CHARLES UNIVERSITY

Faculty of Science

Department of Biochemistry

MSc. Ondřej Skořepa

STRUCTURAL BIOCHEMISTRY OF HUMAN NK CELL RECEPTOR COMPLEX NKP30 AND B7-H6

PhD. Thesis

Supervisor: RNDr. Ondřej Vaněk, Ph.D.

Prague 2021

DECLARATION

I declare that I have worked on this thesis under the guidance of my supervisor and that all sources of the previous knowledge are properly cited. No part of this work was used and will not be used for obtaining any other academic degree than PhD. from Charles University.

Prague, …… ……

Ondřej Skořepa

DECLARATION OF AUTHORSHIP

I declare that Ondřej Skořepa contributed significantly (30-90 %) to the experiments and all three scientific publications contained in this PhD. thesis. He performed most of the experiments, substantially contributed to their planning, and took a significant part in the primary data interpretation and preparation for the publication.

Prague …… ……

RNDr. Ondřej Vaněk, Ph.D.

ACKNOWLEDGEMENTS

At this place, I would like to thank my supervisor Ondřej Vaněk for his patient guidance throughout most of my studies at Charles University. Ondřej has always been a good example for us with his diligence and expertise, and at the same time, he always tries to provide a friendly working environment with the freedom to realise our scientific growth.

Special thanks go to Bára Kalousková, Jan Bláha, Celeste Abreu and Samuel Pažický for their collaboration on the project, as well as for stimulating discussions and for their boundless willingness to give a helping hand (and for reminding me of upcoming deadlines). I express my gratitude for the friendly and inspiring working and learning environment to all former and current lab members. Many thanks to Anna Ammerová for being the good spirit of the Department of Biochemistry.

Thanks to Jan Dohnálek and Tereza Skálová for their collaboration on scientific publications and their interpretation of rather challenging biophysical data.

Last but not least, sincere thanks go to my parents, brother, wife, and daughter for their remarkable patience and for always being my support.

This research was funded by Czech Science Foundation (15-15181S, 18-10687S), the Ministry of Education, Youth and Sports of the Czech Republic (LG14009 and LM2015043 CIISB for CMS BIOCEV, LTC17065 in the frame of the COST Action CA15126 MOBIEU), BIOCEV (ERDF CZ.1.05/1.1.00/02.0109, CZ.02.1.01/0.0/0.0/16_013/0001776), Charles University (GAUK 161216 and 927916, SVV 260079/2014, 260427/2019, 260427/2020, UNCE 204025/2012), the Canadian Institutes of Health Research (FRN 106491 and 159450, to J.R.C.), foundation "Nadání Josefa, Marie a Zdeňky Hlávkových" and BioStruct-X (EC FP7 project 283570). The authors also acknowledge the support and the use of resources of Instruct, a Landmark ESFRI project through the R&D pilot scheme APPID 56 and 286. The authors also acknowledge the support and the use of resources of Instruct-ERIC (PID: 1314) and iNEXT (PID: 2322) infrastructures. The Wellcome Centre for Human Genetics is supported by Wellcome Trust grant 203141/Z/16/Z.

ABSTRACT

Natural killer cells (NK cells for short) are lymphocytes of the non-specific (innate) immune system. They excel in the ability to recognise and eliminate infected or cancerous cells rapidly. Although their role in immune surveillance of malignant transformation was confirmed years ago, ongoing research shows that this process is far from simple. NKp30 is one of the central activating receptors of NK cells with a potential for use in targeted immunotherapy. The oligomerisation of the extracellular ligand-recognition domain of NKp30 in solution depends on the presence of a C-terminal stalk region. However, the structure and role in signal transduction of these oligomers are still unclear. Moreover, the interaction of NKp30 with ligands is influenced by the presence of *N*-linked glycosylation. In this work, we investigated whether and how the oligomerisation of NKp30 depends on its glycosylation. Our results show that NKp30 forms oligomers, regardless of whether glycosylation is complex or uniform (acquired by expression in the HEK293S GnTI$^-$ cell line). In contrast, NKp30 was found to form only monomers when enzymatically deglycosylated. Furthermore, we characterised the interaction with the ligand B7-H6, again concerning oligomerisation and glycosylation. We solved the crystal structure of its complex with glycosylated NKp30, through which we revealed glycosylation-induced dimerisation of NKp30. This work provides new insight into the structural basis of NKp30 oligomerisation and complements our knowledge of how the glycosylation and the presence of the stalk region affect affinity for ligands.

Unravelling of the actual mechanisms underlying NK cell activation, inhibition, and maturation, including the context of cooperation with other lymphocytes, remains a significant challenge. However, understanding these processes is a fundamental prerequisite for rational intervention in NK cell surveillance and its modulation by immunotherapeutics to eliminate tumours when our immunity fails.

ABSTRAKT

Přirozeně zabíječské buňky (zkráceně NK buňky) jsou lymfocyty nespecifického imunitního systému, které vynikají schopností rychle rozpoznat a eliminovat infikované, či nádorové buňky. Přestože jejich schopnost imunitního dohledu nad maligní transformací byla potvrzena již před lety, aktuální výzkum stále ukazuje, že tento proces je velice komplikovaný. NKp30 je jedním z hlavních aktivačních receptorů NK buněk s potenciálem k využití v cílené imunoterapii. Ektodoména NKp30 v roztoku oligomerizuje, tento jev ovšem závisí na přítomnosti C-koncového „stalk" regionu. Struktura oligomerů NKp30 a jejich role v přenosu signálu je zatím nejasná. Interakce NKp30 s ligandy je navíc ovlivněna přítomností *N*-vázané glykosylace. V rámci této práce jsme zjišťovali, zda a jak oligomerizace NKp30 závisí na jeho glykosylaci. Naše výsledky ukazují, že NKp30 tvoří oligomery, ať už je na něm glykosylace přirozená, či jednoduchá (získaná expresí v linii HEK293S GnTI$^-$). Oproti tomu bylo zjištěno, že NKp30 tvoří pouze monomery, je-li enzymaticky deglykosylováno. Dále jsme charakterizovali interakci s ligandem B7-H6, opět s ohledem na oligomerizaci a glykosylaci a vyřešili krystalovou strukturu jeho komplexu s glykosylovaným NKp30, díky které jsme odhalili glykosylací indukovanou dimerizaci NKp30. Tato práce přináší nový pohled na strukturní základ oligomerizace NKp30 a doplňuje naše znalosti o tom, jak glykosylace a přítomnost stalk regionu ovlivňuje afinitu vůči ligandům.

Rozkrývání skutečných mechanismů, které stojí za aktivací, inhibicí a maturací NK buněk, a to i v kontextu kooperace s dalšími lymfocyty, je stále velkou výzvou. Pochopení těchto dějů je ovšem nezbytným předpokladem pro racionální zásah do NK-buněčného dohledu a pro jeho modulaci imunoterapeutiky s cílem eliminovat nádory ve chvílích, kdy vlastní imunita selhává.

ABBREVIATIONS

AA	Amino acid
ADAM	A disintegrin and metalloproteinase
ADCC	Antibody-dependent cellular cytotoxicity
aFGF	Acidic fibroblast growth factor
AUC	Analytical ultracentrifugation
B7-H1	B7 family homolog 1 protein (also PD1-L)
B7-H3	B7 family homolog 3 protein
B7-H6	B7 family homolog 6 protein
BAG6	Bcl2-associated athanogene 6
BAT3	Human leukocyte antigen - B associated transcript 3
CAR-T	Chimeric antigen receptor T cell
CCR7	C-C chemokine receptor type 7
CD152	Cluster of differentiation 152 (cytotoxic T-lymphocyte associated protein 4, CTLA4)
CD16	Cluster of differentiation 16 (also FcγRIII)
CD161	Cluster of differentiation 161 (also KLRB1)
CD244	Cluster of differentiation 244 (also Natural Killer Receptor 2B4)
CD28	Cluster of differentiation 28
CD3	Cluster of differentiation 3
CD335	Cluster of differentiation 335 (also NKp46)
CD336	Cluster of differentiation 336 (also NKp44)
CD337	Cluster of differentiation 337 (also NKp30)
CD3ζ	T-cell surface glycoprotein CD3 zeta chain also known as T-cell receptor T3 zeta chain or CD247 (Cluster of Differentiation 247)
CD4	Cluster of differentiation 4
CD56	Cluster of differentiation 56 (Neural cell adhesion molecule)
$CD56^{bright}$	Natural killer cell with high expression of CD65
$CD56^{dim}$	Natural killer cell with low expression of CD65

CD57	Cluster of differentiation 57
CD8	Cluster of differentiation 8
CD94	Cluster of differentiation 94 (also KLRD1)
Clec2	C-type lectin receptor cluster 2
Clr	C-type lectin related protein
Clr-11	C-type lectin related protein 11
Clr-b	C-type lectin related protein b
CMV	Cytomegalovirus
CTL	C-type lectin
CTLA-4	Cytotoxic T-lymphocyte-associated protein 4
CTLD	C-type lectin-like domain
CTLR	C-type lectin-like receptor
DCs	Dendritic cells
DNA	Deoxyribonucleic acid
ELISA	Enzyme-linked immunosorbent assay
ER	Endoplasmic reticulum
Fab	Fragment antigen-binding
FcγRIIIA	Low-affinity immunoglobulin gamma Fc region receptor III-A, also CD16
FcεRI-γ	High-affinity IgE receptor
GA	Golgi apparatus
GAG	Group-specific antigen
GlcNAc	*N*-Acetylglucosamine
$GlcNAc_2Man_5$	Oligosaccharide consisting of one glucose residue, two *N*-acetylglucosamines and five mannoses.
HA	Influenza hemagglutinin
HEK293T	Human embryonic kidney cell line 293 T
HEK293S $GnTI^-$	Human embryonic kidney cell line 293 S with inactive *N*-acetylglucosaminyltransferase I
HisTag	Polyhistidine affinity tag
HLA-E	Human leukocyte antigen, alpha chain E
Ig	Immunoglobulin

IgC	Immunoglobulin-like domain, C-type
IgG	Immunoglobulin G
Ig-like	Immunoglobulin-like domain
IgV	Immunoglobulin-like domain, V-type
IL-12	Interleukin 12
IL-15	Interleukin 15
IL-18	Interleukin 18
IL-2	Interleukin 2
ILC1	Innate lymphoid cell, group 1
IMAC	Immobilised metal affinity chromatography
INF-γ	Interferon gamma
ITAM	Immunoreceptor tyrosine-based activation motif
ITC	Isothermal titration calorimetry
ITIM	Immunoreceptor tyrosine-based inhibitory motif
K_D	Dissociation constant
KIR	Killer immunoglobulin-like receptor
KLRB1	Killer cell lectin-like receptor family B member 1
LAT	Linker for activation of T cells
LBD	Ligand-binding domain
LIR	Leukocyte immunoglobulin-like receptors
LLT1	Lectin-like transcript 1
lPEI	Linear polyethyleneimine
MALS	Multi Angle Light Scattering
Man	Mannose
MHC	Major histocompatibility complex
MICA	MHC class I polypeptide-related sequence A
MICB	MHC class I polypeptide-related sequence B
MLL5	Mixed lineage leukaemia gene 5
NCR	Natural cytotoxicity receptor
NK	Natural killer (cell)
NKp30	Natural killer protein 30
NKp44	Natural killer protein 44

NKp46	Natural killer protein 46
NKR-P1	Natural killer receptor protein 1
NKT	Natural killer T cell
NTAL	Non-T cell activation linker
PCNA	Proliferating cell nuclear antigen
PD-1	Programmed cell death protein 1
PD1-L	Programmed cell death protein 1 ligand
PDB	Protein databank
PI3K	Phosphoinositide 3-kinase
PLCγ1/2	Phosphoinositide-specific phospholipase C 1/2
SAXS	Small-angle X-ray scattering
SDS-PAGE	Sodium dodecyl sulphate polyacrylamide gel electrophoresis
SEC	Size-exclusion chromatography
SH-2	Src Homology 2 domain
SH-3	Src Homology 3 domain
SHP	SH domain containing protein tyrosine phosphatase
SPR	Surface plasmon resonance
Src	Sarcoma proto-oncogene tyrosine-protein kinase
Syk	Spleen tyrosine kinase
T-BET	T-box protein expressed in T cells
TEV	Tobacco etch virus
TGF-β	Transforming growth factor β
TH1	T helper type 1 cells
TH17	T helper type 17 cells
TH2	T helper type 2 cells
TNF	Tumour necrosis factor
TRAIL	TNF-related apoptosis-inducing ligand
T-reg	Regulatory T cell
UCOE	Ubiquitous chromatin opening element
VPA	Valproic acid
ZAP70	Zeta-chain-associated protein kinase 70

TABLE OF CONTENTS

1. INTRODUCTION

1.1 NATURAL KILLER CELLS

Last year marked the forty-fifth anniversary of discovering large granular lymphocytes, commonly known by the pseudonym "natural killers", or NK cells for short. Their discovery, particularly the first description of their ability to eliminate tumour cells, was described in three publications between 1974-1975 [1-3]. Initially, it was found that the observed cytotoxicity to allogeneic tumours is not of T- or B-cell nature. This effect could be observed because NK cells do not need prior antigen sensitisation for their function and, thanks to a very rapid response to malignantly transformed cells [3, 4], virus-infected cells [5, 6] and parasites [7], they are an essential part of the innate immune system.

NK cells are large granular lymphocytes derived from the common lymphoid progenitor [8]. With approx. two-week blood circulation life span, they are estimated to constitute 5 to 15 % of circulating mononuclear cells [9]. NK cells lack T- and B-cell receptors, and their human phenotype can be characterised as $CD3^{-}CD16^{+/-}$ $CD56^{+}CD161^{+/-}$ [5]. In their most classic definition, human NK cells can be divided into two main subgroups according to the intensity of CD56 surface expression. While NK cells with low CD56 expression ($CD56^{dim}$) predominate in peripheral blood, NK cells found in tissues show much higher CD56 expression ($CD56^{bright}$). The "bright" subset expresses the NKG2A receptor, whereas killer immunoglobulin-like receptors (KIRs) are not represented. $CD56^{bright}$ also show lower cytolytic activity, secrete cytokines (mainly IFN-γ and TNF-α) and are considered non-mature. $CD56^{bright}$ proliferate strongly under IL2 and IL15 signalling. On the other hand, $CD56^{dim}$ have higher cytolytic activity, the ability to rapidly secrete cytokines, and are considered mature. They express NKG2A and/or KIRs on their surface. Interestingly, based on the expression of surface markers, $CD56^{dim}$ can be divided according to differentiation stages. Those are characterised by cytolytic activity that is higher correlated with lower proliferative capacity for more mature cells and vice versa for less mature cells [10, 11]. Completely matured NK cells are KIR^{+} $CD57^{+}$ $CD16^{bright}$ and may express the HLA-E specific activating receptor NKG2C. These cells are subject to expansion during cytomegalovirus (CMV) infections and exhibit adaptive features and characteristics typical to immune memory cells [12-16].

Because expression of CD56 has not been observed on murine NK cells [17, 18], it was suggested that the presence of NKp46, together with the ability to produce IFN-γ, could be a universal common feature of NK cells across the species [17, 19, 20]. Besides that, a recently discovered subset of T-bet-dependent innate cells, the group 1 innate lymphoid cells (ILC1), shares many features with conventional NK cells. However, despite their similarities, ILC1 differ in several important aspects, such as localisation, transcriptional regulation, and phenotype, suggesting that they have different origins and functions [21, 22].

Despite the efforts to correlate the function and fate of NK cell populations with their phenotype (which would be convenient), there are several exceptions and discrepancies in the classical system. For example, while NK cells, defined as $CD56^{dim}CD16^{+}$, are usually thought to be cytotoxic, in fact, $CD56^{bright}$ NK cells have the greatest cytotoxic potential. Again, contrary to convention, it turns out that regulatory NK cells, generally defined as $CD56^{bright}CD16^{-}$, can be CD16 positive. Thus, it is clear that when defining NK cell subtypes and their functions, one cannot rely on the phenotype (Figure 1) but must also consider other properties such as responsiveness and metabolic activity [23].

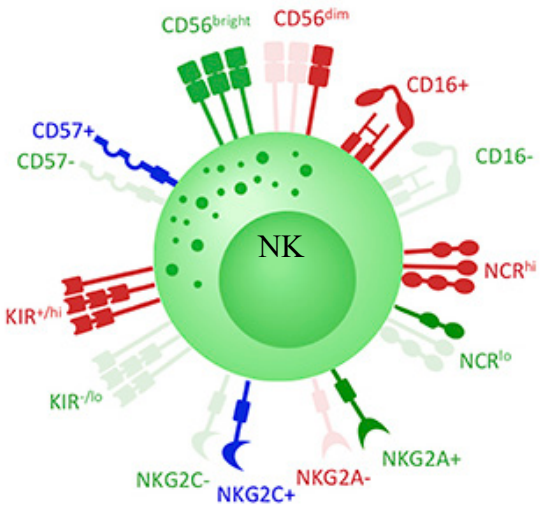

Figure 1: Phenotype does not necessarily imply the NK cell function. For many years, phenotype has been used for the classification of NK cell subsets. Despite the efforts to correlate phenotype with the function and fate of NK cell populations, there are several exceptions and discrepancies in the classical system and the expression of many receptors overlaps. In red receptors associated with cytotoxic NK cells, in green receptors associated with regulatory NK cells, while blue receptors are usually associated with memory NK cells. Modified from [23].

1.2 NK CELL RECOGNITION AND FUNCTION

The mechanism by which NK cells distinguish healthy cells from those which need to be eliminated has not been known for years. Until around 1990, a "missing-self " concept [24] was proposed (Figure 2, page 16). This hypothesis was based on an experiment with a mouse model in which NK cells were able to eliminate tumour cells that lacked major histocompatibility complex-class I (MHC-I), whereas lymphoma cells on which MHC-I expression was preserved were resistant to NK cell-mediated killing [25]. This finding indicated that there are inhibitory receptors present on NK cells to confer self-resistance. And indeed, inhibitory receptors belonging mainly to the Ly49 family were found on murine NK cells [26, 27]. In humans, other inhibitory receptors belonging to the killer-cell immunoglobulin-like receptors (KIR) family [28, 29], as well as leukocyte immunoglobulin-like receptors (LIR) [30], have been found. A representative of inhibitory receptors that is common for both humans and rodents is the heterodimeric CD94/NKG2A(B) complex [31, 32].

Considering the current understanding that the diversity of inhibitory receptors includes a set of more than ten receptors for each organism that do not necessarily belong to the same protein family, and furthermore that each receptor is often specific for different MHC-I polymorphisms, it is important to note that each NK cell typically expresses only 3 – 5 species of these receptors [33-36]. Therefore, it becomes clear that mere inhibition via MHC-I is not sufficient to control NK cell function, alluding, for example, to the fact that targets without (erythrocytes) or with low expression (neurons) of MHC-I molecules do not interfere with NK cells [37]. In addition to receptors corresponding to MHC-I ligands, NK cells also express stimulatory receptors that promote NK cell activity. These are specific for many other target cell surface ligands (induced by stress or DNA damage, for viral ligands and some constitutively expressed ligands). In this "induced-self" recognition, the outcome of the NK cell-target cell encounter is not dependent only on inhibitory signals. For NK cells to lyse target cells or produce cytokines, they must be triggered by stimulatory receptors, similarly to T-cells [38]. The combination of both theories mentioned above is usually referred to as "altered-self" recognition. Considering the importance of the activating receptors and their ligands, they will be discussed further in a separate chapter.

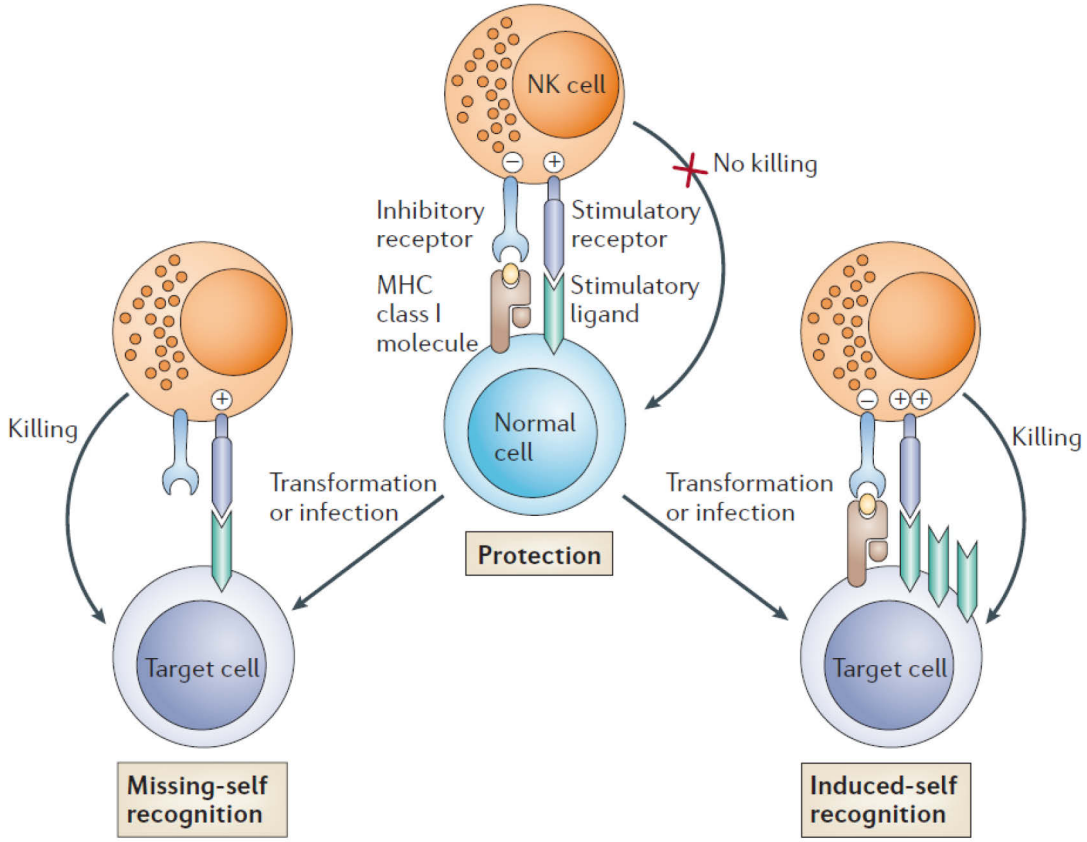

Figure 2: Possible outcomes of NK cell-target cell interaction. When the inhibitory and activating signals are balanced (above), the cell is – usually correctly – considered healthy and spared from NK cell-mediated killing. However, if MHC-I expression has been reduced, for example, due to malignant transformation or virus infection, the signals transmitted by the target cell lead to NK cell activation and subsequent cytotoxicity by the "missing-self" mechanism (left). A similar outcome occurs when malignancy, stress, or infection increases the expression of activating ligands and inhibitory signals are overcome. This condition, called "induced-self", leads again to NK cell activation (right) [38].

The mechanism by which activated NK cells directly eliminate target cells involves the excretion of cytotoxic granules containing perforin, granzymes and Fas ligand [39-41]. In addition, NK cells express the CD16 receptor (FcγRIIIA), through which they recognise IgG opsonised targets [42-44], mediating antibody-dependent cellular cytotoxicity (ADCC). In addition to innate immune surveillance, NK cells can support and regulate immunity through interactions with dendritic cells (DCs), macrophages, and T lymphocytes. NK cells meet dendritic cells in secondary lymphoid organs and peripheral tissues, where they interact in two ways. Firstly, NK cells can influence homeostasis by eliminating immature DCs via a pathway dependent on the TNF-related

apoptosis-inducing ligand (TRAIL) [45]. The second outcome of NK cell interaction with dendritic cells is the promotion of maturation by the action of INF- γ and TNF [43]. These cytokines also induce differentiation of helper T cells into Th1 and Th2 cells. As a result, due to the production of IL-2, IL-12, IL-15 and IL-18 by phagocytosing dendritic cells and macrophages, NK cells proliferate, secrete more cytokines (Figure 3) and have a reduced threshold for triggering cytotoxicity, resulting in a higher cytolytic potential [46-48].

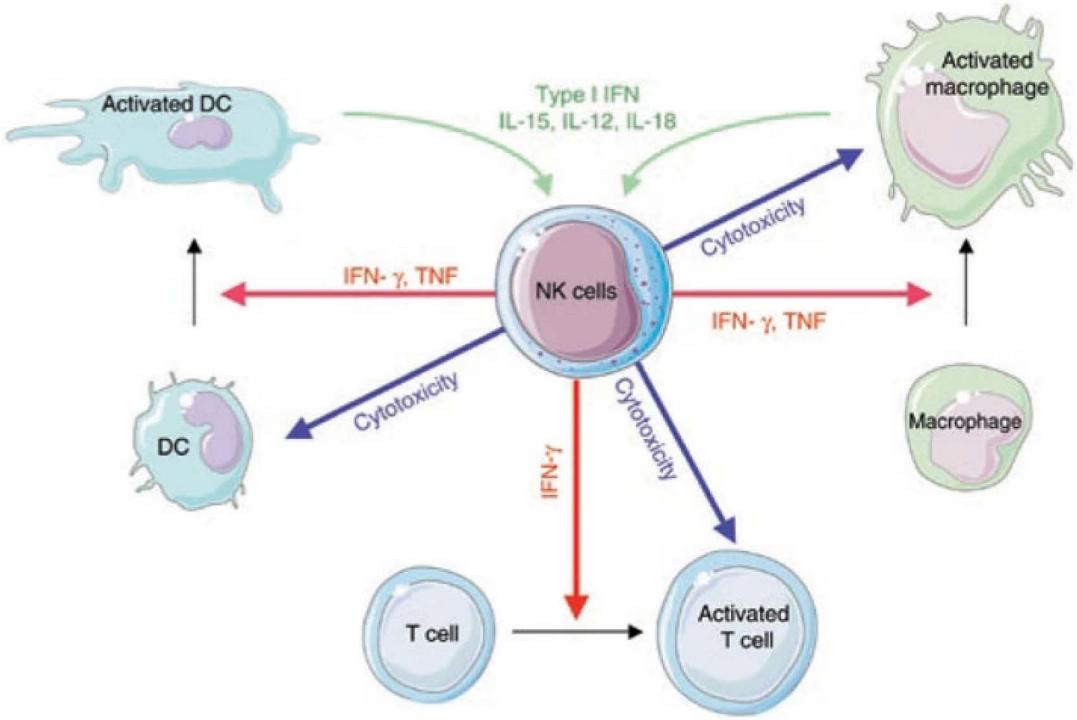

Figure 3: Regulation of immune responses by NK cells. NK cells, primed by several interleukins, can promote maturation and activation of other lymphocytes (red arrows). However, at the same time, they can eliminate unmatured DCs, hyperreactive macrophages and $CD4^+$ T lymphocytes (blue arrows). Such functions are tightly regulated by the balance between signals received by activating and inhibitory receptors present on NK cells [43]. Modified from [43].

Furthermore, it has been discovered that NK cells have the ability to maintain relatively long-term cellular memory after infection-induced clonal expansion. Upon reinfection, these memory-like NK cells represent a reservoir for rapid secondary responses [49, 50]. In this context, NK cells overcome the established notion of "non-adaptive immunity" and represent a highly versatile actor at the interface of adaptive and innate immunity [51].

1.3 MECHANISMS OF TUMOUR ESCAPE FROM NK CELL IMMUNOSURVEILLANCE

Although NK cells often mediate significant anti-tumour response, many proposed therapies fail in the natural environment despite promising *in vitro* results. This failure is because the suppressive microenvironment of solid tumours attenuates the efficacy of NK cells. In addition to hypoxia, which is very common in tumours and lowers NK cell activity, local immunosuppression results from the interaction with many soluble factors (e.g., TGF-β, macrophage migration inhibitory factor [52, 53]). These factors may be produced both by the tumour itself and by the lymphocytes that have been "attracted" by the tumour (including M2 macrophages, myeloid-derived suppressor cells, T-reg and stromal cells) [54]. Ultimately, the final effect on NK cells is the down-regulation of activating receptors. NK cells that could normally eliminate activating ligand-expressing tumours (e.g., B7-H6 [55]) are "disarmed" and unable to recognise the target [16]. Another critical element of tumour escape is the expression of inhibitory checkpoints PD-1 on NK and T cells and corresponding ligands PD1-L on tumour cells, whose engagement results, again, into inhibition [16, 56, 57]. Another way in which tumours escape immune surveillance is through shedding (proteolytic cleavage) and the internalisation of activating receptors. Specific ligands for activating receptors, namely for NKG2D (ligands MICA and MICB [58]) and NKp30 (ligands B7-H6 [59] and BAG6 [60]), are released by tumour cells through the action of specific proteases called ADAMs (a disintegrin and metalloprotease [61]) or are secreted on the surface of exosomes. The consequence of shedding is reducing the amount of activating ligands on the tumour surface and decreasing NK cell responsiveness. In the context of therapeutic intervention, the use of antibodies that would prevent shedding by direct interaction with the activating ligand appears to be a promising approach (inhibition of proteases is not feasible due to their abundance). For example, therapy with a specific antibody against the α domain of MICA/B has shown promising results in this regard, resulting in increased levels of this activating ligand on the target cell surface and, thanks to the NKG2D receptor, to an overall increased NK cell responsiveness [62, 63].

The whole process of escaping immune surveillance is called immunoediting. In principle, it can be described in three phases: elimination, equilibrium, and escape. During the elimination phase (i.e., the immunosurveillance phase), all the newly formed tumour cells are destroyed by the immune system. If the immune system fails to capture all the

malignantly transformed cells, an equilibrium is established where transformed cells carrying mutations that make tumour cells more resistant to killing begin to arise under the selective pressure given by immunocytes. Therefore, at the beginning of the second phase, in equilibrium, the immune system modulates the tumour population and selects for the clones with lower immunogenicity. The consequence may then be a transition of the tumour cell population into the escape phase when the immune system is overwhelmed by the rapid growth of the aggressive tumour. Unfortunately, most tumours do not manifest until the escape phase [64, 65].

1.4 NK CELL RECEPTORS

As already mentioned, NK cells express a wide range of receptors on their surface that determine the outcome of the encounter with the target cell. This outcome can be either activation or inhibition of the NK cell. In principle, NK cell receptors can be divided into activating and inhibitory groups. In the perspective of protection against pathogens and thus activation of the NK cell, we can say that inhibitory receptors scan the surface of the target for MHC-I deficiency, whereas activating receptors look for specific ligands that should not be present on a healthy somatic cell.

After binding the appropriate ligand, the external signal is passed towards the cell through the immunoreceptor tyrosine-based activation motif (ITAM) or the immunoreceptor tyrosine-based inhibitory motif (ITIM). These motifs may be present directly within the receptor's sequence or carried by the adaptor protein (e.g., DAP10 associating with two-domain KIRs, or CD3ζ associating with CD16 and natural cytotoxicity receptors, NCRs [66, 67]). Engagement of ITAM or ITIM motifs triggers the respective signalling cascades (Figure 4, page 20) and determines whether the NK cell is activated or inhibited. Upon binding of activation ligands, the ITAM motif is phosphorylated, resulting in the involvement of Syk family kinases, leading to the activation of cytolytic processes. In contrast, engagement of inhibitory receptors leads to phosphorylation of the ITIM motif, which is mediated by the same Src kinase responsible for ITAM phosphorylation. Phosphorylation of the ITIM motif activates the tyrosine phosphatases SHP1 or SHP2. These subsequently terminate signals emanating from ITAM associated activation receptors by their phosphatase activity, thereby deactivating the NK cell [68-70].

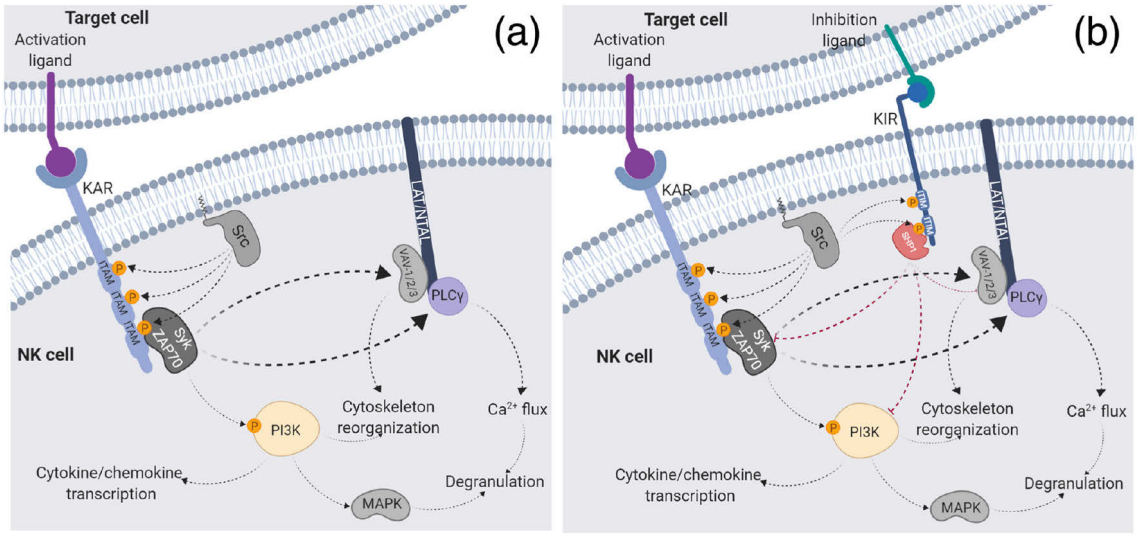

Figure 4: NK cell signalling through ITAM and ITIM motifs. (**a**) After the interaction of the activating receptor with the activating ligand, intracellular ITAM motifs are phosphorylated by Src family enzymes. This activates the phosphorylases Syk and ZAP70, which further phosphorylate the PI3K complex and activate VAV-1/2/3, PLCγ1 and PLCγ2. This subsequently induces cytoskeletal reorganisation and an increase in Ca^{2+} levels. This signalling cascade results in a cytotoxic and cytolytic response in degranulation and production of cytokines and chemokines. (**b**) When inhibitory receptors (KIRs) bearing the ITIM motif are also paired with the corresponding inhibitory ligands, Src kinase-mediated phosphorylation of ITIM follows. This leads to the engagement of SHP1/2 kinases, which terminates ITAM-based activation signalling, thereby deactivating NK cells. The outcome of the engagement of these two pathways is directly proportional to the number of receptors involved. If target cells express more activating than inhibitory ligands, the activation signal will predominate and thus determine the initiation of the NK cell cytotoxic response [70-75].

Certain NK receptors are found in multiple isoforms on NK cells. Sometimes, the isoform exists as a simple point mutation variant, but there may be an entire domain missing in some cases. Such changes can have a significant impact on the resulting function of the protein. Let us take KIR receptors as an example; they can be expressed with a long or short cytoplasmic tail (L and S isoform). Accordingly, they may have either an inhibitory (L) or activating (S) function [76].

In addition to the functional classification into inhibitory and activating receptors, it is advantageous to focus on structural similarities. From this perspective, NK receptors can be divided into two distinct families: C-type lectin-like receptors (CTLR) and

immunoglobulin-like receptors (Ig-like). The first mentioned family structurally includes integral type II membrane proteins. The N-terminal domain mediating signalling is located in the cytosol, followed by a single passage through the cytoplasmic membrane, from which the C-terminal C-type lectin-like domain extends. The most well-characterised proteins in this family are NKR-P1, Clr, Ly49, CD94 and NKG2 receptors [77, 78]. The second mentioned family is comprised of Ig-like receptors. These are integral type I membrane proteins. The extracellular part is formed by two or three Ig domains (depending on the receptor) which usually recognise MHC-I molecules [79]. Here, the best-described proteins are killer-cell immunoglobulin-like receptors (KIRs), leukocyte immunoglobulin-like receptors (LIRs) and natural cytotoxicity receptors (NCRs) [16]. Although the two groups of receptors are very different in terms of extracellular domain structure, it should be noted that they both signal in the same way, i.e., through ITAM and ITIM motifs, and thus both structural groups contain activating and inhibitory receptors.

1.5 C-TYPE LECTIN-LIKE RECEPTORS

Inhibitory Ly-49 or CD94/NKG2A heterodimers, belonging to the lectin-like C-type receptor family, recognise MHC I on the surface of healthy cells and effectively prevent their unwanted elimination. However, during pathological conditions, the expression of their ligands is often lost. That leads to the predominance of activating signals for NK cells and thus the activation of natural cytotoxicity by the "missing-self" mechanism [25]. In addition, these receptors also exhibit "induced-self" recognition, where ligands that are present in limited amounts (or none) on normal cells appear on the surface of the tumour, infected or stressed cells. Such ligands are then recognised by activating receptors. For example, MHC class I-like proteins MICA and MICB are recognised by the C-type lectin-like receptor NKG2D [80, 81].

Next to Ly-49 and CD94/NKG2A, the NKR-P1 (CD161) family is a second large family of receptors that can act on NK cells in activating and inhibitory ways. NKR-P1 receptors were first discovered on rat NK cells [82], and subsequent research has revealed their expression on NKT and $CD8^+$ T cells [83]. This family is encoded by distinct but closely related genes of the NK gene complex. Given the degree of conservation of the genes encoding NKR-P1 (the NK gene complex referred to as *Klrb1*) that occur in birds,

rodents and other mammals, including humans, it seems clear that C-type lectin-like receptors play an important role in innate immunity across species [81, 84].

A typical C-type lectin-like domain (CTLD) exhibits a compact globular double-loop structure with antiparallel β-sheets and two α-helices (α1 and α2). Four disulphide bridges stabilise this structure. A random-coil region of the long loop exits the core of this main domain and enters back at almost the exact location (Figure 5). This extended loop is involved in calcium-dependent carbohydrate-binding and domain swapping dimerisation in lectins [85-89]. C-type lectin-like receptors in NK cells contain a single CTL domain, which is usually glycosylated and forms disulphide homodimers (except for the CD94/NKG2 heterodimer pair already mentioned). However, these receptors do not contain sequences required for carbohydrate-binding except for Dectin-1, which binds certain fungal β-glucans [90].

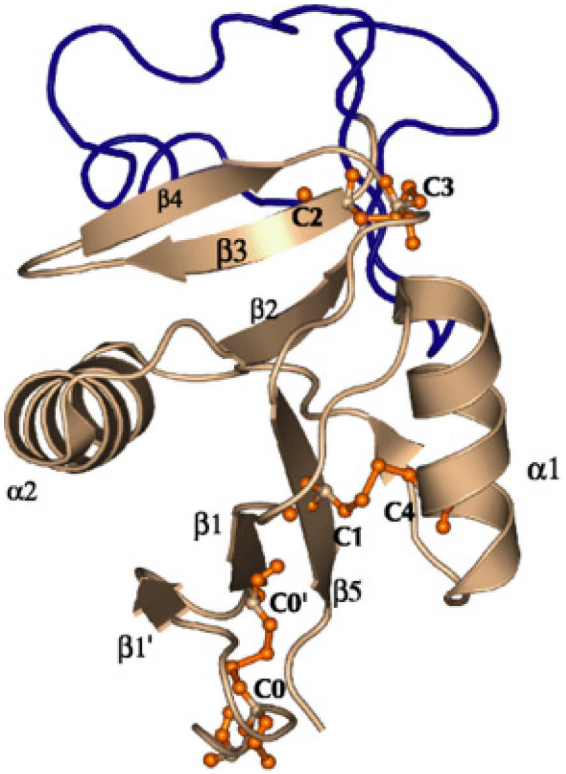

Figure 5: A typical C-type lectin-like domain. A typical CTLD represented as a cartoon of the DC-SIGN receptor (PDB 1K9I). The long loop responsible for Ca^{2+} dependent carbohydrate-binding is shown in blue. The core of the protein containing two β-sheets and two α-helices is represented in brown. Conserved cysteines forming disulphide bridges (orange) are numbered from N-terminus (cystine bridge specific for long-form CTLDs numbered C0-C0′) [91].

The fact that Clr-b expressing cells are partially protected from lysis by NK cells and that it is the murine NKR-P1B receptor that recognises Clr-b was a landmark in understanding the function of NKR-P1 receptors. Indeed, Clr-b is a member of the C-type lectin-related family encoded by the *Clec2* genes, which are intertwined with the *Klrb/f* genes. Their linkage also means that the "self" ligand is always inherited together with its receptor [83, 92]. At the same time, lectin-like receptors have been shown to interact with other proteins in the same family rather than with carbohydrates, whose function at these receptors remains unknown [81].

The human NKR-P1 (CD161, *klrb1* gene) was identified in 1994 and remained the only described human NKR-P1 receptor to date [93]. However, the human NK receptors NKp65 [94] and NKp80 [95] show similarities to NKR-P1 and could therefore be considered activating counterparts to human NKR-P1 [78, 96]. Human NKR-P1 is also expressed on NKT cells [97] and T cell subpopulations [98, 99]. It has also been found on some Tc17 cells [100], which are involved in autoimmune diseases such as multiple sclerosis [101], rheumatoid arthritis [102] and Crohn's disease [103]. It is currently considered a marker of all Th17 cells [104]. NKR-P1 could also play a role in extravasation into immunologically privileged tissues [104-108]. NKR-P1 functions as an inhibitory receptor on NK cells [93, 109, 110] and as a co-stimulatory receptor on NKT and T cells [109, 111], where it promotes IFNγ secretion. The inhibitory function of human NKR-P1 is undesirably exploited by glioblastomas [112] and B-cell non-Hodgkin's lymphomas [113], which overexpress the physiological ligand of NKR-P1 known as lectin-like transcript 1 (LLT1, *clec2d* gene) [109, 110, 114, 115] and thus escape the immune response [116]. Notably, LLT1 is also a type II transmembrane receptor belonging to the C-type lectin-like (CTL) superfamily. As an inhibiting ligand of human NKR-P1, it is expressed mainly on activated lymphocytes (NK cells, T cells, B cells) and antigen-presenting cells, i.e., macrophages and dendritic cells [111, 115].

1.6 IG-LIKE RECEPTORS

In terms of structure, the classical Ig-like domain consists of 7 – 10 β-strands that form two antiparallel β-sheets with typical connectivity called Greek key β-barrel. Due to the high variability of the loops connecting the β-structures and the variability in the number of domains, Ig-like proteins can significantly vary in size [117].

In humans and primates, the missing Ly49 family of CTLR receptors is replaced by functionally similar but structurally distinct killer immunoglobulin-like receptors (KIRs). The similarity between the two groups lies in the fact that they recognise MHC-I and signal through DAP12-ITAM and ITIM motifs and participate in the so-called licensing of NK cells. As among Ly49, both activating and inhibitory receptors are present within KIRs. KIR repertoire on NK cells varies strongly within a single individual with respect to allelic variants and gene expression levels [118].

A less dominant group of Ig-like receptors are leukocyte immunoglobulin-like receptors (LIR). These receptors also bind MHC class I glycoproteins that inhibit NK cells but with significantly lower affinity than KIRs [118]. The exception, in this case, is the LIR-1 receptor, which binds UL18, a human cytomegalovirus class I MHC homolog, in the nM scale and, in contrast to its usual NK cell inhibitory function, activates [119].

The last mentioned and quite unnumbered group is the natural cytotoxicity receptors (NCRs). This group includes the activating receptors NKp30, NKp44 and NKp46 and is discussed in the following chapters.

1.6.1 Natural cytotoxicity receptors

Natural cytotoxicity receptors (NCRs) represent an important component of the NK cell activation repertoire. This group includes three structurally distinct Ig-like receptors, which have been named NKp46 (NCR1; CD335) [19, 120, 121] NKp44 (NCR2; CD336 [122]) and NKp30 (NCR3; CD337[123]) according to their electrophoretic mobility in SDS-PAGE. These receptors are encoded in the germline and are involved in triggering NK cell cytotoxicity against malignant or infected cells. NKp46 and NKp30 are expressed essentially on all resting human NK cells, being up-regulated on activated NK cells and down-regulated on "adaptive" NK cells found in CMV^+ individuals [15, 124].

All NCRs are type I transmembrane proteins that contain one (NKp30, NKp44) or two (NKp46) Ig-like domains, pass through the membrane by a single α-helix and terminate by a short C-terminal chain. The transmembrane helix contains a single positively charged amino acid that mediates association with the membrane regions of the activating adaptor proteins CD3ζ, FcεRI-γ or DAP12 (Figure 6, page 25) [124].

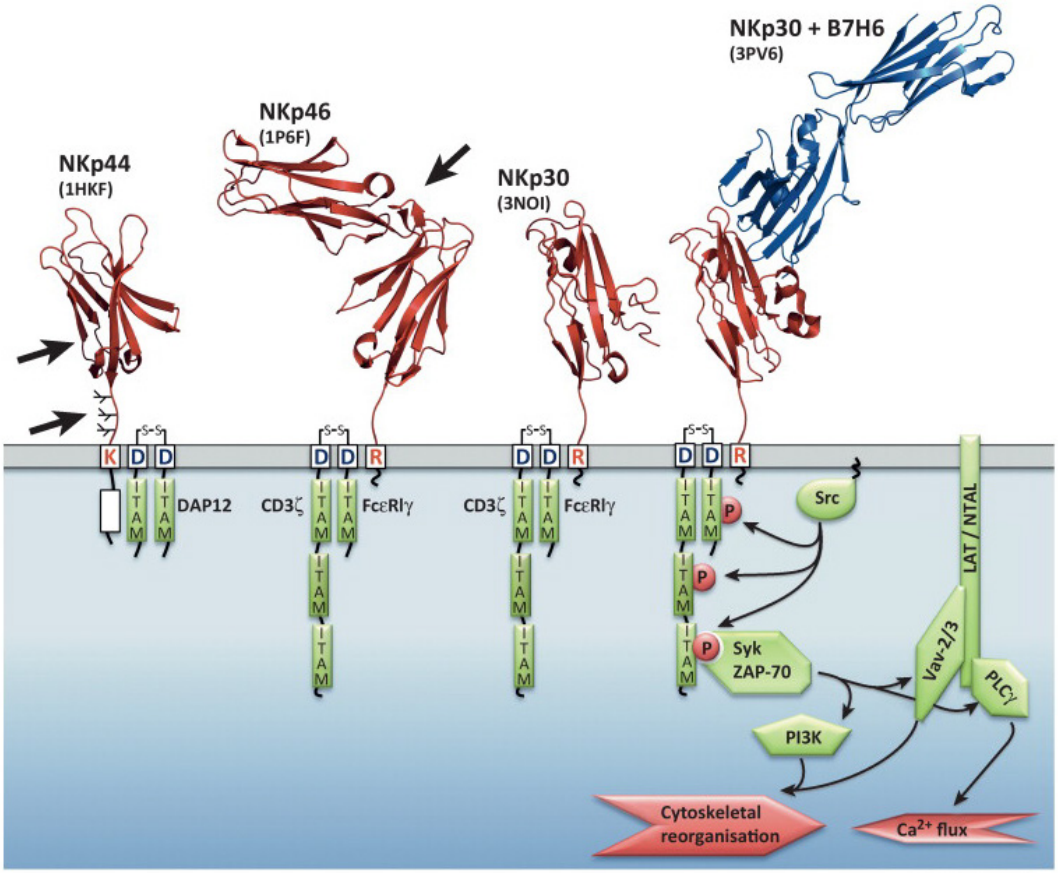

Figure 6: Schematic diagram of the NCRs on the membrane surface. The diagram illustrates the possible arrangement of the domains of human NCRs, NKp30, NKp44 and NKp46. All NCRs are type I membrane proteins, with one (NKp30 and NKp44) or two (NKp46) Ig-like extracellular domains linked to the transmembrane α-helix via a short "stalk region". NKp44 contains one ITIM inhibitory motif on the cytoplasmic chain, but this may not be functional (illustrated as a white rectangle). For signalling, NCRs associate with adaptor proteins (DAP12, CD3ζ) due to opposite amino acid charges in the corresponding transmembrane segments (contact AA are indicated in the membrane segment by a single-letter code). NKp30 is shown as a crystal structure without a bound ligand (PDB 3NOI) and in complex with its ligand B7-H6 (PDB 3PV6). NKp44 and NKp46 are also shown as X-ray crystal structures (PDB 1HKF and 1P6F). The sialic acid moieties within the stalk domain of NKp44 are directly involved in ligand binding (indicated by arrow). In addition, the large groove within the Ig-like domain of NKp44 and the hinge region between the two Ig-like domains of NKp46 are proposed binding sites for yet unidentified protein ligands (indicated by arrows). NCR engagement triggers ITAM phosphorylation mediated by Src family kinases, leading to the recruitment and activation of ZAP70 and Syk kinases. These kinases phosphorylate transmembrane adaptors such as LAT and NTAL, leading to the recruitment and activation of phospholipase C (PLC)γ-1/2, VAV-2/3 and phosphoinositide 3-kinase (PI3K), ultimately leading to degranulation and cytokine secretion via Ca^{2+} flux and cytoskeleton reorganisation, as discussed in Chapter 1.3 [71].

Ligands for the extracellular domains of NCR are very diverse. One group comprises viral ligands, e.g., influenza virus HA activating through NKp46 and NKp44, but inhibiting NKp30, and cytomegalovirus protein pp65 [125, 126], which also counteracts activation through NKp30. Another group of NCR ligands are intracellular proteins (e.g., BAT3/BAG6, MLL5, and PCNA) that appear on the surface in response to stress or because of malignant transformation. For example, BAG6, which is found in the nucleus under physiological conditions, can move to the plasma membrane when exposed to heat shock. It can also be secreted on exosomes' surfaces in some tumours [60, 127, 128]. Similarly, the MLL5 protein is expressed in the nucleus, but one isoform, located on the cytoplasmic membrane, is a ligand for NKp44 [129] Finally, PCNA, a protein involved in replication, DNA repair, and cell cycle control, is found on the surface of some tumour cells or on secreted exosomes, where it functions as a ligand for NKp44 [130].

Extracellular ligands of NKp44 and NKp46 include complement factor P, which binds to NKp46, suggesting a cross-communication between two different mechanisms of response to infection (complement and NK cell cytotoxicity) [131], and a recently identified extracellular ligand of NKp44 is Nidogen-1 [132], whose interaction induces a reduction in cytokine secretion by NK cells [124].

Considering NKp30, the following chapter focuses in more depth on its structure, properties, and ligands.

1.7 HUMAN RECEPTOR NKP30 AND ITS LIGANDS

The activating receptor NKp30 of the NCR family was discovered in 1999 [123]. Since then, its expression on NK cells has been confirmed in humans and other mammals [123, 133-137]. Interestingly, in mice, the gene for NKp30 occurs only as a pseudogene that is terminated prematurely by two stop codons in the canonical sequence. The only known exception to date is *M. caroli* [138]. Another difference from human NKp30 can be found in chimpanzees, where NKp30 expression is induced by NK cell activation, analogous to the human NKp44 [134, 139].

Structurally, NKp30 is similar to the CD28 protein family. The extracellular part consists of a single Ig domain responsible for ligand binding, followed by a 15-amino-acid-long "stalk" region facing the membrane. Previously overlooked, this short domain is essential for signalling, ligand binding, and oligomerisation of NKp30 [67, 140]. The

cytosolic tail itself does not contain the ITAM motif [123]. Interaction with adaptor proteins is mediated by a transmembrane segment and an arginine located at the interface between the membrane and the extracellular space [67]. It is also important to note that NKp30 has three occupied *N*-glycosylation sites on Asn42, Asn68 and Asn121.

Human NKp30 is expressed in six splice variants, designated a – f, thanks to the alternative splicing of exon 2 (extracellular region) and exon 4 [70]. For isoforms a – c, the extracellular Ig domain adopts a V-type Ig structure consisting of complete ectodomain sequences, where the most abundant isoform a represents the canonical NKp30 sequence. The remaining three isoforms d – f lack amino acids 66 – 99 in the sequence, and the extracellular region forms a type-C Ig-domain. The effect of the different structures of the isoforms has so far been observed for variants a – c. When correlating NKp30 splicing variants with prognosis in gastrointestinal sarcoma, it was found that isoforms a and b stimulate the immune system, whereas isoform c exerts immunosuppressive effects [141].

Although most CD28 protein family members have the B7 family proteins [142] as their natural ligands, the first ligands discovered for NKp30 were heparin and heparan sulphate. However, these only interact with glycosylated NKp30 [143, 144]. Nevertheless, the interaction of NKp30 with viral ligands usually inhibits the NK cell response. This is indeed true for pp65 protein released from human cytomegalovirus [126] as well as hemagglutinin of ectromelia and vaccine virus [145]. The mechanism of this inhibition has been described for pp65, which causes dissociation of the pre-assembled NKp30-CD3ζ complex. Although the binding site for pp65 does not sterically hinder the binding of the activating ligands, the activation pathway is already disrupted [126, 143].

Later, three cellular ligands of NKp30 were identified. As expected from the similarity within the CD28 family, a protein of the B7 family, namely B7 homologue 6 (B7-H6), was reported to bind NKp30. This protein is constitutively expressed on the surface of some cancer cells [146]. Another cellular ligand for NKp30 is the soluble fragment of the tumour antigen BCL2-associated athanogene 6 (BAG-6). This protein is found under physiological conditions in the nucleus, where it plays a role in response to DNA damage, regulation of gene expression, protein quality control and immunoregulation. As a result of stress or malignant transformation, it can be located on the cell surface to be recognised

through NKp30 [147]. BAG-6 also exists on the surface of exosomes [147], where, according to recent findings, B7-H6 is rarely present [60]. Furthermore, they can be found in soluble forms produced by proteolytic cleavage from the membrane surface. As previously mentioned, this so-called shedding prevents NK cell activation [59, 147]. The most recently discovered ligand of NKp30 is galectin 3. This protein, belonging to the lectin family, is expressed by some tumours and markedly inhibits NK cell cytotoxicity [148].

Since discovering the clinical potential lying in the activation of NK cell cytotoxicity by forming the B7-H6:NKp30 complex, considerable research efforts have been made to define the specificity of B7-H6 expression in cancer cell lines [55, 142, 149]. B7-H6 is also a type I transmembrane protein [146]. Its extracellular part consists of two Ig-like (IgV and IgC) domains, followed by a single α-helix permeating the cytoplasmic membrane. The protein terminates by a cytoplasmic C-terminal sequence homologous to group-specific antigen (GAG) proteins that carries various signalling motifs, including ITIM-, SH-2- and SH-3 binding motifs [142, 146]. The signalling output is not yet known [142]; however, the role of B7-H6 in non-Hodgkin lymphoma involves cell proliferation, migration and invasion [150]. The structurally closest homologues of B7-H6 are B7-H1 (better known as programmed death-ligand 1 or PD-L1) and B7-H3 [146]. B7-H6 is also heavily glycosylated with six occupied *N*-glycosylation sites out of the six predicted.

B7-H6 also has potential as a tumour marker, given that it has not yet been detected on healthy unstressed cells, whereas it is expressed on some cancer cell lines [142, 146]. In addition to its expression on cancer cells, mechanisms leading to B7-H6 expression in untransformed cells have also been investigated. In vivo, B7-H6 can be induced on the surface of $CD14^+$ $CD16^+$ proinflammatory monocytes and neutrophils by stimulation with Toll-like receptor ligands or proinflammatory cytokines (interleukin-1β and TNF-α). At the same time, the expression of soluble and exosomal B7-H6 was confirmed under the same conditions. B7-H6 was also detected in the serum of patients with Gram-negative sepsis. These findings suggest that B7-H6 is involved in both tumour-associated immune processes and response to infection [151].

Although the structure of NKp30 has already been solved both alone [152] and in complex with B7-H6 [149], both structures overlook glycosylation for the proteins used for crystallisation were expressed in bacteria that generally lack this posttranslational

modification. At the same time, a structure of NKp30 with its stalk domain included is not yet known. As it was shown later, it is both glycosylation and the stalk domain that affect the affinity for ligands [140]. *N*-glycosylation has been shown essential for B7-H6 binding and signal transduction but does not affect the interaction with BAG6 [153]. The presence of the stalk domain of NKp30 influences its oligomerisation, at least for its extracellular part in the solution [153]. It is also worth noting that a dimer can be observed in the crystal structure of NKp30 alone [152] but is not present in the only previously known structure of the NKp30:B7-H6 complex [149]. Regarding the oligomerisation of NKp30, it is worth noting that the oligomeric fraction's presence correlates positively with the affinity for B7-H6 when measured by SPR. However, such increased measured affinity may be due to an avidity contribution caused by oligomerisation of the NKp30 ectodomain [153]. Similarly, different affinities were found for glycosylation mutants generated by targeted mutagenesis of asparagine to glutamine. Glycosylation at Asn42 and Asn68 significantly affects ligand binding, whereas glycosylation on Asn121 does not appear to have any critical role [140].

The following brief review of previously published affinities measured for NKp30 and B7-H6 shows differences in affinity depending on the expression system and the NKp30 construct used. The affinity of the complex ranged from 2.5 to 3.5 μM when both binding partners were expressed in *E. coli* [152]. In contrast, higher affinities of up to 1 μM were provided by measurements when B7-H6 was expressed in the insect cell line Sf9 [149]. Even higher K_D in the range of 80 to 320 nM was provided by measurements where the NKp30 receptor was expressed in the human cell line HEK293T as an Fc IgG-fusion construct (NKp30-Ig). Moreover, in this measurement, the increased affinity correlated positively with the length of the stalk domain of the construct used [140]. The highest affinity was shown by ELISA measurements, for which NKp30 was produced in the HEK293 line and B7-H6 in the Sf9 line. These resulted in an affinity range between 1 – 2 nM, again depending on the oligomeric state of NKp30 [153].

1.8 Glycosylation of Immune Receptors in Cancer

Glycosylation, a post-translational modification of proteins by a carbohydrate moiety, is the most common type of post-translational modification, occurring in more than 50 % of human proteins [154]. Glycosylation is involved in a wide range of biological

processes. It is important for protein folding; it influences protein stability and solubility and is ultimately involved in protein interactions [155, 156]. According to the type of carbohydrate-protein linkage, *N*- and *O*-linked glycosylation is distinguished. *N*-glycosylation represents the covalent attachment of *N*-acetylglucosamine (GlcNAc) to the nitrogen atom on the asparagine (Asn) side chain mediated by *N*-glycosidic linkage. In parallel, *O*-linked glycosylation occurs on the oxygen side groups of serine (Ser) or threonine (Thr).

The process of protein *N*-glycosylation occurs in the endoplasmic reticulum (ER) and Golgi apparatus (GA) and can be described in four steps. The first one is the formation of dolichol phosphate, which contains 14 carbohydrate units (Glc_3-Man_9-$GlcNAc_2$). This precursor is located in the ER lumen and serves as the oligosaccharide donor for the following steps. Secondly, the oligosaccharyltransferase complex catalyses the transfer of this whole oligosaccharide precursor unit to asparagine residues located in the peptide sequence (Asn-X-Ser/Thr) on the nascent polypeptide translocated into the ER lumen [157, 158]. In the third stage, the processing of the glycoprotein occurs in the ER. After conjugation of the 14-monosaccharide-unit precursor to substrates, further trimming mediated by various glycosidases occurs. This process also leads to quality control to ensure the correct fold of the newly synthesised glycoprotein. [159, 160]. The maturation of glycans, and thus the fourth step of glycosylation, occurs in the Golgi apparatus [155, 161]. It is the step responsible for forming a vast repertoire of glycan structures, including high-mannose, hybrid and complex *N*-glycans. Hence, at each glycosylation site, a number of diverse glycan structures can be formed, leading to a large heterogeneity of the so-called glycoforms of a given protein [162].

The glycocalyx, as the coat surrounding cells composed of glycosylated proteins and proteoglycans is called, is located on the exterior of the plasma membrane and plays a vital role in the recognition and interaction processes between cells. It mediates adhesion, intercellular interactions, signalling, and, eventually, interactions in response to pathogens [163-165]. Alterations in glycosylation are associated with many pathological conditions such as immunodeficiency, cancer, and innate immune disorders [163, 166-168]. Several causes and mechanisms that can lead to changes in *N*- and *O*-glycans' structure have already been described. These typically include altered gene expression of enzymes involved in glycosylation or changes in the localisation of these enzymes in the

Golgi apparatus, or even reduced substrate availability. Towards malignant transformation, glycosylation aberrations may lead to altered intercellular adhesion, activation of oncogenic signalling pathways and subsequent induction of pro-metastatic phenotypes. Indeed, metastatic cells must overcome adhesion to leave the original solid tumour and migrate to other tissues [163, 165, 169].

Cadherins, a family of cell adhesion molecules [170-172], are specific examples where altered glycosylation affects tumorigenesis. Similarly, glycosylation alteration on integrins [163, 170] influences tumour cell invasiveness. In addition, specific alterations in glycan structures have already been identified at receptor tyrosine kinases that are often responsible for oncogenic activation [165, 173-175].

Typical changes in glycan structure in cancer cells include alterations in *N*-glycan branching, glycan truncation (also applicable to *O*-linked carbohydrates), increased sialylation and fucosylation, or alteration of glycosaminoglycans [163, 176]. Such modifications are then responsible for modulated interactions with the corresponding binding partners, for instance, with selectins, that mediate cell adhesion between leukocytes and vascular endothelial cells during inflammation. A similar process is used by metastatic tumour cells [164, 177]. The other major category consists of proteins that bind primarily carbohydrates, especially galectins, regulating various processes, including immune surveillance [178, 179]. On the other hand, alterations in glycosylation can infer different stages of tumour progression and thus serve as biomarkers for the diagnosis and prognosis of patients (Figure 7, page 32) [165, 180].

In addition to these general processes, information on the effect of glycosylation in particular cases has been increasing in recent years. The diverse functions of *N*-linked glycosylation at the NKp30 receptor have already been discussed in previous chapters. However, it should be mentioned that NKp30 is not the only representative of glycosylated NK cell (and optionally T cell) receptors. The functional glycosylation has been found both on activating receptors and on their ligands (e.g., TCR [181, 182], CD28 [183], CD244 [184], B7-H6 [185], MICA [186]) and on their inhibitory counterparts (e.g., PD-1/PD-L1 [187], CTLA-4/CD152 [173]), as well as on cytokines and chemokines (e.g., TGF-β [188-190], CCR7 [191]) [162].

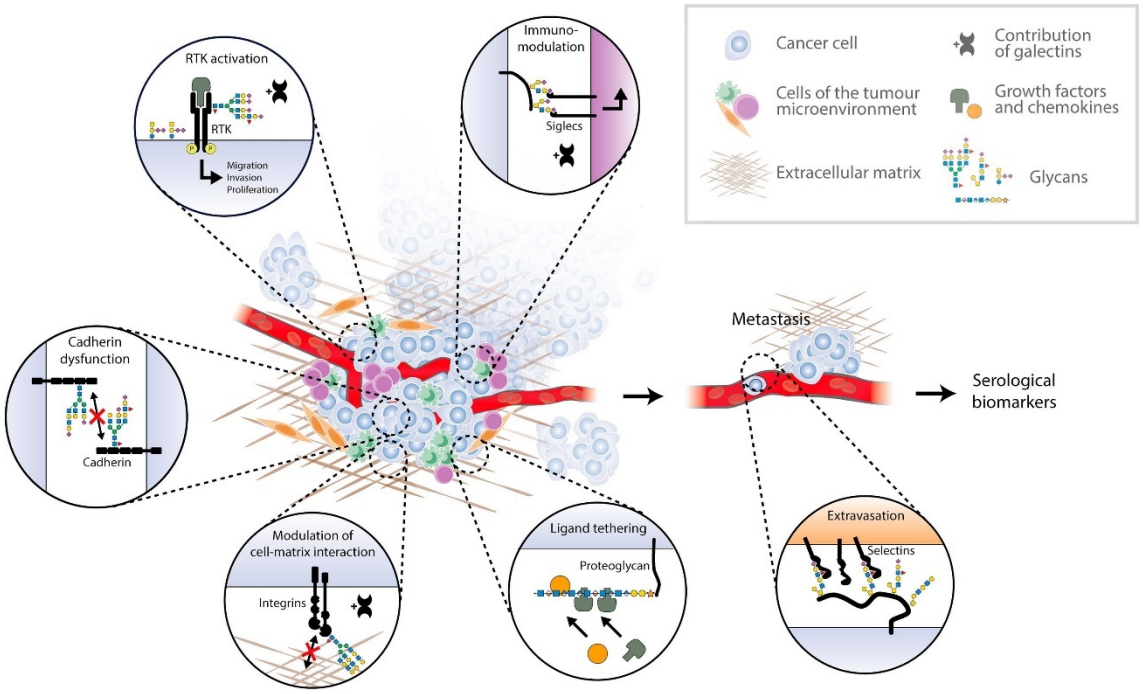

Figure 7: Selected functions of glycoconjugates in cancer metastasis. Glycoconjugates are hallmarks of cancer that promote metastasis. Receptor tyrosine kinases are activated by alternative receptor glycosylation, gangliosides, and galectin expression, leading to increased migration, invasion, and proliferation of cancer cells. Interactions between cells and matrix are modulated by glycosylation, as exemplified by the branched *N*-glycans of cadherins and integrins that result in the migratory phenotypes of cancer cells. Glycosylated growth factors and chemokines determine cell signalling processes. Glycan-binding proteins such as siglecs and galectins regulate the immune response allowing immune tolerance. Sialyl Lewis glycan epitopes are ligands for selectins and contribute to interactions between tumour cells and the endothelium, facilitating extravasation and metastasis. These glycoconjugates can be detected in patients' sera and thus used as diagnostic and predictive biomarkers [165].

In conclusion, understanding glycan structures and their functions or alterations on specific glycoproteins is essential for diagnostic and prognostic purposes and as a source of new targets for therapeutic applications. Immunotherapeutic approaches such as antibodies or glycan-directed CAR-T cells have great potential in cancer therapy. Research in this field is also moving towards applications of inhibitors of glycosylation-related enzymes or blocking specific glycan-recognition molecules. Knowledge of the tumour glycome and unravelling the effects of glycosylation on tumour progression or immune surveillance provides a relatively new ground for novel strategies in cancer treatment and diagnosis [165].

2. AIMS OF THE THESIS

- To optimise transfection in suspension-adapted HEK293T and HEK293S GnTI$^-$ cell lines for the production of NKp30_Stalk, LBD, B7-H6 and BAG6 in various glycosylation forms.

- To characterise receptor-ligand binding by ITC and SPR and to compare results for affinity and avidity.

- To characterise glycosylation and its influence on the oligomeric state of NKp30.

- To characterise the oligomeric state of NKp30 in solution by SEC-MALS and AUC.

- To observe an influence of B7-H6 binding to NKp30 oligomers.

- To test the influence of B7-H6 glycosylation on its binding affinity with NKp30.

- To crystallise and solve a structure of homogeneously glycosylated NKp30_LBD in complex with B7-H6.

- To propose possible position on cell surface and arrangement of NKp30 units in oligomers.

3. METHODS

All methods that were used in this thesis are listed in the attached publications. For this reason, only a list of methods follows, a detailed description of which can be found in the relevant publications.

- Gene cloning and vector design
- Cell culture
- Transfections
- Flow cytometry
- Protein expression and purification
- Electrophoresis and Western blot analysis.
- Protein labelling
- Differential scanning fluorimetry
- Size-exclusion chromatography with multi-angle light scattering
- Mass spectrometry
- Analytical ultracentrifugation
- Isothermal titration calorimetry
- Surface plasmon resonance
- Small-angle X-ray scattering
- Fourier-transform infrared spectroscopy
- Deglycosylation
- Dynamic light scattering
- Protein crystallisation and X-ray crystallography

4. RESULTS AND DISCUSSION

To obtain sufficient amounts of soluble NKp30 receptor ectodomain and its ligand B7-H6, which were the focus of this work, we used an optimised recombinant protein expression procedure in the human cell line HEK293. Optimisation of recombinant protein production system is described in the first two (chronologically) attached publications.

Our standard procedures of cultivating HEK293S GnTI$^-$ and HEK293T lines, adaptation to suspension growth and the method of high-density transfection with linear polyethyleneimine are described by Bláha *et al*. in a publication from 2015 [115]. In the first co-authored publication attached [116], we describe the methodology for expressing the human NK cell receptor NKR-P1. Following unsuccessful experiments based on expression in *E. coli*, which resulted in precipitation of NKR-P1 into inclusion bodies and failed refolding [192], we optimised the procedure for its preparation using the pOPINGTTneo expression vector setting up a stably transfected HEK293S GnTI$^-$ cell line. In the next co-authored [81] publication, we further optimised the expression methodology in the HEK293 line on reporter proteins and tested different ratios of lPEI to DNA and use valproate (VPA) to increase yields. Consequently, the optimised procedure is applied to the expression of rat NKR-P1B and Clr-11.

Recombinant protein production in the HEK293T cell line provides proteins with wild-type mammalian complex post-translational modifications, which can be considered a significant advantage in functional studies. Indisputably advantageous modification is glycosylation, which helps with protein folding and solubility during recombinant expression. Despite this, non-uniform mammalian complex glycosylation can be a bit problematic in protein crystallography. Indeed, the attached oligosaccharides vary in the number of sialic acid and fucose residues, and at some glycosylation sites, the oligosaccharides may be absent, making the sample too heterogeneous. In order to get a more homogeneous sample, several approaches can be used to tackle this inherent variability. Firstly, several endoglycosidases such as endoglycosidase-H or -F are available for deglycosylation. However, these enzymes typically cannot cleave off the wild-type complex *N*-glycans very well for the fucose linked to the core GlcNAc residue and can be disadvantageous in introducing an additional purification step to remove them from the sample. Another approach is the use of kifunensin, an α-mannosidase inhibitor,

during protein expression. Kifunensin prevents cleavage of the mannose structure and thus the subsequent synthesis of complex oligosaccharides [193]. A rather elegant solution is direct intervention in the cellular glycosylation cascade by knocking out the relevant enzyme (*N*-acetylglucosaminyltransferase I), as in the HEK293S GnTI$^-$ line (Figure 8). Such cell lines then provide uniform $GlcNAc_2Man_5$ *N*-glycans. This type of glycosylation can also be readily cleaved by endoglycosidases. A drawback of such cell lines is generally the lower yield of recombinant proteins.

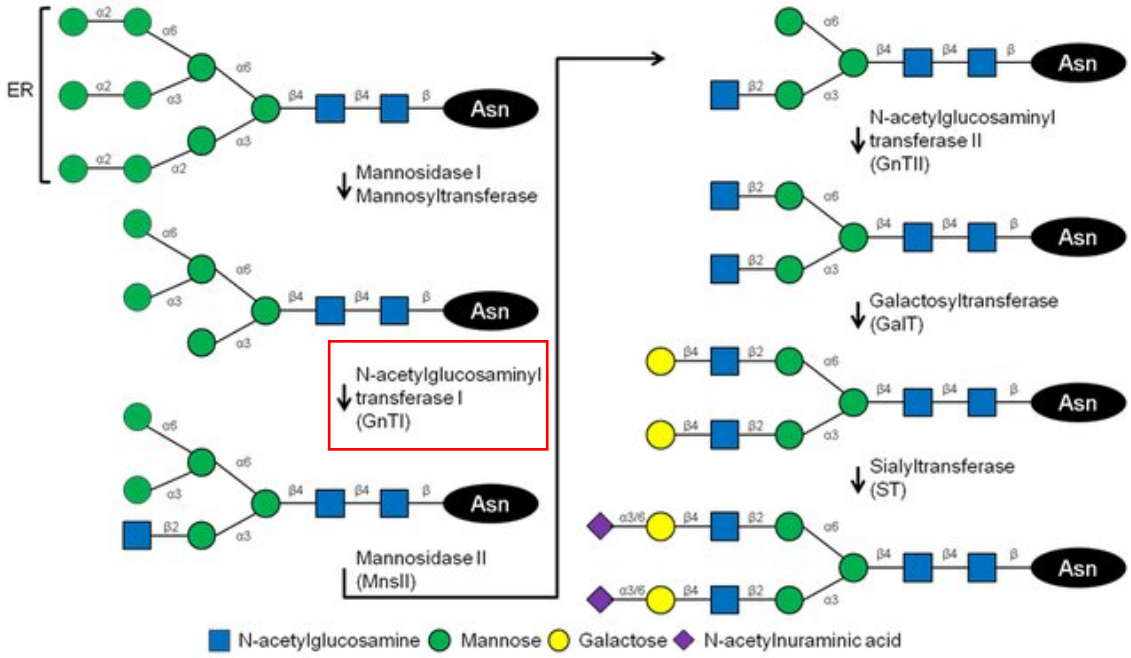

Figure 8: Glycosylation cascade in the HEK293 line. The glycosylation cascade in the HEK293S GnTI$^-$ line is interrupted by the inactivation of *N*-acetylglucosaminyl-transferase I (GnTI, in red square), thus providing a uniform oligomannose *N*-glycosylation of the $GlcNAc_2Man_5$ type [194].

Successful production of human NKR-P1 was previously published using the HEK293 line, but the authors do not report the yield [192], which may not have been high given that the protein has been used only for immobilisation on SPR chip. To verify the published procedure, we performed transient production of the same NKR-P1 construct (G90-S225) in both HEK293T and HEK293S GnTI$^-$ suspension-adapted cell lines. However, the yield was only about 0.1 mg of purified human NKR-P1 per litre of cell culture. For comparison, the typical yield from the expression of LLT1 (the structural homologue and also the ligand of NKR-P1) is about 3 mg per litre of culture using the

same methodology. We repeatedly tried to express the NKR-P1 G90-S225 construct (lacking the stalk domain) because we aimed to crystallise its ectodomain. To date, all well-resolved CTL domain protein structures do not contain a stalk region [114, 195-197]. Therefore, in addition to the construct optimisation trying to express different lengths of the N-terminal stalk domain (in *E. coli*, the insect Sf9 cell line, and the HEK293 cell line), we attempted to establish a stably transfected HEK293S GnTI$^-$ line. For this purpose, we cloned the original construct (G90-S225) into the pOPINGTTneo vector (obtained from the Oxford Protein Production Facility, University of Oxford, UK), which can be used for stable transfection of mammalian cell lines under the selective pressure of Geneticin G418 antibiotics. The selected HEK293S GnTI$^-$ cell line was allowed to grow and produce NKR-P1 for ten days. The yield after affinity chromatography (IMAC) and gel filtration was increased to 2.5 mg per litre of cell culture. NKR-P1 obtained by this method was subsequently successfully crystallised in both glycosylated and deglycosylated states, as well as in complex with its cognate ligand LLT1.

Similarly, the optimised procedures were used to produce several constructs of NKp30 and B7-H6. For transient transfections of both the HEK293T and HEK293S GnTI$^-$ cell lines, the procedure involved high-density transfection with linear polyethyleneimine (lPEI) in 40 ml of cell suspension in EX-CELL293 medium using a DNA:lPEI ratio of 1:3 (1 μg per 10^6 cells). Following consultation with Dr. David Hacker (manager of Protein Expression Core Facility, EPFL, Switzerland), we also reduced the incubation time with DNA and lPEI in high density from 4 hours to 90 minutes. As a result, the viability of the culture after dilution to production concentration (2×10^6 cells/ml) in a 400 ml volume increased while maintaining the transfection efficiency. In addition, we currently use cotransfection by a production plasmid in combination with plasmids carrying genes for anti-apoptotic factors aFGF and p27, which increase yields by up to 50 % more (unpublished data). After dilution to the final volume, valproate (VPA) is added to the cell suspension to a final concentration of 2 mM. Production was typically carried out for six days. Both NKp30 and B7-H6 were secreted into the medium and purified by IMAC using a histidine tag present at the proteins' C-termini. The standard yield from transient expression was approximately 40 mg of NKp30_LBD, 30 mg of NKp30_Stalk, and 50 mg of B7-H6 per litre of HEK293T cell suspension. Yields from the HEK293S GnTI$^-$ line were generally lower, approximately half.

Given the previous success with increasing yields by establishing a stable line, we used the piggyBac system [198]. Optimisation of piggyBac system is described in several theses from our laboratory [199, 200]. It is a system that uses cotransfection with a transiently expressed transposase enzyme that actively inserts an expression cassette from another plasmid into the genome of the transfected cell. Subsequent selection on corresponding antibiotics results in a polyclonal stably transfected cell line pool. In this case, production from stable cell lines allowed for increased yields up to 60 mg per litre of cell suspension for both NKp30_LBD and B7-H6 in the HEK293T line (HEK293S GnTI$^-$ with an approximately half-yield). Compared to the original plasmid [198], a UCOE segment [201] was inserted into the expression cassette by Dr. Jan Bláha to protect the transfected cell line from gene silencing over time. The advantage of stable lines, besides the increase in yield, is the inducibility of expression by the addition of doxycycline. This provides a tuneable expression rate, introducing another possibility for optimising the system, especially for proteins with problematic folding. Furthermore, the stable line can be maintained at -80 °C, and it does not require the time-consuming step of isolating milligram quantities of plasmid DNA (as necessary for large-scale transient transfection), making piggyBac stable cell line generation a very convenient tool.

In the third attached publication, we investigated the effect of glycosylation on the interaction of the NKp30 receptor with the B7-H6 ligand. We inserted the gene coding extracellular domains of NKp30 and B7-H6 into mammalian expression vectors with a C-terminal histidine tag to address these features. Expression in the HEK293 line provided either natural glycosylation (HEK293T) or uniform glycosylation (HEK293S GnTI$^-$). Uniformly glycosylated proteins were enzymatically deglycosylated by endoglycosidase F1 for further experiments (leaving a single GlcNAc unit at each glycosylation site), thus obtaining both binding partners in three different glycosylation states. The presence of the predicted glycan type was further verified by mass spectrometry. The extracellular domain of NKp30 was prepared in two different lengths to investigate the effect of the stalk domain presence on the binding properties and oligomerisation (NKp30_LBD, NKp30_Stalk). Importantly, the three glycosylation sites Asn42, Asn68 and Asn121 are retained on both NKp30 constructs.

The extracellular part of B7-H6 (Asp25-Leu245) consisting of two Ig-like domains was chosen as the B7-H6 construct. Each of these domains contains one disulphide

bridge. The C-terminal Ig domain contains an odd cysteine (Cys212, Figure 9). Initially, we attempted to express a shorter B7-H6 construct consisting of an N-terminal domain (Asp25 – Val140). However, the shorter construct could not be expressed. The extracellular part of B7-H6 is stable only when expressed as a whole. The first attempts to express the whole extracellular domain of B7-H6 were made with a sequence with the odd cysteine 212 preserved. SDS-PAGE analysis and subsequent analytical ultracentrifugation confirmed the presence of a covalent dimer; therefore, we proceeded to mutate the odd cysteine to serine. The B7-H6 (C212S) construct no longer forms a covalent dimer, and, in addition, the introduction of this mutation increased the expression yield up to tenfold. Only the B7-H6 (C212S) construct was used for all further experimental work.

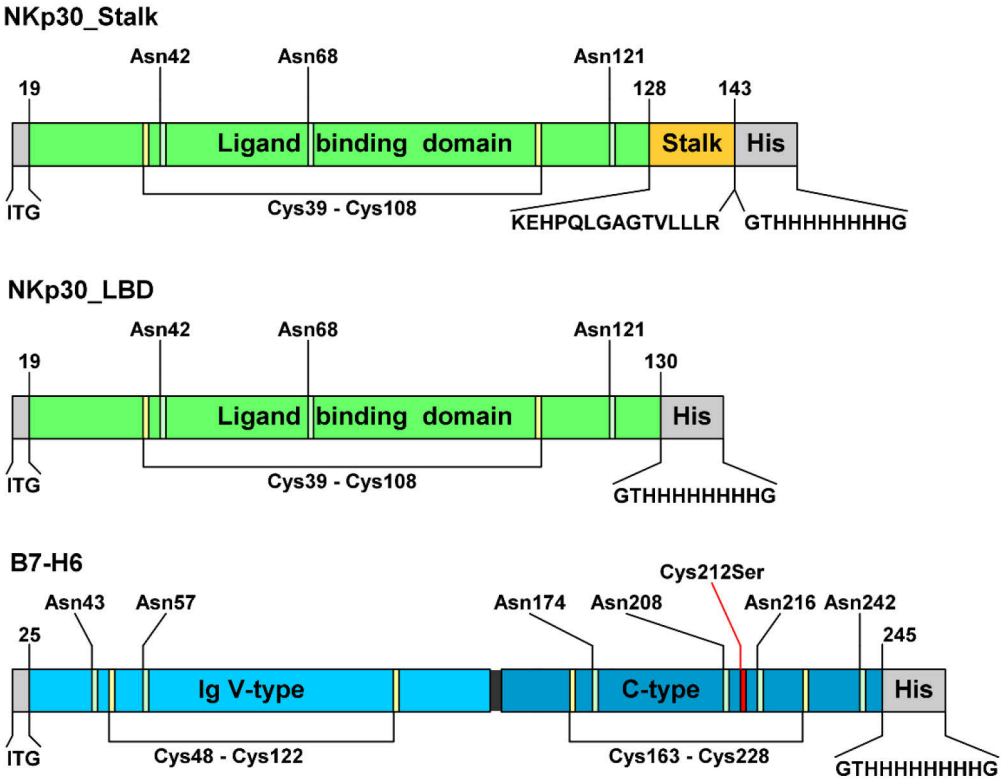

Figure 9: Expression constructs NKp30 and B7-H6. All constructs contain a short segment of three amino acids (ITG) at the N-terminus that remains after cleavage of the secretion signal. An uncleaved affinity tag (His-tag) is present at the C-terminus and is preceded by amino acids GT (remaining from the restriction endonuclease cleavage site). Lines mark cysteines forming disulphide bridges, and bars mark glycosylation sites on the corresponding asparagine. The C212S odd cysteine mutation in B7-H6 is shown in red [185].

In addition to the successful expression of B7-H6, we attempted to prepare another natural ligand of NKp30, BAG6. Unfortunately, despite many optimisations, including preparing a library of constructs, various expression systems (Sf9, *E. coli*) and generation of stably transfected HEK293T lines, we could not prepare soluble BAG6.

The oligomerisation of the extracellular domain of NKp30, which is the focus of this work, has been published previously [153]. For characterisation, the authors used NKp30 expressed in the insect line Sf9, which provides simple paucimannose *N*-glycans. Similarly, two constructs were chosen for expression, one of which contained the stalk domain; however, both constructs still carried a conserved TEV protease cleavage site at the C-terminus upstream of the decahistidine tag, linked to the Ig-like domain of NKp30_LBD itself or the stalk domain of NKp30_Stalk. The authors observed oligomerisation for NKp30_Stalk, consistent with our observations, and to a lesser extent for NKp30_LBD, while our NKp30_LBD construct does not oligomerise. However, AUC analysis of our NKp30_LBD at high concentration shows a small peak that would correspond to the dimeric form and thus confirms some tendency to self-association. To verify the presence of oligomers, we performed sedimentation analysis (AUC) and size-exclusion chromatography with multi-angle light scattering detection (SEC-MALS). Our results show that the NKp30_LBD construct lacking the stalk region is purely monomeric (at lower concentrations), whereas the NKp30_Stalk construct is present in both monomeric and oligomeric forms, significantly present in all our analyses. To conclude, it can be stated that the presence of the stalk domain is a necessary condition for the oligomerisation of NKp30.

Another previous study showed that when glycosylation is present on NKp30, both binding affinity towards B7-H6 and cellular signalling increase [140]. We were able to show that glycosylation is also essential for the oligomerisation of NKp30. While NKp30 produced in the HEK293 line (both S and T) oligomerises extensively, the oligomeric fraction disappears completely after enzymatic deglycosylation (Figure 10, page 41). We verified this effect by both AUC and SEC-MALS. It is noteworthy that, based on the calculated molecular masses of NKp30, the oligomeric fraction appears to contain two dominant oligomer species of eight and sixteen units. In conclusion, both the stalk domain and the glycosylation of NKp30 are necessary for its homooligomerisation.

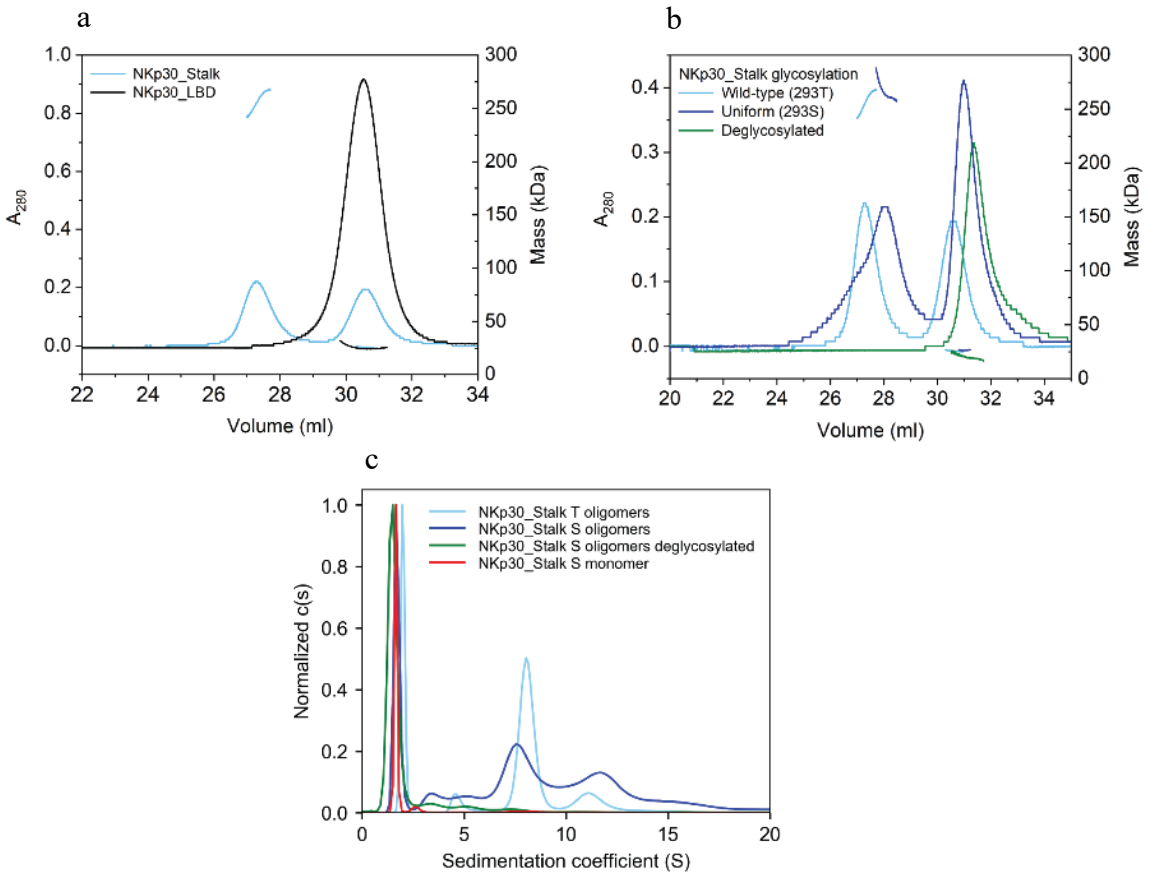

Figure 10: Glycosylation is necessary for NKp30 oligomerisation. (a) SEC-MALS analysis of NKp30_Stalk and NKp30_LBD, confirming that the stalk region is required for oligomerisation. (b) SEC-MALS analysis of recombinantly expressed NKp30_Stalk with wild-type glycosylation (black), uniform, simple glycans (blue), both showing non-covalent oligomers and deglycosylated sample, which does not form oligomers (red). (c) Normalised continuous size distributions of sedimenting species for glycosylated and deglycosylated NKp30_Stalk oligomers and their monomeric fractions. The main peak corresponds to the NKp30_Stalk monomer, whereas a broad distribution of oligomeric species is present in glycosylated NKp30_Stalk samples [185].

Measurements of NKp30 affinity towards B7-H6 performed by Hermann *et al.* [153] showed that the NKp30_Stalk construct has a very low K_D (on the nanomolar scale) when the affinity is measured by surface plasmon resonance (SPR) or enzyme-linked immunosorbent assay (ELISA). Since both methods are based on surface interaction, there may be an apparent increase in affinity by the avidity contribution of the oligomers [153]. Similarly, in our study, the NKp30_Stalk affinity for B7-H6 was higher (especially of the oligomeric fraction) than for NKp30_LBD, measured by SPR with B7-H6 immobilised on the sensor. To test the hypothesis that this is an avidity contribution, we used isothermal titration calorimetry (ITC), a method that can measure affinity in

solution. Using this approach, we found that NKp30_Stalk and NKp30_LBD show similar thermodynamic parameters and affinity for soluble B7-H6; however, the oligomers exhibit significantly lower binding stoichiometry, suggesting that not all the binding sites in the oligomer are available for interaction with B7-H6. This effect is also profound in AUC measurement, where sedimentation coefficient and calculated molecular weight of oligomeric form bound to B7-H6 do not correspond with the expected value.

The original goal of this project was to understand the formation of NKp30 oligomers. Considering the interim results, we expanded this goal to include understanding the role of glycosylation in oligomer formation and interaction with B7-H6. The proposed methods included structural mass spectrometry (crosslinking and hydrogen/deuterium exchange) or cryo-electron microscopy and protein crystallography; only the latter yielded results. We were able to crystallise the homogeneously glycosylated NKp30_LBD:B7-H6 complex and solve its structure. This structure, deposited under PDB code 6YJP, is in principle similar to the previously published structures of NKp30_LBD alone (PDB 3NOI [152]) and the complex with B7-H6 (PDB 3PV6, [149]); however, the previous structures entirely omit glycosylation because the used proteins were produced in bacteria. Despite many efforts and hundreds of crystallisation conditions deployed, we have so far failed to crystallise the NKp30_Stalk construct. Even so, our structure provides new insight into a possible mechanism of NKp30 oligomerisation and possible arrangement on the cell surface.

The NKp30_LBD dimer with bound B7-H6 is present in our structure. Especially noteworthy is the symmetric arrangement of the Asn42 glycosylation site near the C-terminal region of the opposite NKp30_LBD unit. Given that it is the presence of the C-terminal stalk domain that is necessary for NKp30 oligomerisation, this arrangement strengthens our hypothesis that glycosylation influences oligomer formation. For better visualisation, we overlaid the glycosylated NKp30_LBD dimer from our structure with the PDB 3NOI structure, where the same type of dimer is observed, but with a non-glycosylated protein (Figure 11, page 43). It is clear that Asn42, when non-glycosylated, interacts with adjacent side chains between the dimer units. However, such an arrangement is unlikely because of the occupancy of this glycosylation site by an oligosaccharide. In our structure, the position of the second NKp30_LBD unit is shifted

by 9 – 15 Å, bringing Asn42 closer to the C-terminus of the second unit, therefore to the position of the stalk region. It is also worth noting that the PISA score [202], which indicates the relevance of the interaction interface, is 1.0 for our structure, while it is 0.18 for the 3NOI structure.

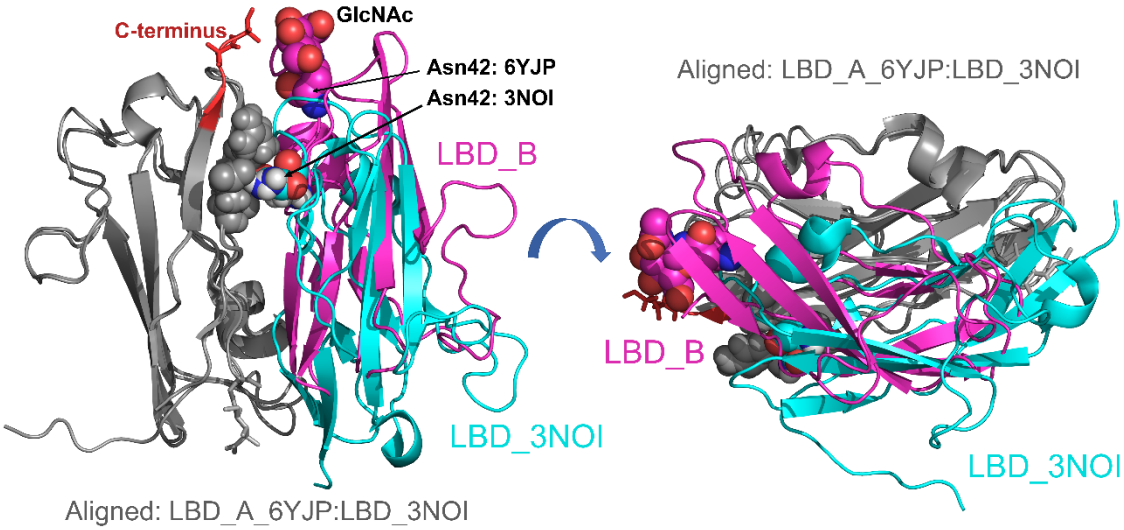

Figure 11: Glycosylation-induced NKp30 dimerisation positions the glycan at Asn42 residue near the C-terminal stalk region. The NKp30_LBD dimers observed in the present crystal structure PDB 6YJP and the PDB 3NOI [152] were aligned using molecules on one side of the dimer only (grey colour). On the left – *N*-glycosylation site at Asn42 of LBD_B, highlighted as spheres, is near the C-terminus of LBD_A (highlighted in red), whereas Asn42 residue in LBD_3NOI is buried within the dimer interface, interacting with Glu26 and Arg28 (all highlighted as spheres). On the right – side view of the dimer interface showing the difference in the arrangement of the two dimers [185].

It is also conceivable that the stalk domains emanating from the sides of the dimer could be given enough flexibility to interact with the stalk domain of the next NKp30 unit and thus enable organisation into higher-order structures. To get a better sense, we performed small-angle X-ray scattering coupled with size exclusion chromatography (SEC-SAXS) measurements for the monomeric and oligomeric fractions of NKp30 even in complex with B7-H6. Given the lack of additional data to model the arrangement of NKp30 units in the fitted SAXS envelopes, we can only conclude that the shape of these envelopes is elongated rather than spherical. In principle, this asymmetry is consistent with the predictions based on the crystal structure and with our sedimentation analysis of the oligomers suggesting asymmetric elongated or flattened particles.

Our structure of the complex is also interesting in the context of publications by Xu *et al*. [203, 204], who investigated the structure of the Fab of inhibitory antibody 17B1.3 in complex with the B7-H6 ectodomain. Although the antibody attaches to a site remote from the B7-H6 interaction interface with NKp30 and does not block this interaction, the experiments in the reporter line show inhibition of signalling through NKp30. Authors speculate that the inhibition may be due to steric hindrance not directly between the ligand-receptor pair but between the close contacts at the NK cell-target cell interface. Our structure then shows a possible arrangement of such a narrow contact, which could be amplified at the surface of interacting cells by oligomerisation of NKp30 (Figure 12).

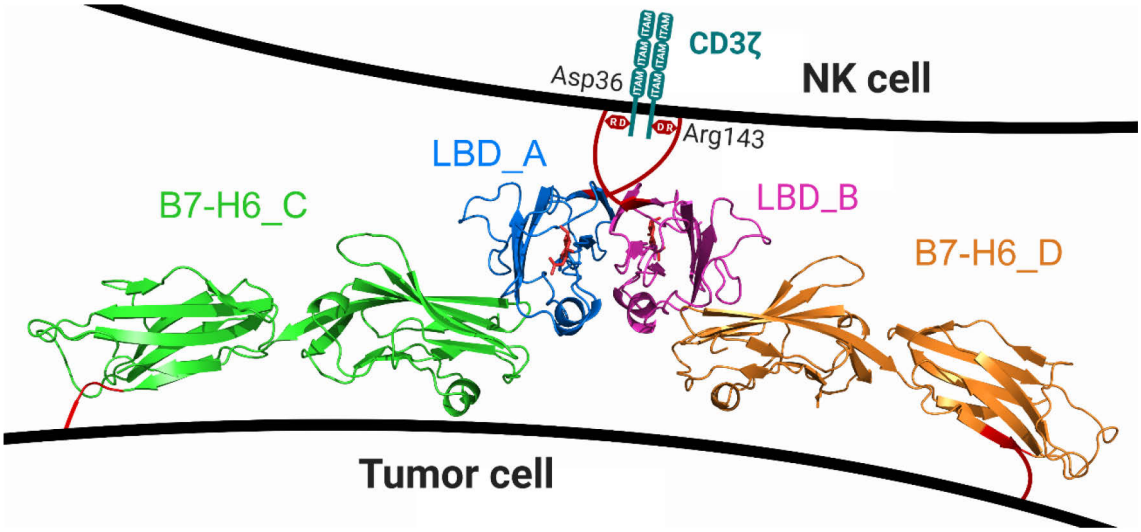

Figure 12: Model of the possible position of the NKp30_LBD:B7-H6 dimeric complex, as observed in the crystal structure (PDB 6YJP), within the NK cell immune synapse. B7-H6 has a very short stalk sequence of several amino acids only, whereas NKp30 has the 15-amino-acid-long stalk region at its C-terminus (red lines). The stalk is long enough to confer flexibility to the NKp30 ligand-binding domain. Such an arrangement would bring the membranes of both cells into very close contact, and such an effect could be further potentiated by NKp30 oligomerisation. Local deformation of the NK cell plasma membrane caused by the conformational change of the stalk region induced by ligand binding might trigger signal transduction through the CD3ζ chains associated with the NKp30 transmembrane domain thanks to the interaction of CD3ζ Asp36 residue with NKp30 Arg143 residue occurring at plasma membrane which is required for NKp30 signalling [67, 185].

Confirmation of the hypothetical arrangement of NKp30 upon interaction with B7-H6, as well as the oligomeric arrangement on the membrane of living cells, will be the subject of further investigation. Given the length of the stalk domain, we are aware that it is unlikely that significantly larger complexes are formed on the membrane, yet this effect could contribute to signalling in a similar way to the apparent increase of affinity using surface methods. Therefore, future immunotherapeutic strategies and agents designed to target or activate the NKp30:B7-H6 system should allow sufficient flexibility with respect to B7-H6 to ensure proper orientation and interaction with NKp30.

5. SUMMARY

- Suspension adapted HEK293T and HEK293S GnTI$^-$ cell lines were optimised to produce NKp30_Stalk, LBD, B7H6_C212S in various glycosylation forms.

- Receptor:ligand binding has been re-evaluated by ITC and SPR and compared to the results published in earlier research reports concerning affinity and avidity. The higher apparent affinity of oligomers measured with surface methods (SPR, ELISA) is caused by the avidity effect and is similar to monomeric protein when measured in the solution (ITC).

- The influence of glycosylation on the oligomeric state of NKp30 has been described. Glycosylation is an essential condition for NKp30 oligomerisation because its oligomers are disrupted upon enzymatic deglycosylation.

- SEC-MALS and AUC have been used to characterise the oligomeric state of NKp30_Stalk in solution. Possible stoichiometry of 8 or 16 units per oligomer has been proposed.

- An influence of B7-H6 binding to NKp30 oligomers has been observed, concluding that B7-H6 binding does not disrupt the oligomerisation of NKp30_Stalk.

- An influence of glycosylation of B7-H6 on its binding affinity with NKp30 has been measured by SPR. It was shown that B7-H6 glycosylation does not affect its binding properties towards NKp30.

- Homogeneously glycosylated NKp30_LBD in complex with enzymatically deglycosylated B7-H6 has been crystallised, and the structure has been solved at 3.1 Å resolution. A possible position on the cell surface and possible arrangement of NKp30 units in oligomers have been proposed.

6. REFERENCES

1. Greenberg, A.H. and J.H. Playfair, *Spontaneously arising cytotoxicity to the P-815-Y mastocytoma in NZB mice.* Clin Exp Immunol, 1974. **16**(1): p. 99-109.
2. Herberman, R.B., M.E. Nunn, and D.H. Lavrin, *Natural cytotoxic reactivity of mouse lymphoid cells against syngeneic acid allogeneic tumors. I. Distribution of reactivity and specificity.* Int J Cancer, 1975. **16**(2): p. 216-29.
3. Kiessling, R., E. Klein, and H. Wigzell, *"Natural" killer cells in the mouse. I. Cytotoxic cells with specificity for mouse Moloney leukemia cells. Specificity and distribution according to genotype.* Eur J Immunol, 1975. **5**(2): p. 112-7.
4. Herberman, R.B*., et al.*, *Natural cytotoxic reactivity of mouse lymphoid cells against syngeneic and allogeneic tumors. II. Characterization of effector cells.* Int J Cancer, 1975. **16**(2): p. 230-9.
5. Trinchieri, G., *Biology of natural killer cells.* Adv Immunol, 1989. **47**: p. 187-376.
6. Hammer, Q. and C. Romagnani, *About Training and Memory: NK-Cell Adaptation to Viral Infections.* Adv Immunol, 2017. **133**: p. 171-207.
7. Walk, J. and R.W. Sauerwein, *Activatory Receptor NKp30 Predicts NK Cell Activation During Controlled Human Malaria Infection.* Front Immunol, 2019. **10**: p. 2864.
8. Kondo, M., I.L. Weissman, and K. Akashi, *Identification of clonogenic common lymphoid progenitors in mouse bone marrow.* Cell, 1997. **91**(5): p. 661-72.
9. Blum, K.S. and R. Pabst, *Lymphocyte numbers and subsets in the human blood. Do they mirror the situation in all organs?* Immunol Lett, 2007. **108**(1): p. 45-51.
10. Moretta, L., *Dissecting CD56dim human NK cells.* Blood, 2010. **116**(19): p. 3689-91.
11. Romagnani, C*., et al.*, *CD56brightCD16- killer Ig-like receptor- NK cells display longer telomeres and acquire features of CD56dim NK cells upon activation.* J Immunol, 2007. **178**(8): p. 4947-55.
12. Bjorkstrom, N.K*., et al.*, *Expression patterns of NKG2A, KIR, and CD57 define a process of CD56dim NK-cell differentiation uncoupled from NK-cell education.* Blood, 2010. **116**(19): p. 3853-64.
13. Hendricks, D.W*., et al.*, *Cutting edge: NKG2C(hi)CD57+ NK cells respond specifically to acute infection with cytomegalovirus and not Epstein-Barr virus.* J Immunol, 2014. **192**(10): p. 4492-6.
14. Della Chiesa, M*., et al.*, *Phenotypic and functional heterogeneity of human NK cells developing after umbilical cord blood transplantation: a role for human cytomegalovirus?* Blood, 2012. **119**(2): p. 399-410.
15. Muccio, L*., et al.*, *Late Development of FcepsilonRgamma(neg) Adaptive Natural Killer Cells Upon Human Cytomegalovirus Reactivation in Umbilical Cord Blood Transplantation Recipients.* Front Immunol, 2018. **9**: p. 1050.
16. Pende, D*., et al.*, *Killer Ig-Like Receptors (KIRs): Their Role in NK Cell Modulation and Developments Leading to Their Clinical Exploitation.* Front Immunol, 2019. **10**: p. 1179.
17. Walzer, T*., et al.*, *Identification, activation, and selective in vivo ablation of mouse NK cells via NKp46.* Proc Natl Acad Sci U S A, 2007. **104**(9): p. 3384-9.

18. Walzer, T.*, et al.*, *Natural killer cells: from CD3(-)NKp46(+) to post-genomics meta-analyses.* Curr Opin Immunol, 2007. **19**(3): p. 365-72.
19. Sivori, S.*, et al.*, *p46, a novel natural killer cell-specific surface molecule that mediates cell activation.* J Exp Med, 1997. **186**(7): p. 1129-36.
20. Moretta, L.*, et al.*, *Human natural killer cells: their origin, receptors and function.* Eur J Immunol, 2002. **32**(5): p. 1205-11.
21. Vivier, E.*, et al.*, *Innate Lymphoid Cells: 10 Years On.* Cell, 2018. **174**(5): p. 1054-1066.
22. Seillet, C., G.T. Belz, and N.D. Huntington, *Development, Homeostasis, and Heterogeneity of NK Cells and ILC1.* Curr Top Microbiol Immunol, 2016. **395**: p. 37-61.
23. Poznanski, S.M. and A.A. Ashkar, *What Defines NK Cell Functional Fate: Phenotype or Metabolism?* Front Immunol, 2019. **10**: p. 1414.
24. Ljunggren, H.G. and K. Karre, *In search of the 'missing self': MHC molecules and NK cell recognition.* Immunol Today, 1990. **11**(7): p. 237-44.
25. Karre, K.*, et al.*, *Selective rejection of H-2-deficient lymphoma variants suggests alternative immune defence strategy.* Nature, 1986. **319**(6055): p. 675-8.
26. Dimasi, N. and R. Biassoni, *Structural and functional aspects of the Ly49 natural killer cell receptors.* Immunol Cell Biol, 2005. **83**(1): p. 1-8.
27. Yokoyama, W.M. and W.E. Seaman, *The Ly-49 and NKR-P1 gene families encoding lectin-like receptors on natural killer cells: the NK gene complex.* Annu Rev Immunol, 1993. **11**: p. 613-35.
28. Andre, P.*, et al.*, *New nomenclature for MHC receptors.* Nat Immunol, 2001. **2**(8): p. 661.
29. Moretta, A.*, et al.*, *Receptors for HLA class-I molecules in human natural killer cells.* Annu Rev Immunol, 1996. **14**: p. 619-48.
30. Davidson, C.L., N.L. Li, and D.N. Burshtyn, *LILRB1 polymorphism and surface phenotypes of natural killer cells.* Hum Immunol, 2010. **71**(10): p. 942-9.
31. Borrego, F.*, et al.*, *Recognition of human histocompatibility leukocyte antigen (HLA)-E complexed with HLA class I signal sequence-derived peptides by CD94/NKG2 confers protection from natural killer cell-mediated lysis.* J Exp Med, 1998. **187**(5): p. 813-8.
32. Vance, R.E.*, et al.*, *Mouse CD94/NKG2A is a natural killer cell receptor for the nonclassical major histocompatibility complex (MHC) class I molecule Qa-1(b).* J Exp Med, 1998. **188**(10): p. 1841-8.
33. Raulet, D.H.*, et al.*, *Specificity, tolerance and developmental regulation of natural killer cells defined by expression of class I-specific Ly49 receptors.* Immunol Rev, 1997. **155**: p. 41-52.
34. Valiante, N.M.*, et al.*, *Functionally and structurally distinct NK cell receptor repertoires in the peripheral blood of two human donors.* Immunity, 1997. **7**(6): p. 739-51.
35. Kubota, A.*, et al.*, *Diversity of NK cell receptor repertoire in adult and neonatal mice.* J Immunol, 1999. **163**(1): p. 212-6.
36. Raulet, D.H., R.E. Vance, and C.W. McMahon, *Regulation of the natural killer cell receptor repertoire.* Annu Rev Immunol, 2001. **19**: p. 291-330.
37. Lanier, L.L., *NK cell recognition.* Annu Rev Immunol, 2005. **23**: p. 225-74.
38. Raulet, D.H. and R.E. Vance, *Self-tolerance of natural killer cells.* Nat Rev Immunol, 2006. **6**(7): p. 520-31.

39. Bossi, G. and G.M. Griffiths, *Degranulation plays an essential part in regulating cell surface expression of Fas ligand in T cells and natural killer cells.* Nat Med, 1999. **5**(1): p. 90-6.
40. de Saint Basile, G., G. Menasche, and A. Fischer, *Molecular mechanisms of biogenesis and exocytosis of cytotoxic granules.* Nat Rev Immunol, 2010. **10**(8): p. 568-79.
41. Voskoboinik, I., J.C. Whisstock, and J.A. Trapani, *Perforin and granzymes: function, dysfunction and human pathology.* Nat Rev Immunol, 2015. **15**(6): p. 388-400.
42. Leibson, P.J., *Signal transduction during natural killer cell activation: inside the mind of a killer.* Immunity, 1997. **6**(6): p. 655-61.
43. Vivier, E.*, et al.*, *Functions of natural killer cells.* Nat Immunol, 2008. **9**(5): p. 503-10.
44. Orange, J.S., *Natural killer cell deficiency.* J Allergy Clin Immunol, 2013. **132**(3): p. 515-525.
45. Hayakawa, Y.*, et al.*, *NK cell TRAIL eliminates immature dendritic cells in vivo and limits dendritic cell vaccination efficacy.* J Immunol, 2004. **172**(1): p. 123-9.
46. Walzer, T.*, et al.*, *Natural-killer cells and dendritic cells: "l'union fait la force".* Blood, 2005. **106**(7): p. 2252-8.
47. Moretta, L.*, et al.*, *Effector and regulatory events during natural killer-dendritic cell interactions.* Immunol Rev, 2006. **214**: p. 219-28.
48. Degli-Esposti, M.A. and M.J. Smyth, *Close encounters of different kinds: dendritic cells and NK cells take centre stage.* Nat Rev Immunol, 2005. **5**(2): p. 112-24.
49. Cooper, M.A.*, et al.*, *Cytokine-induced memory-like natural killer cells.* Proc Natl Acad Sci U S A, 2009. **106**(6): p. 1915-9.
50. Beaulieu, A.M. and J.C. Sun, *Tracking Effector and Memory NK Cells During MCMV Infection.* Methods Mol Biol, 2016. **1441**: p. 1-12.
51. Vivier, E.*, et al.*, *Innate or adaptive immunity? The example of natural killer cells.* Science, 2011. **331**(6013): p. 44-9.
52. Apte, R.S.*, et al.*, *Cutting edge: role of macrophage migration inhibitory factor in inhibiting NK cell activity and preserving immune privilege.* J Immunol, 1998. **160**(12): p. 5693-6.
53. Regis, S.*, et al.*, *NK Cell Function Regulation by TGF-beta-Induced Epigenetic Mechanisms.* Front Immunol, 2020. **11**: p. 311.
54. Vitale, M.*, et al.*, *Effect of tumor cells and tumor microenvironment on NK-cell function.* Eur J Immunol, 2014. **44**(6): p. 1582-92.
55. Chen, Y.*, et al.*, *The B7 Family Member B7-H6: a New Bane of Tumor.* Pathol Oncol Res, 2018. **24**(4): p. 717-721.
56. Pesce, S.*, et al.*, *Identification of a subset of human natural killer cells expressing high levels of programmed death 1: A phenotypic and functional characterization.* J Allergy Clin Immunol, 2017. **139**(1): p. 335-346 e3.
57. Vacca, P.*, et al.*, *Human natural killer cells and other innate lymphoid cells in cancer: Friends or foes?* Immunol Lett, 2018. **201**: p. 14-19.
58. Kaiser, B.K.*, et al.*, *Disulphide-isomerase-enabled shedding of tumour-associated NKG2D ligands.* Nature, 2007. **447**(7143): p. 482-6.

59. Schlecker, E.*, et al.*, *Metalloprotease-mediated tumor cell shedding of B7-H6, the ligand of the natural killer cell-activating receptor NKp30.* Cancer Res, 2014. **74**(13): p. 3429-40.
60. Ponath, V.*, et al.*, *Secreted Ligands of the NK Cell Receptor NKp30: B7-H6 Is in Contrast to BAG6 Only Marginally Released via Extracellular Vesicles.* Int J Mol Sci, 2021. **22**(4).
61. Giebeler, N. and P. Zigrino, *A Disintegrin and Metalloprotease (ADAM): Historical Overview of Their Functions.* Toxins (Basel), 2016. **8**(4): p. 122.
62. Ferrari de Andrade, L.*, et al.*, *Inhibition of MICA and MICB Shedding Elicits NK-Cell-Mediated Immunity against Tumors Resistant to Cytotoxic T Cells.* Cancer Immunol Res, 2020. **8**(6): p. 769-780.
63. Ben-Shmuel, A., G. Biber, and M. Barda-Saad, *Unleashing Natural Killer Cells in the Tumor Microenvironment-The Next Generation of Immunotherapy?* Front Immunol, 2020. **11**: p. 275.
64. Vesely, M.D.*, et al.*, *Natural innate and adaptive immunity to cancer.* Annu Rev Immunol, 2011. **29**: p. 235-71.
65. Guillerey, C. and M.J. Smyth, *NK Cells and Cancer Immunoediting.* Curr Top Microbiol Immunol, 2016. **395**: p. 115-45.
66. Lanier, L.L., *NK cell receptors.* Annu Rev Immunol, 1998. **16**: p. 359-93.
67. Memmer, S.*, et al.*, *The Stalk Domain of NKp30 Contributes to Ligand Binding and Signaling of a Preassembled NKp30-CD3zeta Complex.* J Biol Chem, 2016. **291**(49): p. 25427-25438.
68. Billadeau, D.D. and P.J. Leibson, *ITAMs versus ITIMs: striking a balance during cell regulation.* J Clin Invest, 2002. **109**(2): p. 161-8.
69. Linnartz-Gerlach, B., M. Mathews, and H. Neumann, *Sensing the neuronal glycocalyx by glial sialic acid binding immunoglobulin-like lectins.* Neuroscience, 2014. **275**: p. 113-24.
70. Pinheiro, P.F., G.C. Justino, and M.M. Marques, *NKp30 - A prospective target for new cancer immunotherapy strategies.* Br J Pharmacol, 2020. **177**(20): p. 4563-4580.
71. Koch, J.*, et al.*, *Activating natural cytotoxicity receptors of natural killer cells in cancer and infection.* Trends Immunol, 2013. **34**(4): p. 182-91.
72. Linnartz, B., Y. Wang, and H. Neumann, *Microglial immunoreceptor tyrosine-based activation and inhibition motif signaling in neuroinflammation.* Int J Alzheimers Dis, 2010. **2010**.
73. Linnartz-Gerlach, B., J. Kopatz, and H. Neumann, *Siglec functions of microglia.* Glycobiology, 2014. **24**(9): p. 794-9.
74. Paul, S. and G. Lal, *The Molecular Mechanism of Natural Killer Cells Function and Its Importance in Cancer Immunotherapy.* Front Immunol, 2017. **8**: p. 1124.
75. Watzl, C. and E.O. Long, *Signal transduction during activation and inhibition of natural killer cells.* Curr Protoc Immunol, 2010. **Chapter 11**: p. Unit 11 9B.
76. Bruijnesteijn, J.*, et al.*, *Extensive Alternative Splicing of KIR Transcripts.* Front Immunol, 2018. **9**: p. 2846.
77. Iizuka, K.*, et al.*, *Genetically linked C-type lectin-related ligands for the NKRP1 family of natural killer cell receptors.* Nat Immunol, 2003. **4**(8): p. 801-7.
78. Bartel, Y., B. Bauer, and A. Steinle, *Modulation of NK cell function by genetically coupled C-type lectin-like receptor/ligand pairs encoded in the human natural killer gene complex.* Front Immunol, 2013. **4**: p. 362.

79. D'Andrea, A. and L.L. Lanier, *Killer cell inhibitory receptor expression by T cells.* Curr Top Microbiol Immunol, 1998. **230**: p. 25-39.
80. Raulet, D.H., *Roles of the NKG2D immunoreceptor and its ligands.* Nat Rev Immunol, 2003. **3**(10): p. 781-90.
81. Vanek, O.*, et al.*, *Production of recombinant soluble dimeric C-type lectin-like receptors of rat natural killer cells.* Sci Rep, 2019. **9**(1): p. 17836.
82. Chambers, W.H.*, et al.*, *Monoclonal antibody to a triggering structure expressed on rat natural killer cells and adherent lymphokine-activated killer cells.* J Exp Med, 1989. **169**(4): p. 1373-89.
83. Mesci, A.*, et al.*, *NKR-P1 biology: from prototype to missing self.* Immunol Res, 2006. **35**(1-2): p. 13-26.
84. Hao, L., J. Klein, and M. Nei, *Heterogeneous but conserved natural killer receptor gene complexes in four major orders of mammals.* Proc Natl Acad Sci U S A, 2006. **103**(9): p. 3192-7.
85. Mizuno, H.*, et al.*, *Structure of coagulation factors IX/X-binding protein, a heterodimer of C-type lectin domains.* Nat Struct Biol, 1997. **4**(6): p. 438-41.
86. Feinberg, H.*, et al.*, *Structure of a C-type carbohydrate recognition domain from the macrophage mannose receptor.* J Biol Chem, 2000. **275**(28): p. 21539-48.
87. Hirotsu, S.*, et al.*, *Crystal structure of bitiscetin, a von Willebrand factor-dependent platelet aggregation inducer.* Biochemistry, 2001. **40**(45): p. 13592-7.
88. Mizuno, H.*, et al.*, *Crystal structure of an anticoagulant protein in complex with the Gla domain of factor X.* Proc Natl Acad Sci U S A, 2001. **98**(13): p. 7230-4.
89. Liu, Y. and D. Eisenberg, *3D domain swapping: as domains continue to swap.* Protein Sci, 2002. **11**(6): p. 1285-99.
90. Chaturvedi, N.*, et al.*, *The effect of beta-glucan and its potential analog on the structure of Dectin-1 receptor.* J Mol Graph Model, 2017. **74**: p. 315-325.
91. Zelensky, A.N. and J.E. Gready, *The C-type lectin-like domain superfamily.* FEBS J, 2005. **272**(24): p. 6179-217.
92. Rahim, M.M. and A.P. Makrigiannis, *Ly49 receptors: evolution, genetic diversity, and impact on immunity.* Immunol Rev, 2015. **267**(1): p. 137-47.
93. Lanier, L.L., C. Chang, and J.H. Phillips, *Human NKR-P1A. A disulfide-linked homodimer of the C-type lectin superfamily expressed by a subset of NK and T lymphocytes.* J Immunol, 1994. **153**(6): p. 2417-28.
94. Spreu, J.*, et al.*, *Interaction of C-type lectin-like receptors NKp65 and KACL facilitates dedicated immune recognition of human keratinocytes.* Proc Natl Acad Sci U S A, 2010. **107**(11): p. 5100-5.
95. Welte, S.*, et al.*, *Mutual activation of natural killer cells and monocytes mediated by NKp80-AICL interaction.* Nat Immunol, 2006. **7**(12): p. 1334-42.
96. Vogler, I. and A. Steinle, *Vis-a-vis in the NKC: genetically linked natural killer cell receptor/ligand pairs in the natural killer gene complex (NKC).* J Innate Immun, 2011. **3**(3): p. 227-35.
97. Exley, M.*, et al.*, *CD161 (NKR-P1A) costimulation of CD1d-dependent activation of human T cells expressing invariant V alpha 24 J alpha Q T cell receptor alpha chains.* J Exp Med, 1998. **188**(5): p. 867-76.
98. Fergusson, J.R.*, et al.*, *CD161 defines a transcriptional and functional phenotype across distinct human T cell lineages.* Cell Rep, 2014. **9**(3): p. 1075-88.

99. Afzali, B.*, et al.*, *CD161 expression characterizes a subpopulation of human regulatory T cells that produces IL-17 in a STAT3-dependent manner.* Eur J Immunol, 2013. **43**(8): p. 2043-54.
100. Billerbeck, E.*, et al.*, *Analysis of CD161 expression on human CD8+ T cells defines a distinct functional subset with tissue-homing properties.* Proc Natl Acad Sci U S A, 2010. **107**(7): p. 3006-11.
101. Brucklacher-Waldert, V.*, et al.*, *Phenotypical and functional characterization of T helper 17 cells in multiple sclerosis.* Brain, 2009. **132**(Pt 12): p. 3329-41.
102. Estrada-Capetillo, L.*, et al.*, *Induction of Th17 lymphocytes and Treg cells by monocyte-derived dendritic cells in patients with rheumatoid arthritis and systemic lupus erythematosus.* Clin Dev Immunol, 2013. **2013**: p. 584303.
103. Smith, J.A. and R.A. Colbert, *Review: The interleukin-23/interleukin-17 axis in spondyloarthritis pathogenesis: Th17 and beyond.* Arthritis Rheumatol, 2014. **66**(2): p. 231-41.
104. Cosmi, L.*, et al.*, *Human interleukin 17-producing cells originate from a CD161+CD4+ T cell precursor.* J Exp Med, 2008. **205**(8): p. 1903-16.
105. Poggi, A.*, et al.*, *Phenotypic and functional analysis of CD4+ NKRP1A+ human T lymphocytes. Direct evidence that the NKRP1A molecule is involved in transendothelial migration.* Eur J Immunol, 1997. **27**(9): p. 2345-50.
106. Poggi, A.*, et al.*, *NKRP1A molecule is involved in transendothelial migration of CD4+ human T lymphocytes.* Immunol Lett, 1997. **57**(1-3): p. 121-3.
107. Annibali, V.*, et al.*, *CD161(high)CD8+T cells bear pathogenetic potential in multiple sclerosis.* Brain, 2011. **134**(Pt 2): p. 542-54.
108. Chalan, P.*, et al.*, *Expression of Lectin-Like Transcript 1, the Ligand for CD161, in Rheumatoid Arthritis.* PLoS One, 2015. **10**(7): p. e0132436.
109. Aldemir, H.*, et al.*, *Cutting edge: lectin-like transcript 1 is a ligand for the CD161 receptor.* J Immunol, 2005. **175**(12): p. 7791-5.
110. Rosen, D.B.*, et al.*, *Cutting edge: lectin-like transcript-1 is a ligand for the inhibitory human NKR-P1A receptor.* J Immunol, 2005. **175**(12): p. 7796-9.
111. Germain, C.*, et al.*, *Induction of lectin-like transcript 1 (LLT1) protein cell surface expression by pathogens and interferon-gamma contributes to modulate immune responses.* J Biol Chem, 2011. **286**(44): p. 37964-75.
112. Roth, P.*, et al.*, *Malignant glioma cells counteract antitumor immune responses through expression of lectin-like transcript-1.* Cancer Res, 2007. **67**(8): p. 3540-4.
113. Germain, C.*, et al.*, *Lectin-like transcript 1 is a marker of germinal center-derived B-cell non-Hodgkin's lymphomas dampening natural killer cell functions.* Oncoimmunology, 2015. **4**(8): p. e1026503.
114. Skalova, T.*, et al.*, *Four crystal structures of human LLT1, a ligand of human NKR-P1, in varied glycosylation and oligomerization states.* Acta Crystallogr D Biol Crystallogr, 2015. **71**(Pt 3): p. 578-91.
115. Blaha, J.*, et al.*, *Expression and purification of soluble and stable ectodomain of natural killer cell receptor LLT1 through high-density transfection of suspension adapted HEK293S GnTI(-) cells.* Protein Expr Purif, 2015. **109**: p. 7-13.
116. Blaha, J.*, et al.*, *High-level expression and purification of soluble form of human natural killer cell receptor NKR-P1 in HEK293S GnTI(-) cells.* Protein Expr Purif, 2017. **140**: p. 36-43.

117. Bork, P., L. Holm, and C. Sander, *The immunoglobulin fold. Structural classification, sequence patterns and common core.* J Mol Biol, 1994. **242**(4): p. 309-20.
118. Pegram, H.J.*, et al.*, *Activating and inhibitory receptors of natural killer cells.* Immunol Cell Biol, 2011. **89**(2): p. 216-24.
119. Chapman, T.L., A.P. Heikeman, and P.J. Bjorkman, *The inhibitory receptor LIR-1 uses a common binding interaction to recognize class I MHC molecules and the viral homolog UL18.* Immunity, 1999. **11**(5): p. 603-13.
120. Pessino, A.*, et al.*, *Molecular cloning of NKp46: a novel member of the immunoglobulin superfamily involved in triggering of natural cytotoxicity.* J Exp Med, 1998. **188**(5): p. 953-60.
121. Sivori, S.*, et al.*, *NKp46 is the major triggering receptor involved in the natural cytotoxicity of fresh or cultured human NK cells. Correlation between surface density of NKp46 and natural cytotoxicity against autologous, allogeneic or xenogeneic target cells.* Eur J Immunol, 1999. **29**(5): p. 1656-66.
122. Vitale, M.*, et al.*, *NKp44, a novel triggering surface molecule specifically expressed by activated natural killer cells, is involved in non-major histocompatibility complex-restricted tumor cell lysis.* J Exp Med, 1998. **187**(12): p. 2065-72.
123. Pende, D.*, et al.*, *Identification and molecular characterization of NKp30, a novel triggering receptor involved in natural cytotoxicity mediated by human natural killer cells.* J Exp Med, 1999. **190**(10): p. 1505-16.
124. Sivori, S.*, et al.*, *Human NK cells: surface receptors, inhibitory checkpoints, and translational applications.* Cell Mol Immunol, 2019. **16**(5): p. 430-441.
125. Arnon, T.I., G. Markel, and O. Mandelboim, *Tumor and viral recognition by natural killer cells receptors.* Semin Cancer Biol, 2006. **16**(5): p. 348-58.
126. Arnon, T.I.*, et al.*, *Inhibition of the NKp30 activating receptor by pp65 of human cytomegalovirus.* Nat Immunol, 2005. **6**(5): p. 515-23.
127. Pogge von Strandmann, E.*, et al.*, *Human leukocyte antigen-B-associated transcript 3 is released from tumor cells and engages the NKp30 receptor on natural killer cells.* Immunity, 2007. **27**(6): p. 965-74.
128. Reiners, K.S.*, et al.*, *Soluble ligands for NK cell receptors promote evasion of chronic lymphocytic leukemia cells from NK cell anti-tumor activity.* Blood, 2013. **121**(18): p. 3658-65.
129. Baychelier, F.*, et al.*, *Identification of a cellular ligand for the natural cytotoxicity receptor NKp44.* Blood, 2013. **122**(17): p. 2935-42.
130. Rosental, B.*, et al.*, *Proliferating cell nuclear antigen is a novel inhibitory ligand for the natural cytotoxicity receptor NKp44.* J Immunol, 2011. **187**(11): p. 5693-702.
131. Narni-Mancinelli, E.*, et al.*, *Complement factor P is a ligand for the natural killer cell-activating receptor NKp46.* Sci Immunol, 2017. **2**(10).
132. Gaggero, S.*, et al.*, *Nidogen-1 is a novel extracellular ligand for the NKp44 activating receptor.* Oncoimmunology, 2018. **7**(9): p. e1470730.
133. De Maria, A.*, et al.*, *Identification, molecular cloning and functional characterization of NKp46 and NKp30 natural cytotoxicity receptors in Macaca fascicularis NK cells.* Eur J Immunol, 2001. **31**(12): p. 3546-56.

134. Rutjens, E.*, et al.*, *Differential NKp30 inducibility in chimpanzee NK cells and conserved NK cell phenotype and function in long-term HIV-1-infected animals.* J Immunol, 2007. **178**(3): p. 1702-12.
135. Backman-Petersson, E.*, et al.*, *Molecular characterization of the novel rat NK receptor 1C7.* Eur J Immunol, 2003. **33**(2): p. 342-51.
136. Hsieh, C.L.*, et al.*, *NKp30 is a functional activation receptor on a subset of rat natural killer cells.* Eur J Immunol, 2006. **36**(8): p. 2170-80.
137. Hsieh, C.L.*, et al.*, *Identification, cloning, and characterization of a novel rat natural killer receptor, RNKP30: a molecule expressed in liver allografts.* Transplantation, 2004. **77**(1): p. 121-8.
138. Hollyoake, M., R.D. Campbell, and B. Aguado, *NKp30 (NCR3) is a pseudogene in 12 inbred and wild mouse strains, but an expressed gene in Mus caroli.* Mol Biol Evol, 2005. **22**(8): p. 1661-72.
139. Cantoni, C.*, et al.*, *NKp44, a triggering receptor involved in tumor cell lysis by activated human natural killer cells, is a novel member of the immunoglobulin superfamily.* J Exp Med, 1999. **189**(5): p. 787-96.
140. Hartmann, J.*, et al.*, *The stalk domain and the glycosylation status of the activating natural killer cell receptor NKp30 are important for ligand binding.* J Biol Chem, 2012. **287**(37): p. 31527-39.
141. Delahaye, N.F.*, et al.*, *Alternatively spliced NKp30 isoforms affect the prognosis of gastrointestinal stromal tumors.* Nat Med, 2011. **17**(6): p. 700-7.
142. Kaifu, T.*, et al.*, *B7-H6/NKp30 interaction: a mechanism of alerting NK cells against tumors.* Cell Mol Life Sci, 2011. **68**(21): p. 3531-9.
143. Kruse, P.H.*, et al.*, *Natural cytotoxicity receptors and their ligands.* Immunol Cell Biol, 2014. **92**(3): p. 221-9.
144. Hershkovitz, O.*, et al.*, *Altered glycosylation of recombinant NKp30 hampers binding to heparan sulfate: a lesson for the use of recombinant immunoreceptors as an immunological tool.* Glycobiology, 2008. **18**(1): p. 28-41.
145. Chisholm, S.E. and H.T. Reyburn, *Recognition of vaccinia virus-infected cells by human natural killer cells depends on natural cytotoxicity receptors.* J Virol, 2006. **80**(5): p. 2225-33.
146. Brandt, C.S.*, et al.*, *The B7 family member B7-H6 is a tumor cell ligand for the activating natural killer cell receptor NKp30 in humans.* J Exp Med, 2009. **206**(7): p. 1495-503.
147. Binici, J. and J. Koch, *BAG-6, a jack of all trades in health and disease.* Cell Mol Life Sci, 2014. **71**(10): p. 1829-37.
148. Wang, W.*, et al.*, *Tumor-released Galectin-3, a soluble inhibitory ligand of human NKp30, plays an important role in tumor escape from NK cell attack.* J Biol Chem, 2014. **289**(48): p. 33311-9.
149. Li, Y., Q. Wang, and R.A. Mariuzza, *Structure of the human activating natural cytotoxicity receptor NKp30 bound to its tumor cell ligand B7-H6.* J Exp Med, 2011. **208**(4): p. 703-14.
150. Yang, S.*, et al.*, *B7-H6 Promotes Cell Proliferation, Migration and Invasion of Non-Hodgkin Lymphoma via Ras/MEK/ERK Pathway Based on Quantitative Phosphoproteomics Data.* Onco Targets Ther, 2020. **13**: p. 5795-5805.

151. Matta, J.*, et al.*, *Induction of B7-H6, a ligand for the natural killer cell-activating receptor NKp30, in inflammatory conditions.* Blood, 2013. **122**(3): p. 394-404.
152. Joyce, M.G.*, et al.*, *Crystal structure of human natural cytotoxicity receptor NKp30 and identification of its ligand binding site.* Proc Natl Acad Sci U S A, 2011. **108**(15): p. 6223-8.
153. Herrmann, J.*, et al.*, *Homo-oligomerization of the activating natural killer cell receptor NKp30 ectodomain increases its binding affinity for cellular ligands.* J Biol Chem, 2014. **289**(2): p. 765-77.
154. An, H.J., J.W. Froehlich, and C.B. Lebrilla, *Determination of glycosylation sites and site-specific heterogeneity in glycoproteins.* Curr Opin Chem Biol, 2009. **13**(4): p. 421-6.
155. Helenius, A. and M. Aebi, *Intracellular functions of N-linked glycans.* Science, 2001. **291**(5512): p. 2364-9.
156. Aebi, M., *N-linked protein glycosylation in the ER.* Biochim Biophys Acta, 2013. **1833**(11): p. 2430-7.
157. Ruiz-Canada, C., D.J. Kelleher, and R. Gilmore, *Cotranslational and posttranslational N-glycosylation of polypeptides by distinct mammalian OST isoforms.* Cell, 2009. **136**(2): p. 272-83.
158. Shrimal, S., N.A. Cherepanova, and R. Gilmore, *Cotranslational and posttranslocational N-glycosylation of proteins in the endoplasmic reticulum.* Semin Cell Dev Biol, 2015. **41**: p. 71-8.
159. Olzmann, J.A., R.R. Kopito, and J.C. Christianson, *The mammalian endoplasmic reticulum-associated degradation system.* Cold Spring Harb Perspect Biol, 2013. **5**(9).
160. Ruggiano, A., O. Foresti, and P. Carvalho, *Quality control: ER-associated degradation: protein quality control and beyond.* J Cell Biol, 2014. **204**(6): p. 869-79.
161. Breitling, J. and M. Aebi, *N-linked protein glycosylation in the endoplasmic reticulum.* Cold Spring Harb Perspect Biol, 2013. **5**(8): p. a013359.
162. Sun, R., A.M.J. Kim, and S.O. Lim, *Glycosylation of Immune Receptors in Cancer.* Cells, 2021. **10**(5).
163. Pinho, S.S. and C.A. Reis, *Glycosylation in cancer: mechanisms and clinical implications.* Nat Rev Cancer, 2015. **15**(9): p. 540-55.
164. Marth, J.D. and P.K. Grewal, *Mammalian glycosylation in immunity.* Nat Rev Immunol, 2008. **8**(11): p. 874-87.
165. Rodrigues, J.G.*, et al.*, *Glycosylation in cancer: Selected roles in tumour progression, immune modulation and metastasis.* Cell Immunol, 2018. **333**: p. 46-57.
166. Reis, C.A.*, et al.*, *Alterations in glycosylation as biomarkers for cancer detection.* J Clin Pathol, 2010. **63**(4): p. 322-9.
167. Dube, D.H. and C.R. Bertozzi, *Glycans in cancer and inflammation--potential for therapeutics and diagnostics.* Nat Rev Drug Discov, 2005. **4**(6): p. 477-88.
168. Freeze, H.H. and M. Aebi, *Altered glycan structures: the molecular basis of congenital disorders of glycosylation.* Curr Opin Struct Biol, 2005. **15**(5): p. 490-8.
169. Oliveira-Ferrer, L., K. Legler, and K. Milde-Langosch, *Role of protein glycosylation in cancer metastasis.* Semin Cancer Biol, 2017. **44**: p. 141-152.

170. Carvalho, S., C.A. Reis, and S.S. Pinho, *Cadherins Glycans in Cancer: Sweet Players in a Bitter Process.* Trends Cancer, 2016. **2**(9): p. 519-531.
171. Pinho, S.S.*, et al.*, *Modulation of E-cadherin function and dysfunction by N-glycosylation.* Cell Mol Life Sci, 2011. **68**(6): p. 1011-20.
172. Yoshimura, M.*, et al.*, *Aberrant glycosylation of E-cadherin enhances cell-cell binding to suppress metastasis.* J Biol Chem, 1996. **271**(23): p. 13811-5.
173. Lau, K.S.*, et al.*, *Complex N-glycan number and degree of branching cooperate to regulate cell proliferation and differentiation.* Cell, 2007. **129**(1): p. 123-34.
174. Contessa, J.N.*, et al.*, *Inhibition of N-linked glycosylation disrupts receptor tyrosine kinase signaling in tumor cells.* Cancer Res, 2008. **68**(10): p. 3803-9.
175. Mereiter, S.*, et al.*, *Glycomic analysis of gastric carcinoma cells discloses glycans as modulators of RON receptor tyrosine kinase activation in cancer.* Biochim Biophys Acta, 2016. **1860**(8): p. 1795-808.
176. Fuster, M.M. and J.D. Esko, *The sweet and sour of cancer: glycans as novel therapeutic targets.* Nat Rev Cancer, 2005. **5**(7): p. 526-42.
177. Zarbock, A.*, et al.*, *Leukocyte ligands for endothelial selectins: specialized glycoconjugates that mediate rolling and signaling under flow.* Blood, 2011. **118**(26): p. 6743-51.
178. Johannssen, T. and B. Lepenies, *Glycan-Based Cell Targeting To Modulate Immune Responses.* Trends Biotechnol, 2017. **35**(4): p. 334-346.
179. Chou, F.C.*, et al.*, *Role of Galectins in Tumors and in Clinical Immunotherapy.* Int J Mol Sci, 2018. **19**(2).
180. Taniguchi, N. and Y. Kizuka, *Glycans and cancer: role of N-glycans in cancer biomarker, progression and metastasis, and therapeutics.* Adv Cancer Res, 2015. **126**: p. 11-51.
181. Demetriou, M.*, et al.*, *Negative regulation of T-cell activation and autoimmunity by Mgat5 N-glycosylation.* Nature, 2001. **409**(6821): p. 733-9.
182. Dias, A.M.*, et al.*, *Dysregulation of T cell receptor N-glycosylation: a molecular mechanism involved in ulcerative colitis.* Hum Mol Genet, 2014. **23**(9): p. 2416-27.
183. Ma, B.Y.*, et al.*, *CD28 T cell costimulatory receptor function is negatively regulated by N-linked carbohydrates.* Biochem Biophys Res Commun, 2004. **317**(1): p. 60-7.
184. Agresta, L., K.H.N. Hoebe, and E.M. Janssen, *The Emerging Role of CD244 Signaling in Immune Cells of the Tumor Microenvironment.* Front Immunol, 2018. **9**: p. 2809.
185. Skorepa, O.*, et al.*, *Natural Killer Cell Activation Receptor NKp30 Oligomerization Depends on Its N-Glycosylation.* Cancers, 2020. **12**(7): p. 1998.
186. Mellergaard, M.*, et al.*, *N-glycosylation of asparagine 8 regulates surface expression of major histocompatibility complex class I chain-related protein A (MICA) alleles dependent on threonine 24.* J Biol Chem, 2014. **289**(29): p. 20078-91.
187. Liu, K.*, et al.*, *N-glycosylation of PD-1 promotes binding of camrelizumab.* EMBO Rep, 2020. **21**(12): p. e51444.
188. Mariathasan, S.*, et al.*, *TGFbeta attenuates tumour response to PD-L1 blockade by contributing to exclusion of T cells.* Nature, 2018. **554**(7693): p. 544-548.
189. Batlle, E. and J. Massague, *Transforming Growth Factor-beta Signaling in Immunity and Cancer.* Immunity, 2019. **50**(4): p. 924-940.

190. Liu, M.*, et al.*, *TGF-beta suppresses type 2 immunity to cancer.* Nature, 2020. **587**(7832): p. 115-120.
191. Hauser, M.A.*, et al.*, *Distinct CCR7 glycosylation pattern shapes receptor signaling and endocytosis to modulate chemotactic responses.* J Leukoc Biol, 2016. **99**(6): p. 993-1007.
192. Kamishikiryo, J.*, et al.*, *Molecular basis for LLT1 protein recognition by human CD161 protein (NKRP1A/KLRB1).* J Biol Chem, 2011. **286**(27): p. 23823-30.
193. Elbein, A.D.*, et al.*, *Kifunensine, a potent inhibitor of the glycoprotein processing mannosidase I.* J Biol Chem, 1990. **265**(26): p. 15599-605.
194. Nettleship, J., *Structural Biology of Glycoproteins*. Intech ed. S. Petrescu. 2012.
195. Kolenko, P.*, et al.*, *Molecular architecture of mouse activating NKR-P1 receptors.* J Struct Biol, 2011. **175**(3): p. 434-41.
196. Skalova, T.*, et al.*, *Mouse Clr-g, a ligand for NK cell activation receptor NKR-P1F: crystal structure and biophysical properties.* J Immunol, 2012. **189**(10): p. 4881-9.
197. Vanek, O.*, et al.*, *Soluble recombinant CD69 receptors optimized to have an exceptional physical and chemical stability display prolonged circulation and remain intact in the blood of mice.* FEBS J, 2008. **275**(22): p. 5589-606.
198. Li, Z.*, et al.*, *Simple piggyBac transposon-based mammalian cell expression system for inducible protein production.* Proc Natl Acad Sci U S A, 2013. **110**(13): p. 5004-9.
199. Skořepa, O., *Strukturní studium potkaního NK buněčného receptoru NKR-P1B a jeho ligandu Clrb*. 2016, Univerzita Karlova, Přírodovědecká fakulta, Katedra biochemie.
200. Kalousková, B., *Příprava lidského NK buněčného aktivačního receptoru NKp80 a jeho ligandu AICL*. 2016, Univerzita Karlova, Přírodovědecká fakulta, Katedra biochemie.
201. Muller-Kuller, U.*, et al.*, *A minimal ubiquitous chromatin opening element (UCOE) effectively prevents silencing of juxtaposed heterologous promoters by epigenetic remodeling in multipotent and pluripotent stem cells.* Nucleic Acids Res, 2015. **43**(3): p. 1577-92.
202. Krissinel, E. and K. Henrick, *Inference of macromolecular assemblies from crystalline state.* J Mol Biol, 2007. **372**(3): p. 774-97.
203. Xu, X.*, et al.*, *Expression, crystallization and X-ray diffraction analysis of a complex between B7-H6, a tumor cell ligand for the natural cytotoxicity receptor NKp30, and an inhibitory antibody.* Acta Crystallogr F Struct Biol Commun, 2015. **71**(Pt 6): p. 697-701.
204. Xu, X.*, et al.*, *Structural Insights into the Inhibitory Mechanism of an Antibody against B7-H6, a Stress-Induced Cellular Ligand for the Natural Killer Cell Receptor NKp30.* J Mol Biol, 2016. **428**(22): p. 4457-4466.

7. SELECTED PUBLICATIONS

PUBLICATION I

Bláha J., Kalousková B., Skořepa O., Pažický S., Novák P., Vaněk O.

High-level expression and purification of soluble form of human natural killer cell receptor NKR-P1 in HEK293S GnTI$^-$ cells.

Protein Expr. Purif. 140:36-43 (2017)

My contribution to the publication: performing research (cloning, recombinant protein expression and purification, protein characterisation, cell line cultivation and transfection optimisation)

Protein Expression and Purification 140 (2017) 36–43

Contents lists available at ScienceDirect

Protein Expression and Purification

journal homepage: www.elsevier.com/locate/yprep

High-level expression and purification of soluble form of human natural killer cell receptor NKR-P1 in HEK293S GnTI⁻ cells

Jan Bláha [a], Barbora Kalousková [a], Ondřej Skořepa [a], Samuel Pažický [a], Petr Novák [a, b], Ondřej Vaněk [a, *]

[a] Department of Biochemistry, Faculty of Science, Charles University, Hlavova 2030/8, 12840 Prague, Czech Republic
[b] Institute of Microbiology, The Czech Academy of Sciences, BIOCEV, Průmyslová 595, 25250 Vestec, Czech Republic

ARTICLE INFO

Article history:
Received 29 May 2017
Received in revised form
21 July 2017
Accepted 25 July 2017
Available online 27 July 2017

Keywords:
NKR-P1
CD161
klrb1
NK cells
HEK293
LLT1

ABSTRACT

Human natural killer receptor protein 1 (NKR-P1, CD161, gene *klrb1*) is a C-type lectin-like receptor of natural killer (NK) cells responsible for recognition of its cognate protein ligand lectin-like transcript 1 (LLT1). NKR-P1 is the single human orthologue of the prototypical rodent NKR-P1 receptors. Naturally, human NKR-P1 is expressed on the surface of NK cells, where it serves as inhibitory receptor; and on T and NKT cells functioning as co-stimulatory receptor promoting secretion of IFNγ. Most notably, it is expressed on Th17 and Tc17 lymphocytes where presumably promotes targeting into LLT1 expressing immunologically privileged niches. We tested effect of different protein tags (SUMO, TRX, GST, MsyB) on expression of soluble NKR-P1 in *E. coli*. Then we optimized the expression construct of soluble NKR-P1 by preparing a library of expression constructs in pOPING vector containing the extracellular lectin-like domain with different length of the putative *N*-terminal stalk region and tested its expression in Sf9 and HEK293 cells. Finally, a high-level expression of soluble NKR-P1 was achieved by stable expression in suspension-adapted HEK293S GnTI⁻ cells utilizing pOPINGTTneo expression vector. Purified soluble NKR-P1 is homogeneous, deglycosylatable, crystallizable and monomeric in solution, as shown by size-exclusion chromatography, multi-angle light scattering and analytical ultracentrifugation.

1. Introduction

Natural killer (NK) cells are large granular lymphocytes described to be on the functional borderline of innate and adaptive immunity [1,2]. They are mainly recognized for their singular ability to provide defence against viral infection and tumour development without prior antigen sensitization [3], but they also contribute to the regulation of the adaptive system via secretion of cytokines [1] and are even able to form antigen specific immunologic memory [4–6]. NK cell activity is controlled by a fine balance of signals from its variety of inhibitory and activating receptors [3] that engage a broad range of health and disease markers in the accepted "missing-self" and "induced-self" modes of recognition, respectively [7–11].

NK cell receptors are divided into the immunoglobulin-like [12] and the C-type lectin-like (CTL) structural classes [13,14]. C-type lectins bind calcium and carbohydrates; however, CTL receptors recognize protein ligands instead, despite the fact that they are homologous to C-type lectins [15,16]. The NKR-P1 receptor family, encoded in the Natural Killer Cell (NKC) gene complex (human chromosome 12), encompasses the prototypical NK cell receptors belonging to the CTL class [15]. Unlike many CTL NK receptors that are recognizing MHC class I glycoproteins [14,17,18], NKR-P1 receptors interact with a genetically and structurally highly related ligands from *clec2* gene subfamily [13].

Human NKR-P1 (CD161, gene *klrb1*) was identified in 1994 as a human orthologue of rodent NKR-P1 receptors [19] and up to now remains the only described human NKR-P1 receptor. However, human NK receptors from the *klrf* subfamily – i.e. NKp65 [20] and NKp80 [21] share distinct similarity to NKR-P1 and were proposed to represent activating counterparts of human NKR-P1 [13,22].

Apart from NK cells, human NKR-P1 was found to be expressed on NKT cells [23] and subpopulations of T lymphocytes [24]. Most

Abbreviations: CTL, C-type lectin-like; GnTI⁻, *N*-acetylglucosaminyltransferase I negative; HEK, human embryonic kidney; LLT1, lectin-like transcript 1; lPEI, linear polyethylenimine; MALS, multi-angle light scattering; NK, natural killer; SEC, size-exclusion chromatography.

* Corresponding author.
E-mail address: ondrej.vanek@natur.cuni.cz (O. Vaněk).

http://dx.doi.org/10.1016/j.pep.2017.07.016
1046-5928/

notably, human NKR-P1 is present on regulatory T cells [25] and is currently recognized to be a marker for all Th17 cells [26]. It was found also on some Tc17 cells [27] which are being more and more implicated in autoimmune diseases like multiple sclerosis [28], rheumatoid arthritis [29] and Crohn's disease [30]. It was proposed that NKR-P1 could play a role in targeting of these lymphocytes and promote transendothelial extravasation into immunologically privileged niches [26,31–34].

Under homeostasis NKR-P1 functions as inhibitory receptor of NK cells [19,35,36] and co-stimulatory receptor of NKT and T cells [35,37] promoting secretion of IFNγ. However, it was also described that the inhibitory function of human NKR-P1 is in an undesirable way exploited by glioblastomas [38] and B-cell Non-Hodgkin's lymphomas [39] which overexpress the NKR-P1 physiological ligand – lectin-like transcript 1 (LLT1, gene *clec2d*) [35,36,40,41] and thus escape immune response.

From a protein point of view, human NKR-P1 shares common CTL receptor features. It was identified as a homodimeric type II. transmembrane glycoprotein lacking O-linked glycosylation [19]. Its short intracellular portion contains an immunoreceptor tyrosine-based inhibitory motif that is noncanonical for the presence of alanine residue in the −2 position relative to the tyrosine residue [42]. A transmembrane helix is followed by 25 residues long stalk region that presumably functions as a flexible linker providing a scaffold for cystine homodimerization and a *C*-terminal CTL domain that itself contains 6 conserved cysteine residues stabilizing this domain by formation of three intramolecular disulphide bridges [14].

Although there have been recently promising results for refolding of murine NKR-P1 receptors from inclusion bodies produced in *E. coli* [43,44], so far only an unsuccessful renaturation of the human orthologue have been reported [45]. Mammalian cell lines were used previously to express full-length human NKR-P1 receptor or its extracellular part in low-scale for immunological studies [35,36,40,41] or surface plasmon resonance measurements [45], respectively. Here we present an optimization of the human NKR-P1 ectodomain expression in different expression systems and finally an utilization of HEK293S GnTI$^-$ cells [46] for generation of stably transfected cell line that provides a high yield of soluble human NKR-P1 ectodomain usable for structural studies.

2. Material and methods

2.1. Vectors and NKR-P1 library cloning

A cDNA clone (GenBank accession no. BC114516) containing the entire coding sequence of *klrb1* gene was obtained from Source BioScience (GenomeCUBE IRCMp5012E0732D). A library of NKR-P1 stalk region deletion expression vectors was constructed by In-Fusion cloning at the Oxford Protein Production Facility (OPPF; Oxford, UK) as described before [47,48]. Primers used for amplification of the selected NKR-P1 constructs from the cDNA clone contained In-Fusion overlaps at the 5′ of the specific forward and the reverse primers as described in supplementary data, Table S1. For transient expression in HEK293 cells, NKR-P1 ectodomain (G90-S225) was amplified from the cDNA clone using 5′–AAAAAAACCGGTGGTCTCTTAAACTGCCCAATATATTG–3′ and 5′–AAAAAAGGTACCAGAGTCAGGATACACTTTATTTCTCAC–3′ and using *Age*I and *Kpn*I sites subcloned into pTT28 expression plasmid (kindly provided by Dr. Yves Durocher; a derivative of pTT5 [49] containing *N*-terminal secretion leader and *C*-terminal His_8-tag sequence, thus leaving ITG- and -GTKHHHHHHHHG at expressed protein *N*-and *C*-termini).

2.2. Small-scale NKR-P1 expression tests

Expression of the library of stalk region deletion constructs was performed at OPPF following standard OPPF protocols for high-throughput expression testing in *E. coli* [50] and Sf9 cells [51] as described before.

Briefly, for prokaryotic expression 150 μl of overnight cultures grown from selected colony of *E. coli* Rosetta2(DE3) pLysS or B834(DE3) strains (both Novagen) transformed with the given expression plasmid were used for inoculation of 3 ml of Power Broth (Molecular Dimensions) and Overnight Express Instant TB Medium (TBONEX; Novagen) with an appropriate antibiotic in 24-well deep well blocks. The blocks were shaken at 37 °C until an average OD_{595} reached ca 0.5. The Power Broth cultures were cooled to 20 °C and expression was induced by addition of IPTG to 1 mM final concentration and left to produce overnight. The TBONEX cultures were cooled to 25 °C and left to produce for 20 h.

Bacterial cultures were centrifuged and frozen until analysis. Defrosted cell pellets were resuspended in lysis buffer (50 mM NaH_2PO_4, 300 mM NaCl, 10 mM imidazole, 1% v/v Tween 20, pH 8.0) supplemented with lysozyme and DNAse I, incubated for 30 min and the lysates were cleared by centrifugation in deep-well block (6000 × g, 30 min, 4 °C). Expression levels were analysed by Coomassie stained reducing SDS-PAGE from soluble fraction of cell lysates [50].

For insect cell expression, to generate a P0 virus stock Sf9 cells were co-transfected with linearized bacmid DNA (Bac10:KO_{1629} [52]) and pOPIN vector from the stalk region deletion library as a transfer vector. For small-scale expression tests 3 ml of 1 × 10^6 Sf9 cells/ml in 24-well deep blocks were infected with 3 and 30 μl of P1 virus stock and left to produce at 27 °C for 72 h. For scale up, 800 ml of Sf9 production culture in shaken Thompson flask was infected with 800 μl of P2 virus stock. Media were harvested and purified after 7 days.

For mammalian expression tests, 4 μg of the given expression plasmid and 10 μl of Lipofectamine 2000 (Invitrogen, USA) were each diluted into 25 μl of Freestyle F17 media (Invitrogen, USA), incubated for 5 min, mixed and incubated for 10 min again before addition to 2 × 10^6 HEKT293T cells grown in 1 ml of Freestyle F17 medium on a shaken 24-well culture plate (Corning, USA) at 37 °C, 5% CO_2. After 4 h cell cultures were diluted with 1 ml of EX-CELL293 serum-free medium (Sigma, USA) and left to produce for 72 h.

Expression tests from insect and mammalian cell cultures were analysed by enriching the secreted products by IMAC on Ni-NTA magnetic beads (Qiagen and Biotool, USA) from 1 ml of the production media and either analysed by SDS-PAGE or by Western blot and immunodetection with primary mouse PentaHis anti-His-tag monoclonal antibody (Qiagen, USA) and secondary HRP or AP conjugated anti-mouse IgG antibody (R&D Systems, USA; Sigma, USA).

2.3. Transient NKR-P1 expression in HEK293T cells

HEK293 cell lines were grown in suspension as described in Ref. [41] in mixture of equal volumes of EX-CELL293 and Freestyle F17 media in shaken square-shaped glass bottles within humidified 37 °C, 5% CO2 incubator. For transient expression of soluble NKR-P1 ectodomain, 400 μg of the pTT28 expression plasmid were diluted in PBS, filter-sterilized and 25 kDa linear polyethylenimine (Polysciences, USA) was added in 1:3 (w/w) ratio to 4 ml final volume, the mixture was shaken and incubated for 5 min. Meanwhile, 400 × 10^6 HEK293T cells were centrifuged and resuspended in 200 ml of Freestyle F17 and immediately transfected. Following 4 h incubation, the culture was diluted with 200 ml of EX-CELL293. 5–7 days post-transfection culture medium was harvested by

centrifugation (4000 × g, 30 min), filtered (0.22 μm Steritop filter; Millipore, USA), and stored at −20 °C or immediately processed.

2.4. Stable NKR-P1 expression in HEK293S GnTI⁻ cells

For generation of stably transfected HEK293S GnTI⁻ cell pool, 30 × 10^6 cells were transfected in high cell density [41] with 30 μg of pOPINGTTneo expression plasmid. For selection, Geneticin G418 was added two days post-transfection at 100 μg/ml. The culture was split and the medium was exchanged with fresh addition of the selection antibiotic every three days. Three weeks post-transfection healthy and growing pool of polyclonal stably transfected cell culture was established. The stable culture was maintained in 1:1 mixture of EX-CELL293 and Freestyle F17 with 100 μg/ml of the Geneticin G418. For protein production 400 × 10^6 cells were split into 400 ml of 1:1 mixture of EX-CELL293 and Expi293 (Invitrogen, USA) with 100 μg/ml of the selection antibiotic. Culture medium was harvested after 10–14 days by centrifugation (4000 × g, 30 min), filtered (0.22 μm Steritop filter; Millipore, USA), and stored at −20 °C or immediately processed.

2.5. Protein purification and crystallization

Medium was diluted twofold with 50 mM Na_2HPO_4, 300 mM NaCl, 10 mM NaN_3, pH 7.5 PBS buffer and pH was adjusted to 7.5 if necessary. The His-tagged protein was recovered by IMAC chromatography on HiTrap TALON crude column (GE Healthcare, USA) with subsequent SEC on Superdex 200 10/300 GL column (GE Healthcare, USA) in 10 mM HEPES, 150 mM NaCl, 10 mM NaN_3, pH 7.5 buffer and concentrated to 20 mg/ml on Amicon Ultra concentrator (10000 MWCO; Millipore, USA). The protein was crystallized using sitting drop vapour diffusion method. Drops (100 nl of protein solution and 100 nl of reservoir) were set up using a Cartesian Honeybee 961 robot (Genomic Solutions) at 294 K. The reservoir consisted of 30% w/v PEG 6000, 100 mM Bis-Tris propane pH 9.0 (PegRx screen, condition 39, Hampton Research).

2.6. Mass spectrometry

Disulphide bonds in soluble human NKR-P1 were determined according to the previously published protocol [53]. Briefly, the protein was separated by SDS-PAGE, *N*-linked glycans were cleaved off after the first GlcNAc unit by endoglycosidase Endo Hf (New England Biolabs, USA) and digested by trypsin (Sigma, USA) or Asp-N endoproteinase (Sigma, USA) under nonreducing conditions in the presence of 200 μM cystamine. The peptide mixtures were desalted on peptide MacroTrap and separated on reversed phase MAGIC C18 columns (both Michrom BioResources, USA) connected directly to an APEX-Q 9.4 T FT-ICR mass spectrometer (Bruker Daltonics, USA) using an electrospray ion source. Data were acquired using ApexControl 3.0.0 and processed with DataAnalysis 4.0. The disulphide bonds and saccharide moieties were identified using Links software [54].

2.7. Analytical ultracentrifugation

The oligomeric state of the produced protein was analysed in ProteomeLab XL-I analytical ultracentrifuge equipped with An-50 Ti rotor (Beckman Coulter, USA). For sedimentation velocity experiment, samples of NKR-P1 diluted to the desired concentration with the SEC buffer used for its purification were spun at 48000 rpm at 20 °C and 150 scans with 0.003 cm spatial resolution were recorded in 5 min interval using absorbance optics at 280–300 nm. The data were analysed using Sedfit [55] using a c(s) continuous size distribution model. For sedimentation equilibrium experiment, NKR-P1 at 0.11 mg/ml was spun at 12-15-18-21-24000 rpm at 4 °C and 1 scan with 0.001 cm spatial resolution at 280 nm was recorded after first 34 h and then consecutively after 18 h per each velocity. The data were analysed using Sedphat [56] using multi-speed sedimentation equilibrium and single ideal species model. Buffer density and protein partial specific volume were estimated in SEDNTERP (http://sednterp.unh.edu/), figures were prepared in GUSSI [57].

2.8. SEC-MALS

Molecular weight and polydispersity of NKR-P1 and LLT1(H176C) [41] were analysed by size exclusion chromatography using an HPLC system (Shimadzu, Japan) equipped with refractive index (RI), UV and multi-angle light scattering (MALS) DAWN8 EOS detectors (Wyatt Technology, USA). A microSuperose12 column (GE Healthcare, USA) was used with 10 mM HEPES, 150 mM NaCl, 10 mM NaN_3, pH 7.5 eluent at 0.1 ml/min. Weight-average molecular weights (Mw) were calculated from the light-scattering detector based on the known injected mass while assuming 100%

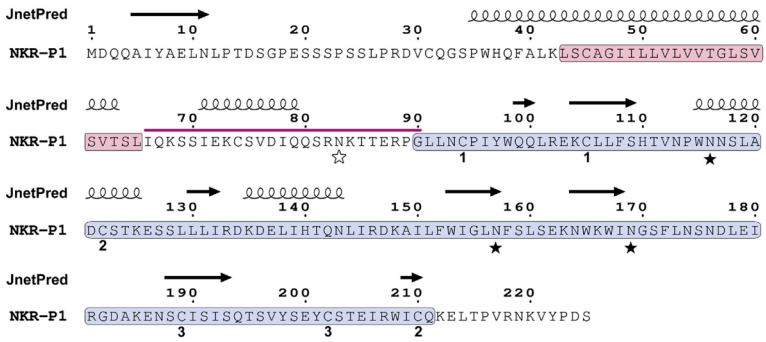

Fig. 1. The primary sequence of human NKR-P1 (CD161, *klrb1*). The transmembrane helix and C-type lectin-like domain predicted by Globplot 2 [59] are highlighted by red and blue rectangles, respectively. The stalk region optimized in this study is marked by magenta line above the sequence. JPred 4 [60] secondary structure prediction is depicted at the top. Identified cystic pairs and *N*-linked glycosylation sites are labelled by numbers and full stars, respectively. The empty star indicates the presumptive *N*-linked glycosylation site present within the stalk region. (For interpretation of the references to colour in this figure legend, the reader is referred to the web version of this article.)

Table 1
List of used expression plasmids with description of peptides flanking the expression construct.

Vector	*N*-terminal	*C*-terminal
pOPINS3C	His_6-SUMO-3C	–
pOPINTRX	His_6-TRX-3C	–
pOPINMSYB	His_6-MsyB-3C	–
pOPINJB	His_6-GST-3C	BAP
pOPINP	SS[PelB]	Lys-His_6
pOPING	SS[RPTPmu]	Lys-His_6
pOPINGTTneo	SS[RPTPmu]	Lys-His_6

His_6 – hexahistidine tag; SUMO – small ubiquitin-like modifier; 3C – cleavage site for 3C protease; TRX – *E. coli* thioredoxin; MsyB – *E. coli* MsyB; GST – glutathione S-transferase; SS[PelB] – PelB signal sequence; SS[RPTPmu] – receptor-like protein tyrosine phosphatase μ signal sequence; BAP – biotin acceptor peptide.

mass recovery. Number-average molecular weights (Mn) were determined by refractive index measurements and were calculated assuming a dn/dc value of 0.185 ml/g. Polydispersity is defined as (Mw/Mn).

3. Results and discussion

3.1. Transient expression of NKR-P1 in HEK293 cell lines

To our best knowledge, successful expression of soluble human NKR-P1 ectodomain has been previously reported only in transiently transfected HEK293 cells [45]. Although the authors haven't stated the production yield, the reported use for immobilization on SPR sensor chip doesn't necessarily suggest high yields. To evaluate this approach, we have performed transient expression of NKR-P1 ectodomain in suspension cultures of HEK293T and HEK293S GnTI$^-$ cells using the same expression construct G90-S225 as reported before [45]. This expression construct corresponds to the CTL domain of NKR-P1 (Fig. 1) and does not contain residues from the stalk region of the receptor. Similar constructs were previously successfully used within our hands for bacterial expression and refolding of mouse NKR-P1A, NKR-P1C, and Clrg ectodomains [43,44,58], as well as of human LLT1 ectodomain that was expressed in the same HEK293 cell lines [41]. However, in case of human NKR-P1 we have obtained on average yields of only about 0.1 mg of pure recombinant protein per litre of production culture from either HEK293 cell line. In contrast, we have recently reported ca 30-times higher yields in the same expression system for LLT1 [41]. Such low yields of NKR-P1 are neither sufficient nor economical for structural studies; therefore, we have attempted further optimization of its expression with regards to the expression system used and to the length of the putative *N*-terminal stalk region in its expression construct.

3.2. Screening of NKR-P1 expression in E. coli

In order to test the solubility effect of a protein tag fusion we

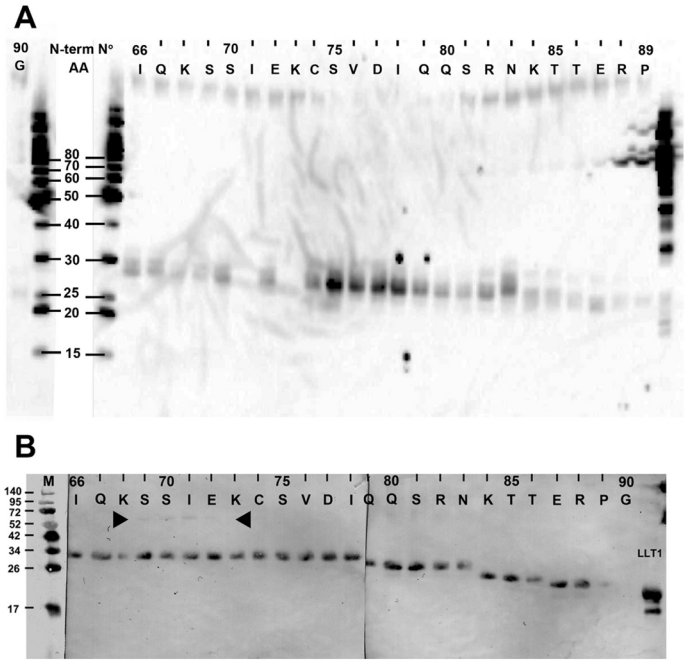

Fig. 2. Screening of the stalk region deletion library of NKR-P1 expression constructs. Western blots of His-tagged products enriched on Ni-NTA magnetic beads from small-scale expression tests of the NKR-P1 stalk region deletion library in pOPING (*C*-terminally His_6-tagged) in (A) Sf9 insect and (B) human HEK293T cell lines. The *N*-terminal residue of the stalk region included in the given construct is annotated at the top. Molecular weight standards are in kDa. Position of putative covalent dimer of NKR-P1 is marked by an arrow. Sample of NKR-P1 ligand, protein LLT1, was added for comparison.

have subcloned three expression constructs of human NKR-P1 differing in the length of the flexible *N*-terminal stalk region while containing the whole CTL domain (I66/Q80/G90-S225) (Fig. 1) into the pOPINS3C, pOPINTRX, pOPINMSYB, pOPINJB, and pOPINP expression vectors from OPPF's suite of pOPIN vectors [48] (see Table 1 for information about the expression cassettes). Expression tests were performed in *E. coli* B834(DE3) and *E. coli* Rosetta2(DE3) pLysS strains using two different production conditions – an overnight production at 20 °C after induction with 1 mM IPTG and a production in TBONEX auto-induction medium at 25 °C for 20 h. Products of 1 ml cultures were enriched using Ni-NTA magnetic beads from soluble fraction of cell lysate and analysed using Coomassie stained reducing SDS-PAGE [50] (Fig. S1). Unfortunately, we cannot report any improvement on expression of soluble human NKR-P1 in *E. coli* for any of the tested fusion constructs or conditions. It is possible that using strains with an oxidizing cytoplasm designed for expression of disulphide-containing proteins like SHuffle or Rosetta-gami would be more efficient; however, based on our previous experiences with these strains for similar constructs of mouse NKR-P1 receptors this seems unlikely, too (not shown).

3.3. Screening of stalk region deletion library in Sf9 and HEK293T cells

For simultaneous expression test in both insect cell baculoviral and mammalian expression systems, we have utilized OPPF's pOPING expression vector allowing for secreted expression with *C*-terminal His_6-tag flanking the protein of interest (Table 1). A series of 25 human NKR-P1 constructs with consecutively shortened *N*-terminal stalk region (I66-G90) (Fig. 1) ending at the CTL domain *C*-terminal S225 were subcloned into the pOPING vector. Expression tests were performed in 3 ml of Sf9 culture infected with P1 generation of baculoviruses and in 2 ml of transiently transfected suspension HEK293T cultures. Expression media were analysed for the presence of desired products 72 h post-transfection by anti-histidine tag immunodetection.

Although positive, only low expression signals were obtained from the insect cell expressions (Fig. 2A). However, a distinct region of best expressing constructs could be distinguished with the *N*-termini of NKR-P1 ranging from C74 to Q79. This could suggest stabilization of these constructs by secondary structure formation. Interestingly, a JPred 4 secondary structure prediction analysis suggests α-helix within this region (Fig. 1). Such structural stabilization could provide a scaffold for the formation of an intermolecular disulphide bridge via the C74 residue.

Analysis of the expression test in mammalian culture showed positive albeit similarly low level of expression for most of the tested constructs (Fig. 2B). Interestingly, a very low signal corresponding to the NKR-P1 covalent dimer could be detected within the range of S69-E72 *N*-terminal NKR-P1 constructs. Also, a sudden shift in the electrophoretic mobility between the N83 and K84 *N*-terminal constructs and presence of NKT consensus sequence suggest presence of *N*-linked glycan at the N83 (Fig. 1).

We have further attempted to scale-up the production of the S75-S225 construct in 800 ml of Sf9 culture infected with P2 generation of the virus. However, the low level of expression was confirmed with yield of only ca 0.4 mg of heavily contaminated protein per litre of production culture (contamination may have been caused by presence of misfolded protein aggregates). Therefore, we cannot report a suitable format of recombinant expression of soluble human NKR-P1 based on baculoviral transduction of Sf9 cells. We cannot exclude the possibility that the sequence following the signal peptide might have a negative impact on secretion in insect cells, rather than the construct itself.

3.4. High-level expression of soluble human NKR-P1 in stable HEK293S GnTI⁻ cell line

In parallel, we have attempted to express the original G90-S225 construct of human NKR-P1 ectodomain in stably transfected pool of HEK293S GnTI⁻ cells and thus test whether higher production yields might be reached by using stable instead of transient transfection. Although this construct performed poorly in the aforementioned transient expression test and may be suboptimal with respect to possible expression yield, based on our previous work on structural elucidation of CTL receptors [40,43,58,61] constructs lacking the *N*-terminal stalk region and containing only the well-defined CTL domain are the most suitable targets for further structural experiments. The expression construct was subcloned into OPPF's vector pOPINGTTneo containing neomycin selection marker. A pool of resistant HEK293S GnTI⁻ cells was selected on Geneticin G418. Following positive expression test (data not shown), the resistant pool was scaled to 300 ml of 1×10^6/ml cell suspension and left to produce for 10 days. The secreted product was purified by IMAC on HiTrap Talon column followed by SEC on Superdex 200 10/300 GL yielding on average 2.5 mg of pure protein per litre of production culture.

The HEK293S GnTI⁻ cell line provides uniform mammalian *N*-linked glycosylation of $GlcNAc_2Man_5$ type that is readily cleavable with endoglycosidase Endo F1 leaving only a single GlcNAc unit (Fig. 3A, lane D). Both under reducing and non-reducing conditions the soluble human NKR-P1 ectodomain migrates on SDS-PAGE as three distinct glycoforms corresponding to the theoretical weight of monomer with one (18.4 kDa), two (19.6 kDa) or three (20.9 kDa)

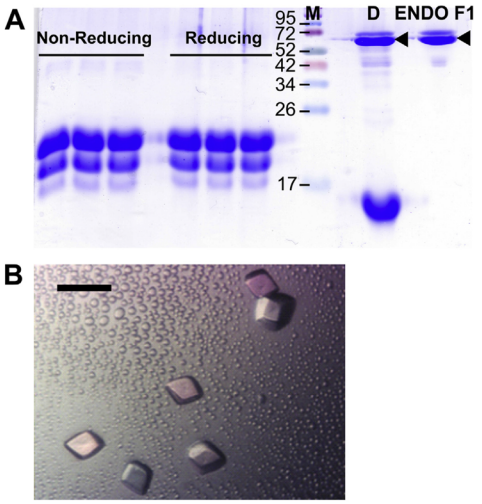

Fig. 3. Soluble NKR-P1 ectodomain forms distinct glycoforms, is easily deglycosylatable and crystallizable. (A) SDS-PAGE analysis of the final product of soluble NKR-P1 (G90-S225) with simple $GlcNAc_2Man_5$ *N*-linked glycosylation from HEK293S GnTI⁻ cells. Both under reducing and non-reducing conditions three distinct glycoforms of NKR-P1 are detectable, that migrate as a single band after cleavage of *N*-glycans with endoglycosidase Endo F1 (leaving single GlcNAc unit; lane D). M – molecular weight standard in kDa. ENDO F1 – endoglycosidase F1 (arrow). (B) Crystals of NKR-P1 produced in HEK293S GnTI⁻ cells grown by sitting drop vapour diffusion method. The black scale bar represents 100 μm.

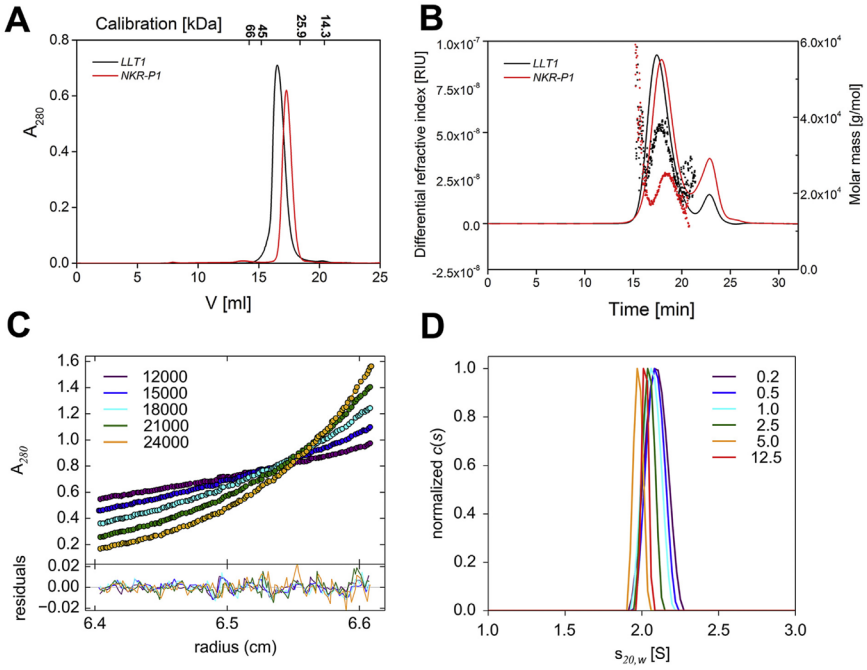

Fig. 4. Soluble NKR-P1 is monomeric in solution. (A) Comparison of size exclusion chromatography profiles of soluble LLT1 H176C mutant (black) and NKR-P1 (red). The LLT1 is forming non-covalent dimer [41] while NKR-P1 migrates rather as monomer. (B) Comparison of size exclusion chromatography with refractive index detection (line plot, left axis) and molar masses determined by multi angle light scattering (scatter plot, right axis) of soluble LLT1 H176C mutant (black) and NKR-P1 (red). (C) Sedimentation equilibrium analysis in analytical ultracentrifuge performed at 0.11 mg/ml concentration showed that NKR-P1 behaves as monomer; upper panel – absorbance data with fitted curves (single non-interacting discrete species model), lower panel – residual plot showing the goodness of fit. (D) Series of sedimentation velocity analyses in analytical ultracentrifuge at increasing protein concentration (given in mg/ml; normalized continuous size distributions of the sedimenting species) showed that NKR-P1 does not self-associate. (For interpretation of the references to colour in this figure legend, the reader is referred to the web version of this article.)

N-linked glycosylation sites occupied with the $GlcNAc_2Man_5$ oligosaccharide moieties (Fig. 3A). Furthermore, the prepared soluble human NKR-P1 with homogeneous $GlcNAc_2Man_5$ *N*-glycans (although still being in-homogeneous with respect to incomplete *N*-glycosylation site occupancy) was readily crystallized using the vapour diffusion method in sitting drop, forming bipyramidal crystals (Fig. 3B) up to 80 μm in size. These initial crystals already diffracted up to resolution of ca 2.0 Å and were later optimized leading to solution of NKR-P1 crystal structure (Bláha *et al.*, submitted).

Utilizing a mass spectrometry approach, we have identified cystic peptides in the soluble NKR-P1 ectodomain confirming canonical configuration of disulphides in CTL domain: C94-C105, C122-C210, and C189-C202 (Table S2, Fig. 1). Furthermore, we have been able to confirm presence of saccharide moieties at the three predicted *N*-linked glycosylation sites – N116, N157, and N169 (Table S2, Fig. 1). The incomplete occupancy of these sites accounts for the three different glycoforms observed on SDS-PAGE (Fig. 3A).

3.5. Stoichiometry of recombinant human NKR-P1 in solution

Comparison of SEC retention volumes for soluble LLT1(H176C) eluting as a non-covalent dimer [41] and for soluble NKR-P1 ectodomain suggests that soluble NKR-P1 elutes rather as a monomer (Fig. 4A). To confirm this, we repeated the analysis with multi-angle light scattering detection (Fig. 4B) providing a molecular weight of ca 22 kDa and 33 kDa for soluble NKR-P1 and LLT1(H176C) respectively, both with low polydispersity (Fig. 4B). Monomeric state of human NKR-P1 was further corroborated by sedimentation equilibrium analysis in analytical ultracentrifuge resulting in estimated molecular weight of 20.7 kDa (Fig. 4C). Sedimentation velocity experiment performed with samples of increasing protein concentration also showed no tendency to form homodimer or oligomeric species (Fig. 4D). Soluble human NKR-P1 behaves as particle with standard sedimentation coefficient $s_{20,w}$ 2.10 S and approximate dimensions of 4.5 × 3.5 nm corresponding well to expected values for monomeric protein.

Human NKR-P1 should form a covalently linked homodimer on the cell surface [19], but the produced soluble form of NKR-P1 lacks the odd cysteine residue in the stalk region implicated in such dimerization [13]. However, soluble ectodomains of the homologous subfamily of related *clec2* receptors – CD69 [61], LLT1 [40], and KACL [62] were previously reported to form stable non-covalent dimers in solution quite easily. On the other hand, recently published structure of NKp65 [62], a member of more closely related *klrf* subfamily, shows this receptor interacting with

its *clec2* ligand KACL while being in a monomeric state and its dimerization in the manner of *clec2* receptors would even hamper the interaction with its *clec2* ligand. Similarly, previously reported mouse NKR-P1A and NKR-P1C(B6) orthologues were observed in solution only as monomers [43,44]. Taken together with the presented low propensity of NKR-P1 to form a non-covalent dimer in solution, a different, less stable mode of dimerization should be expected than that of *clec2* receptors for the human NKR-P1 and its orthologues and close homologues – the *klrf* receptors; that requires covalent stabilization by a disulphide bridge(s) in the putative stalk region.

4. Conclusions

To conclude, we have recombinantly expressed soluble human NKR-P1 ectodomain in stable, deglycosylatable and crystallizable form. To our knowledge, this is the first attempt at structural characterization of human NKR-P1 immunoreceptor. The strategy of construct design described herein for NKR-P1 – i.e. the construction of stalk region deletion library – might be considered also for other C-type lectin-like receptors of NK cells, although in our case, it was rather the choice of proper expression system that was the most important factor. Selection of stably transfected HEK293 cell lines as expression host may be optimal both for protein production aimed at structural characterization and for production of soluble receptor domains that could be utilized in clinical therapy also for other NK cell CTL receptors and their ligands. Depending on the intended use, suitable HEK293 cell line with desired *N*-glycosylation profile could be chosen, i.e. HEK293S GnTI$^-$ or HEK293T cell lines with simple or complex *N*-glycans, respectively.

Acknowledgements

This study was supported by Czech Science Foundation (15-15181S), Ministry of Education, Youth and Sports of the Czech Republic (LG14009 and LM2015043 CIISB for CMS Biocev; LTC17065), Charles University (UNCE 204025/2012, SVV 260079/2014, GAUK 161216), Foundation "Nadání Josefa, Marie a Zdeňky Hlávkových", COST Action CA15126 (MOBIEU), and BioStruct-X (EC FP7 project 283570). The authors also acknowledge the support and the use of resources of Instruct, a Landmark ESFRI project through the R&D pilot scheme APPID 56 and 286.

Appendix A. Supplementary data

Supplementary data related to this article can be found at http://dx.doi.org/10.1016/j.pep.2017.07.016.

References

[1] E. Vivier, D.H. Raulet, A. Moretta, M.A. Caligiuri, L. Zitvogel, L.L. Lanier, W.M. Yokoyama, S. Ugolini, Innate or adaptive immunity? The example of natural killer cells, Science 331 (2011) 44–49.
[2] M.A. Caligiuri, Human natural killer cells, Blood 112 (2008) 461–469.
[3] E. Vivier, E. Tomasello, M. Baratin, T. Walzer, S. Ugolini, Functions of natural killer cells, Nat. Immunol. 9 (2008) 503–510.
[4] A. Cerwenka, L.L. Lanier, Natural killer cell memory in infection, inflammation and cancer, Nat. Rev. Immunol. 16 (2016) 112–123.
[5] E. Vivier, S. Ugolini, Natural killer cells: from basic research to treatments, Front. Immunol. 2 (2011) 18.
[6] M.A. Cooper, M. Colonna, W.M. Yokoyama, Hidden talents of natural killers: NK cells in innate and adaptive immunity, EMBO Rep. 10 (2009) 1103–1110.
[7] D.H. Raulet, N. Guerra, Oncogenic stress sensed by the immune system: role of natural killer cell receptors, Nat. Rev. Immunol. 9 (2009) 568–580.
[8] C.S. Brandt, M. Baratin, E.C. Yi, J. Kennedy, Z. Gao, B. Fox, B. Haldeman, C.D. Ostrander, T. Kaifu, C. Chabannon, A. Moretta, R. West, W. Xu, E. Vivier, S.D. Levin, The B7 family member B7-H6 is a tumor cell ligand for the activating natural killer cell receptor NKp30 in humans, J. Exp. Med. 206 (2009) 1495–1503.
[9] N. Anfossi, P. Andre, S. Guia, C.S. Falk, S. Roetynck, C.A. Stewart, V. Breso, C. Frassati, D. Reviron, D. Middleton, F. Romagne, S. Ugolini, E. Vivier, Human NK cell education by inhibitory receptors for MHC class I, Immunity 25 (2006) 331–342.
[10] C. Bottino, R. Castriconi, L. Moretta, A. Moretta, Cellular ligands of activating NK receptors, Trends Immunol. 26 (2005) 221–226.
[11] K. Karre, H.G. Ljunggren, G. Piontek, R. Kiessling, Selective rejection of H-2-deficient lymphoma variants suggests alternative immune defence strategy, Nature 319 (1986) 675–678.
[12] L.L. Lanier, B. Corliss, J.H. Phillips, Arousal and inhibition of human NK cells, Immunol. Rev. 155 (1997) 145–154.
[13] Y. Bartel, B. Bauer, A. Steinle, Modulation of NK cell function by genetically coupled C-type lectin-like receptor/ligand pairs encoded in the human natural killer gene complex, Front. Immunol. 4 (2013) 362.
[14] W.M. Yokoyama, B.F. Plougastel, Immune functions encoded by the natural killer gene complex, Nat. Rev. Immunol. 3 (2003) 304–316.
[15] D. Rozbesky, L. Ivanova, L. Hernychova, V. Grobarova, P. Novak, J. Cerny, Nkrp1 family, from lectins to protein interacting molecules, Molecules 20 (2015) 3463–3478.
[16] A.N. Zelensky, J.E. Gready, The C-type lectin-like domain superfamily, FEBS J. 272 (2005) 6179–6217.
[17] K.P. Kane, K.J. Lavender, B.J. Ma, Ly-49 receptors and their functions, Crit. Rev. Immunol. 24 (2004) 321–348.
[18] S. Bauer, V. Groh, J. Wu, A. Steinle, J.H. Phillips, L.L. Lanier, T. Spies, Activation of NK cells and T cells by NKG2D, a receptor for stress-inducible MICA, Science 285 (1999) 727–729.
[19] L.L. Lanier, C. Chang, J.H. Phillips, Human NKR-P1A. A disulfide-linked homodimer of the C-type lectin superfamily expressed by a subset of NK and T lymphocytes, J. Immunol. 153 (1994) 2417–2428.
[20] J. Spreu, S. Kuttruff, V. Stejfova, K.M. Dennehy, B. Schittek, A. Steinle, Interaction of C-type lectin-like receptors NKp65 and KACL facilitates dedicated immune recognition of human keratinocytes, Proc. Natl. Acad. Sci. U. S. A. 107 (2010) 5100–5105.
[21] S. Welte, S. Kuttruff, I. Waldhauer, A. Steinle, Mutual activation of natural killer cells and monocytes mediated by NKp80-AICL interaction, Nat. Immunol. 7 (2006) 1334–1342.
[22] I. Vogler, A. Steinle, Vis-a-vis in the NKC: genetically linked natural killer cell receptor/ligand pairs in the natural killer gene complex (NKC), J. Innate Immun. 3 (2011) 227–235.
[23] M. Exley, S. Porcelli, M. Furman, J. Garcia, S. Balk, CD161 (NKR-P1A) costimulation of CD1d-dependent activation of human T cells expressing invariant V alpha 24 J alpha Q T cell receptor alpha chains, J. Exp. Med. 188 (1998) 867–876.
[24] J.R. Fergusson, K.E. Smith, V.M. Fleming, N. Rajoriya, E.W. Newell, R. Simmons, E. Marchi, S. Bjorkander, Y.H. Kang, L. Swadling, A. Kurioka, N. Sahgal, H. Lockstone, D. Baban, G.J. Freeman, E. Sverremark-Ekstrom, M.M. Davis, M.P. Davenport, V. Venturi, J.E. Ussher, C.B. Willberg, P. Klenerman, CD161 defines a transcriptional and functional phenotype across distinct human T cell lineages, Cell Rep. 9 (2014) 1075–1088.
[25] B. Afzali, P.J. Mitchell, F.C. Edozie, G.A. Povoleri, S.E. Dowson, L. Demandt, G. Walter, J.B. Canavan, C. Scotta, B. Menon, P.S. Chana, W. Khamri, S.Y. Kordasti, S. Heck, B. Grimbacher, T. Tree, A.P. Cope, L.S. Taams, R.I. Lechler, S. John, G. Lombardi, CD161 expression characterizes a subpopulation of human regulatory T cells that produces IL-17 in a STAT3-dependent manner, Eur. J. Immunol. 43 (2013) 2043–2054.
[26] L. Cosmi, R. De Palma, V. Santarlasci, L. Maggi, M. Capone, F. Frosali, G. Rodolico, V. Querci, G. Abbate, R. Angeli, L. Berrino, M. Fambrini, M. Caproni, F. Tonelli, E. Lazzeri, P. Parronchi, F. Liotta, E. Maggi, S. Romagnani, F. Annunziato, Human interleukin 17-producing cells originate from a CD161+CD4+ T cell precursor, J. Exp. Med. 205 (2008) 1903–1916.
[27] E. Billerbeck, Y.H. Kang, L. Walker, H. Lockstone, S. Grafmueller, V. Fleming, J. Flint, C.B. Willberg, B. Bengsch, B. Seigel, N. Ramamurthy, N. Zitzmann, E.J. Barnes, J. Thevanayagam, A. Bhagwanani, A. Leslie, Y.H. Oo, S. Kollnberger, P. Bowness, O. Drognitz, D.H. Adams, H.E. Blum, R. Thimme, P. Klenerman, Analysis of CD161 expression on human CD8+ T cells defines a distinct functional subset with tissue-homing properties, Proc. Natl. Acad. Sci. U. S. A. 107 (2010) 3006–3011.
[28] V. Brucklacher-Waldert, K. Stuerner, M. Kolster, J. Wolthausen, E. Tolosa, Phenotypical and functional characterization of T helper 17 cells in multiple sclerosis, Brain J. Neurol. 132 (2009) 3329–3341.
[29] L. Estrada-Capetillo, B. Hernandez-Castro, A. Monsivais-Urenda, C. Alvarez-Quiroga, E. Layseca-Espinosa, C. Abud-Mendoza, L. Baranda, A. Urzainqui, F. Sanchez-Madrid, R. Gonzalez-Amaro, Induction of Th17 lymphocytes and Treg cells by monocyte-derived dendritic cells in patients with rheumatoid arthritis and systemic lupus erythematosus, Clin. Dev. Immunol. 2013 (2013) 584303.
[30] J.A. Smith, R.A. Colbert, Review: the interleukin-23/interleukin-17 axis in spondyloarthritis pathogenesis: Th17 and beyond, Arthritis & Rheumatol. 66 (2014) 231–241.
[31] A. Poggi, P. Costa, M.R. Zocchi, L. Moretta, Phenotypic and functional analysis of CD4+ NKRP1A+ human T lymphocytes. Direct evidence that the NKRP1A molecule is involved in transendothelial migration, Eur. J. Immunol. 27 (1997) 2345–2350.
[32] A. Poggi, P. Costa, M.R. Zocchi, L. Moretta, NKRP1A molecule is involved in

transendothelial migration of CD4+ human T lymphocytes, Immunol. Lett. 57 (1997) 121–123.
[33] V. Annibali, G. Ristori, D.F. Angelini, B. Serafini, R. Mechelli, S. Cannoni, S. Romano, A. Paolillo, H. Abderrahim, A. Diamantini, G. Borsellino, F. Aloisi, L. Battistini, M. Salvetti, CD161(high)CD8+T cells bear pathogenetic potential in multiple sclerosis, Brain J. Neurol. 134 (2011) 542–554.
[34] P. Chalan, J. Bijzet, M.G. Huitema, B.J. Kroesen, E. Brouwer, A.M. Boots, Expression of lectin-like transcript 1, the ligand for CD161, in rheumatoid arthritis, PLoS One 10 (2015) e0132436.
[35] H. Aldemir, V. Prod'homme, M.J. Dumaurier, C. Retiere, G. Poupon, J. Cazareth, F. Bihl, V.M. Braud, Cutting edge: lectin-like transcript 1 is a ligand for the CD161 receptor, J. Immunol. 175 (2005) 7791–7795.
[36] D.B. Rosen, J. Bettadapura, M. Alsharifi, P.A. Mathew, H.S. Warren, L.L. Lanier, Cutting edge: lectin-like transcript-1 is a ligand for the inhibitory human NKR-P1A receptor, J. Immunol. 175 (2005) 7796–7799.
[37] C. Germain, A. Meier, T. Jensen, P. Knapnougel, G. Poupon, A. Lazzari, A. Neisig, K. Hakansson, T. Dong, N. Wagtmann, E.D. Galsgaard, P. Spee, V.M. Braud, Induction of lectin-like transcript 1 (LLT1) protein cell surface expression by pathogens and interferon-gamma contributes to modulate immune responses, J. Biol. Chem. 286 (2011) 37964–37975.
[38] P. Roth, M. Mittelbronn, W. Wick, R. Meyermann, M. Tatagiba, M. Weller, Malignant glioma cells counteract antitumor immune responses through expression of lectin-like transcript-1, Cancer Res. 67 (2007) 3540–3544.
[39] C. Germain, T. Guillaudeux, E.D. Galsgaard, C. Hervouet, N. Tekaya, A.S. Gallouet, J. Fassy, F. Bihl, G. Poupon, A. Lazzari, P. Spee, F. Anjuere, C. Pangault, K. Tarte, P. Tas, L. Xerri, V.M. Braud, Lectin-like transcript 1 is a marker of germinal center-derived B-cell non-Hodgkin's lymphomas dampening natural killer cell functions, Oncoimmunology 4 (2015) e1026503.
[40] T. Skalova, J. Blaha, K. Harlos, J. Duskova, T. Koval, J. Stransky, J. Hasek, O. Vanek, J. Dohnalek, Four crystal structures of human LLT1, a ligand of human NKR-P1, in varied glycosylation and oligomerization states, Acta Crystallogr. D Biol. Crystallogr. 71 (2015) 578–591.
[41] J. Blaha, P. Pachl, P. Novak, O. Vanek, Expression and purification of soluble and stable ectodomain of natural killer cell receptor LLT1 through high-density transfection of suspension adapted HEK293S GnTI(-) cells, Protein Expr. Purif. 109 (2015) 7–13.
[42] J.V. Ravetch, L.L. Lanier, Immune inhibitory receptors, Science 290 (2000) 84–89.
[43] P. Kolenko, D. Rozbesky, O. Vanek, V. Kopecky Jr., K. Hofbauerova, P. Novak, P. Pompach, J. Hasek, T. Skalova, K. Bezouska, J. Dohnalek, Molecular architecture of mouse activating NKR-P1 receptors, J. Struct. Biol. 175 (2011) 434–441.
[44] D. Rozbesky, D. Kavan, J. Chmelik, P. Novak, O. Vanek, K. Bezouska, High-level expression of soluble form of mouse natural killer cell receptor NKR-P1C(B6) in Escherichia coli, Protein Expr. Purif. 77 (2011) 178–184.
[45] J. Kamishikiryo, H. Fukuhara, Y. Okabe, K. Kuroki, K. Maenaka, Molecular basis for LLT1 protein recognition by human CD161 protein (NKRP1A/KLRB1), J. Biol. Chem. 286 (2011) 23823–23830.
[46] P.J. Reeves, N. Callewaert, R. Contreras, H.G. Khorana, Structure and function in rhodopsin: high-level expression of rhodopsin with restricted and homogeneous N-glycosylation by a tetracycline-inducible N-acetylglucosaminyltransferase I-negative HEK293S stable mammalian cell line, Proc. Natl. Acad. Sci. U. S. A. 99 (2002) 13419–13424.
[47] N.S. Berrow, D. Alderton, S. Sainsbury, J. Nettleship, R. Assenberg, N. Rahman, D.I. Stuart, R.J. Owens, A versatile ligation-independent cloning method suitable for high-throughput expression screening applications, Nucleic Acids Res. 35 (2007) e45.
[48] L.E. Bird, High throughput construction and small scale expression screening of multi-tag vectors in Escherichia coli, Methods 55 (2011) 29–37.
[49] Y. Durocher, S. Perret, A. Kamen, High-level and high-throughput recombinant protein production by transient transfection of suspension-growing human 293-EBNA1 cells, Nucleic Acids Res. 30 (2002) E9.
[50] L.E. Bird, H. Rada, J. Flanagan, J.M. Diprose, R.J. Gilbert, R.J. Owens, Application of In-Fusion cloning for the parallel construction of E. coli expression vectors, Methods Mol. Biol. 1116 (2014) 209–234.
[51] J.E. Nettleship, P.J. Watson, N. Rahman-Huq, L. Fairall, M.G. Posner, A. Upadhyay, Y. Reddivari, J.M. Chamberlain, S.E. Kolstoe, S. Bagby, J.W. Schwabe, R.J. Owens, Transient expression in HEK 293 cells: an alternative to E. coli for the production of secreted and intracellular mammalian proteins, Methods Mol. Biol. 1258 (2015) 209–222.
[52] Y. Zhao, D.A. Chapman, I.M. Jones, Improving baculovirus recombination, Nucleic Acids Res. 31 (2003) E6. E6.
[53] P. Pompach, P. Man, D. Kavan, K. Hofbauerova, V. Kumar, K. Bezouska, V. Havlicek, P. Novak, Modified electrophoretic and digestion conditions allow a simplified mass spectrometric evaluation of disulfide bonds, J. Mass Spectrom. JMS 44 (2009) 1571–1578.
[54] M.M. Young, N. Tang, J.C. Hempel, C.M. Oshiro, E.W. Taylor, I.D. Kuntz, B.W. Gibson, G. Dollinger, High throughput protein fold identification by using experimental constraints derived from intramolecular cross-links and mass spectrometry, Proc. Natl. Acad. Sci. U. S. A. 97 (2000) 5802–5806.
[55] P. Schuck, Size-distribution analysis of macromolecules by sedimentation velocity ultracentrifugation and lamm equation modeling, Biophys. J. 78 (2000) 1606–1619.
[56] P. Schuck, On the analysis of protein self-association by sedimentation velocity analytical ultracentrifugation, Anal. Biochem. 320 (2003) 104–124.
[57] C.A. Brautigam, Calculations and publication-quality illustrations for analytical ultracentrifugation data, Methods Enzym. 562 (2015) 109–133.
[58] T. Skalova, K. Kotynkova, J. Duskova, J. Hasek, T. Koval, P. Kolenko, P. Novak, P. Man, P. Hanc, O. Vanek, K. Bezouska, J. Dohnalek, Mouse Clr-g, a ligand for NK cell activation receptor NKR-P1F: crystal structure and biophysical properties, J. Immunol. 189 (2012) 4881–4889.
[59] R. Linding, R.B. Russell, V. Neduva, T.J. Gibson, GlobPlot: exploring protein sequences for globularity and disorder, Nucleic Acids Res. 31 (2003) 3701–3708.
[60] A. Drozdetskiy, C. Cole, J. Procter, G.J. Barton, JPred4: a protein secondary structure prediction server, Nucleic Acids Res. 43 (2015) W389–W394.
[61] O. Vanek, M. Nalezkova, D. Kavan, I. Borovickova, P. Pompach, P. Novak, V. Kumar, L. Vannucci, J. Hudecek, K. Hofbauerova, V. Kopecky Jr., J. Brynda, P. Kolenko, J. Dohnalek, P. Kaderavek, J. Chmelik, L. Gorcik, L. Zidek, V. Sklenar, K. Bezouska, Soluble recombinant CD69 receptors optimized to have an exceptional physical and chemical stability display prolonged circulation and remain intact in the blood of mice, FEBS J. 275 (2008) 5589–5606.
[62] Y. Li, Q. Wang, S. Chen, P.H. Brown, R.A. Mariuzza, Structure of NKp65 bound to its keratinocyte ligand reveals basis for genetically linked recognition in natural killer gene complex, Proc. Natl. Acad. Sci. U. S. A. 110 (2013) 11505–11510.

Supplementary material

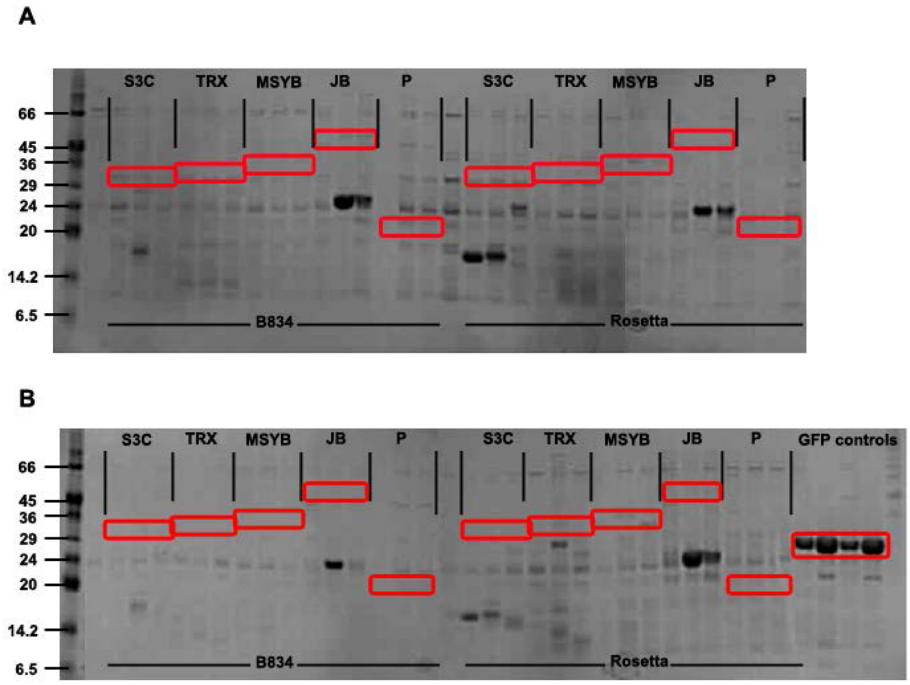

Fig. S1. Screening of the fusion tags for expression of NKR-P1 ectodomain in *E. coli*. Coomassie stained reducing 4-12% SDS-PAGE of His-tagged products enriched on Ni-NTA magnetic beads from soluble fraction of cell lysate of small-scale expression tests of three NKR-P1 constructs - I66/Q80/G90-S225 (displayed in that order); in pOPINS3C (S3C), pOPINTRX (TRX), pOPINMSYB (MSYB), pOPINJB (JB), and pOPINP (P) expression plasmids – annotated at the top. Expression tests were performed in *E. coli* B834(DE3) and Rosetta2(DE3) pLysS strains – annotated at the bottom, using two different production conditions – (A) an overnight production at 20°C after induction with 1 mM IPTG and (B) a production in Overnight Express Instant TB auto-induction media at 25°C for 20 h. Red rectangles highlight approximate area of expected products soluble fusion products. The positive GFP controls for the four experimental conditions are shown in the last four lanes in (B).

Table S1. Table of DNA primers used for PCR amplification. For In-Fusion cloning of the selected NKR-P1 construct into the set of pOPIN vectors, DNA primers contained a 5' overlap designed for the In-Fusion cloning into a linearized vector and a sequence specific for the selected NKR-P1 construct. The first part of the table shows the selected N-terminal/C-terminal NKR-P1 residue with the respective forward/reverse sequence specific for the given NKR-P1 construct. The second part of the table shows the pOPIN vectors used in this study with the respective set of restriction enzymes used for their linearization and specific 5' forward/reverse In-Fusion overlaps.

N-terminal AA	Construct specific forward sequence
I66	5'ATACAGAAATCATCAATAGAAAAATGCAGTGTGG3'
Q67	5'CAGAAATCATCAATAGAAAAATGCAGTGTGG3'
K68	5'AAATCATCAATAGAAAAATGCAGTGTGGAC3'
S69	5'TCATCAATAGAAAAATGCAGTGTGGACATTC3'
S70	5'TCAATAGAAAAATGCAGTGTGGACATTCAAC3'
I71	5'ATAGAAAAATGCAGTGTGGACATTCAACAG3'
E72	5'GAAAAATGCAGTGTGGACATTCAACAG3'
K73	5'AAATGCAGTGTGGACATTCAACAGAGC3'
C74	5'TGCAGTGTGGACATTCAACAGAGCAG3'
S75	5'AGTGTGGACATTCAACAGAGCAGGAATAAAAC3'
V76	5'GTGGACATTCAACAGAGCAGGAATAAAAC3'
D77	5'GACATTCAACAGAGCAGGAATAAAACAACAG3'
I78	5'ATTCAACAGAGCAGGAATAAAACAACAGAG3'
Q79	5'CAACAGAGCAGGAATAAAACAACAGAGAGACC3'
Q80	5'CAGAGCAGGAATAAAACAACAGAGAGACCG3'
S81	5'AGCAGGAATAAAACAACAGAGAGACCGGG3'
R82	5'AGGAATAAAACAACAGAGAGACCGGG3'
N83	5'AATAAAACAACAGAGAGACCGGGTCTCTTAAAC3'
K84	5'AAAACAACAGAGAGACCGGGTCTCTTAAACTG3'
T85	5'ACAACAGAGAGACCGGGTCTCTTAAACTGC3'
T86	5'ACAGAGAGACCGGGTCTCTTAAACTGCC3'
E87	5'GAGAGACCGGGTCTCTTAAACTGCCC3'
R88	5'AGACCGGGTCTCTTAAACTGCCC3'
P89	5'CCGGGTCTCTTAAACTGCCCAATATATTG3'
G90	5'GGTCTCTTAAACTGCCCAATATATTGGC3'
C-Terminal AA	**Construct specific reverse sequence**
S225	5'AGAGTCAGGATACACTTTATTTCTCACAGGTG3'

Vector	Restriction sites	Forward overlap	Reverse overlap
pOPINS3C pOPINTRX pOPINMSYB	KpnI HindIII	5'AAGTTCTGTTTCAGGGCC CG3'	5'ATGGTCTAGAAAGCTTTA3'
pOPINJB	KpnI SfoI	5'AAGTTCTGTTTCAGGGCC CG3'	5'AGATGTCGTTCAGGCC3'
pOPINP	KpnI PmeI	5'GCCCAGCCGGCGATGGC CATG3'	5'GTGATGGTGATGTTT3'
pOPING pOPINTTGneo	KpnI PmeI	5'GCGTAGCTGAAACCGGC3'	5'GTGATGGTGATGTTT3'

Table S2. Table of cystic peptides identified for NKR-P1. First column shows identified peptides/cystic dipeptides (numbered relative to the expressed NKR-P1 construct, i.e. ETG-G90-S225-KHHHHHH) based on which a disulphide bond or N-linked glycosylation was assigned in the second column (presence of N-bound HexNAc is also indicated, in this case this corresponds to the first GlcNAc unit left after the cleavage of protein by endoglycosidase Endo Hf). Theoretical and experimental masses of measured peptides, mass error and intensity are shown in the third, fourth, fifth and sixth column, respectively.

Identified peptide(s)	Cys-Cys cross-link	Theoretical mass	Experimental mass	Error (ppm)	Intensity
35-47/119-137	C122-C210	3834.0408	3834.037	0.9	2.30E+07
100-121	C189-C202	2497.0862	2497.083	1.4	2.40E+08
97-118	C189-C202	2413.0176	2413.012	2.3	4.11E+06
100-121	C189-C202	2497.0862	2497.081	2	1.14E+06
1-39/122-126	C94-C105, C122-C210, N116-HexNAc	5354.5532	5354.544	1.8	2.17E+07
1-34	C94-C105, N116-HexNAc	4146.022	4146.026	1.1	9.91E+08
61-80	N157-HexNAc	2612.3762	2612.372	1.5	1.72E+06
35-75	N157-HexNAc	4948.6133	4948.612	0.3	1.03E+08
48-80	N157-HexNAc	4188.2134	4188.208	1.3	9.24E+05
61-90	N157-HexNAc,N169-HexNAc	3947.9858	3947.98	1.4	4.39E+06
48-90	N157-HexNAc,N169-HexNAc	5523.8232	5523.812	2	9.39E+05
81-95	N169-HexNAc	1980.9666	1980.963	2	3.27E+08
81-99	N169-HexNAc	2352.147	2352.143	1.9	2.80E+07
78-95	N169-HexNAc	2409.1838	2409.179	1.8	5.11E+06
76-90	N169-HexNAc	2039.9827	2039.98	1.4	9.54E+07
81-95	N169-HexNAc	1980.9666	1980.964	1.4	7.60E+07
78-95	N169-HexNAc	2409.1838	2409.18	1.5	2.38E+06

PUBLICATION II

Vaněk O, Celadova P, Skořepa O, Bláha J, Kalousková B, Dvorská A, Poláchová E, Pucholtová H, Kavan D, Pompach P, Hofbauerová K, Kopecký V Jr, Mesci A, Voigt S, Carlyle JR.

Production of recombinant soluble dimeric C-type lectin-like receptors of rat natural killer cells.

Sci. Rep. 9(1):17836 (2019)
Erratum (publisher correction) in: Sci Rep. 10(1):2828 (2020)

My contribution to the publication: performing research (cloning, recombinant protein expression and purification, cell line cultivation and transfection optimisation)

www.nature.com/scientificreports

SCIENTIFIC REPORTS
nature research

OPEN

Production of recombinant soluble dimeric C-type lectin-like receptors of rat natural killer cells

Ondřej Vaněk[1*], Petra Celadova[1], Ondřej Skořepa[1], Jan Bláha[1,6], Barbora Kalousková[1], Anna Dvorská[1], Edita Poláchová[1], Helena Pucholtová[1], Daniel Kavan[1,2], Petr Pompach[2], Kateřina Hofbauerová[2,3], Vladimír Kopecký[3], Aruz Mesci[4], Sebastian Voigt[5] & James R. Carlyle[4]

Working at the border between innate and adaptive immunity, natural killer (NK) cells play a key role in the immune system by protecting healthy cells and by eliminating malignantly transformed, stressed or virally infected cells. NK cell recognition of a target cell is mediated by a receptor "zipper" consisting of various activating and inhibitory receptors, including C-type lectin-like receptors. Among this major group of receptors, two of the largest rodent receptor families are the NKR-P1 and the Clr receptor families. Although these families have been shown to encode receptor-ligand pairs involved in MHC-independent self-nonself discrimination and are a target for immune evasion by tumour cells and viruses, structural mechanisms of their mutual recognition remain less well characterized. Therefore, we developed a non-viral eukaryotic expression system based on transient transfection of suspension-adapted human embryonic kidney 293 cells to produce soluble native disulphide dimers of NK cell C-type lectin-like receptor ectodomains. The expression system was optimized using green fluorescent protein and secreted alkaline phosphatase, easily quantifiable markers of recombinant protein production. We describe an application of this approach to the recombinant protein production and characterization of native rat NKR-P1B and Clr-11 proteins suitable for further structural and functional studies.

Natural killer (NK) cells are innate immune lymphocytes capable of recognizing and destroying a wide variety of target cells, including transformed, infected, transplanted, antibody-coated, and stressed cells[1]. In contrast to T or B cells, NK cells do not express a single dominant activation receptor on their surface. Instead, the functions of these immune effector cells are regulated by a high number of receptors that generate either inhibitory or activation signals through the large "receptor zipper"[2]. These receptors belong to two major protein families similar to members of the immunoglobulin or C-type lectin superfamilies[3]. Inhibitory C-type lectin receptors, such as Ly-49 proteins or CD94/NKG2A heterodimers, recognize MHC class I glycoproteins on the surface of healthy cells and efficiently block the natural killing of these cells. However, in pathological states, target cells often lose inhibitory "self" ligands, leading to enhanced cytotoxicity via NK cell disinhibition. This mode of detection has been termed "missing-self" recognition[4]. Conversely, stressed, transformed or infected cells often overexpress some proteins that are usually in low abundance, on healthy cells. These proteins might be recognized by activating receptors (induced-self-recognition), as in the case of the stress-induced MHC class I-like molecules MICA and MICB, which are recognized by the NKG2D activation C-type lectin-like receptor[5].

In addition to Ly-49, the NKR-P1 (CD161) receptor family, which is the second largest group of receptors encoded by distinct but closely related genes of the NK gene complex, may generate both activation and inhibitory signals in NK cells. This protein family was first identified on the surface of rat natural killer cells using

[1]Department of Biochemistry, Faculty of Science, Charles University, Hlavova 2030/8, 12840, Prague, Czech Republic. [2]Institute of Microbiology, The Czech Academy of Sciences, Vídeňská 1083, 14220, Prague, Czech Republic. [3]Institute of Physics, Faculty of Mathematics and Physics, Charles University, Ke Karlovu 5, 12116, Prague, Czech Republic. [4]Department of Immunology, University of Toronto, 1 King's College Circle, M5S 1A8, Toronto, ON, Canada. [5]Department of Infectious Diseases, Robert Koch Institute, Seestraße 10, 13353, Berlin, Germany. [6]Present address: EMBL Hamburg, c/o DESY, Building 25A, Notkestraße 85, 22603, Hamburg, Germany. *email: ondrej.vanek@natur.cuni.cz

a specific monoclonal antibody 3.2.3[6]. Subsequent studies showed that NKR-P1 (CD161) receptors consist of homodimeric type II transmembrane C-type lectin-like proteins primarily found on NK, NKT, and activated $CD8^+$ T cells[7]. Genes encoding the NKR-P1 family (designated *Klrb1*) appear to be conserved amongst birds, rodents, humans, and other mammals, suggesting that the gene products play a key role in innate immunity across species boundaries[8]. The NKR-P1 receptors consist of N-terminal peptide motifs involved in receptor signalling, a single transmembrane domain, an extended stalk region that includes the putative dimerization cysteine(s), and a large C-terminal ligand binding domain similar to the carbohydrate-recognition domain of C-type lectins[9].

The discovery that physiological ligands of at least some NKR-P1 receptors belong to a family of related C-type lectin-like receptors, the C-type lectin-related (Clr) proteins, which are encoded by a family of *Clec2* genes interspersed among the *Klrb1* genes themselves, was a breakthrough in understanding NKR-P1 function[10,11]. These studies have shown that mouse NKR-P1B recognizes Clr-b and that transfected cells expressing Clr-b are partly protected from lysis by NK cells, thus suggesting that NKR-P1B:Clr-b recognition is a novel form of missing-self recognition designed to monitor the cellular levels of Clr-b. Accordingly, genetic linkage of the *Clec2* and *Klrb1* genes highlighted the importance of this system as a particularly unique self/non-self discrimination tool because the "self" ligand is always coinherited with its cognate receptor[7,12]. These findings established a new paradigm of lectin-like receptors that interact with other lectin-like proteins rather than with carbohydrates, although the role of receptor and ligand glycosylation in these interactions remains unknown.

In addition to mice, this MHC-independent self-recognition system is conserved at least in rats[13] and humans[14,15]. Similarly to MHC-I molecules, this self-recognition system is also subject to viral and tumour evasion of innate and adaptive immunity. In humans, the LLT1 receptor, an orthologue of rodent Clr proteins, is upregulated in glioblastoma[16], in prostate cancer[17] and in B-cell non-Hodgkin's lymphoma[18], in which the receptor mediates immune escape and contributes to the immunosuppressive properties of tumour cells. Conversely, rat cytomegalovirus encodes a protein named RCTL that closely resembles rat Clr-11 (a homolog of mouse Clr-b). Viral infection stimulates Clr-11 loss, which is rapidly counteracted by RCTL surface expression upregulation. RCTL inhibits NK killing of infected cells via direct interaction with NKR-P1B. Thus, RCTL functions as a decoy ligand to subvert NKR-P1B mediated missing-self recognition by NK cells[19]. Interestingly, this subversion is strain-dependent: the NKR-P1B receptor from the WAG rat strain is susceptible to RCTL binding, whereas the NKR-P1B receptor from the SD rat strain is less susceptible, thereby overcoming this decoy inhibition signal. The allelic divergence of rodent NKR-P1 receptors suggests that host genomes are evolving under selection pressure to avert this viral evasion strategy[7,20]. Similarly, in mice, Clr-b loss was observed upon murine cytomegalovirus (MCMV) infection[21]. Furthermore, the MCMV-encoded immunoevasin m12 was observed to engage the inhibitory NKR-P1B receptor, thus subverting the NKR-P1B:Clr-b immune axis. However, a similar host-pathogen evolutionary interplay is revealed by the engagement of some of the m12 alleles through the activating NKR-P1A/C receptors that avert the MCMV decoy strategy[22]. The mouse Clr-b ligand is also a very sensitive marker of cell health that is rapidly downregulated during chemotherapy-induced genotoxic and cellular stress[23] or poxvirus infection[24] or oncogenesis[25]. Concomitantly, recent studies showed that NKR-P1B:Clr-b missing-self recognition plays a key and non-redundant role in bone marrow transplantation[26,27] and cancer immunosurveillance[25] in a mouse models.

Although the structures of a few mouse NKR-P1 and Clr proteins, as well as the structure of the mouse NKR-P1B:m12 complex, were published[22,28,29], only limited structural data on the NKR-P1:Clr receptor complex are available yet. In some cases, the preparation of soluble C-type lectin-like receptor domains by recombinant expression in *E. coli* followed by *in vitro* refolding might be relatively easy[28,29]. However, this strategy also has several disadvantages. The refolding yields are often too low for structural studies, and the number of cysteine residues present in the expression constructs is usually kept as low as possible, leading to monomeric recombinant proteins (or non-covalent dimers, at best). However, native C-type lectin-like NK receptors are often homodimers linked by one or several disulphide bridges[30], and stable dimer formation might also be a prerequisite for complex formation. Moreover, the role of glycosylation in NKR-P1:Clr recognition could not be ascertained using bacterially expressed proteins.

In this report, we describe a eukaryotic expression system based on transient transfection of a human embryonic kidney 293 (HEK293) cell line to produce native dimeric NK cell C-type lectin-like receptors for structural and functional studies. In contrast to stable transfection and cell line generation, transient transfection offers a quick modularity of the expression construct regarding the purification or visualization tag(s), if necessary. Simultaneously, by using cost-effective transfection reagents, affordable cell culture media and strong expression vectors, milligram amounts of recombinant proteins can be generated within days at only moderate costs and production equipment requirements[31,32]. Moreover, successful selenomethionine incorporation and N-linked glycosylation control, which are important for structural biology, particularly for protein crystallography, were shown in HEK293 cell lines[32,33]. Here, we report the successful application of this technique to the recombinant production of rat C-type lectin-like NK cell receptors.

Results

Optimized transient transfection of suspension-adapted HEK293T cells. Transient transfection of adherent HEK293T cell lines with several pHLsec plasmids has been successfully used for recombinant protein expression[32]. However, in our laboratory, the growth of high cell quantities in expanded surface roller bottles was rather difficult due to uneven cell attachment to the surface of the culture bottles. Moreover, the expansion of adherent culture prior to large-scale transient transfection using this method was a time-consuming, labour-intensive, and material-demanding procedure. Therefore, we decided to switch to suspension culture, which is affordable (glass bottles can be autoclaved and reused easily), scalable in a range from a few millilitres to hundreds of litres and may yield potentially higher volumetric productivity.

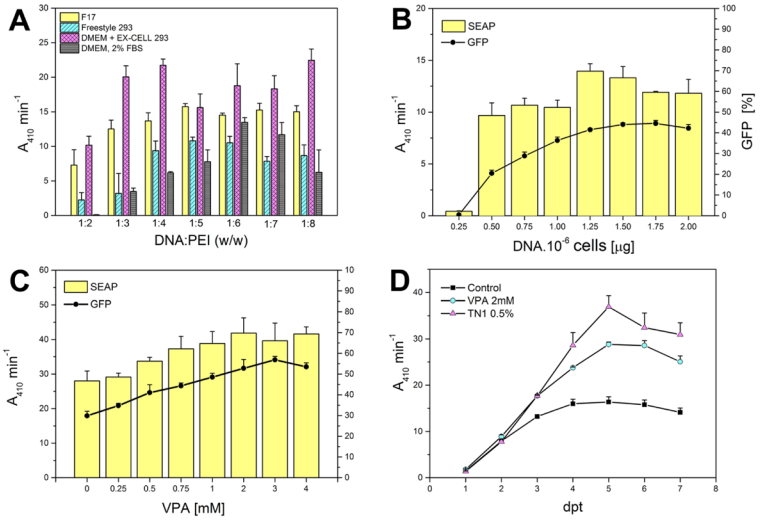

Figure 1. Optimization of transient transfection of suspension adapted HEK293T cells. (**A**) Effect of the DNA-to-PEI ratio on SEAP production in different transfection and production media. (**B**) Effect of the amount of DNA added to the cells. (**C**) Enhancement of transient expression by valproic acid addition at 3 hours post-transfection; transfections were performed in 24-well plates, as described in Materials and Methods, SEAP activity and transfection efficiency were determined 3 days post-transfection (dpt) by measuring the pNPP hydrolysis rate and by flow cytometry (GFP positive viable cells), respectively. (**D**) Transient transfection expression levels as a function of time; SEAP activity was measured each dpt in a control culture, in a culture supplemented with 2 mM VPA and in a culture fed at 2 dpt with 0.5% TN1 hydrolysate; transfections were performed in a 12-well plate, as described in the Materials and Methods section.

An aliquot of 5×10^6 adherent HEK293T cells was thawed and transferred directly into 10 ml of EX-CELL 293 serum-free media, in a 10-cm culture dish. Small floating clumps of cells resumed growth one day later. The culture was pipette-resuspended and split into fresh medium every three days, and we considered the cells fully adapted to serum-free conditions after six splits. Then, we transferred the cell suspension into a square-shaped glass bottle, which was placed on an orbital shaker inside the incubator. Cells resumed growth one day later and grew with a doubling time of approximately 24 h. The EX-CELL 293 medium supports HEK293T high-density cultivation (up to 6×10^6/ml with no apparent loss of viability) and is also suitable for freezing the cells (up to 5×10^7/ml with 5–10% DMSO tested). In contrast, EX-CELL 293 is unsuitable for polyethylenimine (PEI) mediated transfection, most likely due to the presence of negatively charged additives (such as heparin, often used to dissociate cell clumps), which disrupt DNA-PEI transfection polyplexes. We screened several other media for their transfection and production properties using secreted alkaline phosphatase (SEAP) and green fluorescent protein (GFP) as easily quantifiable reporter proteins to monitor secreted protein production and transfection efficiency, respectively. A small volume of cell suspension was transfected with a 19:1 (w/w) mixture of SEAP and GFP expression plasmids, and SEAP activity and transfection efficiency were measured 72 hours later. From the two commercial media tested, F17 medium allows the use of lower DNA:PEI ratios, thus minimizing the risk of potential cytotoxic effects of high PEI concentrations (Fig. 1A). Because the original adherent HEK293T cells were easily transfected in standard DMEM medium supplemented with 2% FBS, we assessed whether these conditions could be modified for suspension conditions. By omitting calcium chloride from the DMEM formulation and by supplementing it with 0.1% Pluronic F-68 instead, we were able to maintain the cells in suspension, although the addition of 2% FBS caused cell aggregation. Conversely, the highest SEAP activities were achieved when transfection was performed in half the desired culture volume of calcium-free DMEM, which was completed with EX-CELL 293 to the full volume 3 hours post-transfection (Fig. 1A). All subsequent transfections were performed in calcium-free DMEM/EX-CELL 293 at a 1:4 (w/w) DNA:PEI ratio.

To maximize the expression yield, we assessed the effect of the DNA amount added to the cells. As shown in Fig. 1B, the amount of DNA necessary for sufficient transfection efficiency and SEAP expression could not be reduced below 1 µg/10^6 cells under these conditions. However, both transfection efficiency and SEAP expression almost doubled when valproic acid was added 3 hours after transfection (Fig. 1C). Valproic acid is a histone deacetylase inhibitor reported to enhance transient gene expression in both HEK293 and CHO cell lines[34] by increasing the overall transcription level while simultaneously inhibiting cell growth[35]. The positive effect of

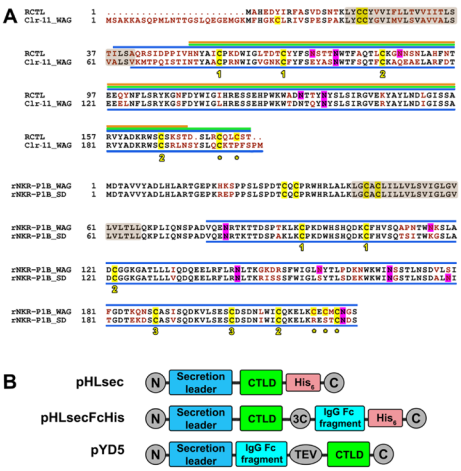

Figure 2. Sequence alignment and design of protein expression constructs. (**A**) Amino acid sequences of rat Clr-11^{WAG}, RCTL, NKR-P1B^{WAG}, and NKR-P1B^{SD} (GenBank accession nos. DQ168419.1, AF302184, EF100678, and EF100684, respectively) were aligned in ClustalW2; non-identical amino acids are indicated in red; transmembrane regions (as predicted by TMHMM 2.0 server) are highlighted in the brown box; cysteine residues are highlighted in yellow, and cysteine residues conserved among C-type lectin-like receptors and forming intramolecular disulphide bridges are numbered according to their linkage, whereas those expected to form intermolecular disulphide bridges are indicated with an asterisk; potential sites of N-glycosylation are highlighted in magenta; the recombinant protein constructs corresponding to C-type lectin-like domain (CTLD) are indicated with blue lines; the following three constructs were generated in case of RCTL: I38-T180 (blue line), H51-T180 (green line), and H51-T170 (orange line). (**B**) Schematic description of protein expression constructs designed using the three plasmids used in this work.

valproic acid (VPA) on transient SEAP expression was confirmed in a time-course study of SEAP expression levels (Fig. 1D). VPA-treated cells analysed by flow cytometry consistently showed a higher level of transfection efficiency and also much higher GFP median fluorescence intensity (data not shown), thus indicating the higher specific productivity of cells transcriptionally activated with VPA. Concurrently, we tried to further boost the expression yield by feeding the cells with casein hydrolysate Tryptone N1 during the production phase, which was previously reported to enhance the productivity of HEK293EBNA cell lines[36]. Peptone additives are often used to replenish nutrients during batch cell culture, and the positive effect of Tryptone N1 (TN1) was also shown in HEK293T cell lines (Fig. 1D). In summary, the optimal values of the transfection and expression parameters were determined for suspension-adapted HEK293T cells through a series of independent experiments, i.e., 1 μg/10^6 cells for DNA, 1:4 for DNA:PEI ratio, calcium-free DMEM and EX-CELL 293 as transfection and production media, respectively, and the expression yield was further enhanced by adding 2 mM VPA and 0.5% TN1, 3 and 48 hours post-transfection, respectively.

Construct design and recombinant expression of soluble rat NK cell lectin-like receptors. We selected rat NK cell C-type lectin-like receptors as a model system to study NKR-P1:Clr interactions. In particular, rat inhibitory NKR-P1B receptors from the WAG and SD rat strains differ in several amino acid residues (Fig. 2A), and these differences lead to differential outcomes when WAG or SD rat strains are challenged by cytomegalovirus infection due to different mechanisms of recognition of the viral RCTL decoy ligand[19]. Conversely, Clr-11 ligand from the WAG and SD rat strains differ only in a single amino acid (R192K in the WAG or SD strain, respectively, not shown) located in the C-terminus of the protein and unlikely involved in receptor binding. Therefore, we consider both Clr-11 sequences functionally equal, and we omitted Clr-11^{SD} from the present study. Clr-11^{WAG} and RCTL sequence alignment (Fig. 2A) shows a highly conserved core of the C-type lectin-like domain surrounded by more variable N- and C-terminal sequences of the extracellular portion of the receptor. The C-type lectin-like domain of NK cell receptors usually contains four to eight conserved cysteine residues responsible for intramolecular disulphide bond formation. These residues are necessary to stabilize the domain fold and several additional cysteine residues in the N- or C-terminal chains involved in dimerization by forming an intermolecular disulphide bridge(s). Furthermore, they are presumably required for stable receptor expression at the cell surface. Interestingly, all four receptors contain their proposed dimerization cysteine residues in their C-termini, suggesting that the N-terminal domain chain may not be necessary for dimer formation in these proteins.

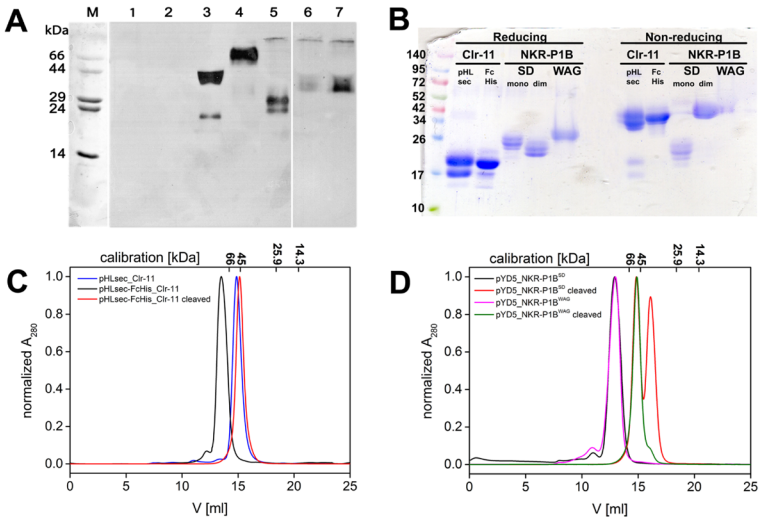

Figure 3. Expression and purification of soluble dimeric rat NK cell C-type lectin-like receptors. (**A**) Small-scale expression test of pHLsec constructs; transfection was performed in a 24-well plate, and 10 µl samples of culture supernatants were collected 3 days later and resolved by 15% SDS-PAGE under non-reducing conditions, transferred onto nitrocellulose membrane and detected by PentaHis mAb; lanes: M, marker; 1, mock transfected; 2, RCTL I38-T180; 3, Clr-11; 4, NKR-P1B^{WAG}; 5, NKR-P1B^{SD}; 6, RCTL H51-T180; 7, RCTL H51-T170. Full-size images of membranes and their photographs are available as Supplementary Information (Figure S1). (**B**) Samples of purified proteins were resolved by 4–20% SDS-PAGE under both reducing and non-reducing conditions; lanes: pHLsec_Clr-11, pHLsec-FcHis_Clr-11 cleaved off by a 3C protease, pYD5_NKR-P1B^{SD} (monomeric and dimeric fractions) and pYD5_ NKR-P1B^{WAG}, both cleaved off by TEV protease. (**C**) Gel filtration profiles of Clr-11, Clr-11-FcHis, and Clr-11 with the FcHis tag cleaved off by a 3C protease. (**D**) Gel filtration profiles of pYD5 Fc-NKR-P1B$^{SD/WAG}$ fusion proteins and NKR-P1B$^{SD/WAG}$ with the Fc tag cleaved off by TEV protease, resulting in the disulphide dimer of NKR-P1B^{WAG} and a mixture of dimer and monomer species of NKR-P1B^{SD}.

Initially, we tried to express the whole extracellular part of RCTL, Clr-11^{WAG}, and both the NKR-P1B^{WAG} and NKR-P1B^{SD} receptors with only slightly shortened N-termini, i.e., including the stalk region. Thus, four expression constructs were generated by PCR amplification from their respective receptor cDNA templates: RCTL I38-T180, Clr-11^{WAG} V65-M207, NKR-P1B^{WAG} V78-S223, and NKR-P1B^{SD} V78-S223. These constructs were cloned to pHLsec expression vector for secreted protein production (Fig. 2B). The vector adds an additional ETG and GTKHHHHHH amino acid sequences to the N- and C-termini of the construct, respectively[32]. Small-scale expression tests (Fig. 3A, lanes 2–5) showed positive expression for all except for the RCTL constructs, moreover, the NKR-P1B^{WAG} were purely dimeric, Clr-11^{WAG} was mostly dimeric, and NKR-P1B^{SD} was monomeric. To also achieve some expression level for the RCTL protein, two shorter constructs were prepared, RCTL H51-T180 and RCTL H51-T170, and the latter was expressed as a monomer, although at a much lower yield (Fig. 3A, lanes 6 and 7). When expressed by transient transfection in square-shaped bottles and purified by IMAC and gel filtration, the final yield of the pure recombinant receptors ranged from 0.2 to 5 mg per litre of production medium, and Clr-11 and RCTL were the best- and worst-produced proteins, respectively.

Generation of dimeric Clr-11^{WAG} by C-terminal Fc fusion. Regarding structural biology and protein crystallography, minor heterogeneities, such as incomplete covalent dimerization of Clr-11^{WAG} (Fig. 3B, lanes pHLsec_Clr-11), potentially leaving some flexible parts unstructured, can be detrimental to the quality and usefulness of the final protein preparation. Additionally, glycosylation heterogeneity or the differential occupation of glycosylation sites (the likely reason for the presence of two bands in Clr-11 preparations, Fig. 3B, lanes pHLsec_Clr-11) may increase sample heterogeneity even further. To overcome the first issue, we cloned the Clr-11^{WAG} expression construct into the pHLsec-FcHis vector. In this vector, the C-terminus of the expression construct is fused to human rhinovirus (HRV) 3C protease cleavage site followed by the hinge and the Fc regions of the human IgG1 molecule, and by a hexahistidine tag (Fig. 2B). This FcHis fusion was used to promote the disulphide bond-mediated dimerization of Clr-11 because IgG is a disulphide-linked dimer itself and therefore IgG hinge dimerization may help to position the Clr-11^{WAG} dimerization cysteine residues close enough to enable disulphide

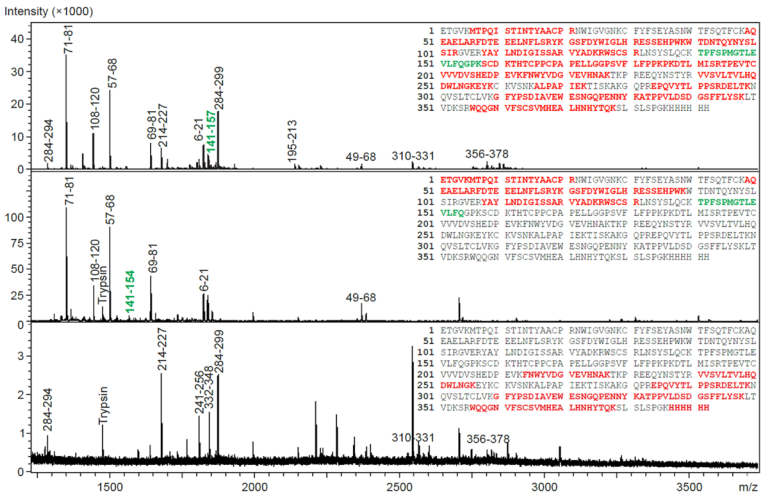

Figure 4. Mass spectrometry analysis of Clr-11-FcHis cleavage with HRV 3C protease. Reduced tryptic digests prepared from SDS-PAGE bands of Clr-11-FcHis (top), Clr-11 with the FcHis fusion cleaved off (middle) and the cleaved FcHis fusion (bottom) were analysed by MALDI-TOF/TOF mass spectrometry. Peptides identified in mass spectra are highlighted in red; peaks in mass spectra are labelled according to corresponding Clr-11-FcHis peptide sequences. The 3C protease cleavage site peptide TPFSPMGTLEVLFQ/GPK is highlighted in green.

bond formation. The expression and purification of Clr-11-FcHis protein was straightforward and at a yield similar to that of the untagged protein, resulting in a purely dimeric fusion Clr-11-FcHis preparation (Fig. 3C, black curve).

The HRV 3C protease preferably cleaves under reducing conditions; however, complete digestion may also be achieved by slightly increasing the protease amount under non-reducing conditions. When applied to the Clr-11-FcHis protein, we observed complete cleavage after one hour at room temperature (data not shown); nevertheless, we chose overnight cleavage at 4 °C for convenience and for lower protease consumption. Because both FcHis fusion and 3C protease contain the histidine tag, we were able to easily separate the cleaved fusion, protease and purely dimeric Clr-11^{WAG} by repeating the purification procedure (Fig. 3C, red curve). Interestingly, the production of Clr-11 with the FcHis fusion also leads to a reduced level of glycosylation heterogeneity, as suggested by the presence of a single band on the SDS-PAGE (Fig. 3B, lane pHLsec-FcHis_Clr-11). When required, glycosylation heterogeneity might be further reduced using N-glycosylation processing inhibitors, such as kifunensine or swainsonine[33], or the N-acetylglucosaminyltransferase I-negative (GnTI$^-$) HEK293S cell line[37], which is unable to synthesize complex N-glycans.

Mass spectrometry characterization of Clr-11-FcHis cleavage and dimerization. To confirm disulphide bond status and correct covalent dimer formation, we analysed the SDS-PAGE bands of uncleaved and cleaved Clr-11-FcHis proteins by mass spectrometry. The protein bands were excised and digested by trypsin directly within the gel; the resulting peptides were extracted, reduced and analysed in MALDI-TOF/TOF mass spectrometer (Fig. 4). All three samples analysed showed good sequence coverage. The cleavage site TPFSPMGTLEVLFQ/GPK was identified in Clr-11-FcHis but not in Clr-11, where the FcHis fusion was cleaved off and replaced by the TPFSPMGTLEVLFQ peptide, corresponding to the correct fusion cleavage. When examining Clr-11-FcHis and Clr-11 tryptic and Asp-N peptides prepared under non-reducing conditions, we were able to confirm the correct intramolecular disulphide bond connection (data not shown) of all four cysteines present in the C-type lectin-like domain (CTLD), i.e., C80-C91 and C108-C190. More importantly, we were also able to distinguish a cystine dipeptide LNSYSLQCK-LNSYSLQCK, corresponding to the correct covalent intermolecular C200-C200 disulphide bond, and stable dimer formation (Fig. 5).

Generation of dimeric NKR-P1B by N-terminal Fc fusion. Subsequently, we tried to apply the same approach to NKR-P1B^{SD} and NKR-P1B^{WAG}, i.e., to produce these expression constructs as C-terminal FcHis fusions to promote their dimerization. Although we were able to express and purify these fusion proteins in a dimeric form and at a good yield (improved in comparison with the untagged proteins; data not shown), we were unable to efficiently cleave off the FcHis fusion with the 3C protease. A possible explanation is that the dimerization cysteines of the receptor and of the IgG hinge region cross-linked with each other. Thus, although

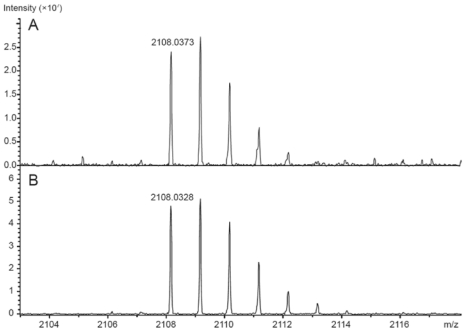

Figure 5. Mass spectrometry analysis of Clr-11 covalent dimerization. MALDI TOF/TOF analyses of tryptic digests of (**A**) Clr-11-FcHis and (**B**) Clr-11 after 3C protease cleavage, both prepared under non-reducing conditions. The m/z value 2108.03 corresponds to the dimerization cystine dipeptide LNSYSLQCK-LNSYSLQCK.

these recombinant fusion proteins are dimeric, their dimerization mode may not be physiological. Reducing the number of cysteine residues in the hinge region or completely removing them from the expression constructs may promote correct dimerization exclusively through the CTLD cysteines.

To overcome this problem, we tested the reverse arrangement of these Fc fusion constructs, i.e., we attached the IgG Fc region to the N-terminus of the NKR-P1B ectodomain using a pYD5 plasmid (Fig. 2B), enabling the subsequent cleavage of the fusion by the tobacco etch virus (TEV) protease. The expression yields of the pYD5_NKR-P1B$^{SD/WAG}$ fusion constructs were similar to those of previous FcHis constructs, and gel filtration showed their correct dimeric state (Fig. 3D, black and magenta curve). Upon cleavage with the TEV protease, we obtained the purely disulphide dimer of the NKR-P1B^{WAG} ectodomain (Fig. 3D, green curve and Fig. 3B, lanes WAG), whereas the NKR-P1B^{SD} ectodomain yielded a mixture of dimeric and monomeric species (Fig. 3D, red curve and Fig. 3B, lanes SD). This difference is likely caused by the fact that NKR-P1B^{WAG} has three cysteine residues in its C-terminus, whereas NKR-P1B^{SD} has a single cysteine in the same position; therefore, disulphide dimerization is more efficient in the NKR-P1B^{WAG} ectodomain.

For the RCTL protein, we were unable to improve its expression yield and dimeric state, even when using FcHis or pYD5 fusion constructs; therefore, we are not yet able to report the successful preparation of any stable soluble form, monomeric or dimeric, of this viral decoy protein in reasonable yield. RCTL is apparently much less stable than its host NK cell counterpart, and its preparation will require further optimization.

Sedimentation analysis confirms dimeric status of prepared proteins. To further characterize the solution behaviour of the prepared dimeric proteins, sedimentation analysis was performed in an analytical ultracentrifuge. Gel filtration suggested that Clr-11 prepared using a histidine-tagged construct (showing incomplete covalent dimerization, Fig. 3B, lanes pHLsec_Clr-11) and the purely dimeric Clr-11 cleaved from the FcHis fusion construct migrate at the same position (Fig. 3C, blue and red curve), thus suggesting that Clr-11 likely forms a stable non-covalent dimer in solution, even in absence of the stabilizing disulphide bridge. Sedimentation velocity experiments performed with the histidine-tagged Clr-11 showed a single peak in the sedimentation coefficient distribution (Fig. 6A, bottom) with an $s_{20,w}$ value of 3.04 ± 0.2 S, which corresponds to a dimeric protein with a moderately elongated shape and with predicted dimensions of approximately 8–10 × 3–4 nm. However, the broad shape of the peak in sedimentation coefficient distribution suggests the presence of monomer-dimer equilibrium at lower protein concentrations. The weight-average molecular weight of 40837 ± 500 Da was calculated based on the results from the sedimentation equilibrium experiment (Fig. 6B), which also matched the value expected for the glycosylated dimer ($2 \times 18211 = 36422$ Da for the dimeric protein itself + mass of up to 4 N-glycosylation sites occupied per dimer).

Similarly, the sedimentation velocity analyses performed for Clr-11 cleaved from pHLsec-FcHis and for both NKR-P1B^{SD} and NKR-P1B^{WAG} cleaved from pYD5 fusion constructs fully confirmed their entirely dimeric state, yielding $s_{20,w}$ values of 3.10 ± 0.05 S, 3.45 ± 0.05 S and 3.68 ± 0.1 S, respectively (Fig. 6C, solid coloured lines). The shift of these individual sedimentation coefficient values reflects the difference in molecular weight of the individual protein expression constructs and differences in the number of their N-glycosylation sites. Compared with histidine-tagged Clr-11 expressed from the pHLsec vector, Clr-11 cleaved from the pHLsec-FcHis construct is much more homogeneous and shows no sign of monomer-dimer equilibrium (Fig. 6C, black vs. red solid lines). We have also analysed the entire Fc-fusion proteins (Fig. 6C, dashed coloured lines). Their resulting peaks of these ca 100 kDa dimeric fusion glycosylated constructs with apparent sedimentation coefficient values ranging from 5 to 5.5 S correspond to the size and shape of expected elongated particles with estimated dimensions of 13–15 × 4–5 nm. Thus, a fusion of extracellular parts of C-type lectin-like receptors to the Fc region of human IgG is not only an efficient method of preparation of disulphide dimers of these receptors, but also a strategy for the generation of immunoactive constructs with therapeutic potential.

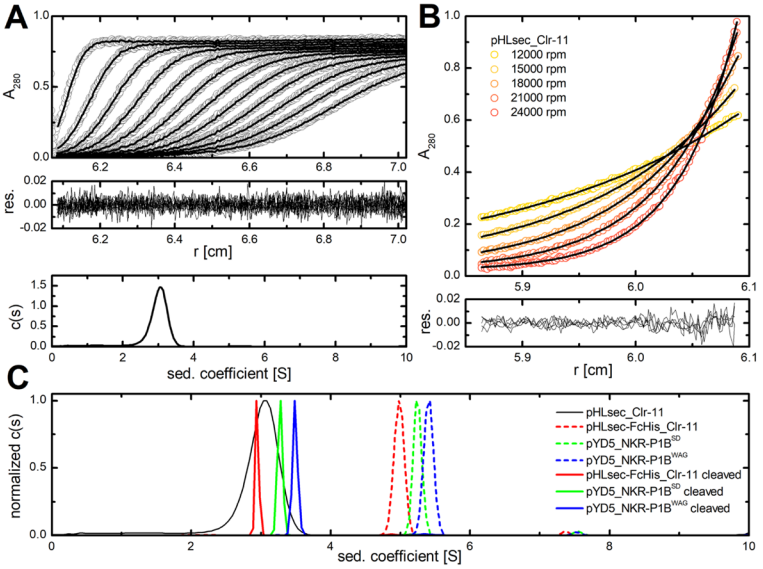

Figure 6. Sedimentation analysis of rat Clr-11 and NKR-P1B dimeric expression constructs. (**A**) pHLsec_Clr-11 protein was analysed by sedimentation velocity; panels show (from top to bottom) absorbance scans recorded at 280 nm (every fifth scan is shown, circles) together with fitted curves (lines), residuals derived from the fitted data, and the resulting c(s) continuous distribution of the sedimentation coefficient. (**B**) pHLsec_Clr-11 was spun at 12–15–18–21–24000 rpm and 4 °C and its sedimentation equilibrium was monitored at 280 nm. The upper panel shows absorbance data (circles) with fitted curves (non-interacting discrete species model, lines), whereas the lower panel shows residuals derived from the fitted data. (**C**) Normalized continuous sedimentation coefficient distributions of pHLsec_Clr-11 (black line), Clr-11 (red line) and both NKR-P1B^{SD} (green line) and NKR-P1B^{WAG} (blue line) cleaved from pHLsec-FcHis and pYD5 Fc fusion constructs, respectively, as well as the distributions of the original uncleaved Fc fusion constructs (the same colour coding, dashed lines).

FTIR spectroscopy analysis of protein secondary structure shows well-folded native proteins. Lastly, the secondary structure of all recombinant soluble receptor constructs was examined by Fourier-transform infrared (FTIR) spectroscopy (Fig. 7 and Table 1). The FTIR spectra of all studied proteins are dominated by two broad bands corresponding to vibrations of the peptide linkage – amide I at ~1639 cm^{-1} (dominated by νCO, i.e., stretching vibrations of CO group) and amide II at ~1550 cm^{-1} (dominated by δNH, i.e., bending vibrations of the NH group, and νCN; Fig. 7A–D). The overall character of these spectra and the maximum of the amide I band correspond to proteins dominated by β-sheet structure. The intensity ratio of amide I and amide II bands, which reflects presence of aggregates, corresponds to fully soluble globular proteins, and no marks of aggregated structures are present (amide I/amide II ratio is close to 3:2 in soluble globular proteins and 1:1 in aggregated structures, whereas the band of intermolecular/aggregated β-sheets at ~1620 cm^{-1} is missing). The second derivative of Clr-11 FTIR spectra clearly shows a high content of β-sheets by the strong negative band at 1637 cm^{-1}, thus confirming that Clr-11 is structurally similar to mouse Clr-g.

The results of secondary structure analysis are summarized in Table 2. The differences between the original FTIR spectra and the fitted curves taken from the protein spectra reference set are very low (lower than 6%, not shown). This translates into reasonable estimations of the protein secondary structure because the relative sums of the estimated structures are < 110%. All estimated secondary structures are very close to each other, as expected for proteins belonging to the same structural family. The estimated secondary structures of monomeric and dimeric NKR-P1B^{SD} are identical, and also the NKR-P1B^{WAG} structure differs only very little. The secondary structure estimated for dimeric NKR-P1B^{SD} in solution and calculated from its crystal structure is very close and inside the margins of errors, which is also true for soluble rat Clr-11 and for the crystal structure of the closely related mouse Clr-g. The values estimated in this study for the dimeric NKR-P1B^{SD} are also very close to values previously estimated for a monomeric, bacterially expressed and refolded, shorter expression construct of rat NKR-P1B[38].

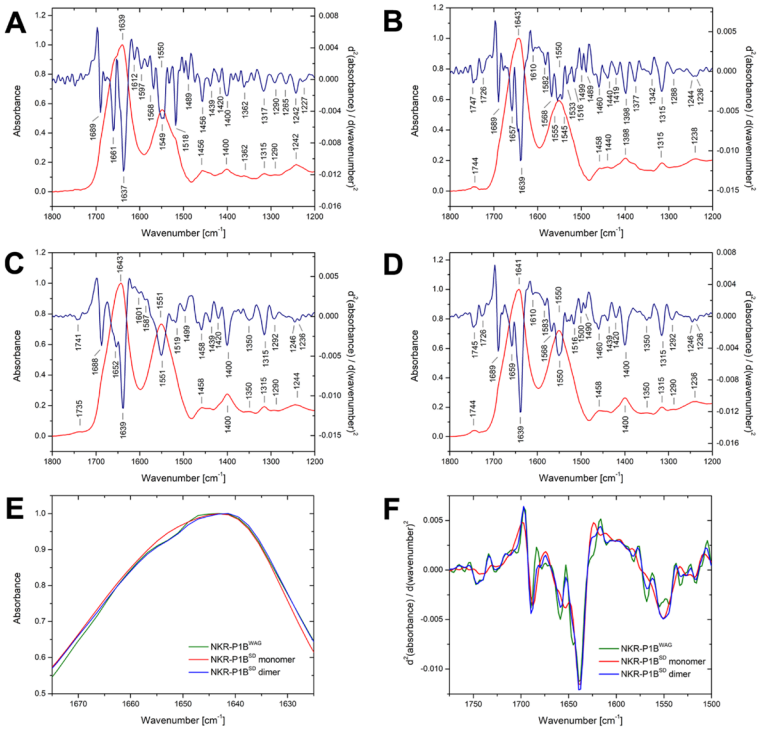

Figure 7. FTIR spectroscopy analysis of recombinant dimeric rat NK cell receptors. Fourier-transform infrared spectra of (**A**) Clr-11 cleaved from pHLsec-FcHis, (**B**) NKR-P1B^{WAG}, (**C**) monomeric, and (**D**) dimeric NKR-P1B^{SD}, all cleaved from pYD5 fusion constructs, in the region of amide I, II and III bands depicted as red curves. The blue line corresponds to the second derivative of the spectrum smoothed by Savitski-Golay function at 7 points; distinct spectral bands are labelled, and band assignment is outlined in Table 1. (**E**) Detailed comparison of the FTIR spectra and their (**F**) second derivatives for monomeric and dimeric NKR-P1B^{SD}, and NKR-P1B^{WAG} in the region of amide I and II bands.

Although the NKR-P1B^{SD} and NKR-P1B^{WAG} dimers are highly similar – both show the same pattern in amide I and II regions – a slight, yet distinct, difference between the NKR-P1B^{SD} monomer and the corresponding dimer is visible at ~1655 cm^{-1} (Fig. 7E), even though their secondary structures show no significant differences (Table 2). The differences are best observed when using the second derivatives (Fig. 7F). The band at 1652 cm^{-1} is shifted at 1659 cm^{-1} upon NKR-P1B^{SD} dimer formation. Unfortunately, this band shift might be attributed both to α-helices or disordered structures[39], or even partly to turns[40]. Slight changes in turns are observed in the region at ~1689 cm^{-1}. However, no changes in β-sheet bands are identified. Thus, β-sheets unlikely participate in NKR-P1B^{SD} dimerization, further confirming that the NKR-P1B^{SD} dimer structure in solution is the same as the crystal structure in which the dimerization interface is formed by α-helices and surrounding turns and loops without involving the β-sheet protein core.

Discussion

Although new detailed structural and functional data are revealing the functional role of NKR-P1 monomers and dimers and the nature of the NKR-P1:Clr interaction, difficulties producing stable covalent NKR-P1 homodimers require using recombinant NKR-P1 proteins from different host organisms in a different stoichiometry. Recently, Hernychová *et al.* reported that only monomeric forms of mouse NKR-P1B could bind to Clr-b on cell surface, suggesting that NKR-P1B monomers might separately participate in the interaction with Clr-b or that the interaction itself might promote NKR-P1B dimerization[41]. Although the signalling efficiency of monomeric NKR-P1B was not evaluated in this study, Hernychová *et al.* concluded that NKR-P1B homodimers are not functional, regardless of the presence of a stalk region, which did not affect the interaction and was not even crucial

Frequency (cm^{-1})	Assignment	References
1227/—/—/—	β-sheet (amide III)/His	39,54–56
1242/1236/1236/1236	β-sheet (amide III)/Tyr–OH	39,54–56
1265/1246/1246/1244	coil (amide III)/Tyr–OH	39,54–56
1290/1292/1292/1288	β-turns (amide III)	54,55
1317/1315/1315/1315	α-helix (amide III)	54,55
1362/1350/1350/1342	Trp	39,56
1400/1400/1400/1398	Asp/Glu ($\nu_s COO^-$)	39,56
—/—/—/1419	Trp/Pro?	39,56
1439/1439/1439/1440	δCH_2, Pro (νCN), His^-(δCH & δCN)	39,56
1456/1458/1460/1460	δCH_2, δCH_3/Tyr/Trp?	39,56
1489/—/1490/1489	Trp? (νCC ring & δCH)	39,56
—/1499/1500/1499	Phe/Tyr–O^- (νCC ring)?	39,56
1518/1519/1516/1516	Tyr–OH (νCC ring & δCH)	39,56
—/—/—/1533	amide II	40,56
—/—/—/1545	amide II	40,56
1549/1551/1550/—	amide II	40,56
—/—/—/1555	amide II	40,56
1568/—/1568/1568	Asp/Glu ($\nu_{as} COO^-$)	39,56
1597/1587/1583/1582	Tyr (νCC ring)	39,56
—/1601/—/—	Tyr–O^- (νCC ring)?	39,56
—/—/1610/1610	Tyr (νCC ring)	39,56
1637/1639/1639/1639	β-sheet (amide I)	40,57
1661/1652/1659/1657	α-helix/coil/turns (amide I)	40,57
1689/1688/1689/1689	β-sheet antiparallel/ turns (amide I)	40,57
—/—/1726/1726	Asp/Glu (νC=O)	39,54,56
—/1741/1745/1747	Asp/Glu (νC=O)	39,54,56

Table 1. Assignment of the infrared bands distinguishable in the second derivatives of Clr-11/monomeric NKR-P1B^{SD}/dimeric NKR-P1B^{SD}/NKR-P1B^{WAG} receptors FTIR spectra shown in Fig. 7 (ν corresponds to stretching, δ to bending, *as* to anti-symmetrical, and *s* to symmetrical vibrations).

NKR-P1B^{WAG}		Clr-11		mouse Clr-g	
Structure	**LSA (%)**	**LSA *N* (%)**	**LSA (%)**	**LSA *N* (%)**	**crystal structure***
α-helix	21 ± 10	20	23 ± 10	22	17
β-sheet	28 ± 9	27	25 ± 9	24	27
β-turn	14 ± 4	13	13 ± 4	12	12
Bend	15 ± 4	14	14 ± 4	13	15
Disordered	27 ± 6	26	30 ± 6	29	29
Sum	105%	100%	105%	100%	100%
NKR-P1B^{SD} monomer		**NKR-P1B^{SD} dimer**		**NKR-P1B^{SD} dimer**	
Structure	**LSA (%)**	**LSA *N* (%)**	**LSA (%)**	**LSA *N* (%)**	**crystal structure***
α-helix	23 ± 10	22	23 ± 10	22	19
β-sheet	28 ± 9	26	28 ± 9	26	28
β-turn	14 ± 4	13	14 ± 4	13	15
Bend	16 ± 4	15	16 ± 4	15	13
Disordered	26 ± 6	24	26 ± 6	24	25
Sum	107%	100%	107%	100%	100%

Table 2. Estimation of the secondary structure content of the prepared proteins using the least-squares method (LSA)[51] analysing amide I & II bands in infrared spectra (*N* marks values normalized to 100%). Given standard deviations are calculated as standard deviations of the used reference set; therefore, they do not reflect the quality of the fits. *Calculated using DSSP[58] on the crystal structures of mouse Clr-g (PDB ID 3RS1)[29] and rat NKR-P1B^{SD} dimer (PDB ID 5J2S). However, in the NKR-P1B^{SD} crystal structure, only 118 amino acid residues are visible, i.e., 29 residues (20%), fewer than those present in the expressed protein construct.Given standard deviations are calculated as standard deviations of the used reference set; therefore, they do not reflect the quality of the fits.

for protein dimerization. Remarkably, in another recent publication Balaji *et al.* showed that only homodimers of mouse NKR-P1B were able to functionally engage CD3ζ-Clr-b chimeras on cells[42]. Moreover, in contrast to the Hernychová *et al.* findings, Balaji *et al.* reported that abrogation of the intermolecular cystine bond was detrimental to functional signalling, precluding the NKR-P1B self-association and higher-order cross-linking of Clr-b. However, NKR-P1B homodimers were not essential for the formation of a stable NKR-P1B:m12 viral immunoevasin complex, most likely because the NKR-P1B:m12 complex has a much higher affinity than the NKR-P1B:Clr-b complex. Unfortunately, discrepancies in the preparations of mouse NKR-P1B protein prevent direct comparisons between these results. Soluble, renatured NKR-P1B, produced in *E. coli*, which results in a mixture of monomers and multiple species of covalent homodimers, was used in the first study[41], whereas Balaji *et al.* was unable to produce covalent homodimers of NKR-P1B in HEK293 cells and instead used tetrameric NKR-P1 particles consisting of four streptavidin-bound biotinylated NKR-P1B monomers.

To meet this need, we developed a rapid method for the preparation of stable soluble covalent NKR-P1 dimers in HEK293 cells suitable for further functional studies and offering therapeutic potential thanks to the presence of IgG Fc fragment, if desired. First, we adapted HEK293T cells for growth in suspension in EX-CELL 293 medium supporting high-density cultures. When compared with adherent cultures, suspension cultures have the potential to be more economical (and ecological) due to their lower requirements for single-use plastic consumables and higher volumetric productivity. However, the likely presence of negatively charged additives (e.g., heparin) may have contributed to ineffective PEI-mediated transfection of HEK293T cells in EX-CELL 293 medium. This is however not a problem in F17 or calcium-free DMEM media in which we were able to optimize transfection parameters (i.e., 1 μg plasmid DNA/10^6 cells, 1:4 (w/w) DNA:PEI ratio, and calcium-free DMEM and EX-CELL 293 as transfection and production media, respectively), and to confirm the positive effect of 2 mM valproic acid added 3 hours post-transfection, as well as of Tryptone N1 added 48 hours post-transfection, on the yield of secreted protein.

To demonstrate the feasibility of preparing covalent disulfidic NKR-P1B dimers in our optimized expression system, we selected the rat inhibitory NKR-P1B:Clr-11 as a model receptor:ligand system – particularly because NKR-P1B receptors from WAG and SD rat strains share their native ligand Clr-11 but differ in their reactivity towards the viral decoy ligand RCTL[19]. Although we have been able to produce dimeric NKR-P1B^{WAG} and mostly dimeric Clr-11, we were unable to obtain covalent dimers of the NKR-P1B^{SD} and RCTL molecules. The RCTL viral decoy ligand proved especially difficult to express, and we obtained only low yields of its monomeric form. The varied dimerization propensity of the NKR-P1B^{WAG} and NKR-P1B^{SD} receptor ectodomains is proportional to the number of available C-terminal dimerization cysteines – the NKR-P1B^{WAG} has three such cysteine residues, whereas NKR-P1B^{SD} contains only one.

Nevertheless, to further promote the covalent dimerization of soluble Clr-11 and NKR-P1B^{SD}, we have prepared fusion constructs with a C-terminally attached Fc fragment of the human IgG1 molecule, cleavable with HRV 3C protease. The C-terminal fusion of Fc fragment was a successful strategy in the case of Clr-11, resulting in stable Cys200-Cys200 bound Clr-11 covalent dimer, as confirmed by mass spectrometry. However, we were unable to cleave off the C-terminal Fc fragment from both NKR-P1B isoforms, most likely due to cross-linking of IgG cysteines with the C-terminal dimerization cysteines of the receptor. This problem caused by the proximity of the C-terminal NKR-P1B to the Fc IgG cysteines was solved by fusing the Fc fragment to the N-terminus of the NKR-P1B ectodomain, thereby efficiently cleaving off the N-terminal Fc fragment and yielding pure NKR-P1B^{WAG} covalent dimer and a separable mixture of NKR-P1B^{SD} monomer and covalent dimer. Thus, we do not recommend C-terminal Fc fragment fusion for rat NKR-P1 expression because it can result in the formation of non-physiological dimers. Conversely, N-terminal Fc fragment fusion is a suitable expression strategy to quickly prepare covalent rat NKR-P1 dimers in milligram quantities.

Further gel filtration and sedimentation velocity analyses showed that monomeric Clr-11 exhibits an equilibrium of monomers and non-covalent dimers in solution, as expected because several *Clec2* orthologues, including mouse Clr-g[29] and Clr-b[42] and human LLT1[43] and CD69[44], have been shown to form non-covalent dimers in solution. Furthermore, the prepared covalent dimers of NKR-P1B^{WAG}, NKR-P1B^{SD} and Clr-11 showed no sign of monomer-dimer equilibrium, thus corroborating the efficiency of our expression strategy. The prepared receptors were also examined by FTIR spectroscopy clearly showing fully soluble globular proteins with no signs of aggregation. Furthermore, analysis of FTIR spectra confirmed the structural similarity of rat Clr-11 to mouse Clr-g. However, the comparison of FTIR spectra of monomeric and dimeric NKR-P1B^{SD} showed that its β-sheets are unlikely to participate in NKR-P1B^{SD} dimerization. This finding corroborates the crystal structure of NKR-P1B^{SD} (PDB ID 5J2S – Vaněk *et al.*, manuscript in preparation), wherein the dimerization interface is mainly formed by α-helices. Combined with the recently reported unconventional dimerization modes of mouse NKR-P1B[41,42], these results indicate that dimerization within the NKR-P1 receptor family differs from that observed in *Clec2* ligands.

Several factors likely hinder the effective formation of covalent dimers of soluble NKR-P1 constructs. When compared with the Clr receptor family, the weaker mode of non-covalent dimerization of NKR-P1B, as revealed in its crystal structures (Balaji *et al.*[42] and PDB ID 5J2S), has rather weak affinity. Therefore, membrane anchoring of the NKR-P1B molecule may be required for the effective formation of disulphide bonds within its stalk region. Thus, by providing such steric anchoring through N-terminal fusion to the Fc-fragment, the dimerization cysteines can be brought into functional proximity and promote the formation of disulphide bridges. The low propensity for non-covalent dimerization is apparently a common feature of NKR-P1 molecules and suggests that the weaker non-conventional mode of dimerization might be conserved throughout the NKR-P1 family. This overall conformational flexibility of NKR-P1 molecules might be also the reason why it is practically impossible to detect and measure the binding of rodent NKR-P1 receptors to their respective Clr ligands in solution. Apparently, the affinity of individual NKR-P1:Clr interaction is extremely weak and largely undetectable by standard biophysical approaches[42]. Yet such behaviour is not uncommon among immune receptor:ligand complexes where it is the

interaction avidity (provided by, e.g., cross-linking of the dimeric receptor:ligand molecules on the cell surface) that plays a major role in signal transduction to the cell.

In summary, the method described herein enables high-level expression of secreted recombinant soluble dimeric forms of rat NK cell C-type lectin-like receptors in quantity and quality sufficient for their biophysical, functional, and structural characterization. Transient transfection is an easily scalable, non-viral, fast and affordable method of recombinant protein production in HEK293 cell lines that allows us to use modular construct design. Furthermore, the fusion of receptor expression constructs to an Fc fragment of human IgG promotes receptor disulphide dimer formation and could be used for purification, detection, or therapy. This approach can be applied to generate other soluble NK cell surface antigens, thus enabling their detailed structural and functional characterization leading to detailed molecular insights necessary for successful rational design of new protein-based immunotherapeutics.

Methods

Chemicals. 25-kDa linear polyethylenimine (Polysciences, USA) was dissolved in water, neutralized with HCl, sterilized by filtration (0.22 μm), aliquoted and stored at −80 °C; a working aliquot was stored at 4 °C. Valproic acid and Pluronic F-68 (both Sigma, USA) were dissolved in water to 0.5 M and 10% (w/v), respectively, sterilized by filtration and stored at −20 °C. Casein hydrolysate Tryptone N1 (Organotechnie, France) was dissolved in F17 medium (GIBCO Invitrogen, USA) to 20% (w/v), sterilized by filtration and stored at 4 °C.

Cell culture. HEK293T cells were kindly provided by Radu A. Aricescu[32] and were maintained as adherent monolayers in standard Dulbecco's Modified Eagle's Medium (DMEM, 4.5 g/l glucose, Institute of Molecular Genetics, The Czech Academy of Sciences, Prague) supplemented with 4 mM L-glutamine, non-essential amino acids and 10% foetal bovine serum (GIBCO Invitrogen, USA) in standard flasks (TPP, Switzerland) in a humidified 37 °C, 5% CO_2 incubator. Suspension adapted HEK293T cells (0.25–6 × 10^6/ml) were maintained in EX-CELL 293 serum-free medium (Sigma, USA) supplemented with 4 mM L-glutamine in standard dishes (TPP, Switzerland) or square-shaped glass bottles with gas permeable caps (DURAN, Germany) using 30–40% of the nominal volume at 135 rpm (Orbit 1000 orbital shaker, rotational diameter 19 mm; Labnet, USA; bottles were fixed with Sticky Pad adhesive mat; New Brunswick Scientific, USA) placed within the same incubator[45].

Vectors, cloning, and DNA purification. The pTTo3c-SSH and pTTo-GFPq vectors containing secreted alkaline phosphatase and green fluorescent protein, respectively, were kindly provided by Dr. Yves Durocher, as well as pYD5 vector (pTT5 derivative with N-terminal human IgG Fc fragment tag cleavable by TEV protease that was in-house modified to contain AgeI/KpnI cloning sites)[31]. The pHLsec and pHLsec-FcHis vectors were kindly provided by Dr. Radu A. Aricescu[32]. Isolation of cDNA of rat NKR-P1B, Clr-11, and RCTL receptors was previously described[19]. Briefly, PCR products were digested, purified and inserted into pHLsec, pHLsec-FcHis or pYD5 vectors using the flanking AgeI and KpnI sites. Positive clones were screened by colony PCR using TaqRed PCR master mix (Top-Bio, Czech Republic). The primers used to amplify the desired expression constructs and the vector-specific primers are listed in Supplementary Information (Table S1). All inserts were sequenced, and the plasmid transfection stocks were prepared using NoEndo JETSTAR 2.0 Plasmid Maxiprep Kit (Genomed, Germany) according to the manufacturer's recommendations. Using a single kit column, 3–4 mg of pure plasmid DNA (A_{260}/A_{280} ratio of 1.8–2.0) was usually obtained from 500 ml of *E. coli* DH5α culture grown in Luria broth medium (in our experience, cultures grown for more than 12-14 h give lower yields).

Small-scale transient transfections. Cells were centrifuged and resuspended in appropriate fresh transfection medium at a density of 0.5 × 10^6/ml. Transfection medium was calcium-free DMEM (as above, but calcium chloride and FBS were not used in the preparation; instead, 0.1% Pluronic F-68 was added) either supplemented with 2% FBS or completed with EX-CELL 293 post-transfection (see below). Alternatively, F17 (supplemented with 4 mM L-glutamine and 0.1% Pluronic F-68) or Glutamax-I Freestyle 293 medium (both GIBCO Invitrogen, USA) were used, as indicated in Results, and 0.5 ml of cell suspension was distributed per well in a 24-well plate (or 1 × 10^6/ml in case of calcium-free DMEM and 0.25 or 1 ml of cell suspension was distributed per well in a 24- or 12-well plate, respectively). The desired amount of DNA (1 μg/10^6 cells unless otherwise noted) was diluted in PBS (in a volume equivalent to one-tenth of the culture to be transfected), PEI was added to desired ratio (w/w; 1:4 unless noted otherwise), and the mixture was immediately vigorously shaken and incubated for 10–15 min at room temperature before adding it to the cells. Following a 3 h incubation with DNA-PEI complexes, the culture medium was completed to 0.5 ml (24-well plate) or 2 ml (12-well plate) with EX-CELL 293 in case of calcium-free DMEM transfections, and VPA was added (concentrations indicated in the text refer to a final culture volume).

SEAP analysis. SEAP activity (ΔA_{410}/min) was determined as previously described[31]. Briefly, culture supernatants were diluted with water as required (typically 1/100 to 1/1000), and 180 μl was transferred to a 96-well plate. The enzymatic reaction was initiated when 20 μl of SEAP assay solution (20 mM *p*-nitrophenyl phosphate; pNPP, 1 mM $MgCl_2$ and 1 M diethanolamine pH 9.8) were added, and absorbance was read at 410 nm in 1 min intervals at room temperature to determine the pNPP hydrolysis rates (Safire microplate reader, Tecan, Austria). Data are expressed as the mean of one experiment performed in triplicate with error bars representing standard deviations. Each sample was independently assayed for SEAP activity three times to minimize pipetting errors.

Flow cytometry. GFP-positive viable cells were estimated using a BD LSR II flow cytometer (BD Biosciences, USA). For each assay, 50 μl of cell suspension were transferred to a round-bottom 96-well plate, diluted with 150 μl of PBS and stained with 10 μl of propidium iodide (PI; 10 μg/ml in PBS) before analysis. Viable transfected cells were quantified using appropriate gating to exclude dead cells, debris and aggregates in a forward vs. side

scatter plot. Data are shown as mean of one experiment performed in triplicate with error bars representing standard deviations.

Transfection in square-shaped bottles. For large-scale recombinant protein production, the respective expression plasmid (1 μg/10^6 of cells to be transfected, typically 400 μg) was diluted in 10 ml of PBS, filter sterilized, and PEI was added at a 1:4 weight ratio (typically 1.6 mg). The mixture was then shaken and incubated for 10 min. Meanwhile, exponentially growing HEK293T cells were centrifuged and resuspended in calcium-free DMEM at a density of 2×10^6/ml (typically in 200 ml of medium in a 1 l square-shaped bottle) and immediately transfected. Following a 3–4 h incubation period with DNA-PEI complexes, the culture medium was completed with an equal volume of EX-CELL 293 (typically 200 ml), and VPA was added to 2 mM concentration. Two days later, the culture was fed with 0.5% TN1. Conditioned culture medium containing secreted recombinant protein was harvested by centrifugation 4–6 days post-transfection and stored at −20 °C until protein purification.

Protein purification. Conditioned medium was thawed, clarified by centrifugation at 25000 × g, and filtered through a 0.22 μm membrane (Steritop filter, Millipore, USA). The medium was diluted twofold with PBS, and the final pH was adjusted to 7.0, when necessary. IMAC purification was performed using cobalt-coated TALON beads (Clontech, USA) in batch mode using 2 l Erlenmeyer flasks. Following a 30-min incubation period with shaking at 110 rpm, the beads were collected in a gravity flow Econo column (Bio-Rad, USA), washed with PBS and the bound His-tagged protein was eluted with PBS containing 250 mM imidazole. The eluate was concentrated with Amicon Ultra device (10 kDa cut-off membrane, Millipore) and subjected to gel filtration on Superdex 200 HR 10/30 column (GE Healthcare, USA). All steps were performed at room temperature. Protein concentration was determined by Bradford assay (Bio-Rad). All pHLsec-FcHis constructs were cleaved with HRV 3C protease overnight, at 4 °C, in non-reducing conditions at a 1:5 target-to-protease mass ratio; all pYD5 constructs were captured on a Protein A column (MabSelect SuRe, GE Healthcare, USA), followed by cleavage with TEV protease and purification by gel filtration, as described above.

Electrophoresis and Western blot analysis. For the rapid screening of new constructs, transfections were performed in 24-well plates using miniprep-purified DNA (JETQUICK Spin Kit, Genomed). Three days post-transfection, 10 μl of conditioned media was resolved on a 15% SDS-PAGE gel, which was subsequently electroblotted onto a BioTrace nitrocellulose membrane (Pall Corporation, USA), followed by Ponceau Red staining and washing with TBS buffer (10 mM Tris, pH 7.5, 150 mM NaCl). The membrane was blocked with 3% BSA in TBS for 1 h at room temperature, and thrice rinsed with TBS-T buffer (20 mM Tris, pH 7.5, 500 mM NaCl, 0.05% Tween-20, 0.2% Triton X-100). After 1 h incubation with PentaHis monoclonal primary antibody (1:1000 dilution in 3% BSA in TBS, Qiagen, Germany) and another 1 h incubation with horseradish peroxidase-conjugated goat anti-mouse IgG polyclonal antibodies (1:2000 in 10% non-fat milk in TBS; Abcam, UK), with extensive washings with the TBS-T and TBS buffers after each step, peroxidase activity was visualized by luminol chemiluminescence.

Mass spectrometry analysis. Mass spectrometry analysis of disulphide bond linkage was performed as previously described[46]. Briefly, to avoid disulphide bond scrambling, 0.2 mM cystamine was added at all stages of sample preparation (i.e., SDS-PAGE gels, sample, running and digestion buffers). Protein bands were excised from the gel and their tryptic and Asp-N peptide digests were extracted and analysed on a MALDI-TOF/TOF mass spectrometer (ULTRAFLEX III, Bruker, Germany). Experimentally determined m/z values were compared with theoretical values created in GPMAW software[47], and cystine peptides were identified using a software LinX (freely available at http://peterslab.org/MSTools/). Routine protein identification and HRV 3C or TEV protease cleavage analysis was similarly performed with reduced tryptic digests.

Sedimentation analysis. The native molecular size and shape as well as the molar mass of the proteins produced were analysed in an analytical ultracentrifuge ProteomeLab XL-I (Beckman Coulter, USA) using both sedimentation velocity and sedimentation equilibrium experiments. Before the experiment, protein samples were diluted with the gel filtration buffer (10 mM HEPES, pH 7.0, 150 mM NaCl, 10 mM NaN_3) to 0.2 mg/ml concentration, and the buffer was used as a reference. Sedimentation velocity experiments were conducted at 48000 rpm and at 20 °C using double-sector cells and An50-Ti rotor. Absorbance scans were recorded at 280 nm, at 5-min intervals. Buffer density, protein partial specific volume, and particle dimensions were estimated in Sednterp (www.jphilo.mailway.com). Data were analysed in Sedfit[48] using a continuous sedimentation coefficient distribution c(s) model. The sedimentation equilibrium experiment was performed with pHLsec_Clr-11 at a concentration of 0.1 mg/ml at 12–15–18–21–24000 rpm and at 4 °C in a six-sector cell, and absorbance scans were collected after 36 h (first scan) or 20 h (consecutive scans) of equilibration. The sedimentation equilibrium data were globally analysed in Sedphat[49] using a non-interacting discrete species model.

Fourier-transform infrared spectroscopy. The proteins were transferred to 10 mM Tris, pH 7.5, 50 mM NaCl buffer using centrifugal filters (10 kDa cut-off, 12000 × g, Millipore, USA) at 20 mg/ml final concentration. Infrared spectra were recorded within a Vector 33 FTIR spectrometer (Bruker, Germany) using a standard MIR source, KBr beam-splitter and a DTGS detector. For each sample 4000 scans were collected with a 4 cm^{-1} spectral resolution using a Blackman-Harris 3-term apodization function. Protein samples were measured at room temperature in a CaF_2-cell with an 8-μm path length (Chevtchenko Optics, Germany). The spectrometer was purged by dry air during all experiments. The spectral contribution of the buffer was corrected following the standard algorithm[50]. The spectrum of water vapour was subtracted; the spectra were offset at 1800 cm^{-1} at zero and normalized to the amide I intensity maximum at one. Data were processed using the software GRAMS/AI (Thermo Electron, USA). The secondary structure of the proteins was estimated from their infrared

spectra using the Dousseau and Pézolet method[51] implemented as a Matlab routine (MathWorks, USA) in the Vibrational Spectroscopy Toolbox and Applications[52]. This method uses least-squares analysis to compare the amide I and amide II bands of a protein of unknown structure with those of the reference set of proteins of known three-dimensional structure (taken from[53]). The main advantage of this method is its independence from band assignments.

Data availability

All data generated or analysed during this study are included in this published article. Raw data, e.g., mass and FTIR spectra or AUC datasets generated in the current study are available from the corresponding author on reasonable request.

Received: 25 March 2019; Accepted: 14 October 2019;
Published online: 28 November 2019

References

1. Lanier, L. L. Up on the tightrope: natural killer cell activation and inhibition. *Nature Immunology* **9**, 495–502, https://doi.org/10.1038/ni1581 (2008).
2. Vivier, E., Tomasello, E., Baratin, M., Walzer, T. & Ugolini, S. Functions of natural killer cells. *Nature Immunology* **9**, 503–510, https://doi.org/10.1038/ni1582 (2008).
3. Lanier, L. L. NK cell recognition. *Annual Review of Immunology* **23**, 225–274, https://doi.org/10.1146/annurev.immunol.23.021704.115526 (2005).
4. Karre, K., Ljunggren, H. G., Piontek, G. & Kiessling, R. Selective rejection of H-2-deficient lymphoma variants suggests alternative immune defence strategy. *Nature* **319**, 675–678, https://doi.org/10.1038/319675a0 (1986).
5. Raulet, D. H. Roles of the NKG2D immunoreceptor and its ligands. *Nature Reviews Immunology* **3**, 781–790, https://doi.org/10.1038/nri1199 (2003).
6. Chambers, W. H. *et al*. Monoclonal antibody to a triggering structure expressed on rat natural killer cells and adherent lymphokine-activated killer cells. *The Journal of Experimental Medicine* **169**, 1373–1389, https://doi.org/10.1084/jem.169.4.1373 (1989).
7. Mesci, A., Ljutic, B., Makrigiannis, A. P. & Carlyle, J. R. NKR-P1 biology: from prototype to missing self. *Immunologic Research* **35**, 13–26, https://doi.org/10.1385/IR:35:1:13 (2006).
8. Hao, L., Klein, J. & Nei, M. Heterogeneous but conserved natural killer receptor gene complexes in four major orders of mammals. *Proceedings of the National Academy of Sciences of the United States of America* **103**, 3192–3197, https://doi.org/10.1073/pnas.0511280103 (2006).
9. Giorda, R. *et al*. NKR-P1, a signal transduction molecule on natural killer cells. *Science* **249**, 1298–1300, https://doi.org/10.1126/science.2399464 (1990).
10. Iizuka, K., Naidenko, O. V., Plougastel, B. F., Fremont, D. H. & Yokoyama, W. M. Genetically linked C-type lectin-related ligands for the NKRP1 family of natural killer cell receptors. *Nature Immunology* **4**, 801–807, https://doi.org/10.1038/ni954 (2003).
11. Carlyle, J. R. *et al*. Missing self-recognition of Ocil/Clr-b by inhibitory NKR-P1 natural killer cell receptors. *Proceedings of the National Academy of Sciences of the United States of America* **101**, 3527–3532, https://doi.org/10.1073/pnas.0308304101 (2004).
12. Rahim, M. M. & Makrigiannis, A. P. Ly49 receptors: evolution, genetic diversity, and impact on immunity. *Immunological Reviews* **267**, 137–147, https://doi.org/10.1111/imr.12318 (2015).
13. Kveberg, L. *et al*. Two major groups of rat NKR-P1 receptors can be distinguished based on chromosomal localization, phylogenetic analysis and Clr ligand binding. *European Journal of Immunology* **39**, 541–551, https://doi.org/10.1002/eji.200838891 (2009).
14. Aldemir, H. *et al*. Cutting edge: lectin-like transcript 1 is a ligand for the CD161 receptor. *Journal of Immunology* **175**, 7791–7795, https://doi.org/10.4049/jimmunol.175.12.7791 (2005).
15. Rosen, D. B. *et al*. Cutting edge: lectin-like transcript-1 is a ligand for the inhibitory human NKR-P1A receptor. *Journal of Immunology* **175**, 7796–7799, https://doi.org/10.4049/jimmunol.175.12.7796 (2005).
16. Roth, P. *et al*. Malignant glioma cells counteract antitumor immune responses through expression of lectin-like transcript-1. *Cancer Research* **67**, 3540–3544, https://doi.org/10.1158/0008-5472.CAN-06-4783 (2007).
17. Mathew, S. O., Chaudhary, P., Powers, S. B., Vishwanatha, J. K. & Mathew, P. A. Overexpression of LLT1 (OCIL, CLEC2D) on prostate cancer cells inhibits NK cell-mediated killing through LLT1-NKRP1A (CD161) interaction. *Oncotarget* **7**, 68650–68661, https://doi.org/10.18632/oncotarget.11896 (2016).
18. Germain, C. *et al*. Lectin-like transcript 1 is a marker of germinal center-derived B-cell non-Hodgkin's lymphomas dampening natural killer cell functions. *Oncoimmunology* **4**, e1026503, https://doi.org/10.1080/2162402X.2015.1026503 (2015).
19. Voigt, S. *et al*. Cytomegalovirus evasion of innate immunity by subversion of the NKR-P1B:Clr-b missing-self axis. *Immunity* **26**, 617–627, https://doi.org/10.1016/j.immuni.2007.03.013 (2007).
20. Carlyle, J. R. *et al*. Molecular and genetic basis for strain-dependent NK1.1 alloreactivity of mouse NK cells. *Journal of Immunology* **176**, 7511–7524, https://doi.org/10.4049/jimmunol.176.12.7511 (2006).
21. Aguilar, O. A. *et al*. Modulation of Clr Ligand Expression and NKR-P1 Receptor Function during Murine Cytomegalovirus Infection. *Journal of Innate Immunity* **7**, 584–600, https://doi.org/10.1159/000382032 (2015).
22. Aguilar, O. A. *et al*. A Viral Immunoevasin Controls Innate Immunity by Targeting the Prototypical Natural Killer Cell Receptor Family. *Cell* **169**, 58–71 e14, https://doi.org/10.1016/j.cell.2017.03.002 (2017).
23. Fine, J. H. *et al*. Chemotherapy-induced genotoxic stress promotes sensitivity to natural killer cell cytotoxicity by enabling missing-self recognition. *Cancer Research* **70**, 7102–7113, https://doi.org/10.1158/0008-5472.CAN-10-1316 (2010).
24. Williams, K. J. *et al*. Poxvirus infection-associated downregulation of C-type lectin-related-b prevents NK cell inhibition by NK receptor protein-1B. *Journal of Immunology* **188**, 4980–4991, https://doi.org/10.4049/jimmunol.1103425 (2012).
25. Tanaka, M. *et al*. The inhibitory NKRP1B: Clr-b recognition axis facilitates detection of oncogenic transformation and cancer immunosurveillance. *Cancer Research* **78**, 3589–3603, https://doi.org/10.1158/0008-5472.CAN-17-1688 (2018).
26. Chen, P. *et al*. Genetic investigation of MHC-independent missing-self recognition by mouse NK cells using an *in vivo* bone marrow transplantation model. *Journal of Immunology* **194**, 2909–2918, https://doi.org/10.4049/jimmunol.1401523 (2015).
27. Rahim, M. M. *et al*. The mouse NKR-P1B:Clr-b recognition system is a negative regulator of innate immune responses. *Blood* **125**, 2217–2227, https://doi.org/10.1182/blood-2014-02-556142 (2015).
28. Kolenko, P. *et al*. Molecular architecture of mouse activating NKR-P1 receptors. *Journal of Structural Biology* **175**, 434–441, https://doi.org/10.1016/j.jsb.2011.05.001 (2011).
29. Skalova, T. *et al*. Mouse Clr-g, a ligand for NK cell activation receptor NKR-P1F: crystal structure and biophysical properties. *Journal of Immunology* **189**, 4881–4889, https://doi.org/10.4049/jimmunol.1200880 (2012).
30. Bartel, Y., Bauer, B. & Steinle, A. Modulation of NK cell function by genetically coupled C-type lectin-like receptor/ligand pairs encoded in the human natural killer gene complex. *Frontiers in Immunology* **4**, 362, https://doi.org/10.3389/fimmu.2013.00362 (2013).

31. Durocher, Y., Perret, S. & Kamen, A. High-level and high-throughput recombinant protein production by transient transfection of suspension-growing human 293-EBNA1 cells. *Nucleic Acids Research* **30**, E9, https://doi.org/10.1093/nar/30.2.e9 (2002).
32. Aricescu, A. R., Lu, W. & Jones, E. Y. A time- and cost-efficient system for high-level protein production in mammalian cells. *Acta Crystallographica Section D, Biological Crystallography* **62**, 1243–1250, https://doi.org/10.1107/S0907444906029799 (2006).
33. Chang, V. T. *et al.* Glycoprotein structural genomics: solving the glycosylation problem. *Structure* **15**, 267–273, https://doi.org/10.1016/j.str.2007.01.011 (2007).
34. Backliwal, G. *et al.* Valproic acid: a viable alternative to sodium butyrate for enhancing protein expression in mammalian cell cultures. *Biotechnology and Bioengineering* **101**, 182–189, https://doi.org/10.1002/bit.21882 (2008).
35. Sunley, K. & Butler, M. Strategies for the enhancement of recombinant protein production from mammalian cells by growth arrest. *Biotechnology Advances* **28**, 385–394, https://doi.org/10.1016/j.biotechadv.2010.02.003 (2010).
36. Pham, P. L. *et al.* Transient gene expression in HEK293 cells: peptone addition posttransfection improves recombinant protein synthesis. *Biotechnology and Bioengineering* **90**, 332–344, https://doi.org/10.1002/bit.20428 (2005).
37. Reeves, P. J., Callewaert, N., Contreras, R. & Khorana, H. G. Structure and function in rhodopsin: high-level expression of rhodopsin with restricted and homogeneous N-glycosylation by a tetracycline-inducible N-acetylglucosaminyltransferase I-negative HEK293S stable mammalian cell line. *Proceedings of the National Academy of Sciences of the United States of America* **99**, 13419–13424, https://doi.org/10.1073/pnas.212519299 (2002).
38. Sovova, Z. *et al.* Structural analysis of natural killer cell receptor protein 1 (NKR-P1) extracellular domains suggests a conserved long loop region involved in ligand specificity. *Journal of Molecular Modeling* **17**, 1353–1370, https://doi.org/10.1007/s00894-010-0837-y (2011).
39. Barth, A. Infrared spectroscopy of proteins. *Biochimica et Biophysica Acta* **1767**, 1073–1101, https://doi.org/10.1016/j.bbabio.2007.06.004 (2007).
40. Fabian, H. & Vogel, H. J. Fourier transform infrared spectroscopy of calcium-binding proteins. *Methods in Molecular Biology* **173**, 57–74, https://doi.org/10.1385/1-59259-184-1:057 (2002).
41. Hernychova, L. *et al.* The C-type lectin-like receptor Nkrp1b: Structural proteomics reveals features affecting protein conformation and interactions. *Journal of Proteomics* **196**, 162–172, https://doi.org/10.1016/j.jprot.2018.11.007 (2019).
42. Balaji, G. R. *et al.* Recognition of host Clr-b by the inhibitory NKR-P1B receptor provides a basis for missing-self recognition. *Nature. Communications* **9**, 4623, https://doi.org/10.1038/s41467-018-06989-2 (2018).
43. Skalova, T. *et al.* Four crystal structures of human LLT1, a ligand of human NKR-P1, in varied glycosylation and oligomerization states. *Acta Crystallographica Section D, Biological Crystallography* **71**, 578–591, https://doi.org/10.1107/S1399004714027928 (2015).
44. Vanek, O. *et al.* Soluble recombinant CD69 receptors optimized to have an exceptional physical and chemical stability display prolonged circulation and remain intact in the blood of mice. *FEBS Journal* **275**, 5589–5606, https://doi.org/10.1111/j.1742-4658.2008.06683.x (2008).
45. Muller, N., Girard, P., Hacker, D. L., Jordan, M. & Wurm, F. M. Orbital shaker technology for the cultivation of mammalian cells in suspension. *Biotechnology and Bioengineering* **89**, 400–406, https://doi.org/10.1002/bit.20358 (2005).
46. Pompach, P. *et al.* Modified electrophoretic and digestion conditions allow a simplified mass spectrometric evaluation of disulfide bonds. *Journal of Mass Spectrometry: JMS* **44**, 1571–1578, https://doi.org/10.1002/jms.1609 (2009).
47. Peri, S., Steen, H. & Pandey, A. GPMAW–a software tool for analyzing proteins and peptides. *Trends in Biochemical Sciences* **26**, 687–689, https://doi.org/10.1016/S0968-0004(01)01954-5 (2001).
48. Schuck, P. Size-distribution analysis of macromolecules by sedimentation velocity ultracentrifugation and lamm equation modeling. *Biophysical Journal* **78**, 1606–1619, https://doi.org/10.1016/S0006-3495(00)76713-0 (2000).
49. Schuck, P. On the analysis of protein self-association by sedimentation velocity analytical ultracentrifugation. *Analytical Biochemistry* **320**, 104–124, https://doi.org/10.1016/S0003-2697(03)00289-6 (2003).
50. Dousseau, F., Therrien, M. & Pezolet, M. On the Spectral Subtraction of Water from the FT-IR Spectra of Aqueous-Solutions of Proteins. *Applied Spectroscopy* **43**, 538–542, https://doi.org/10.1366/0003702894202814 (1989).
51. Dousseau, F. & Pezolet, M. Determination of the secondary structure content of proteins in aqueous solutions from their amide I and amide II infrared bands. Comparison between classical and partial least-squares methods. *Biochemistry* **29**, 8771–8779, https://doi.org/10.1021/bi00489a038 (1990).
52. Pazderka, T. & Kopecky Jr., V. Two-dimensional correlation analysis of Raman optical activity - Basic rules and data treatment. *Vibrational Spectroscopy* **60**, 193–199, https://doi.org/10.1016/j.vibspec.2011.10.002 (2012).
53. Baumruk, V., Pancoska, P. & Keiderling, T. A. Predictions of secondary structure using statistical analyses of electronic and vibrational circular dichroism and Fourier transform infrared spectra of proteins in H O. *Journal of Molecular Biology* **259**, 774–791, https://doi.org/10.1006/jmbi.1996.0357 (1996).
54. Jung, C. Insight into protein structure and protein-ligand recognition by Fourier transform infrared spectroscopy. *Journal of Molecular Recognition* **13**, 325–351. https://doi.org/10.1002/1099-1352(200011/12)13:6<325::AID-JMR507>3.0.CO;2-C (2000).
55. Cai, S. & Singh, B. R. Identification of beta-turn and random coil amide III infrared bands for secondary structure estimation of proteins. *Biophysical Chemistry* **80**, 7–20, https://doi.org/10.1016/S0301-4622(99)00060-5 (1999).
56. Barth, A. The infrared absorption of amino acid side chains. *Progress in Biophysics and Molecular Biology* **74**, 141–173, https://doi.org/10.1016/S0079-6107(00)00021-3 (2000).
57. Barth, A. & Zscherp, C. What vibrations tell us about proteins. *Quarterly Reviews of Biophysics* **35**, 369–430, https://doi.org/10.1017/S0033583502003815 (2002).
58. Kabsch, W. & Sander, C. Dictionary of protein secondary structure: pattern recognition of hydrogen-bonded and geometrical features. *Biopolymers* **22**, 2577–2637, https://doi.org/10.1002/bip.360221211 (1983).

Acknowledgements

This work was supported by the Czech Science Foundation (15-15181S, 18-10687S), the Ministry of Education, Youth and Sports of the Czech Republic (LTC17065 in frame of the COST Action CA15126 MOBIEU), the Canadian Institutes of Health Research (FRN 106491 and 159450, to J.R.C.), and the Charles University (UNCE 204025/2012, SVV 260427/2019, GAUK 161216). The authors also acknowledge the support and the use of resources of Instruct, a Landmark ESFRI project through the R&D pilot scheme APPID 56 and 286.

Author contributions

O.V., P.C., O.S., J.B., B.K., A.D., E.P., H.P. and A.M. participated in cloning, recombinant protein expression and purification, cell line cultivation and transfection optimization, D.K. and P.P. performed mass spectrometry analyses, K.H. and V.K. performed FTIR spectroscopy measurements, J.B., S.V., J.R.C. and O.V. wrote the main manuscript text. All authors reviewed the manuscript.

Competing interests

The authors declare no competing interests.

Additional information

Supplementary information is available for this paper at https://doi.org/10.1038/s41598-019-52114-8.

Correspondence and requests for materials should be addressed to O.V.

Supplementary Information

Production of recombinant soluble dimeric C-type lectin-like receptors of rat natural killer cells

Ondřej Vaněk[1*], Petra Celadova[1], Ondřej Skořepa[1], Jan Bláha[1#], Barbora Kalousková[1], Anna Dvorská[1], Edita Poláchová[1], Helena Pucholtová[1], Daniel Kavan[1,2], Petr Pompach[2], Kateřina Hofbauerová[2,3], Vladimír Kopecký Jr.[3], Aruz Mesci[4], Sebastian Voigt[5], James R. Carlyle[4]

[1] *Department of Biochemistry, Faculty of Science, Charles University, Hlavova 2030/8, 12840 Prague, Czech Republic*

[2] *Institute of Microbiology, The Czech Academy of Sciences, Vídeňská 1083, 14220 Prague, Czech Republic*

[3] *Institute of Physics, Faculty of Mathematics and Physics, Charles University, Ke Karlovu 5, 12116 Prague, Czech Republic*

[4] *Department of Immunology, University of Toronto, 1 King's College Circle, M5S 1A8 Toronto, ON, Canada*

[5] *Department of Infectious Diseases, Robert Koch Institute, Seestraße 10, 13353 Berlin, Germany*

[*] Corresponding author. E-mail address: ondrej.vanek@natur.cuni.cz

[#] *Current address: EMBL Hamburg, c/o DESY, Building 25A, Notkestraße 85, 22603 Hamburg, Germany*

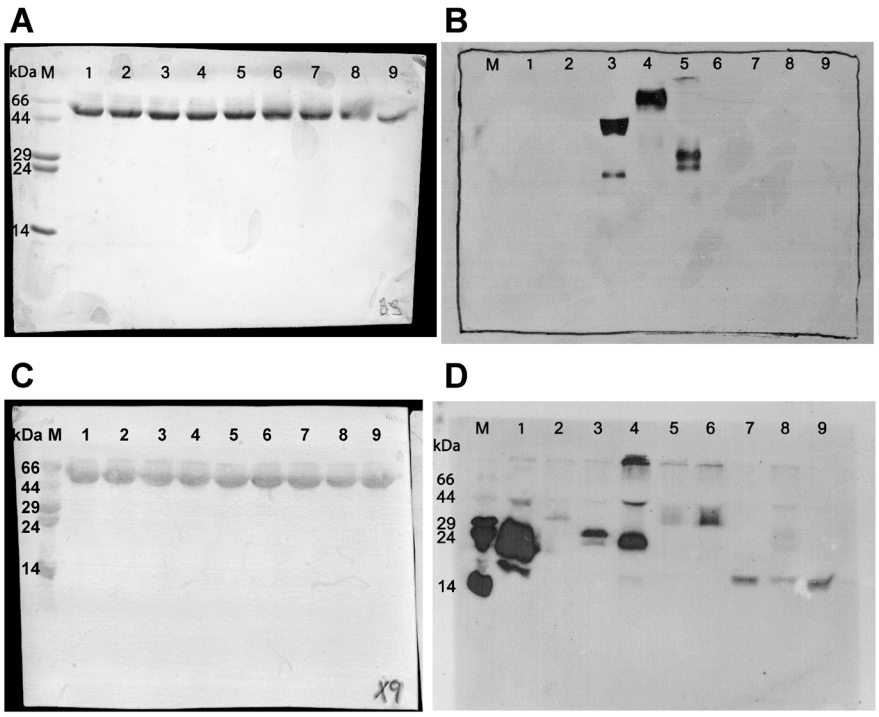

Figure S1. Full-size images of membranes and photographs used to analyse the small-scale expression test of pHLsec constructs in Figure 3A. Samples of transfected cell culture supernatants were resolved by 15% SDS-PAGE under non-reducing conditions, transferred onto nitrocellulose membranes, and transferred proteins were first stained with Ponceau Red (A and C) and then proteins containing histidine tag were detected by primary PentaHis mAb and secondary horseradish peroxidase-conjugated goat anti-mouse IgG polyclonal antibodies, and peroxidase activity was visualized by luminol chemiluminescence captured on photographic films (B and D). Lanes: M, marker; 1, mock transfected; 2, RCTL I38-T180; 3, Clr-11; 4, NKR-P1B^{WAG}; 5, NKR-P1B^{SD} (A and B); M, marker; 5, RCTL H51-T180; 6, RCTL H51-T170 (C and D); other lanes contain unrelated samples of supernatants resulting from expression tests of proteins that are not subject of the present study.

Table S1. Sequences of primers used for PCR amplification of given protein expression constructs and of vector-specific primers used for sequencing. AgeI/KpnI restriction cloning sites are highlighted in bold and underlined.

Target	AA	DNA primer
Clr-11^{WAG}	V65	5'-AAAAAA**ACCGGT**GTAAAAATGACACCACAGATCTCA-3'
	M207	5'-AAAAAA**GGTACC**CATAGGAGAAAAAGGAGTTTTGCA-3'
NKR-P1B^{WAG}	V78	5'-AAAAAA**ACCGGT**GTTCAAGAGAACAGGACAAAAACA-3'
	S223	5'-AAAAAA**GGTACC**GGAGCCATTACACATGCATTCACA-3'
NKR-P1B^{SD}	V78	5'-AAAAAA**ACCGGT**GTTCAAGAGAACAGGACAAAAACA-3'
	S223	5'-AAAAAA**GGTACC**GGAGTCATTGCACGTGCTTTC-3'
pHLsec **pHLsec-FcHis**	FW	5'-GCTGGTTGTTGTGCTGTCTCATC-3'
	REV	5'-CACCAGCCACCACCTTCTGATAG-3'
pYD5	FW	5'-TGATATTCACCTGGCCCGATCTG-3'
	REV	5'-TATGTCCTTCCGAGTGAGAG-3'

PUBLICATION III

Skořepa O, Pazicky S, Kalousková B, Bláha J, Abreu C, Ječmen T, Rosůlek M, Fish A, Sedivy A, Harlos K, Dohnálek J, Skálová T, Vaněk O.

Natural Killer Cell Activation Receptor NKp30 Oligomerization Depends on Its N-Glycosylation.

Cancers 12(7):1998 (2020)

My contribution to the publication: performing research (cloning, protein expression and purification, protein characterisation, biophysical characterisation, crystallisation), data collection, data analysis and interpretation, visualisation, manuscript writing.

cancers

MDPI

Article

Natural Killer Cell Activation Receptor NKp30 Oligomerization Depends on Its *N*-Glycosylation

Ondřej Skořepa [1], Samuel Pazicky [1,†], Barbora Kalousková [1], Jan Bláha [1,†], Celeste Abreu [1], Tomáš Ječmen [1], Michal Rosůlek [1,2], Alexander Fish [3], Arthur Sedivy [4], Karl Harlos [5], Jan Dohnálek [6], Tereza Skálová [6] and Ondřej Vaněk [1,*]

1 Department of Biochemistry, Faculty of Science, Charles University, Hlavova 2030, 12840 Prague, Czech Republic; ondrej.skorepa@natur.cuni.cz (O.S.); spazicky@gmail.com (S.P.); barbora.kalouskova@natur.cuni.cz (B.K.); jahabla@gmail.com (J.B.); celesteabreu22@gmail.com (C.A.); tomas.jecmen@natur.cuni.cz (T.J.); rosulek.michal@gmail.com (M.R.)
2 BIOCEV, Institute of Microbiology, The Czech Academy of Sciences, Průmyslová 595, 25250 Vestec, Czech Republic
3 Department of Biochemistry, Oncode Institute, Netherlands Cancer Institute, Plesmanlaan 121, 1066 CX Amsterdam, The Netherlands; a.fish@nki.nl
4 Protein Technologies, Vienna Biocenter Core Facilities GmbH, Dr. Bohr-Gasse 3, 1030 Vienna, Austria; arthur.sedivy@vbcf.ac.at
5 Division of Structural Biology, Wellcome Centre for Human Genetics, University of Oxford, Roosevelt Drive, Oxford OX3 7BN, UK; karl@strubi.ox.ac.uk
6 BIOCEV, Institute of Biotechnology, The Czech Academy of Sciences, Průmyslová 595, 25250 Vestec, Czech Republic; dohnalek@ibt.cas.cz (J.D.); t.skalova@gmail.com (T.S.)
* Correspondence: ondrej.vanek@natur.cuni.cz
† Present address: EMBL, Hamburg Unit c/o DESY, Notkestrasse 85, 22607 Hamburg, Germany.

Received: 15 April 2020; Accepted: 14 July 2020; Published: 21 July 2020

Abstract: NKp30 is one of the main human natural killer (NK) cell activating receptors used in directed immunotherapy. The oligomerization of the NKp30 ligand binding domain depends on the length of the C-terminal stalk region, but our structural knowledge of NKp30 oligomerization and its role in signal transduction remains limited. Moreover, ligand binding of NKp30 is affected by the presence and type of *N*-glycosylation. In this study, we assessed whether NKp30 oligomerization depends on its *N*-glycosylation. Our results show that NKp30 forms oligomers when expressed in HEK293S GnTI$^-$ cell lines with simple *N*-glycans. However, NKp30 was detected only as monomers after enzymatic deglycosylation. Furthermore, we characterized the interaction between NKp30 and its best-studied cognate ligand, B7-H6, with respect to glycosylation and oligomerization, and we solved the crystal structure of this complex with glycosylated NKp30, revealing a new glycosylation-induced mode of NKp30 dimerization. Overall, this study provides new insights into the structural basis of NKp30 oligomerization and explains how the stalk region and glycosylation of NKp30 affect its ligand affinity. This furthers our understanding of the molecular mechanisms involved in NK cell activation, which is crucial for the successful design of novel NK cell-based targeted immunotherapeutics.

Keywords: NK cell; NKp30; B7-H6; glycosylation; oligomerization

1. Introduction

Natural killer (NK) cells display spontaneous cytotoxic activity without prior sensitization in a process known as natural cytotoxicity. Accordingly, this subset of lymphocytes plays a key role in early immune defense within innate immunity [1,2]. In particular, mature NK cells recognize tumor cells and certain virus-infected cells through a number of inhibitory and activating receptors [3]. The inhibitory

receptors bind to human leukocyte antigen (HLA) molecules, which block NK cell cytotoxicity, whereas their activating receptors bind to specific molecules expressed on target cells, which activate NK cells. Hence, NK cell activation depends on the balance between inhibitory and activating signals coming from their inhibitory and activating receptors [3,4], which are classified primarily into two families: C-type lectin-like and immunoglobulin-like receptors [5].

Natural cytotoxicity receptors (NCRs), namely the natural killer cell proteins NKp30, NKp44, and NKp46 (numbers refer to their molecular weights), stand out for their role in activating NK cells and initiating tumor targeting [5]. NCRs are type I transmembrane proteins that consist of one or two extracellular immunoglobulin-like (Ig-like) domains, a transmembrane α-helix with a positively charged amino acid that facilitates the interaction with signaling adaptor proteins, and a short C-terminal intracellular chain [4].

Natural killer protein 30 (NKp30; also known as natural cytotoxicity receptor 3, NCR3; or CD337) is an Ig-like activating receptor of NK cells [4,6]. Similar to other members of CD28 protein family, the extracellular part of NKp30 consists of a single N-terminal Ig-like domain, followed by a distinct 15 amino acids long stalk region proximal to the plasma membrane, which is important for receptor signaling [7]. Most CD28 family members bind proteins of the B7 family [8]; however, the first molecules that have been shown to interact with NKp30 are heparin and heparin sulfate, that serve as co ligands and only interact with the glycosylated receptor [4,9]. On the other hand, interaction of NKp30 with viral ligands, such as hemagglutinin of the ectromelia and vaccinia virus [10] and protein pp65 released from human cytomegalovirus [10], has inhibitory effects on NK cells [4]. For example, pp65 binding to NKp30 causes NKp30-CD3ζ complex dissociation, thus disrupting the activating signaling pathway, albeit without preventing other ligands from binding to NKp30 because pp65 uses another binding site [4,11].

Further, three specific cellular ligands of NKp30 have been identified. Consistent with the other members of CD28 family, NKp30 binds a member of B7 family, in particular B7 homolog 6 (B7-H6), that is constitutively expressed on the surface of some tumor cells [12]. Another NKp30 cellular ligand, BAG-6, plays a role in DNA damage response, gene expression regulation, protein quality control, and immunoregulation in healthy cells [13], but is recruited to the cell membrane and interacts with NKp30 in some tumor cells or under the stress conditions [13]. Both B7-H6 and BAG-6 also exist on the surface of exosomes [13] and in soluble forms that result from proteolytic shedding of their membrane forms, which hinders NK cell activation [13,14]. Lastly, the most recently discovered NKp30 ligand, galectin 3, expressed on the surface of some tumors, almost completely blocks NK cell cytotoxicity [15].

Since the B7-H6:NKp30 interaction was first discovered, considerable research efforts have been made to define B7-H6 expression specificity in tumor cell lines and its underlying clinical potential [8,16,17]. Similarly to NKp30, B7-H6 is a type I transmembrane protein [12]. It consists of two extracellular Ig-like domains (IgV and IgC), an α-helical transmembrane domain, and a C-terminal sequence homologous to group-specific antigen (GAG) proteins. This C-terminal sequence has various signaling motifs, including ITIM-, SH-2-, and SH-3-binding motifs [8,12], which trigger signal transduction upon NKp30 binding. However, the signal outcome remains unknown [8]. The closest structural homologs of B7-H6 are B7-H1 (more widely known as programmed death-ligand 1 or PD-L1) and B7-H3, all of which belong to the B7 protein family [8,12].

B7-H6 is expressed in several tumor cell lines, both ex vivo and in vivo, but remains undetected in healthy cells thus far, and is therefore an excellent tumor marker [8,12]. In addition, B7-H6 expression has been induced in monocytes and neutrophils [18] using agonists of Toll-like receptors (TLR2, TLR4, TLR5, and TLR8), interleukin IL-1β, and tumor necrosis factor alpha (TNFα), with consistent B7-H6 mRNA and protein expression kinetics. In these phagocytes, B7-H6 mRNA expression peaked early, from 3 to 12 h after induction, returning to baseline within 24 h, whereas its surface expression was stable for up to 48 h after induction. Soluble or exosomal B7-H6 expression has also been induced using the same factors. In in vitro studies, both soluble and membrane forms of B7-H6 were detected in the blood of patients with systemic inflammatory response syndrome, but its cell-surface expression was only

identified in patients presenting with sepsis and selective for $CD14^+$ and $CD161^+$ pro-inflammatory monocytes. In contrast, the blood of patients presenting with sepsis caused by Gram-negative bacteria contains soluble or exosomal forms of B7-H6 [18].

Although crystal structures of NKp30, both unbound [19] and in a complex with B7-H6 [20], have been solved, these structures refer to NKp30 recombinantly expressed in bacteria and therefore lacking glycosylation. However, two *N*-glycosylation sites of NKp30 are crucial for its signal transduction and for B7-H6 but not BAG-6 ligand binding [21]. Moreover, NKp30 lacks the C-terminal 15 amino acids long stalk region that connects the ligand binding domain to the transmembrane helix in these structures. Importantly, both glycosylation and the stalk region affect the binding affinity of NKp30 [22]. The stalk region affects the oligomeric state of NKp30; NKp30 without the stalk region forms only monomer and dimer species in solution, whereas NKp30 with the stalk region forms higher oligomers [21]. Interestingly, the NKp30 dimer is observed in the crystal structure of its unbound (construct without the stalk region produced in *Escherichia coli*) [19] but not in that of its B7-H6-bound state [20]. Nevertheless, the presence of oligomers is positively correlated with NKp30 affinity to its ligands, as previously measured by surface plasmon resonance (SPR), although the differences in the measured affinity are rather small. This increased affinity is due to an avidity effect, which is attributed to NKp30 ectodomain oligomerization [21]. Greater changes in affinity are caused by alterations in *N*-glycosylation; glycosylation at Asn42 is essential for ligand binding, and glycosylation at Asn68 also has a substantial effect, whereas glycosylation at Asn121 does not play a key role, as determined by site-directed mutagenesis [22].

Furthermore, the analysis of NKp30 ligand binding has highlighted differences in affinity as a function of the protein expression system used. NKp30 affinity to B7-H6 ranged from 2.5 to 3.5 μM with both recombinant proteins expressed in *Escherichia coli* [19]. However, this affinity was higher (1 μM) when B7-H6 was expressed in the Sf9 insect cell line [20] and even higher (ranging from 80 to 320 nM) when NKp30-Ig fusion protein was expressed in the human cell line HEK293T (which provides a complex *N*-glycosylation pattern). In the latter case, the affinity of NKp30 to B7-H6 additionally increased with longer stalk region [22]. Even higher affinities were recorded when expressing NKp30 in Sf9 cells and B7-H6 in HEK293T cells, assessing affinities ranging from 1 to 2 nM by ELISA, depending on the oligomeric state of NKp30 [21]. Interestingly, the affinity of NKp30 expressed in HEK293T cells to BAG-6 isolated from an insect cell line was 64 nM. In contrast, its affinity to BAG-6 isolated from *Escherichia coli* was two times higher [23].

In this study, we show that NKp30 oligomerization depends on its *N*-glycosylation. NKp30 produced in HEK293S GnTI$^-$ cells lacking *N*-acetylglucosaminyl-transferase I activity forms oligomers but disassembles to pure monomers after enzymatic deglycosylation. We have further characterized the binding affinity of B7-H6 to NKp30 and its dependence on glycosylation and oligomeric state using proteins expressed in human cell lines, that closely mimic the natural post-translational modifications of this receptor. Finally, we have determined the crystal structure of the NKp30:B7-H6 complex with the glycosylated receptor. Our results suggest that dimerization may be a necessary step for NKp30 oligomerization and stable signal transduction upon B7-H6 binding.

2. Results

2.1. Recombinant Expression and Purification of Stable, Soluble, Glycosylated NKp30, and B7-H6 Proteins

For our studies, we cloned the extracellular domains of NKp30 and B7-H6 into a mammalian expression vector with a C-terminal histidine tag. Both proteins were expressed either in HEK293T cell line that provides the protein with complex wild-type *N*-glycans, or in HEK293S GnTI$^-$ cell line that provides uniform, simple Asn-$GlcNAc_2Man_5$ *N*-glycans, in the latter case allowing also for a possibility of efficient enzymatic deglycosylation, when required [24–26]. Presence of the expected glycan type was verified by mass spectrometry (Figures S1–S3). Two constructs were prepared to study the effect of the C-terminal stalk region of the NKp30 extracellular domain. The NKp30_Stalk construct

contains the whole NKp30 extracellular domain, including the stalk region, whereas the NKp30_LBD (Ligand Binding Domain) lacks the stalk sequence, which is the C-terminal section of the extracellular domain of NKp30 (Figure 1). The entire extracellular portion of B7-H6 (Asp25–Leu245) consisting of two Ig-like domains was used. Each Ig-like domain contains one disulfide bridge, and moreover, the C-terminal domain contains one odd cysteine residue (Cys212).

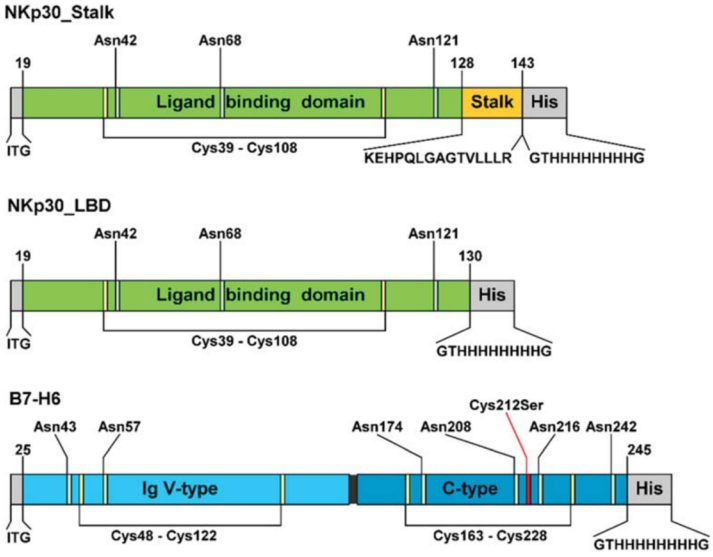

Figure 1. Recombinant NKp30 and B7-H6 expression constructs. All constructs contain three amino acids which remain after the secretion signal is cleaved at the N-terminus and a histidine tag sequence at the C-terminus. Glycosylated asparagine residues and cysteines forming disulfide bridges are indicated, as well as the mutation of the odd cysteine C212S in B7-H6.

B7-H6 expression in HEK293 cells yielded 5 mg of purified protein per liter of cell culture. However, when we analyzed fractions resulting from the SEC peak (Figure 2a, red line) by SDS-PAGE, we noticed that the protein appeared as a monomer of expected size in reducing buffer (33 kDa + *N*-glycosylation), but in non-reducing buffer, a band with a size corresponding to the B7-H6 dimer was identified (Figure 2b, left side, asterisk). These results suggest that the protein formed covalent dimers via its odd cysteine residue. Sedimentation analysis also showed that, although most of the protein behaved as monomers, sedimenting at 2.5 S, a small amount of putative dimer (4 S) and tetramer (6.1 S) species were also present (Figure 2c). The average fitted f/f_0 frictional ratio of 1.5 indicates an elongated shape of the molecule, in line with the published structure. However, mass spectrometry analysis confirmed that disulfide bridges of this wild-type B7-H6 expression construct were not linked correctly (Table S1).

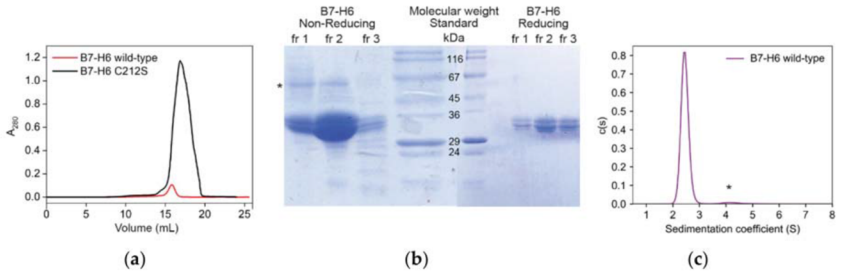

Figure 2. Recombinant B7-H6 is stabilized by the C212S mutation. (**a**) Size-exclusion chromatography (SEC) profiles of recombinantly expressed wild-type B7-H6 and its C212S mutant. (**b**) Fractions of the wild-type B7-H6 SEC peak were analyzed by 15% SDS-PAGE under non-reducing (left) and reducing (right) conditions. (**c**) Sedimentation analysis of wild-type B7-H6 at 0.5 mg/mL shown as continuous size distribution of the sedimenting species c(s). Dimeric species are marked with an asterisk in (**b**,**c**).

The odd cysteine that forms the unwanted covalent dimer of B7-H6 was identified as C212 according to the published structure (PDB 3PV6) [20]; therefore, we mutated this cysteine to serine (C212S). This mutation resulted in the proper folding of B7-H6 (Table S1), and strikingly, promoted the expression yield up to 50 mg per liter of cell culture (Figure 2a, black line). In the present study, only this C212S mutated form of B7-H6 was used and is henceforth referred to as B7-H6 for simplicity. The expression of both NKp30 constructs in HEK293 cell lines was straightforward, yielding 40 and 23 mg of NKp30_LBD, and 27 and 14 mg of NKp30_Stalk per liter of cell culture when expressed in HEK293T and HEK293S GnTI$^-$ cell line, respectively.

2.2. Protein Deglycosylation

To assess the effect of glycosylation on NKp30 oligomerization and on its binding properties, we deglycosylated both NKp30_Stalk and NKp30_LBD. Moreover, as B7-H6 has six predicted *N*-glycosylation sites (Figure 1), the complexity of wild-type mammalian glycosylation might hinder crystallization and therefore we deglycosylated also B7-H6. Additionally, we also assessed the effect of the type of B7-H6 glycosylation on NKp30 receptor binding. The deglycosylated proteins were analyzed by SDS-PAGE (Figure 3).

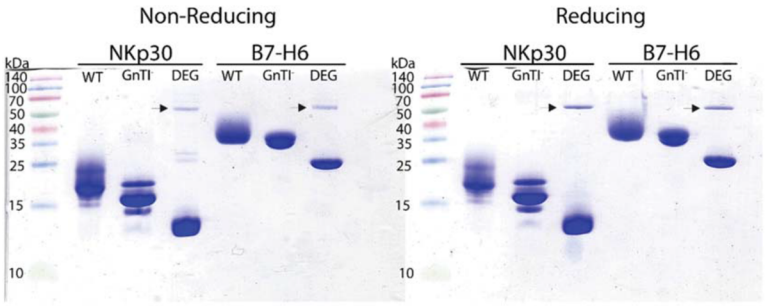

Figure 3. SDS-PAGE analysis of deglycosylated NKp30_LBD and B7-H6 C212S mutant. Different glycosylation states are marked as WT for proteins expressed in HEK293T cells with wild-type (WT) *N*-glycosylation; GnTI$^-$ expressed in HEK293S GnTI$^-$ cells lacking *N*-acetylglucosaminyltransferase I activity which have, therefore, uniform Asn-GlcNAc$_2$Man$_5$ *N*-glycans; and DEG for the GnTI$^-$ proteins deglycosylated (DEG) with endoglycosidase Endo F1 (itself marked by an arrow).

Under standard conditions (10 mM HEPES pH 7.5, 150 mM NaCl, 10 mM NaN_3), B7-H6 deglycosylation caused its precipitation, most likely because of the loss of all its glycans. For this reason, we sought to improve the buffer conditions for deglycosylation and the storage of this protein by differential scanning fluorimetry. Twenty-five conditions were screened by analyzing protein melting point temperatures (Figure 4). The initial melting temperature T_m of the protein in the HEPES buffer was 50 °C and changing the pH of the buffer had no effect. Similarly, adding salts or stabilizers such as L-Arginine had virtually no effect either. Conversely, the highest T_m was recorded when adding 0.5 M saccharose (58 °C). However, at 20% glycerol, the T_m increased similarly (56 °C) and B7-H6 aggregation was completely prevented during deglycosylation. Therefore, glycerol was added to a final concentration of 20% (*v*/*v*) for convenience and used for further B7-H6 deglycosylation and storage at low temperatures (−20 °C). Glycerol was always removed by buffer exchange on desalting columns prior to subsequent experiments.

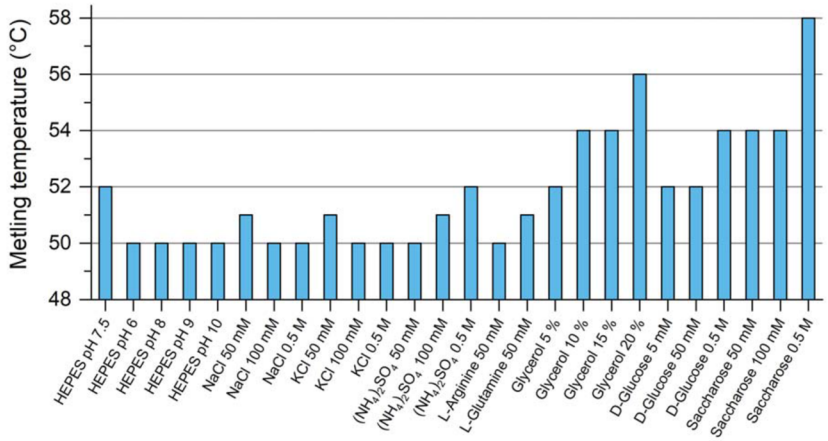

Figure 4. B7-H6 is stabilized by glycerol and saccharose addition. Differential scanning fluorimetry was used to analyze changes in protein melting temperature when adding various reagents. The concentrations given in the graph correspond to the final concentrations present in the sample.

2.3. NKp30 Glycosylation Promotes Its Oligomerization

The extracellular part of the NKp30 receptor has three *N*-glycosylation sites (Figure 1). In previous study, the presence of its *N*-glycans has been shown to enhance B7-H6 ligand binding [22] and associated cell signaling. In addition, NKp30 also forms non-covalent oligomers when the construct contains the C-terminal stalk region [21]. Accordingly, we determined the size of these oligomers by analytical ultracentrifugation (AUC) and SEC with multi-angle light scattering (MALS) detection. Notably, the NKp30_LBD construct lacking the stalk region is purely monomeric, whereas the NKp30_Stalk construct is present in both monomeric and oligomeric species (Figure 5a). Surprisingly, we could show that not only the stalk region, but also *N*-glycosylation is essential for the formation of NKp30 oligomers. Whereas NKp30_Stalk expressed in HEK293T or HEK293S GnTI$^-$ cell line contains a prominent fraction of oligomers, the deglycosylation of NKp30 with Endo F1 (leaving a single GlcNAc unit at the glycosylation site) completely depletes the sample of oligomers (Figure 5b). Elution profile of concentrated oligomeric fraction of NKp30_Stalk shows that most of the protein remains in the oligomeric form and only a minor fraction dissociates to monomers, highlighting slow kinetics of the oligomer dissociation. However, deglycosylation of the same oligomeric fraction again depletes the oligomers and only monomeric protein remains in the sample.

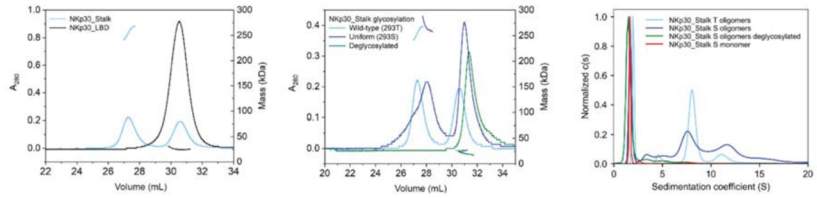

Figure 5. Glycosylation is necessary for NKp30 oligomerization. (**a**) SEC-MALS analysis of NKp30_Stalk and NKp30_LBD, confirming that the stalk region is required for oligomerization. (**b**) SEC-MALS analysis of recombinantly expressed NKp30_Stalk with wild-type glycosylation (black), uniform, simple glycans (blue), both showing non-covalent oligomers, and deglycosylated sample, which does not form oligomers (red). (**c**) Normalized continuous size distributions of sedimenting species for glycosylated and deglycosylated NKp30_Stalk oligomers and for its monomeric fraction. The main peak corresponds to the NKp30_Stalk monomer, whereas a broad distribution of oligomeric species is present in glycosylated NKp30_Stalk samples.

We repeated the same experiment and analyzed it using analytical ultracentrifugation, which led to the same conclusion; NKp30_Stalk does not form oligomers when deglycosylated (Figure 5c). Sedimentation analysis provided better resolution of the oligomeric species than SEC and thus allowed us to estimate their size. The main peak at 1.8 S, with a predicted molar mass of 18.8 kDa, matches the expected mass of the glycosylated NKp30_Stalk monomer (18.9 kDa). The molar masses predicted for the peaks corresponding to the oligomeric species indicated the presence of oligomers with 3, 5, 10, and 20 units, on average. The fitted f/f_0 ratio of 1.6 suggests that the oligomers have a considerably elongated or flattened shape. Interestingly, NKp30_Stalk with wild-type glycosylation expressed in HEK293T cells (20–25 kDa) showed a more homogeneous oligomer profile with one dominant species of ca 8 units and with secondary species of ca 16 units, based on their calculated molar masses of 180 and 320 kDa, respectively. These findings corroborate the molar masses calculated from the MALS signal (Figure 5b), which are within the same range. In summary, not only the presence of the stalk domain but also the glycosylation is essential for the formation of NKp30 oligomers.

2.4. B7-H6 Forms Equimolar Complex with Monomeric NKp30, But Not with Its Oligomeric Form

To study the impact of B7-H6 on NKp30 oligomers, we followed the NKp30:B7-H6 interaction using hydrodynamic approaches. NKp30_Stalk and B7-H6 were analyzed by SEC-MALS separately and in a complex at a 1:1 molar ratio (Figure 6a). Shifts in the elution volume and in the calculated molar mass suggest the formation of the complex in the monomeric and oligomeric fractions of the NKp30_Stalk construct. The ratio between the areas of monomeric and oligomeric peaks did not change, indicating that B7-H6 binding does not disrupt or induce NKp30 oligomerization. Subsequently, we analyzed the binding of the monomeric and oligomeric fractions separately by AUC. The monomeric fraction of glycosylated NKp30_Stalk sedimented predominantly at 1.7 S (monomer) and marginally at 3.5 S (dimeric or trimeric species). B7-H6 sedimented as monomer at 2.4 S. The equimolar mixture of these proteins sedimented as a 1:1 complex at 3.1 S, with a relatively small peak observed at 1.7 S, which is most likely an excess of the free monomer of NKp30 (Figure 6b).

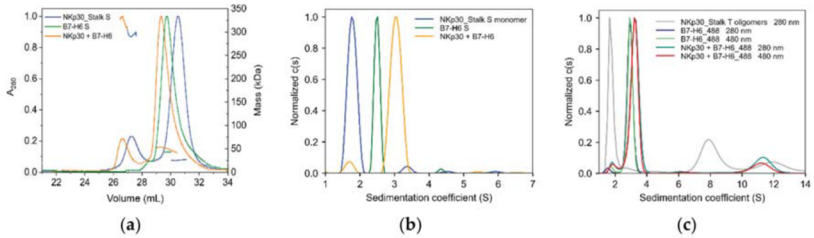

Figure 6. NKp30_Stalk oligomers cannot be saturated by B7-H6. (**a**) Normalized SEC (Size Exclusion Chromatography) elution profiles of NKp30_Stalk, B7-H6 and their equimolar mixture with MALS detection. (**b**) Sedimentation analysis of complex formation for B7-H6 and NKp30_Stalk monomeric fraction and (**c**) of NKp30_Stalk oligomeric fraction with B7-H6 labeled with ATTO488 dye performed at two wavelengths. Letters S and T denote the type of protein glycosylation (HEK293S GnTI$^-$ or HEK293T *N*-glycans, respectively).

To monitor the binding of the oligomeric fraction, we labelled B7-H6 with NHS-ATTO488 fluorescent dye and performed the experiment at 280 nm (total signal) and 480 nm (B7-H6 only) wavelengths (Figure 6c). The bimodal distribution of NKp30_Stalk HEK293T oligomers changed to a single oligomeric complex upon the addition of B7-H6, with a sedimentation coefficient of 11.2 S that corresponds to ca 340 kDa at the fitted overall f/f_0 ratio of 1.7. This value is lower than expected for the fully saturated NKp30_Stalk_HEK293T putative octamer (ca 180 kDa plus eight times 30–33 kDa for each glycosylated B7-H6, i.e., approximately 420–440 kDa for the fully saturated 1:1 complex). This suggests that not all NKp30 binding sites in the oligomeric species are accessible for B7-H6 binding and that NKp30 molecules might sterically block the access to the neighboring binding sites within the oligomer itself or with the B7-H6 molecules bound to it. The modest increase in MALS-calculated molar mass for the oligomeric NKp30:B7-H6 complex (Figure 6a) supports these inferences. Indeed, the ratio between the areas of monomeric and oligomeric NKp30:B7-H6 differs between 280 nm and 480 nm, which indicates that the amount of B7-H6 present in oligomers is smaller than the amount of NKp30 in oligomers (Figure 6c). Finally, the areas under the oligomeric peak are not equal between the two wavelengths, suggesting that only approximately 60% of the NKp30 binding sites are occupied by B7-H6 in the oligomers. This matches well with the observed mass difference between the oligomeric complex (340 kDa) and the oligomers (180 kDa), resulting in ca 160 kDa of B7-H6 bound to the oligomers, or approximately five B7-H6 molecules per eight NKp30 molecules in the oligomeric complex. Hence, B7-H6 binds both monomers and oligomers of NKp30, but only sub-equimolar amount of NKp30 binding sites is available for B7-H6 binding in the oligomeric fraction.

2.5. Affinity of NKp30:B7-H6 Interaction Differs between Surface and Solution

To reevaluate the impact of glycosylation on the interaction of B7-H6 and NKp30, we measured the affinity of this interaction using proteins with different glycosylation patterns. B7-H6 has six predicted *N*-glycosylation sites, five of which were confirmed by our MS analysis (Table S1). B7-H6 in wild-type (T), simple (S), and Endo F1-deglycosylated (D) glycosylation states were immobilized on the SPR chip. The same analyte, the monomeric fraction of NKp30_Stalk, was measured in individual cells. Neither the dissociation constant K_D nor the maximal response B_{max} values significantly differed among all tested B7-H6 variants (Figure 7a). Therefore, B7-H6 glycosylation does not significantly affect the NKp30 receptor binding.

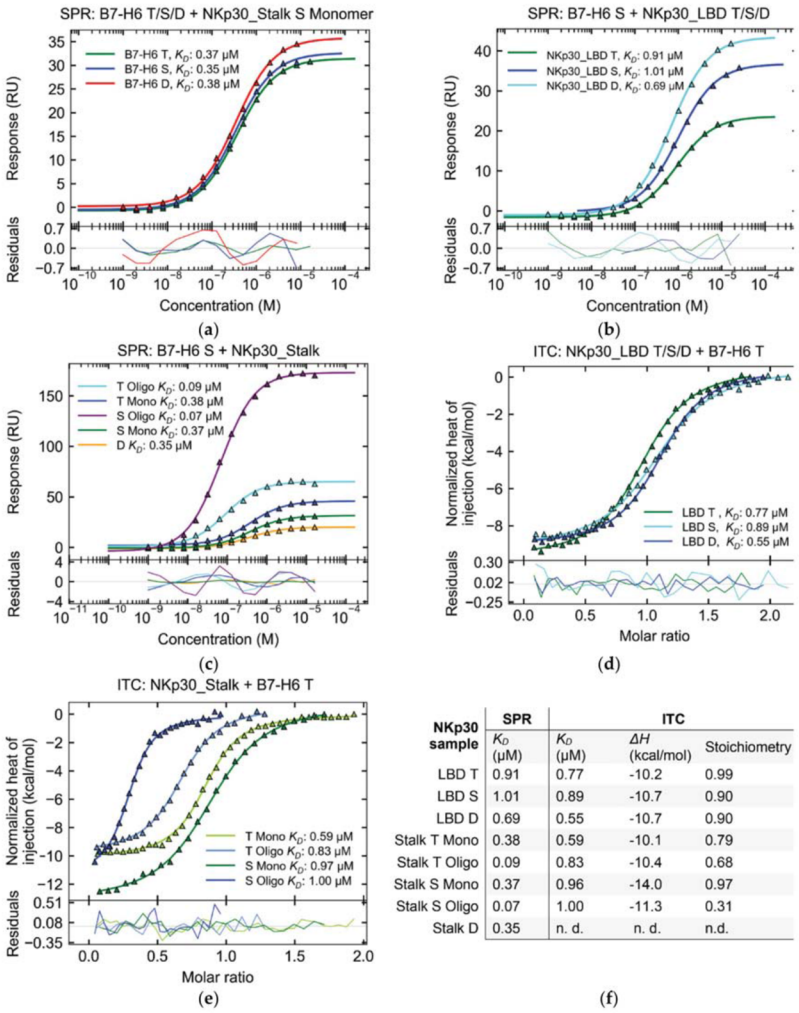

(f)

NKp30 sample	SPR	ITC		
	K_D (µM)	K_D (µM)	ΔH (kcal/mol)	Stoichiometry
LBD T	0.91	0.77	-10.2	0.99
LBD S	1.01	0.89	-10.7	0.90
LBD D	0.69	0.55	-10.7	0.90
Stalk T Mono	0.38	0.59	-10.1	0.79
Stalk T Oligo	0.09	0.83	-10.4	0.68
Stalk S Mono	0.37	0.96	-14.0	0.97
Stalk S Oligo	0.07	1.00	-11.3	0.31
Stalk D	0.35	n. d.	n. d.	n.d.

Figure 7. Characterization of the NKp30:B7-H6 interaction by SPR and ITC. Type of protein glycosylation: T—wild-type, S—uniform, D—deglycosylated, Mono—monomeric, Oligo—oligomeric fraction of NKp30_Stalk. Titles above individual graphs describe the given experiment: SPR or ITC, protein bound to SPR sensor or present in ITC cell + protein flown over the sensor or titrated into the cell, respectively. (**a**) B7-H6 glycosylation does not affect NKp30 binding. (**b**,**d**) Glycosylation of NKp30 weakens its interaction with B7-H6. (**c**,**e**) Stalk region and oligomerization of NKp30 enhance its affinity to B7-H6 in SPR but not in ITC. (**f**) Comparison of all thermodynamic parameters measured for the NKp30:B7-H6 interaction with different protein variants.

Subsequently, we investigated the effect of NKp30 deglycosylation on B7-H6 ligand binding. A previous study had already shown that the point mutation of the glycosylation site Asn68 (N68Q)

reduces the affinity for the B7-H6 ligand, whereas the N42Q mutation of the Asn42 glycosylation site almost completely abrogates binding [22]. For this reason, we performed a binding assay with NKp30 deglycosylated with Endo F1. Interestingly, in comparison with the aforementioned study, the affinity of both deglycosylated NKp30_LBD and NKp30_Stalk did not significantly differ from that of their wild-type or uniformly glycosylated counterparts in both SPR and isothermal titration calorimetry (ITC) measurements (Figure 7b–e). In fact, for NKp30_LBD, the affinity even moderately increased from uniform glycans to wild-type glycans to deglycosylated protein (Figure 7b,d). Similarly, only slight differences in affinity were found among NKp30_Stalk glycosylation variants (Figure 7c,e). However, Endo F1 treatment leaves a single GlcNAc unit at each glycosylation site, whereas point mutations completely block glycosylation. Hence, these results cannot be compared directly.

In contrast, NKp30_Stalk variants showed higher affinity than the shorter NKp30_LBD construct when analyzed by SPR (Figure 7c), thus confirming earlier observations that the stalk region contributes significantly to B7-H6 binding. The affinity of the NKp30_Stalk monomeric fraction was approximately two times higher than that of NKp30_LBD, as shown by both SPR and ITC analyses (Figure 7b,d). Even higher affinities were recorded by SPR for the NKp30_Stalk oligomeric fraction, which was bound approximately ten times more strongly than NKp30_LBD and four times more strongly than the NKp30_Stalk monomeric fraction. Simultaneously, the B_{max} was higher, as expected for oligomer binding (Figure 7c) and in line with a previous study, thus jointly concluding that the observed increase in affinity results from the avidity contribution of the oligomers [21].

Surprisingly, the affinity of the NKp30:B7-H6 interaction was similar when comparing NKp30_LBD with the monomeric and oligomeric fractions of NKp30_Stalk by ITC (Figure 7d,e), albeit with a tenfold decrease in affinity of the oligomeric fraction compared to SPR results. In addition, ITC results showed lower stoichiometry for the oligomeric fractions of NKp30_Stalk (Figure 7f), thus suggesting that not all binding sites of the oligomer are saturated and that they might be sterically blocked and inaccessible for B7-H6 binding. These findings match our results from the sedimentation analysis (Figure 6c), i.e., only 60–70% NKp30_Stalk T oligomers are accessible.

2.6. Crystal Structure of Glycosylated NKp30:B7-H6 Complex

To understand the role of glycosylation in the NKp30:B7-H6 interaction in more detail, we solved the crystal structure of NKp30 with uniform glycosylation in complex with Endo F1-deglycosylated B7-H6. Although we were unable to crystallize this complex with the oligomer-forming NKp30_Stalk construct, we obtained diffracting crystals using the NKp30_LBD monomeric protein. The structure (PDB 6YJP) was solved at 3.1 Å resolution, and the refinement parameters are summarized in Table 1. The asymmetric unit of the crystal contains two NKp30_LBD molecules (LBD_A/B) and three B7-H6 molecules (B7-H6_C/D/E), as shown in Figure 8 below. The molecules are completely localized, except for two missing loops in B7-H6 (residues 151–159 and 149–155 in chains D and E, respectively). In fact, one more NKp30_LBD chain that interacts with B7-H6 (chain E) is present in the crystal but its loose localization did not allow us to build it in the structure.

When viewing neighboring symmetry-related molecules, surrounding the asymmetric unit of the crystal, a dimer of two NKp30_LBD:B7-H6 complexes (LBD_A:B7-H6_C and LBD_B:B7-H6_D) becomes apparent (Figure 9). The interaction interfaces between NKp30 and B7-H6 are conserved and highly similar to the interaction surface observed in the 3PV6 structure; the contact between NKp30_LBD_A and B7-H6_C chains comprises four hydrogen bonds or salt bridges (chain A Gly51 N—chain C Thr127 OG1, chain A Val53 N—chain C Pro128 O, chain A Glu111 OE1—chain C Lys130 NZ and chain A Glu111 OE2—chain C Lys130 NZ), and the interface has a Pisa server complex formation significance score of 0.225 [27]. The contact between chains NKp30_LBD_B and the symmetry-related B7-H6_D comprises five hydrogen bonds or salt bridges: four analogical to the aforementioned bonds and an additionally B47 Arg NH1—D84 Asp OD1 bond. The interface has the same score, 0.225, according to the Pisa server.

Table 1. Data collection statistics and structure refinement parameters for the NKp30_LBD:B7-H6 crystal structure. Values in parentheses refer to the highest resolution shell.

PDB Code	6YJP
Data processing statistics	
Space group	C2
Unit-cell parameters *a*, *b*, *c* (Å); α, β, γ (°)	166.0, 86.5, 111.3; 90, 97.6 90
Resolution range (Å)	48.95-3.1 (3.29-3.1)
No. of observations	99061 (12123)
No. of unique reflections	27102 (3968)
Data completeness (%)	95 (87)
Average redundancy	3.7 (3.1)
Mosaicity (°)	0.09
Average $I/\sigma(I)$	5.7 (0.8)
Solvent content (%)	65
Matthews coefficient (Å^3/Da)	3.54
Wilson B-factor (Å^2)	105.5
R_{merge}	0.104 (0.971)
R_{pim}	0.081 (0.804)
CC1/2	0.995 (0.645)
Structure refinement parameters	
R_{work}	0.272
R_{free}	0.322
R_{all}	0.275
Average *B*-factor (Å^2)	155.6
RMSD bond lengths from ideal (Å)	0.005
RMSD bond angles from ideal (°)	1.59
Number of non-hydrogen atoms	6907
Number of water molecules	0
Ramachandran statistics: residues in allowed/favored region (%)	99.5/92.9

$R_{merge} = \sum_h \sum_i |I_{hi} - \langle I_h \rangle| / \sum_h \sum_i I_{hi}$, $R_{pim} = \sum_h \sum_i (n_h - 1)^{-1/2} |I_{hi} - \langle I_h \rangle| / \sum_h \sum_i I_{hi}$, and $R = \sum_h \left| |F_{h,obs}| - |F_{h,calc}| \right| / \sum_h |F_{h,obs}|$, where I_{hi} is the observed intensity, $\langle I_h \rangle$ is the mean intensity of multiple observations of symmetry-related reflections, and $F_{h,obs}$ and $F_{h,calc}$ are the observed and calculated structure factor amplitudes. R_{work} is the R factor calculated on 95% of reflections excluding a random subset of 5% of reflections marked as "free". The final structure refinement was performed on all observed structure factors. RMSD, root-mean-square deviation, PDB, published structure.

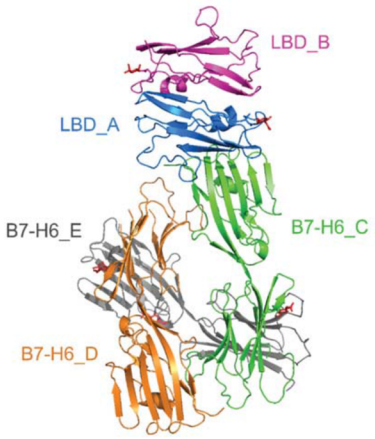

Figure 8. Crystal structure of uniformly glycosylated NKp30_LBD in complex with deglycosylated B7-H6. The asymmetric unit contains two molecules of NKp30_LBD (chains LBD_A and B) and three molecules of B7-H6 (chains B7-H6_C, D and E). Interaction interface between chains LBD_A and B7-H6_C corresponds to the interaction surface observed in the previously published structure of this complex (PDB 3PV6) [20].

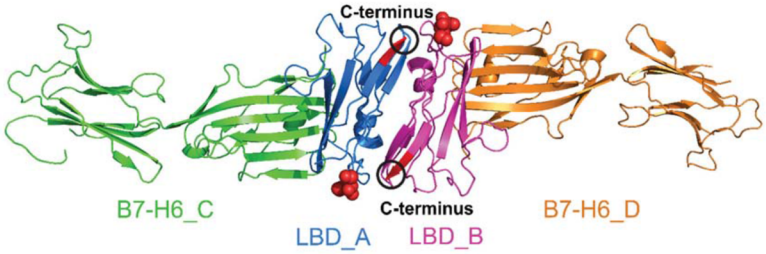

Figure 9. A dimer of the NKp30_LBD:B7-H6 complex is observed in the presented crystal structure. Within the NKp30:B7-H6 complex, both pairs of molecules bind to each other almost identically, and the binding mode of the two proteins is also very similar to that described based on the previously published structure of the complex (PDB 3PV6) [20]. However, the structure of the NKp30_LBD dimer is distinct to the previously published structure of NKp30_LBD itself (PDB 3NOI) [19]. The dimer has a two-fold rotation symmetry, and the *N*-glycosylation site at Asn42 of LBD_A (GlcNAc residue highlighted as spheres) is close to C-terminus of LBD_B (highlighted in red) and vice-versa.

In the crystal structure, electron density maps allowed us to model *N*-acetylglucosamine at NKp30_LBD asparagine residues 42 (chains A and B), and B7-H6 residues 208 (chains C and D) and 43 (chain E). Furthermore, low-quality peaks in the electron density map, corresponding to glycans, were observed near NKp30_LBD asparagine residues 68 (chain A) and 121 (chain B), and near B7-H6 residues 43 (chains C,D), 57 (chains C,D,E), 174 (chains C,D,E), 208 (chain E), and 242 (chains C,E). In the case of NKp30_LBD Asn42, the glycosylation changes the orientation of the Asn42 side chain and main chain and consequently, the placement of residue Ala43 in comparison with NKp30_LBD in PDB 3NOI and 3PV6. Noticeably, the glycosylation site at Asn42 of one NKp30_LBD molecule (LBD_A) localizes in the proximity of the C-terminus of the other NKp30_LBD molecule (LBD_B) and vice versa (Figure 9). In NKp30_Stalk or in full-length NKp30 receptor, this C-terminal part of its ligand binding domain would be followed by the 15 amino acids long stalk region. Both the glycosylation and the stalk regions are required for NKp30 oligomerization, suggesting that this NKp30_LBD dimer may be the building block of these oligomers.

NKp30_LBD chains A and B form a dimer different from that observed in the crystal structure of NKp30 itself (PDB 3NOI) [19], whereas NKp30 was only monomeric in the crystal structure of the NKp30:B7-H6 complex (PDB 3PV6) [20]. Both dimers have two-fold symmetry and a similar patch of mutual contacts (residues Arg28, Asn42, Gln45, and Glu128 participate in hydrogen bonds in both cases); however, their mutual orientation is very different: when chains A are superimposed, the positions of the same residues in chain B differ by 9–15 Å (Figure 10). The NKp30 dimer in PDB 3NOI comprises sixteen hydrogen bonds or salt bridges, and the interface scores 0.176 in the Pisa server, whereas the dimer observed in the present structure PDB 6YJP comprises eleven hydrogen bonds or salt bridges, and its interface scores 1.0 in the Pisa score, which indicates a more stable interaction and relevant interface. Interestingly, Asn42 of NKp30_LBD is positioned directly at the dimer interface in PDB 3NOI, and in close contact with Glu26 and Arg28 from the second chain, whereas GlcNAc at Asn42 in PDB 6YJP is located outside of the interface, right next to the C-terminus of the second chain—at the beginning of the stalk region.

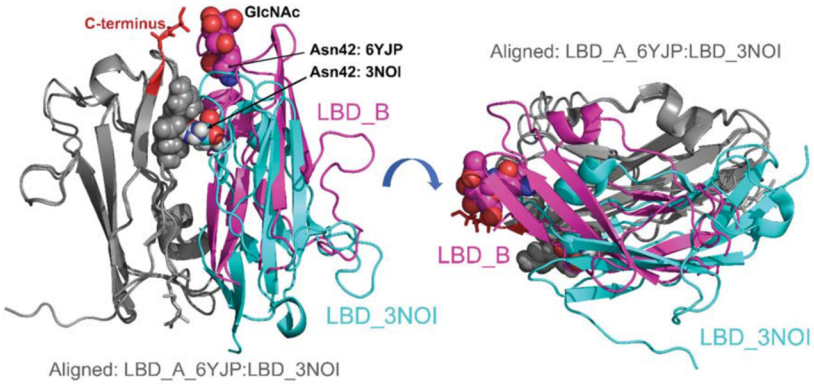

Figure 10. Glycosylation-induced NKp30 dimerization positions the glycans at Asn42 residues near the C-terminal stalk regions. The NKp30_LBD dimers observed in the present crystal structure PDB 6YJP and the PDB 3NOI [19] were aligned using molecules on one side of the dimer only (grey color). On the left —the *N*-glycosylation site at Asn42 of LBD_B, highlighted as spheres, is near the C-terminus of LBD_A (highlighted in red), whereas the Asn42 residue in LBD_3NOI is buried within the dimer interface, interacting with Glu26 and Arg28 (all highlighted as spheres). On the right—side view of the dimer interface showing the difference in arrangement of the two dimers.

3. Discussion

The first key stage of this study was the preparation of the stable, soluble, extracellular part of the B7-H6 protein. Members of the B7 family have moved to the forefront of cancer research for their underlying involvement in tumorigenesis [17] and tumor recognition [16] and for their role as regulators of immune responses and immunotherapy outcomes, such as B7-H1, also known as PD-L1, one of the most discussed checkpoint inhibitors in recent years [28]. Because B7-H6 can induce NKp30-dependent NK activation and cytokine secretion [12], therapeutic interventions based on the NKp30:B7-H6 interaction may provide a new strategy for tumor treatment. Wu et al. [29] have shown that the B7-H6-specific bispecific T cell engager (BiTE) directs host T cells to mediate cellular cytotoxicity and interferon-γ secretion, which is therefore a potential therapeutic strategy for B7-H6$^+$ hematological and solid tumors. More recently, T cells expressing B7-H6-specific human single-chain fragment variable (scFv) as chimeric antigen receptor (CAR) have been shown to induce potent anti-tumor activity in vitro and in vivo against tumors expressing high amounts of B7-H6 [30].

Although B7-H6 was the target molecule in these approaches, other strategies have been developed exploring the potential of B7-H6 as a natural ligand for the activating receptor NKp30. Kellner et al. [31,32] generated a fusion protein consisting of the ectodomain of B7-H6 and of the CD20-specific scFv 7D8. In the functional assay, the authors found that the B7-H6:7D8 fusion protein could stimulate NKp30-mediated NK cell cytotoxicity. The same strategy was successfully applied to create a HER2-specific B7-H6 fusion protein targeting HER2$^+$ tumors [33]. In our study, we initially tried to express not only the B7-H6 construct described above (Figure 1), but also a shorter construct corresponding to the N-terminal IgV B7-H6 domain (Asp25—Val140) only. However, this shorter construct could not be expressed at all, thus suggesting that, although the two Ig-like domains of B7-H6 are structurally well separated, the extracellular part of B7-H6 is stable only when expressed as a whole. Furthermore, we found that mutating the odd cysteine in the B7-H6 IgC domain (Cys212Ser) greatly stabilizes the molecule by promoting correct disulfide bond formation, reaching a ten-fold increase in yield over the wild-type B7-H6 ectodomain. Moreover, glycerol addition was optimal for long-term B7-H6 storage, both in solution and in frozen state, preventing its aggregation, especially

at higher protein concentrations. This optimized protocol for recombinant B7-H6 production may be useful for further studies involving B7-H6 fusion immunotherapeutics or requiring large-scale expression of this tumor antigen in a stable and well-folded form.

Oligomerization of the NKp30 ectodomain has been previously characterized using constructs expressed in Sf9 insect cells providing uniform, simple paucimannose *N*-glycans, similar to those present in HEK293S GnTI$^-$ cell lines. When recombinantly expressing these constructs, the authors found that both NKp30_Stalk and NKp30_LBD oligomerized in their study, although the latter to a lesser extent [21]. However, both proteins had a considerable number of additional amino acid residues at both their N- and C-termini, namely ADLGS and GSENLYFQGGS followed by a decahistidine tag, respectively. In our study, we used the same LBD and Stalk regions of the NKp30 ectodomain, but we expressed these NKp30 constructs in human cell lines, providing uniform mannose- or wild-type glycosylation, and with a limited number of flanking amino acids. Regardless of the glycosylation type or presence, at low concentration the NKp30_LBD construct showed no tendency to oligomerize. At high sample concentration, however, dimer formation has been observed for this construct in our sedimentation analysis (Figure S4). Thus, we can conclude that although the ligand binding domain of NKp30 itself shows some tendency to self-associate (as evidenced by dimer formation observed at high concentration in solution by AUC and by dimeric arrangement found in the crystal), presence of the stalk region is a prerequisite for stable NKp30 oligomerization in solution.

In addition, the ability of the NKp30_Stalk construct to oligomerize is lost upon its deglycosylation with endoglycosidase F1, thereby highlighting the unappreciated but key role of glycosylation in NKp30 oligomerization. Hermann et al. [21] observed that NKp30_Stalk oligomers bound to immobilized B7-H6-Ig have an extremely low nanomolar K_D, as assessed by SPR and ELISA (both surface-based interaction methods), and hypothesized that the increase in apparent ligand binding affinity of the oligomers is caused by the increase in the avidity of higher-molecular-order NKp30 complexes under these conditions. We noted a similar trend in our SPR analysis when using immobilized B7-H6, observing a higher affinity for NKp30_Stalk than for NKp30_LBD, and an even higher affinity for the NKp30_Stalk oligomeric fraction. In contrast, when analyzing the same system by AUC and ITC (solution-based techniques), we found that both monomeric and oligomeric fractions of NKp30_Stalk, and NKp30_LBD, showed similar thermodynamic parameters and affinity to soluble B7-H6, but the oligomers exhibited significantly lower binding stoichiometry. This suggests that interaction data on immobilized B7-H6 and oligomerizing NKp30_Stalk construct collected using surface methods might not correctly express K_D values for interactions of individual binding sites and that the NKp30 oligomers might not be completely biologically active species, at least when present in solubilized form and not on the cell surface.

Another important aspect of the NKp30:B7-H6 interaction is the glycosylation of the NKp30 ectodomain, especially on Asn42 and Asn68 sites, as shown by Hartmann et al. [22] in binding experiments with NKp30 human IgG1-Fc fusion constructs expressed in HEK293T cell lines. Interestingly, mutating these glycosylation sites affected binding to B7-H6, but not to BAG-6, as determined by SPR or ELISA, respectively. Moreover, NKp30_Stalk-Ig binding to natural ligands, in various tumor cell lines, was even stronger in the absence of glycosylation, albeit abrogated in B7-H6$^+$ reporter cell lines. This key role of glycosylation and of the stalk region in signal transduction was further corroborated by using various NKp30-transfected CD3ζ reporter cell lines stimulated by B7-H6$^+$ target cells [22]. In our study, we did not observe marked differences in NKp30:B7-H6 affinity between the NKp30_Stalk and NKp30_LBD constructs, and neither between the NKp30 variants expressed with wild-type human or uniform oligomannose *N*-glycans, or deglycosylated, independent of the method that we used to measure these interactions. The deglycosylated proteins used in our study still had a single GlcNAc residue at each glycosylation site, in contrast to the disruptive Asn-Gln mutations used in the previous study, which may account for the differences in the results. Nevertheless, our findings indicate that glycosylation most likely does not directly affect the NKp30:B7-H6 interaction and instead primarily affects the ability of NKp30 to oligomerize. Impaired oligomerization would then translate

into lower apparent binding affinities, when using surface-based methods such as SPR and ELISA, and into impaired signal transduction in cell-based experiments. The role of the stalk domain in CD3ζ-mediated activation of NK cells was thoroughly characterized by Memmer et al. [7] who showed that mutations in the stalk region close to LBD weaken the K_D of B7-H6-Fc whereas BAG-6 binding, again, remained mostly unaffected, although NKp30-Fc IgG fusions and SPR detection were used in these experiments. Subsequent reporter cell-based assays showed that Arg143 (end of the NKp30 stalk region) alignment with the aspartate of CD3ζ is required for signal transduction and that this alignment might be achieved by ligand-induced receptor clustering and/or stalk-dependent conformational changes [7]. NKp46, another member of the NCR family, exhibits similar complex behavior on the cell surface. It forms dimers and later on also clusters within the immune synapse, which activate NK cell polarization [34,35].

Although NKp30 constructs artificially dimerized through IgG-Fc fusion may not be the best tools to describe the natural behavior of this receptor at the plasma membrane of NK cells, their thorough characterization should be useful for developing immunotherapeutics. Over ten years ago, Arnon et al. [36] demonstrated using human prostate cancer cell lines that treatment with NKp30-Ig dramatically inhibits tumor growth in vivo in mice by successfully recruiting activated macrophages via antibody-dependent cellular cytotoxicity (ADCC). Strikingly, while IgG1 Fc-fusions are regularly used in NCR-related immunology research, no immunotherapy product based on them has been developed thus far.

The original motivation for our work was to understand better how NKp30 oligomers are formed and structured. To this end, we used multiple techniques, but not all of them produced conclusive results, such as structural mass spectrometry (cross-linking and H/D exchange) or cryo-electron microscopy. We also tried to crystallize the NKp30_Stalk construct and thus solve its oligomeric structure, albeit to no avail. Neither this protein nor its complex with B7-H6 formed crystals. Nevertheless, we solved the structure of the glycosylated NKp30_LBD:B7-H6 complex, which is somewhat similar to the previously known structures of NKp30_LBD (PDB 3NOI, [19]) and of the NKp30_LBD:B7-H6 complex (PDB 3PV6, [20]). However, both previously published structures were solved using bacterially expressed, non-glycosylated refolded NKp30_LBD. Therefore, our structure provides new insights into the mechanism of oligomerization of this protein.

Most interestingly, our crystal structure shows the formation of an NKp30_LBD dimer in the bound state with B7-H6. The symmetrical arrangement of Asn42 glycosylation sites, near the C-terminal stalk region beginnings on both sides of the dimer, strengthens our hypothesis of glycosylation-supported, stalk region-mediated NKp30 oligomerization. In contrast to the structure of the glycosylated NKp30_LBD dimer, in the dimer of the refolded NKp30_LBD observed in the PDB 3NOI crystal structure, the Asn42 residue is in close contact with neighboring side chains of other amino acids of the dimerization interface. With such a bulky glycan chain bound to the Asn42, this type of dimer is unlikely to exist. Therefore, we may assume that glycosylation induces the observed dimer arrangement and that this arrangement is further stabilized by the interaction between the glycan moiety and the stalk region of full-length NKp30.

Moreover, for soluble NKp30_Stalk, the stalk regions that extend on both sides of the dimer would be free to interact with stalk regions of other NKp30_Stalk dimers, thereby forming linear oligomers composed of such dimers. To acquire at least some low-resolution data on the structure of these oligomers, we have also performed SEC-SAXS analysis of the NKp30_LBD, NKp30_Stalk monomeric and oligomeric fractions, and their complexes with B7-H6 (Figure S5). Representative examples of the resultant ab initio molecular envelopes calculated from the collected SAXS data are shown in Figure S6 [37,38]. The lack of further structural data on how individual NKp30_Stalk molecules or their possible dimers are arranged in space precludes any further modelling of molecular arrangements of these oligomers. Nevertheless, the overall shape of the calculated envelopes is highly asymmetrical, that is, prolate or oblate rather than spherical, and this asymmetry is in perfect agreement not only with

the prediction based on the crystal structure but also with our sedimentation analysis of the oligomers indicating asymmetrical elongated or flattened particles.

Another interesting aspect of our crystal structure is the overall topology of the dimer of the NKp30_LBD:B7-H6 complex observed in the crystal lattice. Its arrangement is compatible with both NKp30 molecules inserted within the same NK cell membrane and B7-H6 in the cell membrane of a target tumor cell (Figure 11). Such arrangement would bring the membranes of both cells into close contact, and such an effect could be further potentiated by NKp30 oligomerization. Importantly, Xu et al. [39,40] analyzed the crystal structure of the Fab of inhibitory antibody 17B1.3 in complex with the ectodomain of B7-H6 and found that 17B1.3 could bind to a site on B7-H6 that was completely different from the binding site on NKp30 (PDB 4ZSO). Using an NKp30 reporter cell line and B7-H6-expressing P815 tumor cells, they concluded that the bulky 17B1.3 antibody acts by sterically interfering with close cell–cell contacts at the NK cell–target cell interface, thereby blocking immunological synapse formation and NK cell activation [40].

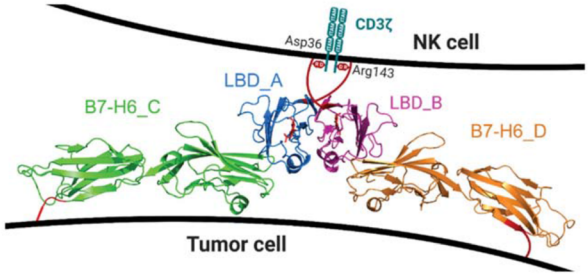

Figure 11. Model of the possible position of the NKp30_LBD:B7-H6 dimeric complex, as observed in the crystal structure (PDB 6YJP), within the NK cell immune synapse. B7-H6 has a very short stalk sequence of several amino acids only, whereas NKp30 has the 15 amino acids long stalk region at its C-terminus (red lines). The stalk is long enough to confer flexibility to the NKp30 ligand binding domain. Such an arrangement would bring the membranes of both cells into very close contact, and such an effect could be further potentiated by NKp30 oligomerization. Local deformation of the NK cell plasma membrane caused by the conformational change of the stalk region induced by ligand binding might trigger signal transduction through the CD3ζ chains associated with the NKp30 transmembrane domain thanks to the interaction of CD3ζ Asp36 residue with NKp30 Arg143 residue occurring at plasma membrane which is required for NKp30 signaling [7].

These results support the proposed close interaction mediated by the NKp30 dimer ligated with two B7-H6 monomers, as observed in the presented crystal structure. However, further studies are required to confirm such an arrangement directly on the membrane of living NK cells, as well as the oligomeric arrangement of NKp30. Considering the short length of the stalk region, it is unlikely that NKp30 forms octameric, decameric, or even larger oligomers through its stalk region on the cell surface, in contrast to its oligomerization in solution. Therefore, data on NKp30 receptor oligomers collected in solution, using its solubilized ectodomains interacting in three-dimensional (3D) space, should not be directly extrapolated to its natural habitat within the plasma membrane and to a 2.5D space on the cell surface. Moreover, all future immunotherapeutic strategies and reagents designed to target or trigger this NK cell receptor:ligand system should also allow enough flexibility with respect to the B7-H6 moiety, thus ensuring its proper orientation and interaction with NKp30.

4. Materials and Methods

4.1. Cell Culture and Vector Design

HEK293T cells were kindly provided by Radu A. Aricescu [24]. HEK293T and HEK293S GnTI$^-$ cells [25] (0.3–6 × 10^6/mL) were maintained in ExCELL293 serum-free medium (Sigma, St. Louis, MT, USA) supplemented with 4 mM L-glutamine in square-bottom glass DURAN flasks with gas permeable caps (DWK Life Sciences, Wertheim, Germany) using 30–40% of the nominal volume at 135 rpm on orbital shaker placed within the incubator at 37 °C and 5% CO_2 [26]. Transient expression in both HEK293T and HEK293S GnTI$^-$ cell lines was performed using the plasmid pTW5sec, a derivative of the pTT5 plasmid backbone [41] modified in-house to contain a woodchuck hepatitis virus post-transcriptional regulatory element (WPRE) and a leader peptide of secreted alkaline phosphatase in frame with AgeI and KpnI cloning sites, followed by a C-terminal histidine tag. Therefore, proteins recombinantly expressed using this plasmid were secreted into the cell culture media and purified by immobilized metal affinity chromatography (IMAC).

4.2. Protein Expression and Purification

For high-density transfection, 800 × 10^6 HEK293 cells were centrifuged for 5 min at 90× *g*. Cells were resuspended in 34 mL of ExCELL293 medium in an empty flask and 800 μg of DNA (1 μg/10^6 cells) were diluted in 6 mL of phosphate-buffered saline (PBS) and filtered through a 0.22 μm filter into the flask with cells. Subsequently, linear 25 kDa polyethyleneimine (lPEI) was added in a 1:3 DNA:lPEI (*w*/*w*) ratio. Cells were incubated in high density on a shaker for 1.5–4 h at 37 °C. Afterwards, up to 400 mL ExCELL293 medium and 0.5 M valproic acid [42] were added to a final concentration of 2 mM. Cells were harvested after 7 days or earlier, when viability dropped below 70%, by centrifugation for 30 min at 15000× *g* at 20 °C. The supernatant was filtered through a 0.2 μm filter, diluted two-fold with PBS buffer, and loaded onto a pre-equilibrated 5 mL HiTrap TALON column using an ÄKTAprime FPLC system (GE Healthcare, Chicago, IL, USA). Protein was eluted with 250 mM imidazole in PBS, concentrated using Amicon Ultra (MWCO 10000; Sigma, St. Louis, MT, USA) concentrators, filtered using spin filter and subjected to size-exclusion chromatography on Superdex 200 Increase 10/300 GL column (GE Healthcare, USA) as a final purification step with HEPES buffer (10 mM HEPES pH 7.5, 150 mM NaCl, 10 mM NaN_3) as the mobile phase. For NKp30_Stalk, fractions were collected separately for oligomeric and monomeric species, and immediately frozen in liquid nitrogen. Protein glycosylation and disulfide bonds pairing were characterized by mass spectrometry (for details see Supplementary Methods) [43–45].

4.3. Protein Labelling

B7-H6 expressed in HEK293S GnTI$^-$ cells was stained with ATTO 488 fluorescent dye (Sigma, USA) using NHS labelling chemistry according to the manufacturer's instructions. Nine volumes of B7-H6 solution in HEPES buffer were mixed with one volume of 1 M bicarbonate buffer, pH 8.5. ATTO 488-NHS ester was added to the protein solution at a molar ratio of 1:3 (protein:ATTO488-NHS). Reaction mixture was incubated for 60 min in the dark at room temperature on a roller shaker at 35 rpm. The labelled protein was purified on a HiTrap Desalting column (GE Healthcare, USA) connected to an ÄKTA basic HPLC system.

4.4. Deglycosylation

For deglycosylation of NKp30 and B7-H6 expressed in HEK293S GnTI$^-$ cell lines, the proteins in HEPES buffer at 1 mg/mL concentration were mixed with recombinant GST-tagged endoglycosidase F1 (Endo F1) [46] in a 200:1 (*w*/*w*) ratio (target protein:Endo F1). For B7-H6, the buffer was supplemented with 20% glycerol to increase protein stability. The mixture was incubated for 3 h at 37 °C or at 4 °C overnight while mixing. Then, the solution was loaded onto a 5 mL GST-trap column (GE Healthcare, Chicago, IL, USA) connected to the fast protein liquid chromatography (FPLC) system to capture

the Endo F1, while collecting the flow-through containing deglycosylated protein. The solution was concentrated to 200 µL and loaded onto a Superdex 200 Increase 10/300 GL (GE Healthcare, Chicago, IL, USA) column for further purification and characterization of the deglycosylated proteins. Samples from collected fractions were used for SDS-PAGE analysis.

4.5. Differential Scanning Fluorimetry

Differential scanning fluorimetry was performed using SYPRO Orange Protein Gel Stain (Thermo Scientific, Waltham, MA, USA). Its 5000× DMSO stock solution was diluted to 50× concentrated solution. The samples were prepared by mixing 4 µL of B7-H6 expressed in HEK293S GnTI$^-$ cells with 10 µL of 2× concentrated screen buffer and 1 µL of 50× concentrated stain solution and complemented by HEPES buffer up to 20 µL. The sample without protein was used as a blank, and the sample with no additive was used as a reference. Data were collected on a Rotor-Gene 2000 Real Time Cycler (Corbett Research, Sydney, Australia) at an excitation wavelength of 300 nm. Fluorescence was measured at 570 nm. The temperature increased stepwise, 0.5 °C each 30 s from 25 °C to 95 °C. The data were evaluated using OriginPro 8 software (version 8.500161). Melting points can be extrapolated by finding the inflection point of sigmoid melting curves. By depicting the data as a negative derivative of relative fluorescence (−d(RF)/T), the melting points correspond to the minima of the melting curves.

4.6. Sedimentation Analysis

Sedimentation velocity measurements were performed on an analytical ultracentrifuge ProteomeLab XL-I (Beckman Coulter, Brea, CA, USA). Protein samples were purified by gel filtration, using the mobile phase buffer (10 mM HEPES pH 7.5, 150 mM NaCl, 10 mM NaN_3) as a reference. Sedimentation velocity experiments were conducted with 20 µM protein samples using double sector cells and An50-Ti rotor at 20 °C and 36,000 or 48,000 rpm for oligomeric or monomeric samples, respectively. Absorbance scans were recorded at 280 or 480 nm at 3–7 min intervals. Buffer density, protein partial specific volume, and particle dimensions were estimated in Sednterp (www.jphilo.mailway.com). Data were analyzed in Sedfit [47] using the continuous sedimentation coefficient distribution c(s) model. Analysis of NKp30_LBD at high concentration was performed with its 20 mg/mL sample at 50,000 rpm using 3 mm centerpiece; scans were recorded every 2 min using the interference optics. The data were fitted with the nonideal c(s) model in Sedfit [48].

4.7. Size-Exclusion Chromatography with Multi-Angle Laser Light Scattering (SEC-MALS)

SEC-MALS experiments were performed using an FPLC station equipped with miniDAWN Tristar light scattering (Wyatt Technologies, Santa Barbara, CA, USA) and Shodex RI-101 (Showa Denko K.K., Tokyo, Japan) refractive index detectors with a Superose 6 Increase 10/300 GL column (GE Healthcare, Chicago, IL, USA) equilibrated in 20 mM HEPES pH 7.5, 150 mM NaCl, 10 mM NaN_3 buffer. Single proteins or protein complexes, typically at 1 mg/mL concentration, were loaded onto the column. The molecular weight was estimated using the refractive index as measure of concentration. The results were analyzed using Astra software (Wyatt Technologies, Santa Barbara, CA, USA).

4.8. Isothermal Titration Calorimetry

Thermodynamic parameters of NKp30:B7-H6 interactions were determined using the PEAQ-ITC instrument (Malvern Panalytical, Westborough, MA, USA). All measurements were performed in the 10 mM HEPES pH 7.5, 150 mM NaCl, 10 mM NaN_3 buffer. First, control heat was determined by buffer–buffer titration. For protein interaction measurements, 200 µL of 20–30 µM NKp30 variants were loaded into the cell and 40 µL of 200–300 µM B7-H6 into the syringe (these concentrations varied slightly in different experiments). An initial injection of 0.4 µL of B7-H6 was followed by 25 injections of 1.5 µL. Injection duration was 2 s, in 120 s intervals, performing the measurements at 25 °C and stirring the cell solution at 750 rpm. The data were evaluated using NITPIC [49], Sedphat [50], and GUSSI software [51].

4.9. Surface Plasmon Resonance

Surface plasmon resonance (SPR) experiments were performed to measure NKp30_Stalk and NKp30_LBD binding, in three different *N*-glycosylation states (wild-type glycans, simple glycans, and deglycosylated with Endo F1), to B7-H6, also in three glycosylation states. Measurements were performed using the Biacore T200 system (GE Healthcare, Chicago, IL, USA) in a buffer composed of 10 mM HEPES pH 7.5, 150 mM NaCl, 1 mg/mL dextran, and 0.05% Tween-20. Three glycosylation variants of B7-H6 were biotinylated (EZ-Link NHS-Biotin; Thermo Fisher Scientific, Waltham, MA, USA) according to the manufacturer's instructions and immobilized to the streptavidin sensor. Binding experiments were performed in single cycle kinetics mode with 15 sequential injections of NKp30 samples in each cycle with concentrations ranging from 1 nM to 16.3 μM. Data from a reference flow cell with an empty channel were subtracted and fitted using the Biacore T200 evaluation software (version 3.0). Maximal fitted responses from each cycle were analyzed using Sedphat [50] software using the AB hetero-association model.

4.10. Protein Crystallization

Protein crystallization was performed at the Division of Structural Biology of the Wellcome Centre for Human Genetics, University of Oxford. Initial screening was performed using the sitting drop method in 300 nL (100 nL of protein solution and 200 nL of crystallization reagents) using the Hydra and Cartesian instruments. All crystallization plates were stored in Rock Imager (Formulatrix, Bedford, MA, USA) at 21 °C. Four commercially available screens (Index, Proplex, PACTpremier, Crystal screen) were used for the equimolar mixture of deglycosylated B7-H6 with NKp30_Stalk or NKp30_LBD, both expressed in HEK293S GnTI$^-$ cells; the mixture was concentrated to 10 mg/mL before the drop set-up. Initially, needle-shaped crystals of NKp30_LBD:B7-H6 complex were obtained in 0.1 M sodium citrate pH 5.0, 20% PEG 8000. These crystals were crushed and used for seeding in optimization performed using the sitting drop method in 300 nL (200 nL of protein solution and 100 nL of crystallization reagents). The number of crystals grew in the drops that were seeded, and diffraction data were collected for a few of them. 25% glycerol was used as cryoprotectant and data were collected at 100 K. The best diffraction data were collected from crystals grown in 0.1 M sodium citrate pH 6.7, 11.7% PEG 6000.

4.11. Diffraction Data Collection

Eleven diffraction data sets were collected at the Diamond Light Source (Didcot, Oxfordshire, UK) at beamline I02 using a wavelength of 0.97949 Å and a PILATUS 6M-F detector (Dectris, Baden-Daettwil, Switzerland). The resolution of all data sets was 3–4 Å and the crystals degraded during the data collection. Eventually, three data sets from three crystals (set B7x1: images 1 to 800 (80°), set B8x5:1 to 800 (80°), and set B8x3:1 to 450 (45°)) were merged to process the data for optimal results. The data were integrated in XDS [52] and merged and scaled in AIMLESS from the CCP4 software package [53], in space group *C*2 (recommended by POINTLESS and ZANUDA) and alternatively in P1. Finally, *C*2 was selected as the correct space group based on the phase problem solution and refinement. Data suffered by strong anisotropy, with effective resolution in the direction of axis *a* being the lowest, ca. 4.4 Å. Anisotropy corrections were not applied to the data. Final data processing statistics are shown in Table 1.

4.12. Structure Solution and Refinement

The phase problem was solved in space group *C*2, using MORDA [54] and PHASER [55], data cut off 3.8 Å and already known structures of NKp30 and B7-H6 as models (PDB code 3PV6 for both molecules). The asymmetric unit in *C*2 contains three B7-H6 protein chains and two NKp30 chains. After refinement trials in REFMAC5 [56], considering manual optimization of restraints, B-values and translation, rotation, and screw-rotation (TLS) parameterization, the structures were

refined in LORESTR (automatic REFMAC5 pipeline for low-resolution structure refinement, [57]), using atomic B-factors, without TLS and with restraints to homologs optimized specially for each run of the refinement. Five percent of reflections were used as a test set (R_{free} set). Manual editing was performed in COOT [58]. Structure quality was checked using the validation tools implemented in MOLPROBITY [59]. There are four Ramachandran outliers (chain C Gly83 and Val152, chain D Gly83, and chain E Gln182), which is 0.5% of refined residues. The final structure parameters are outlined in Table 1.

4.13. Data and Structure Deposition

Diffraction data have been deposited in the SBGrid Data Bank under code 753 (doi:10.15785/SBGRID/753). The crystal structure has been deposited in the Protein Data Bank under code 6YJP.

5. Conclusions

Glycosylation is an essential post-translational modification of cell surface proteins, not only stabilizing them in the extracellular environment but also providing new functional modalities. Moreover, glycosylation is crucial for immune recognition and self-non-self discrimination, especially when involving receptors of the innate immune system, which often bind to their ligands with weak affinities. Accordingly, their ability to transduce the signal into the cell should significantly vary as a function of their glycosylation presence and its type. Glycans may help these receptors to create stable signaling complexes through dimerization and oligomerization or to organize them within complex dynamic structures of the immune synapse. In this study, we exemplified this behavior for the NK cell activation receptor NKp30, whose oligomerization depends on its *N*-glycosylation. Furthermore, we solved the first crystal structure of a glycosylated NKp30 ligand binding domain, in a complex with its tumor ligand B7-H6, highlighting why glycosylation is crucial for the NKp30 oligomerization and for signal transduction. Furthermore, our results indicate that glycosylation should not be overlooked when planning or conducting structure-function studies. In conclusion, our structure of the complex between glycosylated NKp30 and B7-H6 provides a template for designing molecules to stimulate NKp30-mediated cytolytic activity for tumor immunotherapy.

Supplementary Materials: The following are available online at http://www.mdpi.com/2072-6694/12/7/1998/s1, Supplementary methods of mass spectrometry and small-angle X-ray scattering, Figure S1: Direct mass spectrometry of NKp30_Stalk with uniform glycans produced by the HEK293S GnTI$^-$ cell line., Figure S2: Fragmentation spectrum of *N*-glycans produced by the HEK293S GnTI$^-$ cell line, Figure S3: Fragmentation spectrum of *N*-glycans produced by the HEK293T cell line, Figure S4: Sedimentation analysis of NKp30_LBD at high concentration, Figure S5: SEC-SAXS data collected for NKp30_LBD, NKp30_Stalk monomeric and oligomeric fractions, B7-H6 and its complex with NKp30_Stalk monomeric and oligomeric fractions, Figure S6: DAMMIF envelopes ab initio calculated from the SAXS data for the abovementioned proteins, Table S1: Mass spectrometry analysis of disulfide bonds in the prepared recombinant proteins.

Author Contributions: Conceptualization, O.V.; methodology, A.F., A.S., K.H., J.D., T.S., and O.V.; formal analysis, O.S., J.B., T.J., M.R., A.F., A.S., J.D., T.S., and O.V.; investigation, O.S., S.P., B.K., J.B., C.A., T.J., M.R., A.F., A.S., K.H., J.D., T.S., and O.V.; resources, A.F., A.S., and K.H.; data curation, T.S. and J.D.; writing—original draft preparation, O.S. and O.V.; writing—review and editing, O.S., S.P., J.D., T.S. and O.V.; visualization, O.S. and O.V.; supervision, project administration, funding acquisition, O.V. All authors have read and agree to the published version of the manuscript.

Funding: This research was funded by Czech Science Foundation (18-10687S), MEYS of the Czech Republic (LTC17065, CZ.02.1.01/0.0/0.0/16_013/0001776), BIOCEV (ERDF CZ.1.05/1.1.00/02.0109), and Charles University (GAUK 927916, SVV 260427/2020). CIISB research infrastructure project LM2015043 funded by MEYS CR is gratefully acknowledged for the financial support of experiments at the CMS. The authors also acknowledge the support and the use of resources of Instruct-ERIC (PID: 1314) and iNEXT (PID: 2322) infrastructures. The Wellcome Centre for Human Genetics is supported by Wellcome Trust grant 203141/Z/16/Z. O.S. and O.V. received short-term scientific mission support from the COST Action CA15126.

Acknowledgments: We thank Diamond Light Source (Didcot, Oxfordshire, UK) for beamtime (proposal mx10627) and the staff of beamlines I02 and B21 for assistance with data collection. The authors wish to thank Carlos V. Melo for editing the manuscript. The authors also thank the VBCF ProTech facility for technical assistance. Figure 11 was partially created using the tools available from BioRender.com.

Conflicts of Interest: The authors declare no conflict of interest.

References

1. Kiessling, R.; Klein, E.; Wigzell, H. „Natural" killer cells in the mouse. I. Cytotoxic cells with specificity for mouse Moloney leukemia cells. Specificity and distribution according to genotype. *Eur. J. Immunol.* **1975**, *5*, 112–117. [CrossRef] [PubMed]
2. Herberman, R.B.; Nunn, M.E.; Holden, H.T.; Lavrin, D.H. Natural cytotoxic reactivity of mouse lymphoid cells against syngeneic and allogeneic tumors. II. Characterization of effector cells. *Int. J. Cancer* **1975**, *16*, 230–239. [CrossRef] [PubMed]
3. Pegram, H.J.; Andrews, D.M.; Smyth, M.J.; Darcy, P.K.; Kershaw, M. Activating and inhibitory receptors of natural killer cells. *Immunol. Cell Biol.* **2011**, *89*, 216–224. [CrossRef] [PubMed]
4. Kruse, P.H.; Matta, J.; Ugolini, S.; Vivier, E. Natural cytotoxicity receptors and their ligands. *Immunol. Cell Biol.* **2014**, *92*, 221–229. [CrossRef]
5. Biassoni, R. Human Natural Killer Receptors, Co-Receptors, and Their Ligands. *Curr. Protoc. Immunol.* **2009**, *84*. [CrossRef]
6. Pende, D.; Parolini, S.; Pessino, A.; Sivori, S.; Augugliaro, R.; Morelli, L.; Marcenaro, E.; Accame, L.; Malaspina, A.; Biassoni, R.; et al. Identification and Molecular Characterization of Nkp30, a Novel Triggering Receptor Involved in Natural Cytotoxicity Mediated by Human Natural Killer Cells. *J. Exp. Med.* **1999**, *190*, 1505–1516. [CrossRef]
7. Memmer, S.; Weil, S.; Beyer, S.; Zöller, T.; Peters, E.; Hartmann, J.; Steinle, A.; Koch, J. The Stalk Domain of NKp30 Contributes to Ligand Binding and Signaling of a Preassembled NKp30-CD3ζ Complex. *J. Biol. Chem.* **2016**, *291*, 25427–25438. [CrossRef]
8. Kaifu, T.; Escalière, B.; Gastinel, L.N.; Vivier, E.; Baratin, M. B7-H6/NKp30 interaction: A mechanism of alerting NK cells against tumors. *Cell. Mol. Life Sci.* **2011**, *68*, 3531–3539. [CrossRef]
9. Hershkovitz, O.; Jarahian, M.; Zilka, A.; Bar-Ilan, A.; Landau, G.; Jivov, S.; Tekoah, Y.; Glicklis, R.; Gallagher, J.T.; Hoffmann, S.C.; et al. Altered glycosylation of recombinant NKp30 hampers binding to heparan sulfate: A lesson for the use of recombinant immunoreceptors as an immunological tool. *Glycobiology* **2008**, *18*, 28–41. [CrossRef]
10. Chisholm, S.E.; Reyburn, H.T. Recognition of Vaccinia Virus-Infected Cells by Human Natural Killer Cells Depends on Natural Cytotoxicity Receptors. *J. Virol.* **2006**, *80*, 2225–2233. [CrossRef]
11. Arnon, T.I.; Achdout, H.; Levi, O.; Markel, G.; Saleh, N.; Katz, G.; Gazit, R.; Gonen-Gross, T.; Hanna, J.; Nahari, E.; et al. Inhibition of the NKp30 activating receptor by pp65 of human cytomegalovirus. *Nat. Immunol.* **2005**, *6*, 515–523. [CrossRef]
12. Brandt, C.S.; Baratin, M.; Yi, E.C.; Kennedy, J.; Gao, Z.; Fox, B.; Haldeman, B.; Ostrander, C.D.; Kaifu, T.; Chabannon, C.; et al. The B7 family member B7-H6 is a tumor cell ligand for the activating natural killer cell receptor NKp30 in humans. *J. Exp. Med.* **2009**, *206*, 1495–1503. [CrossRef] [PubMed]
13. Binici, J.; Koch, J. BAG-6, a jack of all trades in health and disease. *Cell. Mol. Life Sci.* **2014**, *71*, 1829–1837. [CrossRef] [PubMed]
14. Schlecker, E.; Fiegler, N.; Arnold, A.; Altevogt, P.; Rose-John, S.; Moldenhauer, G.; Sucker, A.; Paschen, A.; Von Strandmann, E.P.; Textor, S.; et al. Metalloprotease-Mediated Tumor Cell Shedding of B7-H6, the Ligand of the Natural Killer Cell-Activating Receptor NKp30. *Cancer Res.* **2014**, *74*, 3429–3440. [CrossRef] [PubMed]
15. Wang, W.; Guo, H.; Geng, J.; Zheng, X.; Wei, H.; Sun, R.; Tian, Z. Tumor-released Galectin-3, a Soluble Inhibitory Ligand of Human NKp30, Plays an Important Role in Tumor Escape from NK Cell Attack. *J. Biol. Chem.* **2014**, *289*, 33311–33319. [CrossRef] [PubMed]
16. Chen, Y.; Mo, J.; Jia, X.; He, Y. The B7 Family Member B7-H6: A New Bane of Tumor. *Pathol. Oncol. Res.* **2018**, *24*, 717–721. [CrossRef] [PubMed]
17. Hu, Y.; Zeng, T.; Xiao, Z.; Hu, Q.; Li, Y.; Tan, X.; Yue, H.; Wang, W.; Tan, H.; Zou, J. Immunological role and underlying mechanisms of B7-H6 in tumorigenesis. *Clin. Chim. Acta* **2020**, *502*, 191–198. [CrossRef]
18. Matta, J.; Baratin, M.; Chiche, L.; Forel, J.-M.; Cognet, C.; Thomas, G.; Farnarier, C.; Piperoglou, C.; Papazian, L.; Chaussabel, D.; et al. Induction of B7-H6, a ligand for the natural killer cell–activating receptor NKp30, in inflammatory conditions. *Blood* **2013**, *122*, 394–404. [CrossRef]

19. Joyce, M.G.; Tran, P.; Zhuravleva, M.A.; Jaw, J.; Colonna, M.; Sun, P.D. Crystal structure of human natural cytotoxicity receptor NKp30 and identification of its ligand binding site. *Proc. Natl. Acad. Sci. USA* **2011**, *108*, 6223–6228. [CrossRef]
20. Li, Y.; Wang, Q.; Mariuzza, R.A. Structure of the human activating natural cytotoxicity receptor NKp30 bound to its tumor cell ligand B7-H6. *J. Exp. Med.* **2011**, *208*, 703–714. [CrossRef]
21. Herrmann, J.; Berberich, H.; Hartmann, J.; Beyer, S.; Davies, K.E.; Koch, J. Homo-oligomerization of the Activating Natural Killer Cell Receptor NKp30 Ectodomain Increases Its Binding Affinity for Cellular Ligands. *J. Biol. Chem.* **2014**, *289*, 765–777. [CrossRef]
22. Hartmann, J.; Tran, T.-V.; Kaudeer, J.; Oberle, K.; Herrmann, J.; Quagliano, I.; Abel, T.; Cohnen, A.; Gatterdam, V.; Jacobs, A.; et al. The Stalk Domain and the Glycosylation Status of the Activating Natural Killer Cell Receptor NKp30 Are Important for Ligand Binding. *J. Biol. Chem.* **2012**, *287*, 31527–31539. [CrossRef] [PubMed]
23. Binici, J.; Hartmann, J.; Herrmann, J.; Schreiber, C.; Beyer, S.; Güler, G.; Vogel, V.; Tumulka, F.; Abele, R.; Mäntele, W.; et al. A Soluble Fragment of the Tumor Antigen BCL2-associated Athanogene 6 (BAG-6) Is Essential and Sufficient for Inhibition of NKp30 Receptor-dependent Cytotoxicity of Natural Killer Cells. *J. Biol. Chem.* **2013**, *288*, 34295–34303. [CrossRef] [PubMed]
24. Aricescu, A.R.; Lu, W.; Jones, E.Y. A time- and cost-efficient system for high-level protein production in mammalian cells. *Acta Crystallogr. Sect. D Biol. Crystallogr.* **2006**, *62*, 1243–1250. [CrossRef] [PubMed]
25. Reeves, P.J.; Callewaert, N.; Contreras, R.; Khorana, H.G. Structure and function in rhodopsin: High-level expression of rhodopsin with restricted and homogeneous N-glycosylation by a tetracycline-inducible N-acetylglucosaminyltransferase I-negative HEK293S stable mammalian cell line. *Proc. Natl. Acad. Sci. USA* **2002**, *99*, 13419–13424. [CrossRef]
26. Bláha, J.; Maraun, M.; Novák, P.; Vaněk, O. Expression and purification of soluble and stable ectodomain of natural killer cell receptor LLT1 through high-density transfection of suspension adapted HEK293S GnTI^{-} cells. *Protein Expr. Purif.* **2015**, *109*, 7–13. [CrossRef] [PubMed]
27. Krissinel, E.; Henrick, K. Inference of Macromolecular Assemblies from Crystalline State. *J. Mol. Biol.* **2007**, *372*, 774–797. [CrossRef] [PubMed]
28. Ni, L.; Dong, C. New B7 Family Checkpoints in Human Cancers. *Mol. Cancer Ther.* **2017**, *16*, 1203–1211. [CrossRef]
29. Wu, M.-R.; Zhang, T.; Gacerez, A.T.; Coupet, T.A.; Demars, L.R.; Sentman, C.L. B7H6-Specific Bispecific T Cell Engagers Lead to Tumor Elimination and Host Antitumor Immunity. *J. Immunol.* **2015**, *194*, 5305–5311. [CrossRef]
30. Gacerez, A.T.; Hua, C.K.; Ackerman, M.E.; Sentman, C.L. Chimeric antigen receptors with human scFvs preferentially induce T cell anti-tumor activity against tumors with high B7H6 expression. *Cancer Immunol. Immunother.* **2018**, *67*, 749–759. [CrossRef]
31. Kellner, C.; Maurer, T.; Hallack, D.; Repp, R.; Van De Winkel, J.G.J.; Parren, P.W.H.I.; Valerius, T.; Humpe, A.; Gramatzki, M.; Peipp, M.; et al. Mimicking an Induced Self Phenotype by Coating Lymphomas with the NKp30 Ligand B7-H6 Promotes NK Cell Cytotoxicity. *J. Immunol.* **2012**, *189*, 5037–5046. [CrossRef] [PubMed]
32. Kellner, C.; Günther, A.; Humpe, A.; Repp, R.; Klausz, K.; Derer, S.; Valerius, T.; Ritgen, M.; Brüggemann, M.; Van De Winkel, J.G.; et al. Enhancing natural killer cell-mediated lysis of lymphoma cells by combining therapeutic antibodies with CD20-specific immunoligands engaging NKG2D or NKp30. *OncoImmunology* **2016**, *5*, e1058459. [CrossRef]
33. Peipp, M.; Derer, S.; Lohse, S.; Staudinger, M.; Klausz, K.; Valerius, T.; Gramatzki, M.; Kellner, C. HER2-specific immunoligands engaging NKp30 or NKp80 trigger NK-cell-mediated lysis of tumor cells and enhance antibody-dependent cell-mediated cytotoxicity. *Oncotarget* **2015**, *6*, 32075–32088. [CrossRef] [PubMed]
34. Jaron-Mendelson, M.; Yossef, R.; Appel, M.; Zilka, A.; Hadad, U.; Afergan, F.; Rosental, B.; Engel, S.; Nedvetzki, S.; Braiman, A.; et al. Dimerization of NKp46 Receptor Is Essential for NKp46-Mediated Lysis: Characterization of the Dimerization Site by Epitope Mapping. *J. Immunol.* **2012**, *188*, 6165–6174. [CrossRef] [PubMed]
35. Hadad, U.; Thauland, T.J.; Martinez, O.M.; Butte, M.J.; Porgador, A.; Krams, S.M. NKp46 Clusters at the Immune Synapse and Regulates NK Cell Polarization. *Front. Immunol.* **2015**, *6*, 216. [CrossRef]

36. Arnon, T.I.; Markel, G.; Bar-Ilan, A.; Hanna, J.H.; Fima, E.; Benchetrit, F.; Galili, R.; Cerwenka, A.; Benharroch, D.; Sion-Vardy, N.; et al. Harnessing Soluble NK Cell Killer Receptors for the Generation of Novel Cancer Immune Therapy. *PLoS ONE* **2008**, *3*, e2150. [CrossRef]
37. Franke, D.; Petoukhov, M.V.; Konarev, P.V.; Panjkovich, A.; Tuukkanen, A.; Mertens, H.D.T.; Kikhney, A.G.; Hajizadeh, N.R.; Franklin, J.M.; Jeffries, C.M.; et al. ATSAS 2.8: A comprehensive data analysis suite for small-angle scattering from macromolecular solutions. *J. Appl. Crystallogr.* **2017**, *50*, 1212–1225. [CrossRef]
38. Pettersen, E.F.; Goddard, T.D.; Huang, C.C.; Couch, G.S.; Greenblatt, D.M.; Meng, E.C.; Ferrin, T.E. UCSF Chimera—A visualization system for exploratory research and analysis. *J. Comput. Chem.* **2004**, *25*, 1605–1612. [CrossRef]
39. Xu, X.; Li, Y.; Gauthier, L.; Chen, Q.; Vivier, E.; Mariuzza, R.A. Expression, crystallization and X-ray diffraction analysis of a complex between B7-H6, a tumor cell ligand for the natural cytotoxicity receptor NKp30, and an inhibitory antibody. *Acta Crystallogr. Sect. F Struct. Biol. Commun.* **2015**, *71*, 697–701. [CrossRef]
40. Xu, X.; Narni-Mancinelli, E.; Cantoni, C.; Li, Y.; Guia, S.; Gauthier, L.; Chen, Q.; Moretta, A.; Vély, F.; Eisenstein, E.; et al. Structural Insights into the Inhibitory Mechanism of an Antibody against B7-H6, a Stress-Induced Cellular Ligand for the Natural Killer Cell Receptor NKp30. *J. Mol. Biol.* **2016**, *428*, 4457–4466. [CrossRef]
41. Durocher, Y. High-level and high-throughput recombinant protein production by transient transfection of suspension-growing human 293-EBNA1 cells. *Nucleic Acids Res.* **2002**, *30*, 9e. [CrossRef]
42. Backliwal, G.; Hildinger, M.; Kuettel, I.; Delegrange, F.; Hacker, D.L.; Wurm, F.M. Valproic acid: A viable alternative to sodium butyrate for enhancing protein expression in mammalian cell cultures. *Biotechnol. Bioeng.* **2008**, *101*, 182–189. [CrossRef]
43. Pompach, P.; Man, P.; Kavan, D.; Hofbauerová, K.; Kumar, V.; Bezouska, K.; Havlicek, V.; Novák, P. Modified electrophoretic and digestion conditions allow a simplified mass spectrometric evaluation of disulfide bonds. *J. Mass Spectrom.* **2009**, *44*, 1571–1578. [CrossRef] [PubMed]
44. Young, M.M.; Tang, N.; Hempel, J.C.; Oshiro, C.M.; Taylor, E.W.; Kuntz, I.D.; Gibson, B.W.; Dollinger, G. High throughput protein fold identification by using experimental constraints derived from intramolecular cross-links and mass spectrometry. *Proc. Natl. Acad. Sci. USA* **2000**, *97*, 5802–5806. [CrossRef]
45. Kukačka, Z.; Rosulek, M.; Strohalm, M.; Kavan, D.; Novák, P. Mapping protein structural changes by quantitative cross-linking. *Methods* **2015**, *89*, 112–120. [CrossRef]
46. Grüninger, F.; D'Arcy, A.; D'Arcy, B.; Chène, C. Deglycosylation of proteins for crystallization using recombinant fusion protein glycosidases. *Protein Sci.* **1996**, *5*, 2617–2622. [CrossRef]
47. Schuck, P. Size-Distribution Analysis of Macromolecules by Sedimentation Velocity Ultracentrifugation and Lamm Equation Modeling. *Biophys. J.* **2000**, *78*, 1606–1619. [CrossRef]
48. Chaturvedi, S.; Ma, J.; Brown, P.H.; Zhao, H.; Schuck, P. Measuring macromolecular size distributions and interactions at high concentrations by sedimentation velocity. *Nat. Commun.* **2018**, *9*, 4415. [CrossRef] [PubMed]
49. Scheuermann, T.H.; Brautigam, C.A. High-precision, automated integration of multiple isothermal titration calorimetric thermograms: New features of NITPIC. *Methods* **2015**, *76*, 87–98. [CrossRef] [PubMed]
50. Zhao, H.; Piszczek, G.; Schuck, P. SEDPHAT—A platform for global ITC analysis and global multi-method analysis of molecular interactions. *Methods* **2015**, *76*, 137–148. [CrossRef] [PubMed]
51. Brautigam, C.A. Calculations and Publication-Quality Illustrations for Analytical Ultracentrifugation Data. *Methods Enzymol.* **2015**, *562*, 109–133. [CrossRef]
52. Kabsch, W. XDS. *Acta Crystallogr. Sect. D Biol. Crystallogr.* **2010**, *66*, 125–132. [CrossRef]
53. Winn, M.; Ballard, C.C.; Cowtan, K.; Dodson, E.J.; Emsley, P.; Evans, P.R.; Keegan, R.M.; Krissinel, E.B.; Leslie, A.G.W.; McCoy, A.; et al. Overview of the CCP4 suite and current developments. *Acta Crystallogr. Sect. D Biol. Crystallogr.* **2011**, *67*, 235–242. [CrossRef]
54. Vagin, A.; Lebedev, A. MoRDa, an automatic molecular replacement pipeline. *Acta Crystallogr. Sect. A Found. Adv.* **2015**, *71*, S19. [CrossRef]
55. McCoy, A.J.; Grosse-Kunstleve, R.W.; Adams, P.D.; Winn, M.D.; Storoni, L.C.; Read, R.J. Phaser crystallographic software. *J. Appl. Crystallogr.* **2007**, *40*, 658–674. [CrossRef] [PubMed]
56. Murshudov, G.N.; Skubak, P.; Lebedev, A.A.; Pannu, N.S.; Steiner, R.A.; Nicholls, R.; Winn, M.D.; Long, F.; Vagin, A.A. REFMAC5 for the refinement of macromolecular crystal structures. *Acta Crystallogr. Sect. D Biol. Crystallogr.* **2011**, *67*, 355–367. [CrossRef] [PubMed]

57. Kovalevskiy, O.; Nicholls, R.; Murshudov, G. Automated refinement of macromolecular structures at low resolution using prior information. *Acta Crystallogr. Sect. D Struct. Biol.* **2016**, *72*, 1149–1161. [CrossRef] [PubMed]
58. Emsley, P.; Lohkamp, B.; Scott, W.G.; Cowtan, K. Features and development of Coot. *Acta Crystallogr. Sect. D Biol. Crystallogr.* **2010**, *66*, 486–501. [CrossRef]
59. Chen, V.B.; Arendall, W.B.; Headd, J.J.; Keedy, D.; Immormino, R.M.; Kapral, G.J.; Murray, L.W.; Richardson, J.S.; Richardson, D.C. MolProbity: All-atom structure validation for macromolecular crystallography. *Acta Crystallogr. Sect. D Biol. Crystallogr.* **2010**, *66*, 12–21. [CrossRef]

cancers

MDPI

Article

Natural Killer Cell Activation Receptor NKp30 Oligomerization Depends on its *N*-Glycosylation

Ondřej Skořepa, Samuel Pazicky, Barbora Kalousková, Jan Bláha, Celeste Abreu, Tomáš Ječmen, Michal Rosůlek, Alexander Fish, Arthur Sedivy, Karl Harlos, Jan Dohnálek, Tereza Skálová, Ondřej Vaněk

Supplementary Materials

Supplementary Methods

1. Mass spectrometry

Disulfide bonds in produced proteins were determined according to the previously published protocol [43]. Briefly, proteins were separated by SDS-PAGE, deglycosylated by ENDO Hf (New England Biolabs, Ipswich, MA, USA), and digested by trypsin (Sigma, St. Louis, MT, USA) under non-reducing conditions in the presence of 200 μM cystamine. The peptide mixtures were desalted on reversed phase trap column (Acclaim PepMap 100, C18, 0.1 × 20 mm, 5 μm) and separated on reversed phase analytical column (Acclaim PepMap 100, C18, 0.075 × 150 mm, 3 μm; both columns Thermo Scientific, Waltham, MA, USA) connected directly to solariX XR 12T FT-ICR mass spectrometer (Bruker Daltonics, Billerica, MA, USA) using an electrospray ion source. Data were acquired using SolarixControl 3.0.0 and processed with DataAnalysis 4.2. The disulfide bonds and saccharide moieties were identified using the Links software [44].

Glycosylation on the NKp30_Stalk protein expressed in HEK293S GnTI$^-$ cell line was characterized using an ESI FT-ICR MS according to previously published protocol [45]. Briefly, 10 μg of the protein was desalted on protein microtrap column (C4 phase, Michrom Bioresources, Auburn, CA, USA) according to the manufacturer instructions, and eluted in 50 μL of 80% acetonitrile/1% acetic acid directly to solariX XR 12T FT-ICR mass spectrometer (Bruker Daltonics, Billerica, MA, USA) using an electrospray ion source. Acquisition of mass spectra was done in the positive mode with the following parameters: the *m*/*z* range 250–3000, 1 M data points transient, 0.2 s ion accumulation, 4 scans accumulation. Acquired data were interpreted by DataAnalysis 4.2. A glycosylation pattern of NKp30_Stalk protein was verified by qCID MSMS analysis of isolated most abundant two times glycosylated form at *m*/*z* 1105.43, z = 16 (Figure S2). Acquisition of MS-MS spectra was done with 0.8 s ion accumulation and eight scans accumulation at the same *m*/*z* range and data points transient as MS spectra.

For glycopeptide analysis of B7-H6 expressed in HEK293T cell line the protein sample was diluted by 50 mM ammonium bicarbonate to 2 μg/μl, the disulfide bonds were reduced 60 min at 60 °C by 5 mM dithiothreitol and alkylated 60 min at room temperature in the dark by 15 mM iodoacetamide. The protein was digested overnight at 37 °C by trypsin at enzyme-to-protein ratio of 1:20 (*w*/*w*). Peptides were desalted on a peptide microtrap column (Michrom Bioresources, Auburn, CA, USA), lyophilized, reconstituted in aqueous 0.1% formic acid, and loaded onto reversed phase column (ZORBAX Eclipse Plus C18, 2.1 × 100 mm, 1.8 μm; Agilent Technologies, Santa Clara, CA, USA). The mobile phase consisted of 0.1% formic acid in water (solvent A) and 0.1% formic acid in acetonitrile (solvent B). The separation was carried out at 0.25 mL/min flow rate, the column temperature was 40 °C, and the following gradient was used (min/% B): 0/3, 1/6, 21/30, 26/80, 28/80, 29/3, 30/3. The measurement was performed on qTOF maXis mass spectrometer (Bruker Daltonics, Billerica, MA, USA) using an electrospray ion source. Acquisition of mass spectra was done in positive mode with following parameters: *m*/*z* range 150–2200, with CID fragmentation (precursor *m*/*z* range 600–2200, charge range 2–5, collision energy 70 eV). DataAnalysis 4.4 and ProteinScape 4

were used for data evaluation and assigned tandem mass spectra of glycopeptides were verified manually.

2. SEC-SAXS Measurements

Size exclusion chromatography–small-angle X-ray scattering (SEC-SAXS) data for NKp30_LBD, NKp30_Stalk, B7-H6 and its complex with NKp30_Stalk were collected at the Diamond Light Source (Didcot, Oxfordshire, UK) at beamline 21 using an Agilent 1200 HPLC system with a 2.4 mL Superdex 200 PC 3.2/30 column (GE Healthcare, Chicago, IL, USA) and a Pilatus P3-2M detector at 12.4 keV of radiation and at 4.014 m of sample-to-detector distance. NKp30_LBD and NKp30_Stalk were expressed in HEK293T cell line with wild-type human N-glycosylation, whereas the B7-H6 ectodomain was expressed in HEK293S GnTI$^-$ cell line with uniform Asn-$GlcNAc_2Man_5$ glycans. Proteins were diluted in 10 mM HEPES pH 7.5, 150 mM NaCl, 10 mM NaN_3. Complex was mixed at a 1:1 molar ratio. The data were collected at 293 K for buffer and protein samples at a loading concentration of 5 mg/mL for NKp30_LBD and B7-H6, and at 10 mg/mL for NKp30_Stalk and for its equimolar mixture with B7-H6. The data in selected intervals (monomeric and oligomeric fractions of NKp30_Stalk, as well as of its mixture with B7-H6, were analyzed separately) were solvent-subtracted in SCÅTTER (developed by Robert Rambo at the Diamond Light Source, http://www.bioisis.net/tutorial/9), and merged and characterized using the ATSAS64 package [37]. As a proof of the data quality, scattering and Guinier plots, for all data ranges, are shown in Figure S5. Using the pair distance distribution functions P(r), twenty ab initio structure models were calculated with DAMMIF 2.7.265 for each of the data intervals. The models were compared using the DAMSEL command and averaged using DAMAVER 5.0 (r10553). The final models were visualized in UCSF Chimera [38] and are shown in Figure S6

Table S1. Mass spectrometry analysis of disulfide bonds in the prepared recombinant proteins.

Exp. Mass	Thr. Mass	Error	Peptide	Chain	Modification	Disulfide Bond
				B7-H6 wild-type (deglycosylated)		
2633.251	2633.251	0.21	B7-H6_WT (122-130) [A]-B7-H6_WT (202-214) [B]	CEVVVTPLK-NMDGTFNVTSCLK	GlcNAc (208)	(122-212)
2879.427	2879.428	0.14	B7-H6 _WT (122-130) [A]-B7-H6_WT (215-231) [B]	CEVVVTPLK-LNSSQEDPGTVYQCVVR		(122-228)
3743.666	3743.672	0.70	B7-H6_WT (202-214) [A]-B7-H6_WT (215-231) [B]	NMDGTFNVTSCLK-LNSSQEDPGTVYQCVVR	GlcNAc (208); GlcNAc (216)	(212-228)
4086.855	4086.855	0.09	B7-H6 _WT (122-130) [A]-B7-H6_WT (156-179) [B]	CEVVVTPLK-ENEDKYMCESSGFYPEAINITWEK	GlcNAc (174)	(122-163)
4748.019	4748.019	0.06	B7-H6 _WT (156-179) [A]-B7-H6_WT (202-214) [B]	ENEDKYMCESSGFYPEAINITWEK-NMDGTFNVTSCLK	GlcNAc (174); GlcNAc (208)	(163-212)
5197.274	5197.276	0.33	B7-H6_WT (156-179) [A]-B7-H6_WT (215-231) [B]	ENEDKYMCESSGFYPEAINITWEK-LNSSQEDPGTVYQCVVR	GlcNAc (174); GlcNAc (216)	(163-228)
				B7-H6 C212S mutant (HEK293S GnTI-)		
5181.28	5181.28	−0.9	B7-H6_C212S (156, 179) [A]-B7-H6_C212S (215, 231) [B]	ENEDKYMCESSGFYPEAINITWEK-LNSSQEDPGTVYQCVVR	GlcNAc (A.174); GlcNAc (B.216)	(163-228)
4978.20	4978.20	−0.4	B7-H6_C212S (156, 179) [A]-B7-H6_C212S (215, 231) [B]	ENEDKYMCESSGFYPEAINITWEK-LNSSQEDPGTVYQCVVR	GlcNAc (A.174) ǀ GlcNAc (B.216)	(163-228)
6178.85	6178.84	1.03	B7-H6_C212S (147, 179) [A]-B7-H6_C212S (215, 231) [B]	LLLDQVGMKENEDKYMCESSGFYPEAINITWEK-LNSSQEDPGTVYQCVVR	GlcNAc (A.174); GlcNAc (B.216)	(163-228)
6071.96	6071.95	1.65	B7-H6_C212S (28, 68) [A]-B7-H6_C212S (122, 130) [B]	VEMMAGGTQITPLNDNVTIFCNIFYSQPLNITSMGITWFWK-CEVVVTPLK	GlcNAc (A.43), GlcNAc (A.57)	(48-122)
4566.03	4566.03	0.03	B7-H6_C212S (161, 179) [A]-B7-H6_C212S (215, 231) [B]	YMCESSGFYPEAINITWEK-LNSSQEDPGTVYQCVVR	GlcNAc (A.174); GlcNAc (B.216)	(163-228)
5975.77	5975.76	1.15	B7-H6_C212S (147, 179) [A]-B7-H6_C212S (215, 231) [B]	LLLDQVGMKENEDKYMCESSGFYPEAINITWEK-LNSSQEDPGTVYQCVVR	GlcNAc (A.174) ǀ GlcNAc (B.216)	(163-228)
4362.95	4362.95	0.04	B7-H6_C212S (161, 179) [A]-B7-H6_C212S (215, 231) [B]	YMCESSGFYPEAINITWEK-LNSSQEDPGTVYQCVVR	GlcNAc (A.174) ǀ GlcNAc (B.216)	(163-228)
9554.39	9554.38	1.03	B7-H6_C212S (28, 68) [A]-B7-H6_C212S (109, 130) [B]	VEMMAGGTQITPLNDNVTIFCNIFYSQPLNITSMGITWFWK-LPGIQLEEAGEYRCEVVVTPLK	$GlcNAc_2Man_5$ (A.43), $GlcNAc_2Man_5$ (A.57)	(48-122)
4978.20	4978.20	0.58	B7-H6_C212S (156, 179) [A]-B7-H6_C212S (215, 231) [B]	ENEDKYMCESSGFYPEAINITWEK-LNSSQEDPGTVYQCVVR	GlcNAc (A.174) ǀ GlcNAc (B.216)	(163-228)
4775.12	4775.12	0.1	B7-H6_C212S (156, 179) [A]-B7-H6_C212S (215, 231) [B]	ENEDKYMCESSGFYPEAINITWEK-LNSSQEDPGTVYQCVVR		(163-228)

7207.98	7207.97	1.58	B7-H6_C212S (156, 179) [A]-B7-H6_C212S (215, 231) [B]	ENEDKYMCESSGFYPEAINITWEK-LNSSQEDPGTVYQCVVR	$GlcNAc_2Man_5$ (A.174); $GlcNAc_2Man_5$ (B.216)	(163-228)
7527.69	7527.69	0.61	B7-H6_C212S (28, 68) [A]-B7-H6_C212S (109, 130) [B]	VEMMAGGTQITPLNDNVTIFCNIFYSQPLNITSMGITWFWK-LPGIQLEEAGEYRCEVVVTPLK	GlcNAc (A.43), GlcNAc (A.57)	(48-122)
9121.55	9121.54	1.15	B7-H6_C212S (28, 68) [A]-B7-H6_C212S (109, 146) [B]	VEMMAGGTQITPLNDNVTIFCNIFYSQPLNITSMGITWFWK-LPGIQLEEAGEYRCEVVVTPLKAQGTVQLEVVASPASR	GlcNAc (A.43), GlcNAc (A.57)	(48-122)
				NKp30_Stalk (deglycosylated)		
3292.49	3292.50	−1.7	NKp30_Stalk (29, 47) [A]-NKp30_Stalk (100, 94) [B]	TLEGSSAFLPCSFNASQGR-GHDASIYVCR	GlcNAc (A.42)	(39-108)
3292.50	3292.50	0.79	NKp30_Stalk (29, 47) [A]-NKp30_Stalk (100, 109) [B]	TLEGSSAFLPCSFNASQGR-GHDASIYVCR	GlcNAc (A.42)	(39-108)
3292.50	3292.50	0.78	NKp30_Stalk (29, 47) [A]-NKp30_Stalk (100, 109) [B]	TLEGSSAFLPCSFNASQGR-GHDASIYVCR	GlcNAc (A.42)	(39-108)
3089.42	3089.42	−0.3	NKp30_Stalk (29, 47) [A]-NKp30_Stalk (100, 109) [B]	TLEGSSAFLPCSFNASQGR-GHDASIYVCR		(39-108)
3662.69	3662.70	−0.8	NKp30_Stalk (29, 47) [A]-NKp30_Stalk (97, 109) [B]	TLEGSSAFLPCSFNASQGR-DVRGHDASIYVCR	GlcNAc (A.42)	(39-108)

The measured and predicted masses of the identified cystic dipeptides are given below for B7-H6_WT, B7-H6_C212S, and NKp30_Stalk expression constructs. For the wild-type B7-H6 construct we confirmed mismatch disulfide pairing with an odd cysteine 212. This mismatch was completely solved by site-directed mutagenesis (C212S) that resulted in correct disulfide pairing, i.e., only the expected disulfides between cysteines 48–122 and 163–228 were identified for the B7-H6_C212S mutant protein. For NKp30 the expected disulfide pairing between cysteines 39–108 was confirmed as well. Glycosylation of NKp30_Stalk construct produced in HEK293S GnTI$^-$ cells was analyzed by mass spectrometry. Three *N*-glycosylation sites are predicted from its amino acid sequence. By direct protein mass spectrometry, measured mass of the intact protein was majorly 17671.87 Da which suggested that the protein has two occupied *N*-glycosylation sites (Figure S1). Minor form with higher mass corresponding to three occupied *N*-glycosylation sites was also detected, albeit at much lower intensities in the mass spectrum, therefore it should be significantly less abundant in the sample. By LC MS analysis of peptide fragments, Asn42 and Asn121 were detected as fully occupied, while Asn68 was just partially glycosylated. Fragmentation spectra further confirmed the expected Asn-GlcNAc$_2$Man$_5$ composition of *N*-glycan chains produced by the HEK293S GnTI$^-$ cell line (Figure S2).

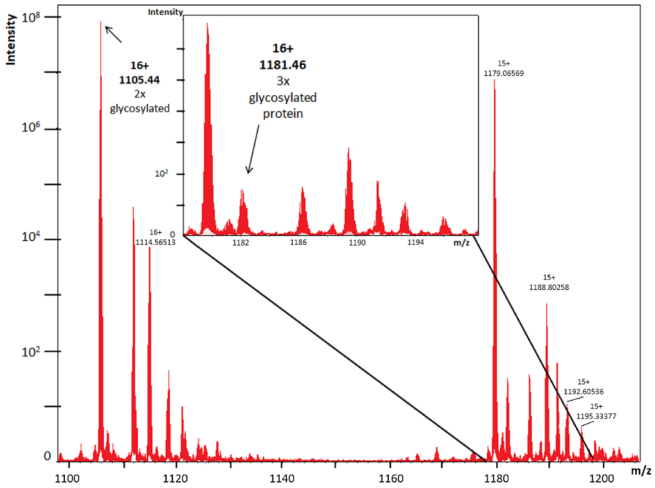

Figure S1. Direct mass spectrometry of NKp30_Stalk with uniform glycans produced by the HEK293S GnTI$^-$ cell line. Peak with the observed *m*/*z* value of 1105.44 corresponds to the 16× charged protein with two occupied *N*-glycosylation sites. Intensity of this peak is at 10^8 order of magnitude. Peak with the observed *m*/*z* value of 1181.46 and intensity at 10^2 corresponds to the 16× charged protein with three occupied *N*-glycosylation sites which is thus considerably less abundant in the sample.

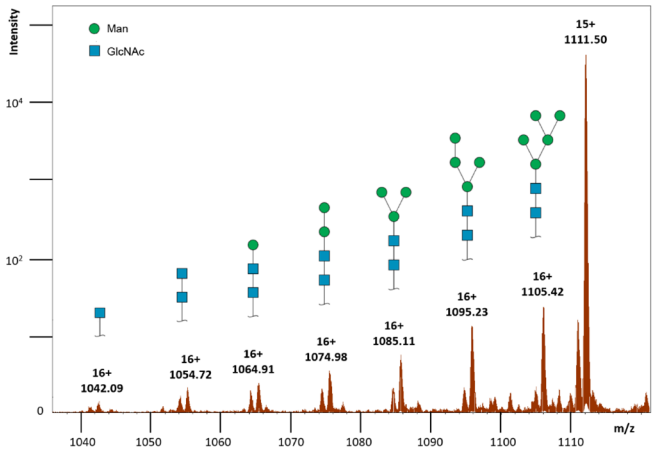

Figure S2. Fragmentation spectrum of *N*-glycans produced by the HEK293S GnTI⁻ cell line. The highest 16× charged peak corresponds to NKp30_Stalk protein with full Asn-GlcNAc$_2$Man$_5$ *N*-glycosylation. Loss of mass in other peaks due to fragmentation corresponds to loss of one mannose unit (rel. mol. mass 162, which is 10.2 on *m*/*z* x-axis with charge z = 16). Loss of mass of the first peak in spectrum from the left corresponds to loss of one *N*-acetylglucosamine unit (rel. mol. mass 203, which is 12.7 on *m*/*z* x-axis with charge z = 16). Predicted oligosaccharide structures corresponding to distinct fragments are depicted by symbolic nomenclature of monosaccharide representation.

As an example of wild-type complex *N*-glycans expressed by the HEK293T cell line, fragmentation spectrum of B7-H6 glycopeptide NMDGTFNVTSSLK is shown below (Figure S3).

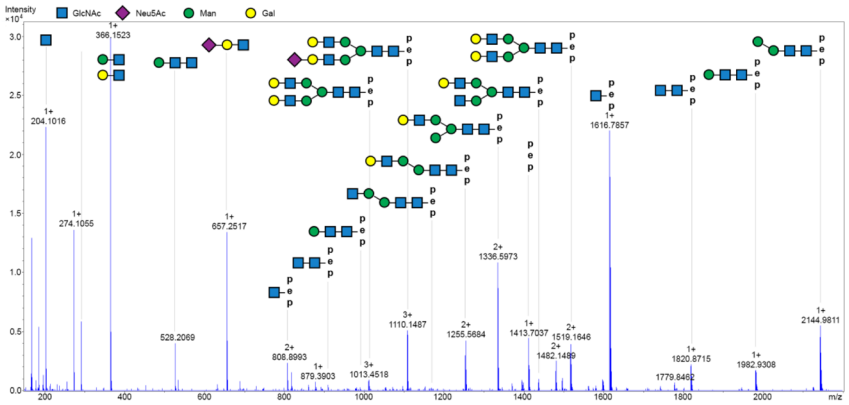

Figure S3. Fragmentation spectrum of *N*-glycans produced by the HEK293T cell line. B7-H6 was digested with trypsin, resultant peptides were desalted and subjected to LC-MS separation and analysis. The fragmentation spectrum of the triply charged precursor with *m*/*z* value of 1110.149 corresponding to peptide NMDGTFNVTSSLK with full Asn-HexNAc$_4$Hex$_5$NeuAc$_1$ *N*-glycosylation is shown together with the predicted oligosaccharide structures corresponding to distinct fragments depicted by symbolic nomenclature of monosaccharide representation.

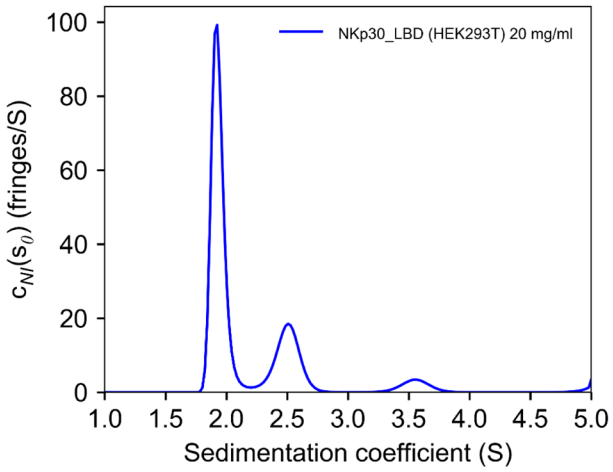

Figure S4. Sedimentation analysis of NKp30_LBD at high concentration. Sample of NKp30_LBD expressed in HEK293T cell line was analyzed by analytical ultracentrifugation at 20 mg/mL concentration using a 3-mm centerpiece and an interference optics. Resultant data were fitted using the nonideal c(s) model implemented in the latest version of Sedfit software [48]. NKp30_LBD is exclusively monomeric at low concentration; however, monomeric, dimeric, and most probably trimeric species are observed at high concentration.

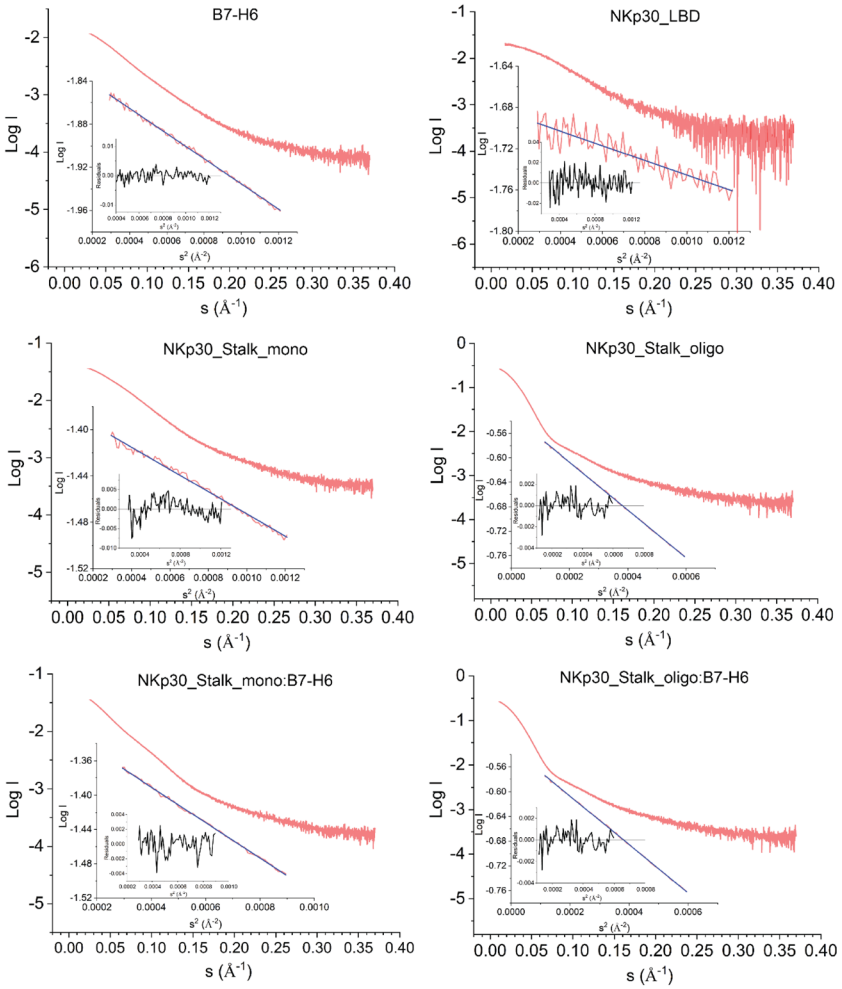

Figure S5. Size exclusion chromatography–small-angle X-ray scattering (SEC-SAXS) data collected for NKp30_LBD, NKp30_Stalk monomeric and oligomeric fractions, B7-H6 and its complex with NKp30_Stalk monomeric and oligomeric fractions. SAXS scattering curves in logarithmic scale (red) are shown for data quality assessment of the merged data, together with the corresponding Guinier plots shown in the lower left corner.

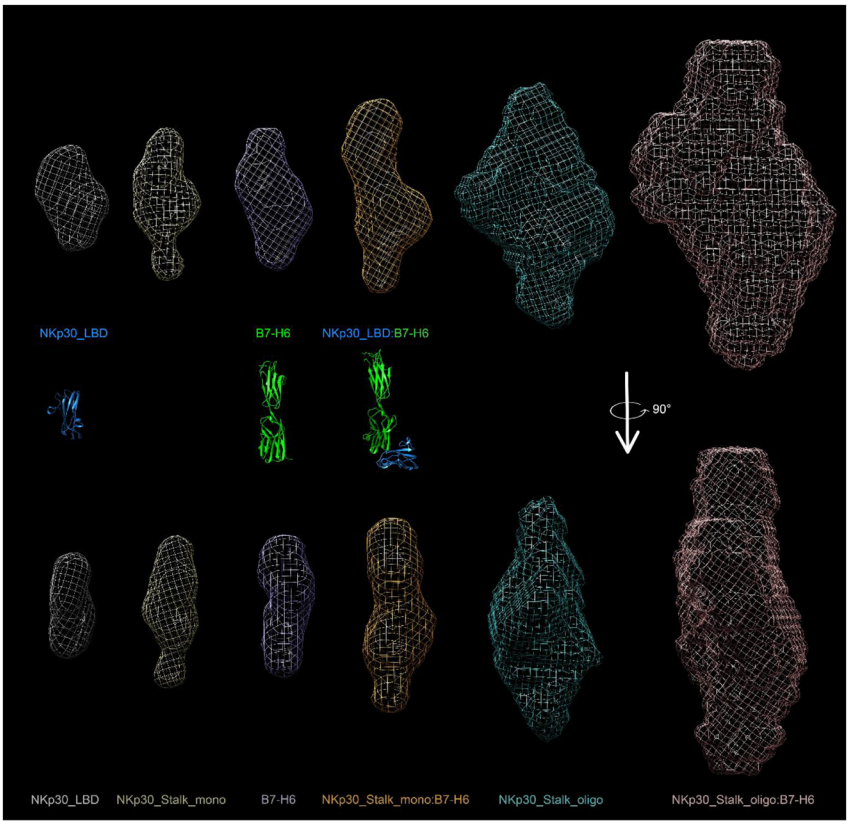

Figure S6. Averaged and filtered DAMMIF envelopes ab initio calculated from the SAXS data for NKp30_LBD, NKp30_Stalk monomeric and oligomeric fractions, B7-H6 and its complex with NKp30_Stalk monomeric and oligomeric fractions. For comparison, NKp30_LBD, B7-H6, and NKp30_LBD:B7-H6 complex, as observed in the presented crystal structure (PDB 6YJP), are shown with the same scale of magnification. The analyzed proteins are glycosylated, and the glycan moieties account for a significant proportion of their molecular mass and hydrodynamic volume; therefore, the envelopes are clearly larger than the naked molecules displayed in the crystal structures.

References

1. Kiessling, R.; Klein, E.; Wigzell, H. „Natural" killer cells in the mouse. I. Cytotoxic cells with specificity for mouse Moloney leukemia cells. Specificity and distribution according to genotype. *Eur. J. Immunol.* 1975, *5*, 112–117, doi:10.1002/eji.1830050208.
2. Herberman, R.B.; Nunn, M.E.; Holden, H.T.; Lavrin, D.H. Natural cytotoxic reactivity of mouse lymphoid cells against syngeneic and allogeneic tumors. II. Characterization of effector cells. *Int. J. Cancer* 1975, *16*, 230–239, doi:10.1002/ijc.2910160205.
3. Pegram, H.J.; Andrews, D.M.; Smyth, M.J.; Darcy, P.K.; Kershaw, M. Activating and inhibitory receptors of natural killer cells. *Immunol. Cell Biol.* 2011, *89*, 216–224, doi:10.1038/icb.2010.78.
4. Kruse, P.H.; Matta, J.; Ugolini, S.; Vivier, E. Natural cytotoxicity receptors and their ligands. *Immunol. Cell Biol.* 2014, *92*, 221–229, doi:10.1038/icb.2013.98.

5. Biassoni, R. Human Natural Killer Receptors, Co-Receptors, and Their Ligands. *Curr. Protoc. Immunol.* 2009, *84*, doi:10.1002/0471142735.im1410s84.
6. Pende, D.; Parolini, S.; Pessino, A.; Sivori, S.; Augugliaro, R.; Morelli, L.; Marcenaro, E.; Accame, L.; Malaspina, A.; Biassoni, R.; et al. Identification and Molecular Characterization of Nkp30, a Novel Triggering Receptor Involved in Natural Cytotoxicity Mediated by Human Natural Killer Cells. *J. Exp. Med.* 1999, *190*, 1505–1516, doi:10.1084/jem.190.10.1505.
7. Memmer, S.; Weil, S.; Beyer, S.; Zöller, T.; Peters, E.; Hartmann, J.; Steinle, A.; Koch, J. The Stalk Domain of NKp30 Contributes to Ligand Binding and Signaling of a Preassembled NKp30-CD3ζ Complex. *J. Biol. Chem.* 2016, *291*, 25427–25438, doi:10.1074/jbc.M116.742981.
8. Kaifu, T.; Escalière, B.; Gastinel, L.N.; Vivier, E.; Baratin, M. B7-H6/NKp30 interaction: A mechanism of alerting NK cells against tumors. *Cell. Mol. Life Sci.* 2011, *68*, 3531–3539, doi:10.1007/s00018-011-0802-7.
9. Hershkovitz, O.; Jarahian, M.; Zilka, A.; Bar-Ilan, A.; Landau, G.; Jivov, S.; Tekoah, Y.; Glicklis, R.; Gallagher, J.T.; Hoffmann, S.C.; et al. Altered glycosylation of recombinant NKp30 hampers binding to heparan sulfate: A lesson for the use of recombinant immunoreceptors as an immunological tool. *Glycobiology* 2008, *18*, 28–41, doi:10.1093/glycob/cwm125.
10. Chisholm, S.E.; Reyburn, H.T. Recognition of Vaccinia Virus-Infected Cells by Human Natural Killer Cells Depends on Natural Cytotoxicity Receptors. *J. Virol.* 2006, *80*, 2225–2233, doi:10.1128/jvi.80.5.2225-2233.2006.
11. Arnon, T.I.; Achdout, H.; Levi, O.; Markel, G.; Saleh, N.; Katz, G.; Gazit, R.; Gonen-Gross, T.; Hanna, J.; Nahari, E.; et al. Inhibition of the NKp30 activating receptor by pp65 of human cytomegalovirus. *Nat. Immunol.* 2005, *6*, 515–523, doi:10.1038/ni1190.
12. Brandt, C.S.; Baratin, M.; Yi, E.C.; Kennedy, J.; Gao, Z.; Fox, B.; Haldeman, B.; Ostrander, C.D.; Kaifu, T.; Chabannon, C.; et al. The B7 family member B7-H6 is a tumor cell ligand for the activating natural killer cell receptor NKp30 in humans. *J. Exp. Med.* 2009, *206*, 1495–1503, doi:10.1084/jem.20090681.
13. Binici, J.; Koch, J. BAG-6, a jack of all trades in health and disease. *Cell. Mol. Life Sci.* 2014, *71*, 1829–1837, doi:10.1007/s00018-013-1522-y.
14. Schlecker, E.; Fiegler, N.; Arnold, A.; Altevogt, P.; Rose-John, S.; Moldenhauer, G.; Sucker, A.; Paschen, A.; Von Strandmann, E.P.; Textor, S.; et al. Metalloprotease-Mediated Tumor Cell Shedding of B7-H6, the Ligand of the Natural Killer Cell-Activating Receptor NKp30. *Cancer Res.* 2014, *74*, 3429–3440, doi:10.1158/0008-5472.can-13-3017.
15. Wang, W.; Guo, H.; Geng, J.; Zheng, X.; Wei, H.; Sun, R.; Tian, Z. Tumor-released Galectin-3, a Soluble Inhibitory Ligand of Human NKp30, Plays an Important Role in Tumor Escape from NK Cell Attack. *J. Biol. Chem.* 2014, *289*, 33311–33319, doi:10.1074/jbc.M114.603464.
16. Chen, Y.; Mo, J.; Jia, X.; He, Y. The B7 Family Member B7-H6: A New Bane of Tumor. *Pathol. Oncol. Res.* 2018, *24*, 717–721, doi:10.1007/s12253-017-0357-5.
17. Hu, Y.; Zeng, T.; Xiao, Z.; Hu, Q.; Li, Y.; Tan, X.; Yue, H.; Wang, W.; Tan, H.; Zou, J. Immunological role and underlying mechanisms of B7-H6 in tumorigenesis. *Clin. Chim. Acta* 2020, *502*, 191–198, doi:10.1016/j.cca.2019.12.030.
18. Matta, J.; Baratin, M.; Chiche, L.; Forel, J.-M.; Cognet, C.; Thomas, G.; Farnarier, C.; Piperoglou, C.; Papazian, L.; Chaussabel, D.; et al. Induction of B7-H6, a ligand for the natural killer cell–activating receptor NKp30, in inflammatory conditions. *Blood* 2013, *122*, 394–404, doi:10.1182/blood-2013-01-481705.
19. Joyce, M.G.; Tran, P.; Zhuravleva, M.A.; Jaw, J.; Colonna, M.; Sun, P.D. Crystal structure of human natural cytotoxicity receptor NKp30 and identification of its ligand binding site. *Proc. Natl. Acad. Sci. USA* 2011, *108*, 6223–6228, doi: 10.1073/pnas.1100622108.
20. Li, Y.; Wang, Q.; Mariuzza, R.A. Structure of the human activating natural cytotoxicity receptor NKp30 bound to its tumor cell ligand B7-H6. *J. Exp. Med.* 2011, *208*, 703–714, doi:10.1084/jem.20102548.
21. Herrmann, J.; Berberich, H.; Hartmann, J.; Beyer, S.; Davies, K.E.; Koch, J. Homo-oligomerization of the Activating Natural Killer Cell Receptor NKp30 Ectodomain Increases Its Binding Affinity for Cellular Ligands. *J. Biol. Chem.* 2014, *289*, 765–777, doi:10.1074/jbc.m113.514786.
22. Hartmann, J.; Tran, T.-V.; Kaudeer, J.; Oberle, K.; Herrmann, J.; Quagliano, I.; Abel, T.; Cohnen, A.; Gatterdam, V.; Jacobs, A.; et al. The Stalk Domain and the Glycosylation Status of the Activating Natural Killer Cell Receptor NKp30 Are Important for Ligand Binding. *J. Biol. Chem.* 2012, *287*, 31527–31539, doi:10.1074/jbc.m111.304238.

23. Binici, J.; Hartmann, J.; Herrmann, J.; Schreiber, C.; Beyer, S.; Güler, G.; Vogel, V.; Tumulka, F.; Abele, R.; Mäntele, W.; et al. A Soluble Fragment of the Tumor Antigen BCL2-associated Athanogene 6 (BAG-6) Is Essential and Sufficient for Inhibition of NKp30 Receptor-dependent Cytotoxicity of Natural Killer Cells. *J. Biol. Chem.* 2013, *288*, 34295–34303, doi:10.1074/jbc.M113.483602.
24. Aricescu, A.R.; Lu, W.; Jones, E.Y. A time- and cost-efficient system for high-level protein production in mammalian cells. *Acta Crystallogr. Sect. D Biol. Crystallogr.* 2006, *62*, 1243–1250, doi:10.1107/s0907444906029799.
25. Reeves, P.J.; Callewaert, N.; Contreras, R.; Khorana, H.G. Structure and function in rhodopsin: High-level expression of rhodopsin with restricted and homogeneous N-glycosylation by a tetracycline-inducible N-acetylglucosaminyltransferase I-negative HEK293S stable mammalian cell line. *Proc. Natl. Acad. Sci. USA* 2002, *99*, 13419–13424.
26. Bláha, J.; Maraun, M.; Novák, P.; Vaněk, O. Expression and purification of soluble and stable ectodomain of natural killer cell receptor LLT1 through high-density transfection of suspension adapted HEK293S GnTI− cells. *Protein Expr. Purif.* 2015, *109*, 7–13, doi:10.1016/j.pep.2015.01.006.
27. Krissinel, E.; Henrick, K. Inference of Macromolecular Assemblies from Crystalline State. *J. Mol. Biol.* 2007, *372*, 774–797, doi:10.1016/j.jmb.2007.05.022.
28. Ni, L.; Dong, C. New B7 Family Checkpoints in Human Cancers. *Mol. Cancer Ther.* 2017, *16*, 1203–1211, doi:10.1158/1535-7163.MCT-16-0761.
29. Wu, M.-R.; Zhang, T.; Gacerez, A.T.; Coupet, T.A.; Demars, L.R.; Sentman, C.L. B7H6-Specific Bispecific T Cell Engagers Lead to Tumor Elimination and Host Antitumor Immunity. *J. Immunol.* 2015, *194*, 5305–5311, doi:10.4049/jimmunol.1402517.
30. Gacerez, A.T.; Hua, C.K.; Ackerman, M.E.; Sentman, C.L. Chimeric antigen receptors with human scFvs preferentially induce T cell anti-tumor activity against tumors with high B7H6 expression. *Cancer Immunol. Immunother.* 2018, *67*, 749–759, doi:10.1007/s00262-018-2124-1.
31. Kellner, C.; Maurer, T.; Hallack, D.; Repp, R.; Van De Winkel, J.G.J.; Parren, P.W.H.I.; Valerius, T.; Humpe, A.; Gramatzki, M.; Peipp, M.; et al. Mimicking an Induced Self Phenotype by Coating Lymphomas with the NKp30 Ligand B7-H6 Promotes NK Cell Cytotoxicity. *J. Immunol.* 2012, *189*, 5037–5046, doi:10.4049/jimmunol.1201321.
32. Kellner, C.; Günther, A.; Humpe, A.; Repp, R.; Klausz, K.; Derer, S.; Valerius, T.; Ritgen, M.; Brüggemann, M.; Van De Winkel, J.G.; et al. Enhancing natural killer cell-mediated lysis of lymphoma cells by combining therapeutic antibodies with CD20-specific immunoligands engaging NKG2D or NKp30. *OncoImmunology* 2016, *5*, e1058459, doi:10.1080/2162402X.2015.1058459.
33. Peipp, M.; Derer, S.; Lohse, S.; Staudinger, M.; Klausz, K.; Valerius, T.; Gramatzki, M.; Kellner, C. HER2-specific immunoligands engaging NKp30 or NKp80 trigger NK-cell-mediated lysis of tumor cells and enhance antibody-dependent cell-mediated cytotoxicity. *Oncotarget* 2015, *6*, 32075–32088, doi:10.18632/oncotarget.5135.
34. Jaron-Mendelson, M.; Yossef, R.; Appel, M.; Zilka, A.; Hadad, U.; Afergan, F.; Rosental, B.; Engel, S.; Nedvetzki, S.; Braiman, A.; et al. Dimerization of NKp46 Receptor Is Essential for NKp46-Mediated Lysis: Characterization of the Dimerization Site by Epitope Mapping. *J. Immunol.* 2012, *188*, 6165–6174, doi:10.4049/jimmunol.1102496.
35. Hadad, U.; Thauland, T.J.; Martinez, O.M.; Butte, M.J.; Porgador, A.; Krams, S.M. NKp46 Clusters at the Immune Synapse and Regulates NK Cell Polarization. *Front. Immunol.* 2015, *6*, 216, doi:10.3389/fimmu.2015.00495.
36. Arnon, T.I.; Markel, G.; Bar-Ilan, A.; Hanna, J.H.; Fima, E.; Benchetrit, F.; Galili, R.; Cerwenka, A.; Benharroch, D.; Sion-Vardy, N.; et al. Harnessing Soluble NK Cell Killer Receptors for the Generation of Novel Cancer Immune Therapy. *PLoS ONE* 2008, *3*, e2150, doi:10.1371/journal.pone.0002150.
37. Franke, D.; Petoukhov, M.V.; Konarev, P.V.; Panjkovich, A.; Tuukkanen, A.; Mertens, H.D.T.; Kikhney, A.G.; Hajizadeh, N.R.; Franklin, J.M.; Jeffries, C.M.; et al. ATSAS 2.8: A comprehensive data analysis suite for small-angle scattering from macromolecular solutions. *J. Appl. Crystallogr.* 2017, *50*, 1212–1225, doi:10.1107/s1600576717007786.
38. Pettersen, E.F.; Goddard, T.D.; Huang, C.C.; Couch, G.S.; Greenblatt, D.M.; Meng, E.C.; Ferrin, T.E. UCSF Chimera–a visualization system for exploratory research and analysis. *J. Comput. Chem.* 2004, *25*, 1605–1612.

39. Xu, X.; Li, Y.; Gauthier, L.; Chen, Q.; Vivier, E.; Mariuzza, R.A. Expression, crystallization and X-ray diffraction analysis of a complex between B7-H6, a tumor cell ligand for the natural cytotoxicity receptor NKp30, and an inhibitory antibody. *Acta Crystallogr. Sect. F Struct. Biol. Commun.* 2015, *71*, 697–701, doi:10.1107/s2053230x15006755.
40. Xu, X.; Narni-Mancinelli, E.; Cantoni, C.; Li, Y.; Guia, S.; Gauthier, L.; Chen, Q.; Moretta, A.; Vély, F.; Eisenstein, E.; et al. Structural Insights into the Inhibitory Mechanism of an Antibody against B7-H6, a Stress-Induced Cellular Ligand for the Natural Killer Cell Receptor NKp30. *J. Mol. Biol.* 2016, *428*, 4457–4466, doi:10.1016/j.jmb.2016.09.011.
41. Durocher, Y. High-level and high-throughput recombinant protein production by transient transfection of suspension-growing human 293-EBNA1 cells. *Nucleic Acids Res.* 2002, *30*, 9e, doi:10.1093/nar/30.2.e9.
42. Backliwal, G.; Hildinger, M.; Kuettel, I.; Delegrange, F.; Hacker, D.L.; Wurm, F.M. Valproic acid: A viable alternative to sodium butyrate for enhancing protein expression in mammalian cell cultures. *Biotechnol. Bioeng.* 2008, *101*, 182–189, doi:10.1002/bit.21882.
43. Pompach, P.; Man, P.; Kavan, D.; Hofbauerová, K.; Kumar, V.; Bezouska, K.; Havlicek, V.; Novák, P. Modified electrophoretic and digestion conditions allow a simplified mass spectrometric evaluation of disulfide bonds. *J. Mass Spectrom.* 2009, *44*, 1571–1578, doi:10.1002/jms.1609.
44. Young, M.M.; Tang, N.; Hempel, J.C.; Oshiro, C.M.; Taylor, E.W.; Kuntz, I.D.; Gibson, B.W.; Dollinger, G. High throughput protein fold identification by using experimental constraints derived from intramolecular cross-links and mass spectrometry. *Proc. Natl. Acad. Sci. USA* 2000, *97*, 5802–5806.
45. Kukačka, Z.; Rosulek, M.; Strohalm, M.; Kavan, D.; Novák, P. Mapping protein structural changes by quantitative cross-linking. *Methods* 2015, *89*, 112–120, doi:10.1016/j.ymeth.2015.05.027.
46. Grüninger, F.; D'Arcy, A.; D'Arcy, B.; Chène, C. Deglycosylation of proteins for crystallization using recombinant fusion protein glycosidases. *Protein Sci.* 1996, *5*, 2617–2622, doi:10.1002/pro.5560051224.
47. Schuck, P. Size-Distribution Analysis of Macromolecules by Sedimentation Velocity Ultracentrifugation and Lamm Equation Modeling. *Biophys. J.* 2000, *78*, 1606–1619, doi:10.1016/s0006-3495(00)76713-0.
48. Chaturvedi, S.; Ma, J.; Brown, P.H.; Zhao, H.; Schuck, P. Measuring macromolecular size distributions and interactions at high concentrations by sedimentation velocity. *Nat. Commun.* 2018, *9*, 4415, doi:10.1038/s41467-018-06902-x.
49. Scheuermann, T.H.; Brautigam, C.A. High-precision, automated integration of multiple isothermal titration calorimetric thermograms: New features of NITPIC. *Methods* 2015, *76*, 87–98, doi:10.1016/j.ymeth.2014.11.024.
50. Zhao, H.; Piszczek, G.; Schuck, P. SEDPHAT--a platform for global ITC analysis and global multi-method analysis of molecular interactions. *Methods* 2015, *76*, 137–148, doi:10.1016/j.ymeth.2014.11.012.
51. Brautigam, C.A. Calculations and Publication-Quality Illustrations for Analytical Ultracentrifugation Data. *Methods Enzymol.* 2015, *562*, 109–133, doi:10.1016/bs.mie.2015.05.001.
52. Kabsch, W. XDS. *Acta Crystallogr. Sect. D Biol. Crystallogr.* 2010, *66*, 125–132, doi:10.1107/S0907444909047337.
53. Winn, M.; Ballard, C.C.; Cowtan, K.; Dodson, E.J.; Emsley, P.; Evans, P.R.; Keegan, R.M.; Krissinel, E.B.; Leslie, A.G.W.; McCoy, A.; et al. Overview of the CCP4 suite and current developments. *Acta Crystallogr. Sect. D Biol. Crystallogr.* 2011, *67*, 235–242, doi:10.1107/S0907444910045749.
54. Vagin, A.; Lebedev, A. MoRDa, an automatic molecular replacement pipeline. *Acta Crystallogr. Sect. A Found. Adv.* 2015, *71*, S19, doi:10.1107/s2053273315099672.
55. McCoy, A.J.; Grosse-Kunstleve, R.W.; Adams, P.D.; Winn, M.D.; Storoni, L.C.; Read, R.J. Phaser crystallographic software. *J. Appl. Crystallogr.* 2007, *40*, 658–674, doi:10.1107/S0021889807021206.
56. Murshudov, G.N.; Skubak, P.; Lebedev, A.A.; Pannu, N.S.; Steiner, R.A.; Nicholls, R.; Winn, M.D.; Long, F.; Vagin, A.A. REFMAC5 for the refinement of macromolecular crystal structures. *Acta Crystallogr. Sect. D Biol. Crystallogr.* 2011, *67*, 355–367, doi:10.1107/S0907444911001314.
57. Kovalevskiy, O.; Nicholls, R.; Murshudov, G. Automated refinement of macromolecular structures at low resolution using prior information. *Acta Crystallogr. Sect. D Struct. Biol.* 2016, *72*, 1149–1161, doi:10.1107/S2059798316014534.
58. Emsley, P.; Lohkamp, B.; Scott, W.G.; Cowtan, K. Features and development of Coot. *Acta Crystallogr. Sect. D Biol. Crystallogr.* 2010, *66*, 486–501, doi:10.1107/S0907444910007493.

59. Chen, V.B.; Arendall, W.B.; Headd, J.J.; Keedy, D.; Immormino, R.M.; Kapral, G.J.; Murray, L.W.; Richardson, J.S.; Richardson, D.C. MolProbity: All-atom structure validation for macromolecular crystallography. *Acta Crystallogr. Sect. D Biol. Crystallogr.* 2010, *66*, 12–21, doi:10.1107/S0907444909042073.

List of publications

Bláha J, Kalousková B, Skořepa O, Pažický S, Novák P, Vaněk O. "High-level expression and purification of soluble form of human natural killer cell receptor NKR-P1 in HEK293S GnTI$^-$ cells." Protein Expression and Purification 2017; 140: 36-43. doi: 10.1016/j.pep.2017.07.016

Vaněk O, Celadova P, Skořepa O, Bláha J, Kalousková B, Dvorská A, Poláchová E, Pucholtová H, Kavan D, Pompach P, Hofbauerová K, Kopecký V Jr, Mesci A, Voigt S, Carlyle JR. "Production of recombinant soluble dimeric C-type lectin-like receptors of rat natural killer cells." Scientific Reports 2019; 9(1): 17836. doi: 10.1038/s41598-019-52114-8

Skořepa O, Pazicky S, Kalousková B, Bláha J, Abreu C, Ječmen T, Rosůlek M, Fish A, Sedivy A, Harlos K, Dohnálek J, Skálová T, Vaněk O. "Natural Killer Cell Activation Receptor NKp30 Oligomerization Depends on Its *N*-Glycosylation." Cancers 2020; 12(7): 1998. doi: 10.3390/cancers12071998

Peleg Y, Vincentelli R, Collins B, Chen K, Livingstone E, Weeratunga S, Leneva N, Guo Q, Remans K, Perez K, Bjerga G, Larsen O, Vaněk O, Skořepa O, Jacquemin S, Poterszman A, Kjaer S, Christodoulou E, Albeck S, Dym O, Ainbinder E, Unger T, Schuetz A, Matthes S, Bader M, de Marco A, Storici P, Semrau M, Stolt-Bergner P, Aigner Ch, Suppmann S, Goldenzweig A, Fleishman S. "Community-wide experimental evaluation of the PROSS stability-design method." Journal of Molecular Biology 2021; 433(13): 166964. doi: 10.1016/j.jmb.2021.166964